Peptidoglycan-Modifying Enzymes: Mechanistic Studies and Substrate and Inhibitor Design

by

Timin Hadi

B.Sc., The University of British Columbia, 2005

A THESIS SUBMITTED IN PARTIAL FULFILLMENT OF
THE REQUIREMENTS FOR THE DEGREE OF

DOCTOR OF PHILOSOPHY

in

THE FACULTY OF GRADUATE STUDIES

(Chemistry)

THE UNIVERSITY OF BRITISH COLUMBIA

(Vancouver)

July 2011

Abstract

Peptidoglycan is a key component of the bacterial cell wall and is an essential structure for protecting the cell from lysis due to high osmotic pressure. Because of its importance, peptidoglycan has become a prominent target for antibiotic design as well as a number of host defense mechanisms. In response, many bacteria have developed methods of evading or minimizing the effects of these antibiotics and defense mechanisms through the modification of their peptidoglycan. One such modification, found in a number of bacterial species, is the *O*-acetylation of *N*-acetylmuramic acid (MurNAc) residues of peptidoglycan. This modification decreases the hydrolytic activity of lysozyme, an enzyme that is released as a response to bacterial infection, on peptidoglycan, and results in increased bacterial pathogenicity and virulence. The enzyme *O*-acetylpeptidoglycan esterase (Ape1) from *Neisseria gonorrhoeae* is an important enzyme involved in the bacterial *O*-acetylation/deacetylation pathway, and has been shown to be essential for bacterial viability. In this thesis, we detail the design and testing of water-soluble monosaccharide and disaccharide substrates of Ape1 (compounds **1** and **2**) and preliminary work towards the design and testing of small-molecule inhibitors of the enzyme. Disaccharide **1** and monosaccharide **2** both served as substrates of Ape1, indicating that a polymeric substrate is not required for efficient catalysis. Our monosaccharide scaffold was chosen for the design of future generations of inhibitors.

The enzyme *N*-acetylmuramic acid 6-phosphate hydrolase (MurQ) is essential for the recycling of MurNAc residues in peptidoglycan. This recycling process serves to reincorporate cell wall components into synthetic precursors that can be used in peptidoglycan biosynthesis as well as other basic metabolic pathways. MurQ catalyzes the

conversion of MurNAc 6-phosphate to GlcNAc 6-phosphate through cleavage of a lactyl ether. In this thesis, studies on the mechanism through which MurQ catalyzes hydrolysis of the lactyl ether of MurNAc 6-phosphate are reported. By probing the reaction with chemically synthesized substrate and substrate analogues, an E1cB-like mechanism with an (*E*)-alkene intermediate is proposed. The amino acids Glu83 and Glu114 are implicated as important residues in catalysis, and their specific roles are also explored in the context of our proposed mechanism.

Preface

A version of Chapter 2 has been published and some figures are reproduced with permission from: Hadi, T.; Pfeffer, J. M.; Clarke, A. J.; Tanner, M. E.; *Journal of Organic Chemistry* **2011**, *76*, 1118-1125 (© 2011 American Chemical Society). The testing of compounds **1**, **2**, and **15** with Ape1 were carried out by John M. Pfeffer at the University of Guelph under the supervision of Professor Anthony J. Clarke. The remaining experiments were performed by the author of this thesis, under the supervision of Professor Tanner.

A version of Chapter 3 has been published and some figures are reproduced with permission from: Hadi, T.; Dahl, U.; Mayer, C.; Tanner, M. E.; *Biochemistry* **2008**, *47*, 11547-11558 (© 2008 American Chemical Society). The plasmid pUB9 was obtained from Professor Mayer (University of Konstanz), and all work on the structural model of MurQ, as well as the multiple sequence alignments, was performed by Ulrike Dahl and Professor Mayer at the University of Konstanz. The plasmids containing the genes for the MurQ mutants Glu83Ala and Asp115Asn were obtained from Professor Mayer, while the plasmids containing the genes for the MurQ mutants Glu83Gln and Glu114Gln were constructed by the author of this thesis. Preliminary work on the design and testing of MurQ inhibitors was aided by Yi Han, an undergraduate research assistant in the Tanner group. The gene expression of both mutant and wild-type forms of MurQ, and all mechanistic investigations, were performed by the author of this thesis, under the supervision of Professor Tanner.

Table of Contents

Abstract ..... **ii**

Preface ..... **iv**

Table of Contents ..... **v**

List of Tables ..... **x**

List of Figures ..... **xi**

List of Symbols and Abbreviations ..... **xvii**

Acknowledgements ..... **xxiv**

Dedication ..... **xxv**

Chapter 1: Metabolism and Modification of Peptidoglycan **1**

1.1 Peptidoglycan Structure and Function 1

1.2 Biosynthesis of Peptidoglycan 6

1.2.1 Synthesis of the Muropeptide Subunit 6

1.2.2 Insertion of Lipid II into the Murein Sacculus 10

1.2.3 The Penicillin-Binding Proteins – Prominent Antibacterial Targets 13

1.3 Peptidoglycan Turnover and Recycling 15

1.3.1 Peptidoglycan Amidases and Peptidases 17

1.3.2 Muramidases and Glucosaminidases 19

1.3.3 Peptidoglycan Recycling 22

1.3.3.1 Peptidoglycan Amino Acid-Recycling Enzymes 23

1.3.3.2 Peptidoglycan Amino Sugar-Recycling Enzymes 27

1.4 Lysozymes: Host Muramidases 30

1.5 Glycan Modification in Peptidoglycan 32

1.5.1 *O*-Acetylation of Peptidoglycan 34

1.5.1.1 Peptidoglycan *O*-Acetyltransferases 36

1.5.1.2 *O*-Acetylpeptidoglycan Esterases 39

1.6 The Role of Peptidoglycan Metabolism in Physiological Processes 40

1.7 Thesis Aims 41

Chapter 2: Substrate and Inhibitor Design for the Enzyme *O*-Acetylpeptidoglycan Esterase (Ape1) from *Neisseria gonorrhoeae*..... 44

2.1 Catalytic Mechanism of Ape1..... 45

2.2 Previous Attempts at Assaying Ape1 Enzymatic Activity..... 46

2.3 Design and Synthesis of Peptidoglycan-Like Substrate Analogues of Ape1..... 49

2.3.1 Synthesis of Disaccharide Substrate (**1**)..... 51

2.3.2 Synthesis of Monosaccharide Substrate (**2**)..... 59

2.4 Testing of Compounds **1** and **2** with Ape1..... 60

2.5 Synthesis of Phosphate Inhibitor (**15**) and Testing with Ape1..... 64

2.6 Summary..... 66

2.7 Future Directions..... 67

2.8 Experimental Procedures..... 69

2.8.1 Materials and General Methods..... 69

2.8.2 Synthesis of Disaccharide (**1**)..... 70

2.8.2.1 Methyl 2-acetamido-2-deoxy-β-D-glucopyranoside (**3**)..... 70

2.8.2.2 Methyl 2-acetamido-4,6-*O*-benzylidene-2-deoxy-β-D-glucopyranoside (**4**)..... 71

2.8.2.3 Methyl 2-acetamido-4,6-*O*-benzylidene-2-deoxy-3-*O*-((*R*)-1-carboxyethyl)-β-D-glucopyranoside (**5**)..... 72

2.8.2.4 Methyl 4,6-*O*-benzylidene-β-D-*N*-acetylmuramylpyranoside-L-alanine methyl ester (**6**)..... 72

2.8.2.5 Methyl 6-*O*-benzyl-β-D-*N*-acetylmuramylpyranoside-L-alanine methyl ester (**7**)..... 73

2.8.2.6 Methyl 3,4,6-tri-*O*-acetyl-2-deoxy-2-trichloroacetamido-β-D-glucopyranosyl-(1→4)-6-*O*-benzyl-β-D-*N*-acetylmuramylpyranoside-L-alanine methyl ester (**9**)..... 74

2.8.2.7 Methyl 3,4,6-tri-*O*-acetyl-2-acetamido-2-deoxy-β-D-glucopyranosyl-(1→4)-6-*O*-benzyl-β-D-*N*-acetylmuramylpyranoside-L-alanine methyl ester (**10**)..... 75

2.8.2.8 Methyl 2-acetamido-2-deoxy-3,4,6-tri-*O*-levulinoyl-β-D-glucopyranosyl-(1→4)-6-*O*-benzyl-β-D-*N*-acetylmuramylpyranoside-L-alanine methyl ester (**11**)..... 76

2.8.2.9 Methyl 2-acetamido-2-deoxy-β-D-glucopyranosyl-(1→4)-6-*O*-acetyl-β-D-*N*-acetylmuramylpyranoside-L-alanine methyl ester (**1**)..... 77

2.8.3 Synthesis of Monosaccharide (**2**)..... 78

2.8.3.1 Methyl 2-acetamido-4,6-*O*-benzylidene-2-deoxy-3-*O*-((*R*)-1-(methoxycarbonyl)ethyl)-β-D-glucopyranoside (**12**)..... 78

2.8.3.2 Methyl 2-acetamido-4-*O*-benzyl-2-deoxy-3-*O*-((*R*)-1-(methoxycarbonyl)ethyl)-β-D-glucopyranoside (**13**) 79
2.8.3.3 Methyl 2-acetamido-6-*O*-acetyl-4-*O*-benzyl-3-*O*-((*R*)-1-carboxyethyl)-2-deoxy-β-D-glucopyranoside monosodium salt (**2**) 80
2.8.4 Synthesis of Monosaccharide Phosphate Inhibitor (**15**) 81
2.8.4.1 Methyl 2-acetamido-4-*O*-benzyl-2-deoxy-6-*O*-dibenzylphosphoryl-3-*O*-((*R*)-1-(methoxycarbonyl)ethyl)-β-D-glucopyranoside (**14**) 81
2.8.4.2 Methyl 2-acetamido-4-*O*-benzyl-2-deoxy-3-*O*-((*R*)-1-(methoxycarbonyl)ethyl)-β-D-glucopyranoside 6-dihydrogen phosphate (**15**) 82
2.8.5 Ape1 Enzyme Production and Enzymatic Activity Assays 83
2.8.5.1 Bacterial Strains and Growth Media 83
2.8.5.2 Production and Purification of Ape1 84
2.8.5.3 Enzyme Assays 85

Chapter 3: Mechanistic Studies on *N*-Acetylmuramic Acid 6-Phosphate Hydrolase (MurQ) from *Escherichia coli* 87

3.1 Previous Characterization of MurQ 89
3.2 Proposed Mechanism of MurQ Action 97
3.3 Synthesis of the Substrate and Product of the MurQ Reaction 100
3.3.1 Synthesis of MurNAc 6-Phosphate 100
3.3.2 Synthesis of GlcNAc 6-Phosphate 102
3.3.3 Synthesis of [2-^{2}H]MurNAc 6-Phosphate 103
3.4 Kinetic Studies on Wild-Type MurQ 104
3.4.1 Kinetic Isotope Effect Measurement on the Wild-Type MurQ Reaction 107
3.5 Monitoring the MurQ Reaction by ^{1}H NMR Spectroscopy and Mass Spectrometry: Solvent Deuterium Incorporation and Intermediate Release 109
3.6 Determination of the Nature of the Unsaturated Sugar Intermediate 115
3.7 Studies with 3-Chloro-3-Deoxy-*N*-Acetylglucosamine 6-Phosphate 119
3.7.1 Synthesis of 3-Chloro-3-Deoxy-GlcNAc 6-Phosphate 120
3.7.2 Studies with 3-Chloro-3-Deoxy-GlcNAc 6-Phosphate 122
3.7.3 Testing of 3-Chloro-3-Deoxy-GlcNAc 6-Phosphate as a Substrate of MurQ 125
3.8 Solvent-Derived ^{18}O Isotope Incorporation Catalyzed by MurQ 126
3.9 Comparison of a Structural Model of MurQ with GlmS and Identification of Potential Active Site Residues 130

3.9.1 Construction and Kinetic Characterization of MurQ Mutants 134
3.9.2 Monitoring the MurQ Mutant Reactions by ^{1}H NMR Spectroscopy and Mass Spectrometry 138
3.9.2.1 Reaction of MurNAc 6-Phosphate with the Glu83Ala MurQ Mutant 139
3.9.2.2 Reaction of MurNAc 6-Phosphate with the Glu114Gln MurQ Mutant 142
3.9.3 Testing of Glu114Gln and Glu83Ala MurQ Mutants with Alternate Substrates 146
3.10 Summary 147
3.11 Future Work 152
3.12 Experimental Procedures 154
3.12.1 Materials and General Methods 154
3.12.2 Synthesis of MurNAc 6-Phosphate (**23**) 155
3.12.2.1 Benzyl 2-acetamido-2-deoxy-α-D-glucopyranoside (**18**) 155
3.12.2.2 Benzyl 2-acetamido-4,6-*O*-benzylidene-2-deoxy-α-D-glucopyranoside (**19**) 155
3.12.2.3 Benzyl 2-acetamido-4,6-*O*-benzylidene-2-deoxy-3-*O*-[(*R*)-1-carboxyethyl]-α-D-glucopyranoside (**20**) 156
3.12.2.4 Benzyl 2-acetamido-4-*O*-benzyl-3-*O*-[(*R*)-1-carboxyethyl]-2-deoxy-α-D-glucopyranoside (**21**) 157
3.12.2.5 Benzyl 2-acetamido-4-*O*-benzyl-3-*O*-[(*R*)-1-carboxyethyl]-2-deoxy-6-*O*-dibenzylphosphoryl-α-D-glucopyranoside (**22**) 157
3.12.2.6 2-Acetamido-3-*O*-[(*R*)-1-carboxyethyl]-2-deoxy-α,β-D-glucose 6-dihydrogen phosphate (**23** - MurNAc 6-phosphate) 158
3.12.3 Synthesis of GlcNAc 6-Phosphate 159
3.12.3.1 Benzyl 2-acetamido-2-deoxy-6-*O*-diphenylphosphoryl-α-D-glucopyranoside (**24**) 159
3.12.3.2 2-Acetamido-2-deoxy-α,β-D-glucose 6-dihydrogen phosphate (**25** - GlcNAc 6-phosphate) 160
3.12.4 Synthesis of [2-^{2}H]MurNAc 6-Phosphate (**26**) 161
3.12.5 Overexpression and Purification of Wild-Type *E. coli* MurQ 161
3.12.6 Coupled Kinetic Assay for MurQ Activity 163
3.12.7 Monitoring the MurQ reaction in D_2O using ^{1}H NMR spectroscopy 164
3.12.8 Reduction of the unsaturated intermediate with $NaBH_4$ 164
3.12.9 Synthesis of 3-Chloro-3-Deoxy-GlcNAc 6-Phosphate 165

3.12.9.1 Benzyl 2-benzamido-4,6-*O*-benzylidene-2-deoxy-6-*O*-toluene-*p*-sulfonyl-α-D-glucopyranoside (**28**) 165
3.12.9.2 Benzyl 2-amino-4,6-*O*-benzylidene-3-chloro-2,3-dideoxy-α-D-glucopyranoside (**29**) 165
3.12.9.3 Benzyl 2-acetamido-4,6-*O*-benzylidene-3-chloro-2,3-dideoxy-α-D-glucopyranoside (**30**) 166
3.12.9.4 Benzyl 2-acetamido-4-*O*-benzyl-3-chloro-2,3-dideoxy-α-D-glucopyranoside (**31**) 167
3.12.9.5 Benzyl 2-acetamido-4-*O*-benzyl-3-chloro-6-*O*-dibenzylphosphoryl-2,3-dideoxy-α-D-glucopyranoside (**32**) 168
3.12.9.6 2-Acetamido-3-chloro-2,3-dideoxy-α,β-D-glucose 6-(dihydrogen phosphate) (**33**) 169
3.12.10 Non-Enzymatic Production of Alkene Intermediate from 3-Chloro-3-Deoxy-GlcNAc 6-Phosphate 169
3.12.11 ^{18}O-Isotope Incorporation Experiment 170
3.12.12 Structural Modeling of *E. coli* MurQ and Multiple Sequence Alignment 171
3.12.13 Preparation and Expression of Mutant MurQ Plasmids 171
3.12.14 Solvent-Derived Deuterium Incorporation into MurNAc 6-Phosphate with Wild-Type and Glu83Ala MurQ 172

References 174

Appendix: NMR Spectra of Selected Compounds 178

List of Tables

Table 2.1 Specific activity of Ape1-catalyzed hydrolysis of test substrates..... 47

Table 2.2 Kinetic parameters for the Ape1-catalyzed hydrolysis of synthetic substrates **1** and **2**. 63

Table 2.3 Bacterial strains and plasmids used in this study. 84

Table 3.1 Kinetic constants for the reactions catalyzed by MurQ and its mutants..... 138

List of Figures

Figure 1.1 Chemical structures of polysaccharide polymers found in nature..... 2
Figure 1.2 Schematic diagram of the (a) Gram-positive and (b) Gram-negative bacterial cell wall. 3
Figure 1.3 Chemical structure of a cross-linked muropeptide subunit in peptidoglycan. 4
Figure 1.4 The orientation of glycan strands and peptide cross-links in peptidoglycan..... 5
Figure 1.5 Chemical structure of UDP-GlcNAc. 6
Figure 1.6 Enzymatic conversion of UDP-GlcNAc to UDP-MurNAc by MurZ and MurB... 7
Figure 1.7 Enzymatic addition of the pentapeptide side chain to UDP-MurNAc. 7
Figure 1.8 General mechanism of ligase-catalyzed peptide bond formation..... 8
Figure 1.9 Attachment of UDP-MurNAc-pentapeptide to undecaprenyl phosphate and the synthesis of Lipid II. 10
Figure 1.10 Transglycosylation of Lipid II and reuse of undecaprenyl phosphate. 12
Figure 1.11 Mechanism of PBP-catalyzed transpeptidation of peptidoglycan. 13
Figure 1.12 Structural similarities between β-lactams and the natural substrate of penicillin D-Ala-D-Ala 14
Figure 1.13 Mechanism of PBP-inactivation by β-lactam antibiotics. 15
Figure 1.14 Sites of action of peptidoglycan hydrolases 17
Figure 1.15 Mechanism of lytic transglycosylase-catalyzed cleavage of peptidoglycan. 20
Figure 1.16 (A) Stabilization of the oxocarbenium ion through formation of an intramolecular oxazolinium ion. (B) Structure of the lytic transglycosylase inhibitor GlcNAc thiazoline 20
Figure 1.17 Peptidoglycan degradation products of lytic transglycosylases (left) and β-*N*-acetylglucosaminidases (right)..... 21
Figure 1.18 The major degradation product GlcNAc-anhMurNAc-tetrapeptide is imported into the cytoplasm by the membrane transporter AmpG. 23
Figure 1.19 The peptidoglycan amino acid-recycling pathway. 24
Figure 1.20 Deletion of LdcA causes alternative Lipid II production and impaired cross-linking of new peptidoglycan strands 26

Figure 1.21 The degradation product GlcNAc-anhMurNAc is converted into UDP-GlcNAc for use in peptidoglycan biosynthesis. 27
Figure 1.22 Conversion of GlcNAc to UDP-GlcNAc via the peptidoglycan recycling pathway. 29
Figure 1.23 Conversion of anhMurNAc into GlcNAc 6-phosphate by AnmK and MurQ.... 30
Figure 1.24 Mechanism of lysozyme-catalyzed hydrolysis of peptidoglycan. 32
Figure 1.25 Covalent modifications of peptidoglycan 34
Figure 1.26 Peptidoglycan *O*-acetylation at the C-6 hydroxyl group of MurNAc residues. . 35
Figure 1.27 Peptidoglycan *O*-acetylation/deacetylation and the action of lytic transglycosylase. 36
Figure 1.28 One-component (left) and two-component (right) models for peptidoglycan *O*-acetylation. 37
Figure 1.29 Hydrolysis of *O*-acetylated peptidoglycan by the *O*-acetylpeptidoglycan esterase, Ape1. 42
Figure 1.30 Conversion of MurNAc 6-phosphate to GlcNAc 6-phosphate by the MurNAc 6-phosphate hydrolase, MurQ 43
Figure 2.1 Proposed mechanism of Ape1-catalyzed hydrolysis of *O*-acetylated peptidoglycan. 46
Figure 2.2 Proposed water-soluble disaccharide (**1**) and monosaccharide (**2**) substrates of Ape1. 49
Figure 2.3 Glycosidic coupling reaction using a glycosyl donor and a glycosyl acceptor. ... 52
Figure 2.4 Formation of an oxazolinium intermediate in glycosidic coupling reactions using GlcNAc donors slows transfer to the glycosyl acceptor. 53
Figure 2.5 Functional groups used to increase the donor properties of 2-*N*-acetyl-containing monosaccharides in oligosaccharide synthesis. 54
Figure 2.6 Synthesis of disaccharide substrate (**1**) 55
Figure 2.7 Mechanism of levulinate ester cleavage by hydrazine. 58
Figure 2.8 Synthesis of monosaccharide substrate (**2**) 60
Figure 2.9 Plot of initial velocity vs. substrate concentration for Ape1's reaction with disaccharide substrate (**1**) 61

Figure 2.10 Plot of initial velocity vs. substrate concentration for Ape1's reaction with monosaccharide substrate (**2**)..... 62
Figure 2.11 Synthesis of monosaccharide phosphate (**15**)..... 65
Figure 2.12 Potential reversible covalent inhibitors of Ape1. 68
Figure 2.13 Proposed mode of action of reversible covalent Ape1 inhibitors (**16**) and (**17**). 69
Figure 3.1 Conversion of anhMurNAc to GlcNAc 6-phosphate by AnmK and MurQ..... 88
Figure 3.2 Assay for the detection of 2-*N*-acetylated amino sugars using Ehrlich's reagent. 92
Figure 3.3 Incubation of MurQ with MurNAc 6-phosphate or GlcNAc 6-phosphate produces a compound that reacts with Ehrlich's reagent..... 93
Figure 3.4 The reaction catalyzed by glucosamine 6-phosphate synthase, GlmS. 94
Figure 3.5 Mechanism of glucose 6-phosphate synthesis and glucosamine 6-phosphate synthesis by GlmS..... 96
Figure 3.6 Proposed mechanism of MurQ catalysis. 99
Figure 3.7 Chemical synthesis of MurNAc 6-phosphate..... 101
Figure 3.8 Chemical synthesis of GlcNAc 6-phosphate. 102
Figure 3.9 Chemical synthesis of [2-^{2}H]MurNAc 6-phosphate..... 104
Figure 3.10 SDS-PAGE gel showing the purification of MurQ. 105
Figure 3.11 Continuous coupled assay measuring the release of D-lactate by MurQ. 106
Figure 3.12 Plot of initial velocity vs. MurNAc 6-phosphate concentration for the wild-type MurQ reaction..... 107
Figure 3.13 Plot of initial velocity vs. substrate concentration for the wild-type MurQ reaction with [2-^{2}H]MurNAc 6-phosphate (circles) and MurNAc 6-phosphate (squares)... 109
Figure 3.14 ^{1}H NMR (D_2O, 400 MHz) spectra of the MurQ reaction with MurNAc 6-phosphate. 111
Figure 3.15 ^{1}H NMR spectra from monitoring the reaction of MurNAc 6-phosphate with MurQ in buffered D_2O 113
Figure 3.16 An equilibrium ratio of alkene intermediate and GlcNAc 6-phosphate is formed through the reversible dehydration of GlcNAc 6-phosphate by MurQ and occasional release of the alkene intermediate into solution..... 115

Figure 3.17 Possible structures of the alkene intermediate of the MurQ reaction following its release from the active site into solution. 116
Figure 3.18 ^{1}H NMR spectra of the α,β-unsaturated aldehyde intermediate before (A) and after (B) reduction with $NaBH_4$. 118
Figure 3.19 Favored structures of the (*E*)-α,β-unsaturated aldehyde intermediate of the MurQ reaction. 119
Figure 3.20 Proposed mechanism for the reaction of the alternate substrate 3-chloro-3-deoxy-GlcNAc 6-phosphate with MurQ. 120
Figure 3.21 Synthesis of 3-chloro-3-deoxy-GlcNAc 6-phosphate. 121
Figure 3.22 ^{1}H NMR spectra showing the decomposition of 3-chloro-3-deoxy-GlcNAc 6-phosphate (**33**) when incubated at 42 °C in deuterated phosphate buffer (50 mM, pD 7.9) 124
Figure 3.23 Incubation of (*E*)-alkene intermediate (produced non-enzymatically) with MurQ to test for catalytic competence. 125
Figure 3.24 ^{1}H NMR spectra from monitoring the conversion of 3-chloro-3-deoxy-GlcNAc 6-phosphate into an equilibrium mixture of alkene intermediate and GlcNAc 6-phosphate. 126
Figure 3.25 Possible isotopically-labeled forms of GlcNAc 6-phosphate that could be formed when [1-^{18}O]GlcNAc 6-phosphate is incubated with MurQ in 50:50 $H_2{}^{18}O$:$H_2{}^{16}O$ 128
Figure 3.26 Mass spectra showing the reaction of [1-^{18}O]GlcNAc 6-phosphate with MurQ in a buffer prepared from a 50:50 mixture of $H_2{}^{18}O$ and $H_2{}^{16}O$ 129
Figure 3.27 Structural model of MurQ modeled as a homodimer (top) and structure of the isomerase module of GlmS (PDB code: 1MOR) 132
Figure 3.28 Identification of putative active site residues using a multiple sequence alignment and the structural model of *E. coli* MurQ 133
Figure 3.29 Structural changes of mutated residues for the Glu83Gln, Glu83Ala, Glu114Gln, and Asp115Asn MurQ mutant enzymes. 134
Figure 3.30 Plot of initial velocity vs. MurNAc 6-phosphate concentration for the Glu83Ala MurQ mutant. 135

Figure 3.31 Plot of initial velocity vs. MurNAc 6-phosphate concentration for the Glu114Gln MurQ mutant. 136
Figure 3.32 Plot of initial velocity vs. MurNAc 6-phosphate concentration for the Asp114Asn MurQ mutant. 136
Figure 3.33 ^{1}H NMR spectra from monitoring the reaction of MurNAc 6-phosphate with the Glu83Ala mutant in deuterated buffer. 140
Figure 3.34 Schematic of the reactions catalyzed by wild-type (top) and Glu83Ala MurQ (bottom) 141
Figure 3.35 Proposed catalytic mechanism of MurQ with Glu83 playing the role of B_2 142
Figure 3.36 ^{1}H NMR spectra monitoring the reaction of MurNAc 6-phosphate with the Glu114Gln MurQ mutant in deuterated buffer 143
Figure 3.37 Schematic of the reactions catalyzed by wild-type (top) and Glu114Gln MurQ (bottom) 144
Figure 3.38 Proposed catalytic mechanism of MurQ with Glu114 playing the role of B_1. 146
Figure 3.39 Mechanism of glycoside hydrolysis catalyzed by the Family 4 glycosidase BglT 150
Figure 3.40 Structures of potential reversible non-covalent inhibitors of MurQ. 153

Figure A. 1 ^{1}H NMR (400 MHz, $CDCl_3$) spectrum of compound **6**. 179
Figure A. 2 ^{13}C NMR (100 MHz, $CDCl_3$) spectrum (APT) of compound **6**. 180
Figure A. 3 ^{1}H NMR (400 MHz, $CDCl_3$) spectrum of compound **7**. 181
Figure A. 4 ^{13}C NMR (100 MHz, $CDCl_3$) spectrum (APT) of compound **7**. 182
Figure A. 5 ^{1}H NMR (400 MHz, MeOD) spectrum of compound **9**. 183
Figure A. 6 ^{13}C NMR (100 MHz, MeOD) spectrum of compound **9**. 184
Figure A. 7 ^{1}H NMR (400 MHz, MeOD) spectrum of compound **10**. 185
Figure A. 8 ^{13}C NMR (100 MHz, MeOD) spectrum (APT) of compound **10**. 186
Figure A. 9 ^{1}H NMR (400 MHz, MeOD) spectrum of compound **11**. 187
Figure A. 10 ^{13}C NMR (100 MHz, MeOD) spectrum (APT) of compound **11**. 188
Figure A. 11 ^{1}H NMR (400 MHz, D_2O) spectrum of compound **1**. 189

Figure A. 12 ^{13}C NMR (100 MHz, D_2O) spectrum (APT) of compound **1**. 190
Figure A. 13 ^{1}H NMR (400 MHz, $CDCl_3$) spectrum of compound **13**. 191
Figure A. 14 ^{13}C NMR (100 MHz, $CDCl_3$) spectrum (APT) of compound **13**. 192
Figure A. 15 ^{1}H NMR (400 MHz, MeOD) spectrum of compound **2**. 193
Figure A. 16 ^{13}C NMR (100 MHz, MeOD) spectrum of compound **2**. 194
Figure A. 17 ^{1}H NMR (300 MHz, $CDCl_3$) spectrum of compound **14**. 195
Figure A. 18 ^{13}C NMR (75 MHz, $CDCl_3$) spectrum of compound **14**. 196
Figure A. 19 ^{1}H NMR (400 MHz, D_2O) spectrum of compound **15**. 197
Figure A. 20 ^{13}C NMR (100 MHz, D_2O) spectrum of compound **15**. 198
Figure A. 21 ^{1}H NMR (400 MHz, DMSO-d_6) spectrum of compound **19**. 199
Figure A. 22 ^{1}H NMR (400 MHz, DMSO-d_6) spectrum of compound **20**. 200
Figure A. 23 ^{1}H NMR (400 MHz, MeOD) spectrum of compound **21**. 201
Figure A. 24 ^{1}H NMR (400 MHz, MeOD) spectrum of compound **22**. 202
Figure A. 25 ^{1}H NMR (400 MHz, D_2O) spectrum of compound **23**. 203
Figure A. 26 ^{1}H NMR (400 MHz, MeOD) spectrum of compound **24**. 204
Figure A. 27 ^{1}H NMR (400 MHz, D_2O) spectrum of compound **25**. 205
Figure A. 28 ^{1}H NMR (400 MHz, $CDCl_3$) spectrum of compound **28**. 206
Figure A. 29 ^{1}H NMR (400 MHz, $CDCl_3$) spectrum of compound **29**. 207
Figure A. 30 ^{1}H NMR (400 MHz, $CDCl_3$) spectrum of compound **30**. 208
Figure A. 31 ^{1}H NMR (400 MHz, $CDCl_3$) spectrum of compound **31**. 209
Figure A. 32 ^{1}H NMR (400 MHz, $CDCl_3$) spectrum of compound **32**. 210
Figure A. 33 ^{1}H NMR (400 MHz, D_2O) spectrum of compound **33** 211

List of Symbols and Abbreviations

α-NA	alpha-naphthyl
δ	chemical shift (ppm)
Å	angstrom
A_2pm	diaminopimelic acid
Ac	acetyl
Ac_2O	acetic anhydride
AcOH	acetic acid
AIBN	azobisisobutyronitrile
amu	atomic mass unit
anhMurNAc	1,6-anhydro-*N*-acetylmuramic acid
ATP	adenosine triphosphate
Ape	*O*-acetylpeptidoglycan esterase
Bn	benzyl
BnOH	benzyl alcohol
BSA	bovine serum albumin
Bu	butyl
Bz	benzoyl
CAZy	Carbohydrate-Active Enzymes
CE	Carbohydrate Esterase
CoA	coenzyme A
COSY	correlation spectroscopy
CV	column volumes

D	deuterium (^{2}H)
DAP	diaminopimelic acid
DCM	dichloromethane; methylene chloride
DIPC	*N*,*N'*-diisopropylcarbodiimide
DMA	*N*,*N*-dimethylacetamide
DMF	*N*,*N*-dimethylformamide
DMM	dimethylmaleoyl
DMSO	dimethylsulfoxide
DTT	dithiothreitol
E1cB	elimination unimolecular conjugate base
[E]	enzyme concentration
E. coli	*Escherischia coli*
EDC	1-ethyl-3-(3-dimethylaminopropyl)carbodiimide
EDTA	ethylenediaminetetraacetate, disodium salt
ESI-MS	electrospray ionization mass spectrometry
Et	ethyl
EtOH	ethanol
Et_2O	diethyl ether
EtOAc	ethyl acetate
FAD	flavin adenine dinucleotide
Glc	glucose
GlcN	glucosamine
GlcNAc	*N*-acetylglucosamine

H. influenzae	*Haemophilus influenzae*
His_6	hexahistidine tag
HMQC	Heteronuclear Multiple Quantum Coherence
HOBt	hydroxybenzotriazole
HRMS	high-resolution mass spectrometry
INT	*para*-iodonitrotetrazolium violet
IPTG	isopropyl 1-thio-β-D-galactopyranoside
J	coupling constant (NMR)
k_{cat}	catalytic rate constant
k_H, k_D	rate of reaction involving protiated and deuterated substrates
kDa	kilodalton
K_M	Michaelis constant
k_{cat}/K_M	specificity constant; second-order rate constant
KIE	kinetic isotope effect
LB	Luria-Bertani medium
LC	liquid chromatography
Lev	levulinate; 4-oxo-pentanoate
LT	lytic transglycosylase
m	*meso*
m/z	mass to charge ratio (mass spectrometry)
Me	methyl
MeOH	methanol
MS	mass spectrometry

MurNAc	*N*-acetylmuramic acid
MW	molecular weight
MWCO	molecular weight cut-off
N. gonorrhoeae	*Neisseria gonorrhoeae*
NAD^+	nicotinamide adenine dinucleotide, oxidized form
NADH	nicotinamide adenine dinucleotide, reduced form
$NADP^+$	nicotinamide adenine dinucleotide phosphate, oxidized form
NADPH	nicotinamide adenine dinucleotide phosphate, reduced form
NEt_3	triethylamine
$Ni^{2+}NTA$	nickel nitrilotriacetic acid
NMR	nuclear magnetic resonance
OD_{600}	optical dispersion at 600 nm
p-NP	*para*-nitrophenol
p-tolSO_2Cl	*para*-toluenesulfonyl chloride
p-tolSO_3H	*para*-toluenesulfonic acid
Pat	peptidoglycan *O*-acetyl transferase
PBPs	penicillin-binding proteins
PDB	protein data bank
PEP	phosphoenolpyruvic acid
PG	peptidoglycan
Ph	phenyl
poa	peptidoglycan *O*-acetylation
ppm	parts per million

PSI	pounds per square inch
pyr	pyridine
R_f	retention factor
rpm	revolutions per minute
rt	room temperature
S. aureus	*Staphylococcus aureus*
sat.	saturated
SDS-PAGE	sodium dodecylsulfate polyacrylamide gel electrophoresis
SIS	sugar phosphate isomerase/sugar phosphate binding
THF	tetrahydrofuran
TfOH	trifluoromethanesulfonic acid
TLC	thin layer chromatography
TMS	trimethylsilyl
Tos	tosyl; *p*-toluenesulfonyl
trien	triethanolamine
UDP	uridine diphosphate
UV-Vis	Ultraviolet-Visible
v_0	initial reaction velocity (rate)
WT	wild type
xs	excess

Common Amino Acid Abbreviations

A	Ala	alanine
C	Cys	cysteine

D	Asp	aspartate
E	Glu	glutamate
F	Phe	phenylalanine
G	Gly	glycine
H	His	histidine
I	Ile	isoleucine
K	Lys	lysine
L	Leu	leucine
M	Met	methionine
N	Asn	asparagine
P	Pro	proline
Q	Gln	glutamine
R	Arg	arginine
S	Ser	serine
T	Thr	threonine
V	Val	valine
W	Trp	tryptophan
Y	Tyr	tyrosine

Nucleotide Base Abbreviations

A	adenine
C	cytosine
G	guanine

T	thymine
U	uracil

Acknowledgements

I would like to thank my supervisor, Professor Martin E. Tanner, for not turning me away from the lab when I showed up for my first day of work covered entirely in blue paint. Without his understanding (and perhaps misguided decision-making), I would have undoubtedly missed out on what has been a truly enjoyable academic experience. I would also like to thank past and present members of the Tanner lab for sharing their experience and expertise, and ensuring that there was never a dull moment in the lab. In particular, I am indebted to Dr. James Morrison for taking the time to ensure that I became a properly trained and fully functional graduate research assistant. I would also like to thank the outstanding support staff of the UBC Chemistry Department for providing an excellent environment to conduct research in. Specifically, I would like to thank Dr. Elena Polishchuk and Jessie Chen in the Biological Services Laboratory, Dr. Yun Ling and David Wong in the Mass Spectrometry facility, and Dr. Maria Ezhova in the NMR facility for their technical help and assistance.

Finally, I would like to thank my friends and family for their encouragement along the way, and for putting up with me for ten years while I sheltered myself from the real world.

Dedicated to

curious scientists examining interesting questions.

Chapter 1: Metabolism and Modification of Peptidoglycan

1.1 Peptidoglycan Structure and Function

The murein sacculus (or peptidoglycan) is an essential component of the cell wall in both Gram-positive and Gram-negative bacteria.[1, 2] It allows bacteria to maintain their shape and is involved in a host of other cellular functions, but peptidoglycan's most important role is to protect the cell from lysis due to high osmotic pressure. The term murein, derived from the Latin word *murus* for "wall," was first used to identify the rigid, polymeric structure surrounding the bacterial cell by Weidel and Pelzer; the term murein sacculus refers to the polymer's existence as a single bag-shaped molecule.[1] Its structure is comprised of alternating *N*-acetylglucosamine (GlcNAc) and *N*-acetylmuramic acid (MurNAc) monosaccharide residues connected to each other via β-(1→4)-glycosidic linkages (Figure 1.1). Each MurNAc residue possesses a D-lactate group at the C-3 position that bears a peptide side chain. The repeating disaccharide unit of murein that consists of one MurNAc and one GlcNAc residue is termed a muropeptide and the polymeric structure as a whole is referred to as a peptidoglycan due to its approximately equal composition of polysaccharides and peptides. Since virtually all members of the class of peptidoglycan polymers are mureins, the two terms have become synonymous and are used interchangeably in the literature.

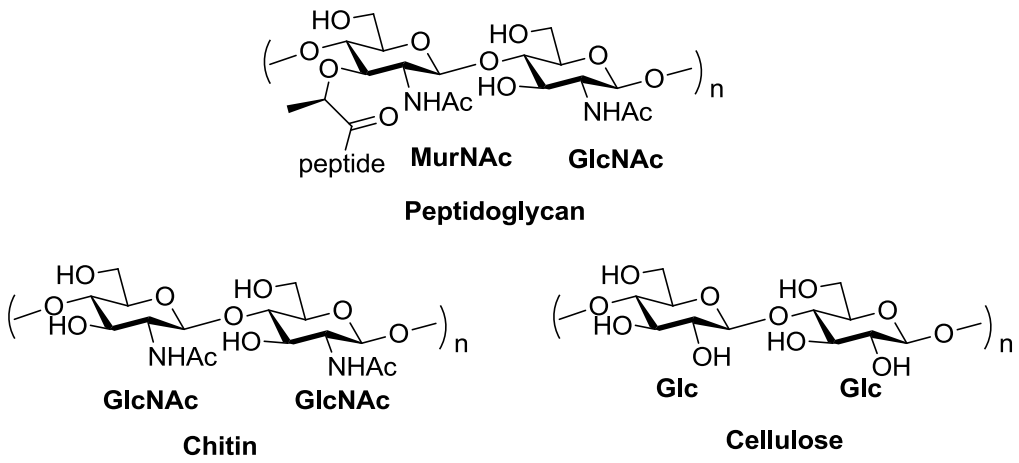

Figure 1.1 Chemical structures of polysaccharide polymers found in nature.

The structures that make up the bacterial cell wall differ in Gram-positive and Gram-negative bacteria (Figure 1.2). In Gram-positive bacteria, the cell wall consists of a cytoplasmic membrane surrounded by a thick layer of peptidoglycan. In Gram-negative bacteria, the cell is surrounded by both an outer membrane and a cytoplasmic membrane and the space between these two structures is termed the periplasm.[1] The murein sacculus is found in the periplasmic space of Gram-negative bacteria, and is relatively thin when compared to the peptidoglycan found in Gram-positive bacteria. Sections 1.2 and 1.3 will focus on the biosynthesis and turnover of peptidoglycan in the Gram-negative bacteria, *Escherichia coli*. Although the metabolism of peptidoglycan differs from species to species, the well-studied processes that occur during the growth of *E. coli* will serve as an excellent model for the understanding of the biosynthetic machinery involved.

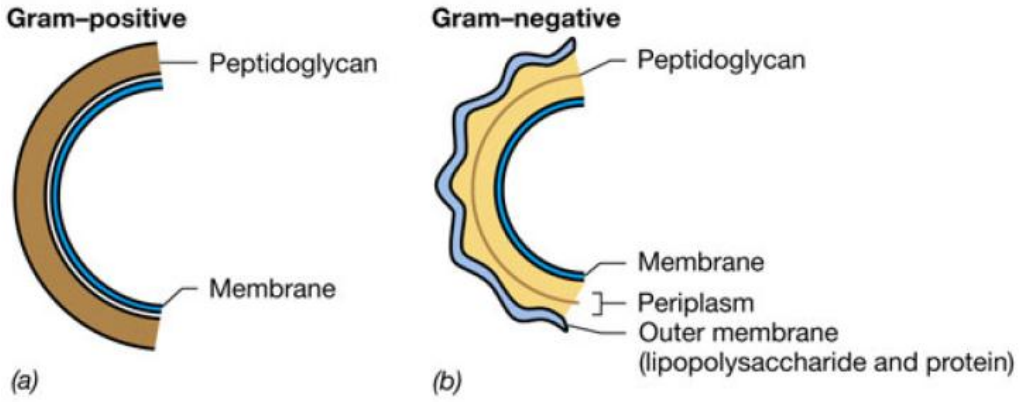

Figure 1.2 Schematic diagram of the (a) Gram-positive and (b) Gram-negative bacterial cell wall.

The polysaccharide backbone of peptidoglycan bears a structural resemblance to both the plant polymer cellulose and the invertebrate polymer chitin. All of these polymers contain polysaccharides linked together in a β-(1→4) fashion (Figure 1.1) but differ in the composition of their respective repeating units (glucose (Glc) in cellulose, GlcNAc in chitin).[1] The increased functional group complexity of peptidoglycan imparted by the C-3 lactate group and amino acid side chain on the MurNAc residues has structural consequences that give the polymer some its unique properties. The peptide side chain on the MurNAc residues of mature peptidoglycan consists of L-alanine, D-glutamic acid, L-*meso*-diaminopimelic acid (*m*-A_2pm or *meso*-DAP) and D-alanine (Figure 1.3). An additional D-alanine is appended to this tetrapeptide in newly-synthesized (or nascent) peptidoglycan, and a peptide bond with a neighbouring strand is found in tri-linked peptidoglycan.[1] There are a small percentage of peptide chains that contain additional or modified amino acids but this four amino acid sequence is by far the most common. Neighbouring strands of peptidoglycan are cross-linked through their stem peptides creating a three-dimensional network that surrounds the entire bacterial cell. Approximately 50% of the peptide side

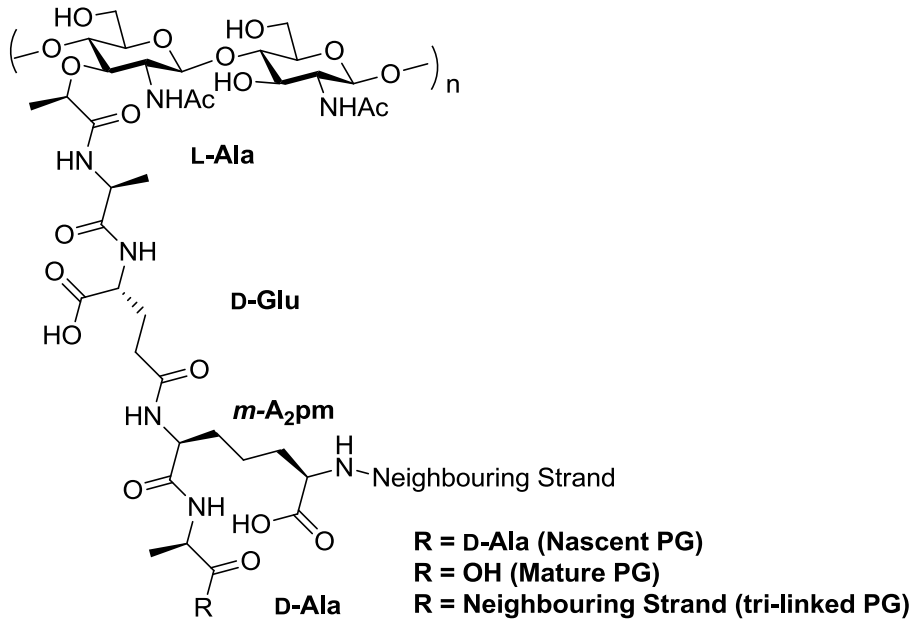

Figure 1.3 Chemical structure of a cross-linked muropeptide subunit in peptidoglycan.

chains are cross-linked to neighbouring strands, and 5% of these are found to be tri-linked.[1] Although its structure was first thought to resemble that of chitin with all the sugar residues residing in a single flat plane, it was later proposed that the sugar backbone of peptidoglycan is slightly tilted. This tilt results in a helical structure with successive peptide side chains extruded at 90 degrees relative to each of its neighbours. One out of every four peptides will be in position to form a cross-link to a parallel strand to its right, while the same ratio will be in position to form a cross-link to a parallel strand on its left (Figure 1.4).[1] This model provides a rationale for the observed percentage of peptide cross-linking in the analysis of peptidoglycan digestion products.

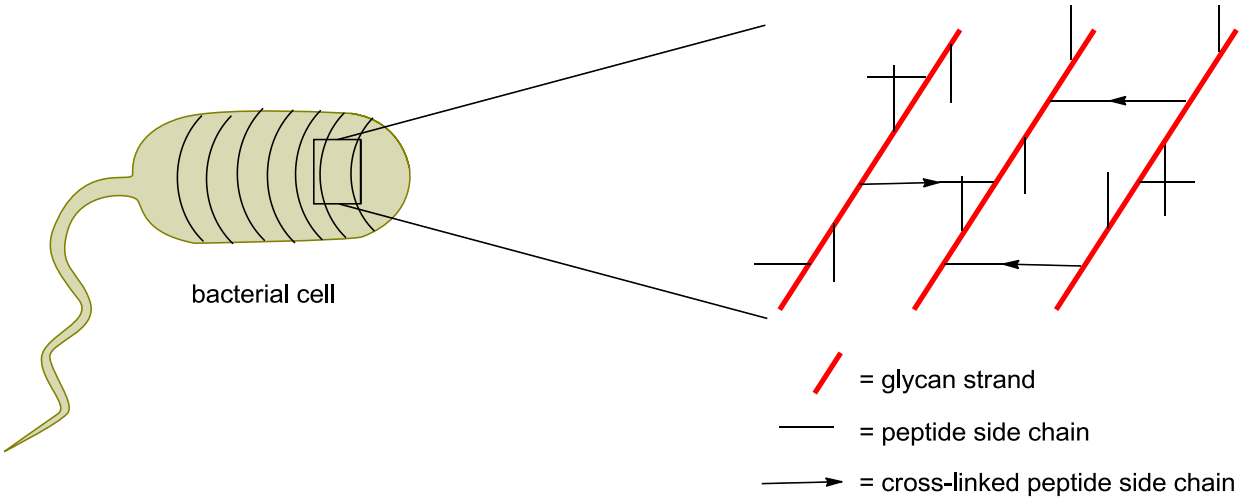

Figure 1.4 The orientation of glycan strands and peptide cross-links in peptidoglycan.

Detailed analyses of the properties of peptidoglycan are complicated by the fact that the polymer takes on the shape of the cell. While the overall shape of peptidoglycan isolated from bacteria is maintained, a number of the native three-dimensional properties of the intact sacculus are absent due to the lack of cellular pressure exerted upon the polymer.[3] It is generally thought that the glycan strands of peptidoglycan run parallel to each other and perpendicular to the long axis of the bacterial cell (Figure 1.4).[1] These strands form a monolayer around the bacterial cell although parts of the peptidoglycan layer have been shown to exist as a triple layer. The average length of these strands is 30 muropeptide units, but over 70% of the strands have lengths of less than 9 units.[1, 3] In order to span the circumference of the cell a large number of parallel strands must be attached together, necessitating the high level of cross-linking found in peptidoglycan.

1.2 Biosynthesis of Peptidoglycan

1.2.1 Synthesis of the Muropeptide Subunit

The biosynthesis of muropeptide subunits and their assimilation into existing peptidoglycan is a relatively well-characterized process. An exhaustive review of this pathway will not be conducted in this dissertation, but a summary of the key steps and enzymes involved will be presented. The pathway begins with the nucleotide sugar uridine diphosphate *N*-acetylglucosamine (UDP-GlcNAc, Figure 1.5), an activated form of GlcNAc used in many different cellular processes. The enzyme MurZ catalyzes the transfer of

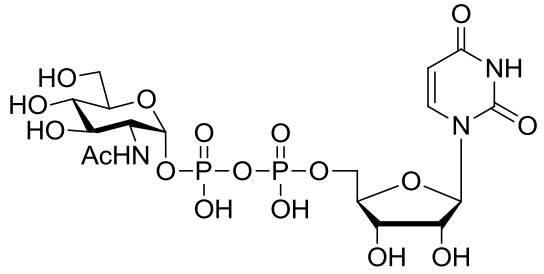

Figure 1.5 Chemical structure of UDP-GlcNAc.

phosphoenol pyruvate (PEP) onto the C-3 hydroxyl group of UDP-GlcNAc to generate UDP-GlcNAc-enolpyruvate (Figure 1.6).[4] The enol-pyruvate moiety on the C-3 position is then reduced by the enzyme MurB to generate UDP-MurNAc with the aid of both a flavin adenine dinucleotide (FAD) and a nicotinamide adenine dinucleotide phosphate (NADP) cofactor (Figure 1.6).[4] This reduction results in the conversion of the enol-pyruvate into the D-lactate group that distinguishes MurNAc from GlcNAc.

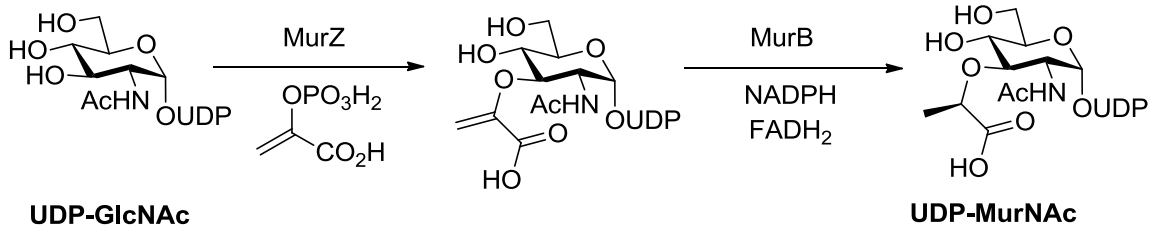

Figure 1.6 Enzymatic conversion of UDP-GlcNAc to UDP-MurNAc by MurZ and MurB.

As discussed previously, the D-lactate group of MurNAc in peptidoglycan is appended with a number of amino acids. The first amino acid attached via an amide bond to D-lactate is the L-stereoisomer of alanine. This isomer is the form that is commonly used in protein synthesis, and as such does not require a specific route for its synthesis and use in peptidoglycan. The D-isomers of glutamate and alanine however, require specific racemases to convert the naturally occurring L-stereoisomer to the D- forms found in peptidoglycan. The dibasic amino acid *meso*-DAP is an intermediate in the biosynthetic pathway for lysine. The enzymes MurC, MurD, and MurE, respectively catalyze the addition of L-Ala, D-Glu, and *meso*-DAP to UDP-MurNAc to generate the corresponding UDP-MurNAc-tripeptide (Figure 1.7).[4] A D-Ala-D-Ala ligase uses ATP to couple two individual D-Ala amino acids

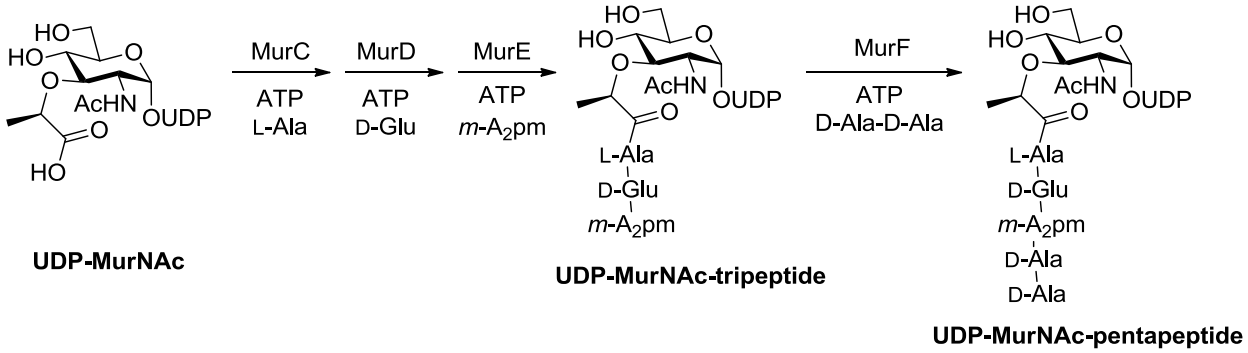

Figure 1.7 Enzymatic addition of the pentapeptide side chain to UDP-MurNAc.

into the corresponding dipeptide, and this dipeptide is transferred onto the UDP-MurNAc-tripeptide donor by the ligase MurF (Figure 1.7).[4] All four of these amino acid-ligating enzymes proceed via essentially the same mechanism. Activation of the terminal carboxyl group of the donor with ATP generates a phosphorylated intermediate with release of ADP. The amino group of the acceptor amino acid or peptide then displaces the phosphate moiety via a tetrahedral anionic intermediate (Figure 1.8).

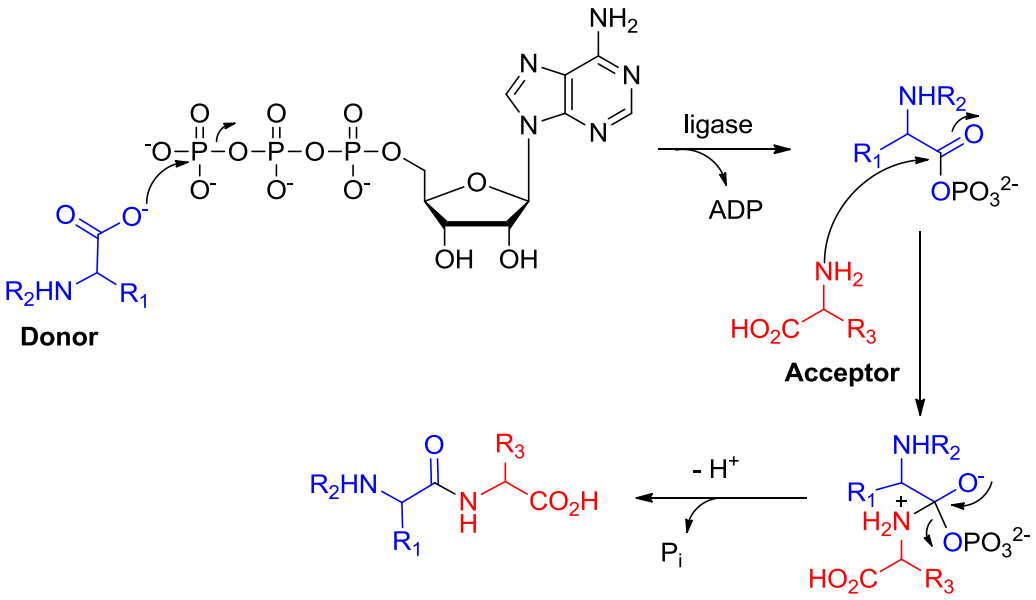

Figure 1.8 General mechanism of ligase-catalyzed peptide bond formation.

The enzymes involved in the formation of UDP-MurNAc-pentapeptide are all localized within the cytoplasm. Eventually however, the muropeptide precursors must be transported through the cytoplasmic membrane and into the periplasmic space where they can be incorporated into the existing peptidoglycan network. In order to accomplish this, bacteria first couple the UDP-MurNAc-pentapeptide precursor to the membrane-associated undecaprenyl phosphate (Figure 1.9).[4] This transfer is catalyzed by the membrane-associated translocase MraY and results in the formation of Lipid I and the release of UMP.[3, 4] This enzymatic reaction is readily reversible and MraY has also been shown to catalyze the

exchange of the nucleotide phosphate groups of UMP and UDP-MurNAc-pentapeptide. The membrane-associated Lipid I is the substrate for the enzyme MurG that transfers GlcNAc onto the C-4 hydroxyl group of the MurNAc moiety of Lipid I using the nucleotide donor UDP-GlcNAc (Figure 1.9). The undecaprenol-linked disaccharide-pentapeptide (Lipid II) is translocated to the periplasmic side of the inner membrane where it is then inserted into the murein sacculus via transglycosylation and transpeptidation reactions.[3, 4] The transglycosylation reaction proceeds with the release of membrane-associated undecaprenyl pyrophosphate; this is subsequently hydrolyzed to undecaprenyl phosphate and is made available to participate in the synthesis of other membrane-bound intermediates.

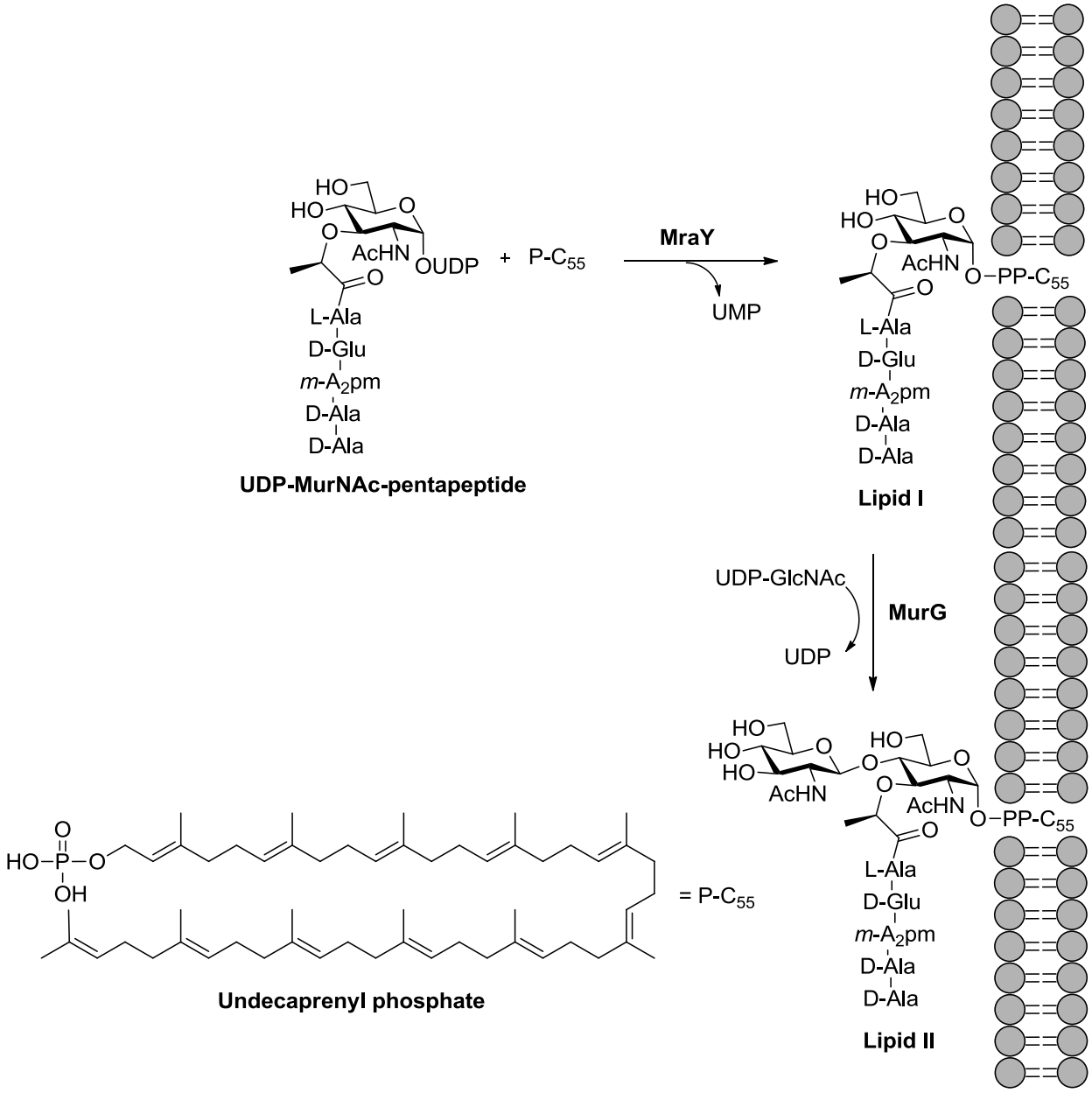

Figure 1.9 Attachment of UDP-MurNAc-pentapeptide to undecaprenyl phosphate and the synthesis of Lipid II.

1.2.2 Insertion of Lipid II into the Murein Sacculus

For the Lipid II precursor to be assimilated into the existing peptidoglycan network it must be transglycosylated onto a growing glycan chain, cleaved from the membrane-associated undecaprenyl phosphate, and in some cases cross-linked to a neighbouring strand

via a peptide linkage. The transglycosylation and transpeptidation reactions are carried out by a class of enzymes called penicillin-binding proteins (PBPs). These enzymes contain both transglycosylation and transpeptidation domains that are located at the *N*-terminal and *C*-terminal ends of the protein, respectively.[4] They are named penicillin-binding proteins because they all contain a conserved serine residue in their transpeptidation domain that will react irreversibly with the β-lactam penicillin. The PBPs are present in many bacterial species, but vary in size, the number present, and their affinity for β-lactam antibiotics.

The prevailing theory regarding the PBP-catalyzed transglycosylation of Lipid II into peptidoglycan strands is that the C-4 hydroxyl group of the GlcNAc moiety of Lipid II acts as an acceptor for the pyrophosphate-linked MurNAc residue of an existing lipid-linked peptidoglycan precursor.[4] Undecaprenyl pyrophosphate is released from the lipid-linked peptidoglycan precursor during this transglycosylation and the resultant molecule is lengthened by two monosaccharide units and can serve as a donor substrate for the transfer of another Lipid II molecule (Figure 1.10). As described earlier, the cleaved undecaprenyl pyrophosphate from the lipid-linked peptidoglycan precursor is hydrolyzed to regenerate the carrier lipid undecaprenyl phosphate and translocated to the cytoplasmic side of the membrane for further use (Figure 1.10). The mechanism that bacteria use to control the length of the newly-formed chains is unclear, but the release of the chain from the membrane-associated lipid carrier occurs with the simultaneous formation of a 1,6-anhydro linkage in the terminal MurNAc residue of the peptidoglycan strand.[4] This 1,6-anhydroMurNAc (anhMurNAc) moiety is consequently found at the end of each linear strand of peptidoglycan and is a valuable marker in determining properties such as the average chain length.

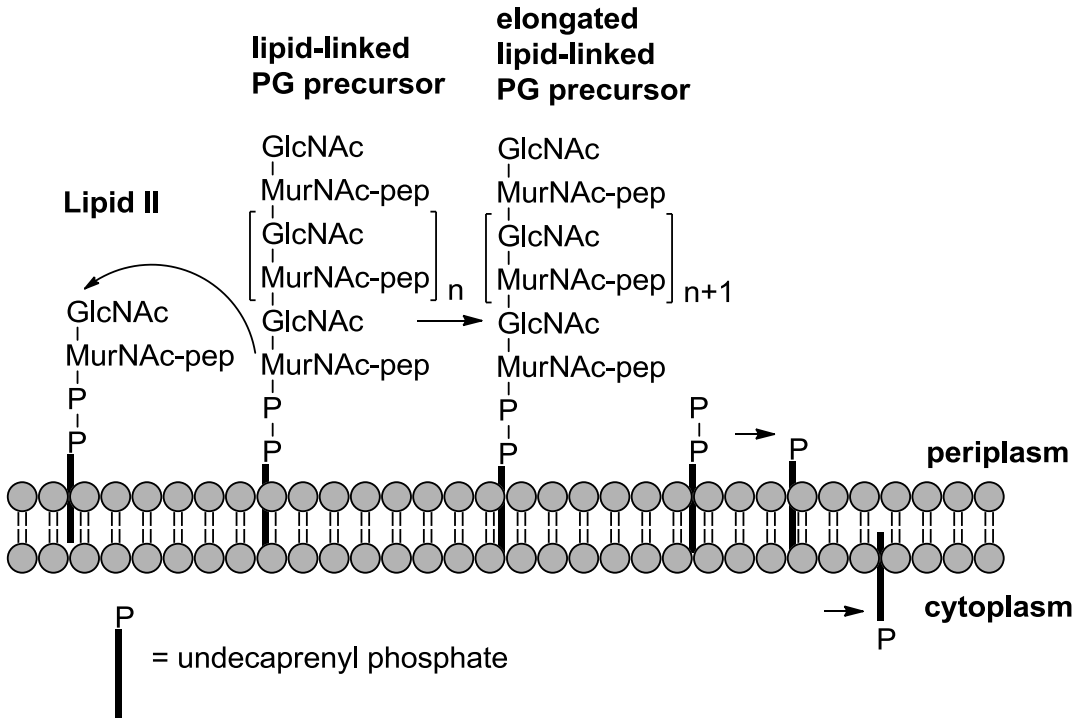

Figure 1.10 Transglycosylation of Lipid II and reuse of undecaprenyl phosphate.

The newly-synthesized chain of peptidoglycan must also be cross-linked to other growing strands in order to be incorporated into the cell-surrounding peptidoglycan network. This linkage occurs via peptide bonds between appropriately positioned amino acid side chains of neighbouring strands. The muropeptide subunits of a growing strand each contain a pentapeptide that terminates with two D-alanine amino acids. This D-Ala-D-Ala linkage is recognized by the transpeptidation domain of the PBPs and the peptide bond between them is cleaved by a catalytic serine nucleophile found in the enzyme active site.[4] This results in the formation of a covalent acyl-enzyme intermediate with the release of D-Ala occurring during the process (Figure 1.11). This covalent enzyme intermediate then serves as a donor for transfer to an amino group of an appropriately positioned acceptor peptide. In most cases the ε-amino group on the *meso*-DAP residue of the acceptor peptide intercepts this enzyme intermediate and forms a peptide bond between the two glycan chains. The cleavage of the

D-Ala-D-Ala bond drives this intermolecular coupling reaction so the pentapeptide substrate is consequently termed the donor peptide. The D,D-linkage between *meso*-DAP and D-Ala is the predominant linkage found in peptidoglycan. However, L,D-linkages between two *meso*-DAP groups have been shown to occur to a minor extent, though the mechanism for their formation as well as the physiological significance of these linkages are both unknown.[4]

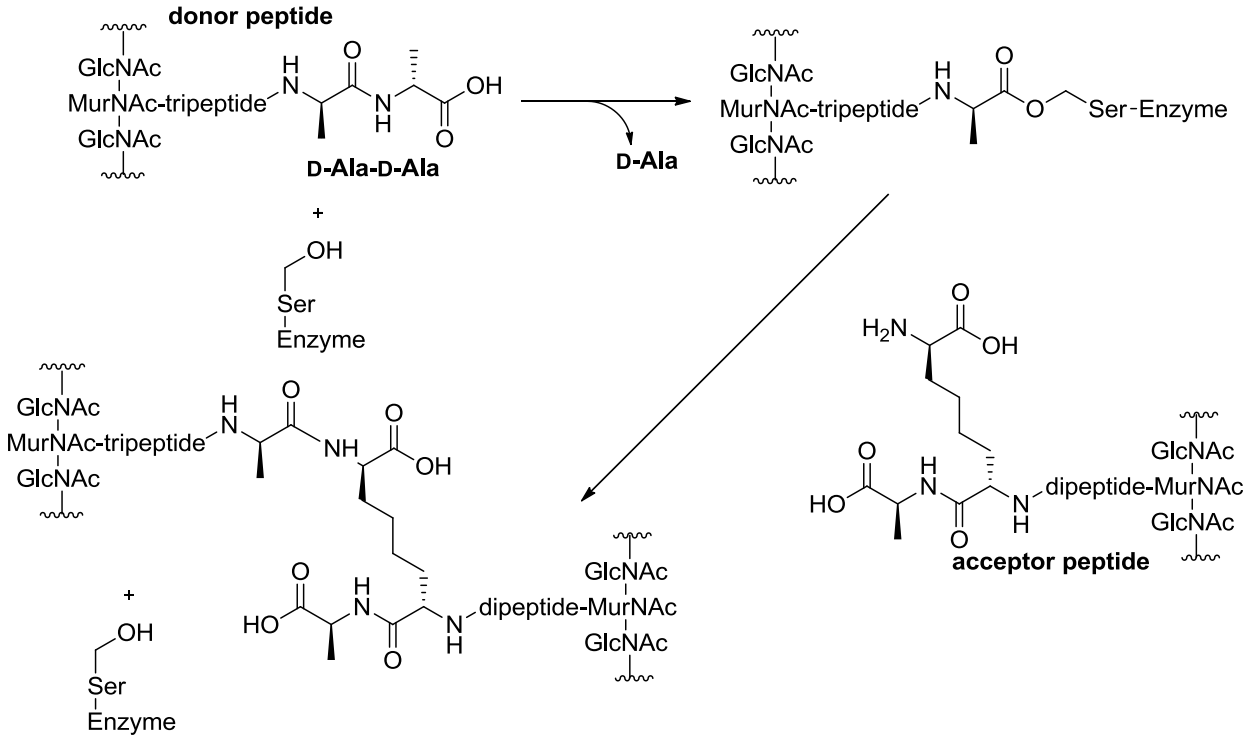

Figure 1.11 Mechanism of PBP-catalyzed transpeptidation of peptidoglycan.

1.2.3 The Penicillin-Binding Proteins – Prominent Antibacterial Targets

Because they catalyze both the transglycosylation and transpeptidation of Lipid II precursors into the existing peptidoglycan network, the penicillin-binding proteins are essential for the maintenance of bacterial viability. An active-site serine nucleophile in the transpeptidation domain of the PBPs is responsible for the interaction of these proteins with the β-lactam class of antibiotics. This broad class of antibiotics contains a β-lactam ring

structure that mimics the D-Ala-D-Ala linkage found in the natural donor peptide substrate, and has carbonyl and carboxylate groups properly positioned to fit in the negative electrostatic wells found in the enzyme active site (Figure 1.12).[5] The β-lactam ring reacts with the active site serine in a similar fashion to the normal transpeptidation reaction to generate a covalent penicilloyl-enzyme intermediate (Figure 1.13). Unlike the normal reaction however, this acyl-enzyme complex is hydrolyzed very slowly and persists within

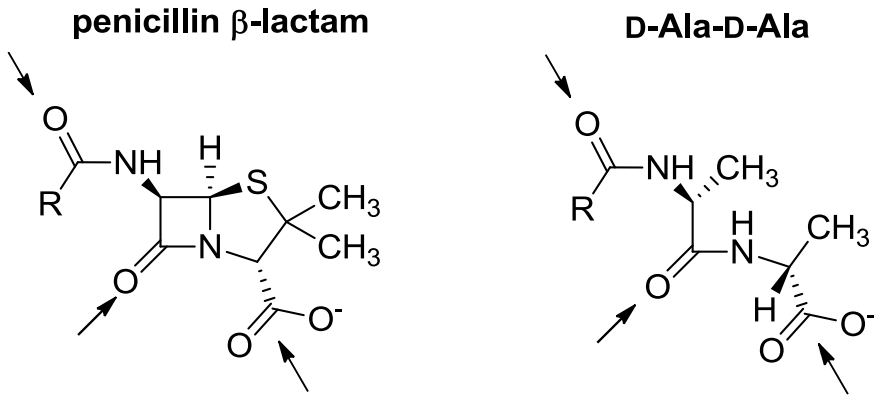

Figure 1.12 Structural similarities between β-lactams and the natural substrate of penicillin D-Ala-D-Ala. Arrows indicate the regions of negative electrostatic potential.

the cell, acting as a suicide inhibitor of the PBP.[5] The inhibition of PBPs results in the cessation of cell growth and can eventually result in cell lysis. This is most likely due to the decreased cell wall integrity caused by an imbalance in peptidoglycan metabolism and lack of cross-linking in newly-synthesized peptidoglycan strands.

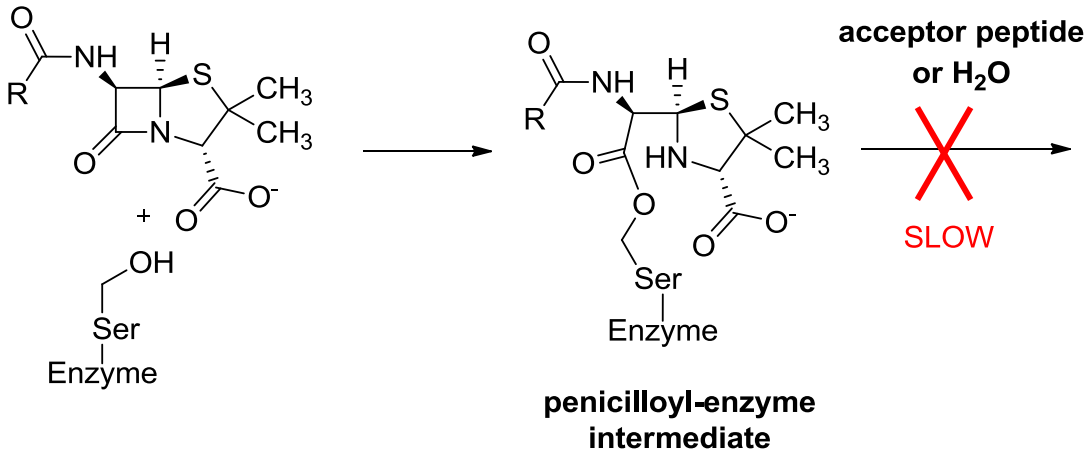

Figure 1.13 Mechanism of PBP-inactivation by β-lactam antibiotics.

Shortly after the introduction of penicillin antibiotics, strains that displayed resistance to their effects began to appear. A number of different resistance mechanisms have been found to occur in various bacterial species. These include decreasing the permeability of the outer membrane, the degradation of penicillin through the expression of β-lactamases, and the production of PBPs with low affinities for β-lactams.[5] Some Gram-negative bacteria have also evolved methods for antibiotic exportation. The many avenues that bacteria possess to combat penicillin antibiotics that target the PBPs have made the discovery and introduction of new drugs very troublesome.[5] Their ability to produce modified PBPs that have lowered affinities towards β-lactam antibiotics has also put into question whether the PBPs are sustainable antibiotic targets.

1.3 Peptidoglycan Turnover and Recycling

The controlled synthesis and breakdown of peptidoglycan is absolutely essential for bacterial cell growth. As the bacterial cell elongates and eventually separates into two daughter cells, it must carefully break and replace its peptidoglycan in order to maintain

cellular integrity while still allowing for cell division to occur.[4, 6] The biosynthesis of muropeptide fragments and their insertion into existing layers of peptidoglycan are only part of the complex cycle that comprises peptidoglycan metabolism. This critical process employs numerous intermediates and enzymes beyond the biosynthetic machinery discussed in Section 1.2. Although an exhaustive review of peptidoglycan metabolism and its involvement in physiological processes would be prohibitive in length, a summary of some of the enzymes involved in key steps in this dynamic process will be presented.

It is well-known that both Gram-positive and Gram-negative bacteria breakdown their peptidoglycan into varying forms of their chemical constituents during cell growth and division. In *E. coli* for example, between 40-50% of the peptidoglycan layer is turned over per generation.[7] The term peptidoglycan (or murein) hydrolases has been used to describe the wide array of enzymes that catalyze the breakdown of peptidoglycan in its various forms (Figure 1.14). The catalytic activities and substrate specificities of each enzyme are used to group common classes together. Amidases, carboxypeptidases, and endopeptidases belong to the general class of peptidoglycan hydrolases responsible for the cleavage of peptide-like bonds during turnover.[7] *N*-Acetylglucosaminidases and *N*-acetyl-β-D-muramidases belong to the general class of peptidoglycan hydrolases responsible for the cleavage of glycosidic bonds during turnover.

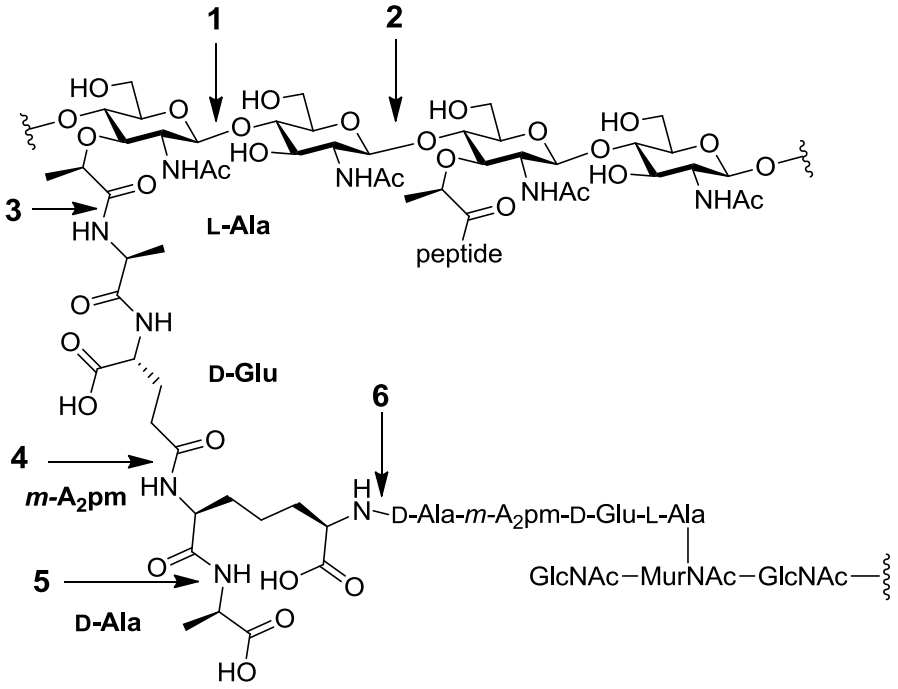

Figure 1.14 Sites of action of peptidoglycan hydrolases: *N*-acetyl-β-D-muramidases (1), *N*-acetylglucosaminidases (2), L-Ala-amidases (3), D,L-endopeptidases (4), L,D-carboxypeptidases (5), D,D-endopeptidases (6).

1.3.1 Peptidoglycan Amidases and Peptidases

Three main types of linkages are found within the stem peptides found in the MurNAc residues of peptidoglycan; amide bonds between the carboxylic acid of D-lactate and the α-amino group of L-Ala, amide bonds between two D-amino acids (D,D-peptide bonds), and amide bonds between an L- and D-amino acid (L,D-peptide bonds). *N*-Acetylmuramyl-L-alanine-amidases cleave the stem peptide from the glycan chain by hydrolyzing the bond between D-lactate and L-Ala, allowing the byproducts to be further processed by other enzymes or reused as intermediates in the synthesis of new muropeptide subunits.[6, 7] Carboxypeptidases cleave amino acids at the C-terminus while endopeptidases hydrolyze bonds within a peptide chain. The carboxypeptidases and endopeptidases that are responsible for breaking down the stem peptide of peptidoglycan degradation products are

identified by both the type of linkage (D,D- or L,D-) and the amino acids that form the peptide bond that they hydrolyze.[6] Carboxypeptidases and endopeptidases cleave peptide bonds that by definition must occur between a α-carboxy and α-amino group of two adjacent amino acids. However, many amide bonds found in the stem peptides of peptidoglycan polymers would not be considered peptide bonds if this definition was applied rigorously.[6] To be consistent with the previous literature, carboxypeptidases and endopeptidases will be used to refer to enzymes catalyzing the hydrolysis of an amide bond between two amino acids, regardless of position, in peptidoglycan throughout this dissertation. There are a number of different L-Ala-amidases present in bacteria that cleave the bond between the D-lactate group on MurNAc and L-Ala. Each amidase possesses a range of substrate specificities that is greatly influenced by their cell-wall binding domain. These domains enhance the activity of enzymes by placing their catalytic machinery in close proximity with the type of substrate they are specific for. Thus, some amidases will act on intact peptidoglycan strands, while others will act on various fragmented forms of peptidoglycan. Depending on their substrate specificity, amidases can be localized to the periplasm via a signal peptide sequence, or can remain in the cytoplasm.[6, 7]

The number of different carboxypeptidases and endopeptidases involved in the hydrolysis of the stem peptides in peptidoglycan is much greater than the number of amidases due to the wider variety of possible substrates. Similar to the L-Ala-amidases, certain carboxy- and endopeptidases hydrolyze linkages in high molecular weight peptidoglycan substrates while others hydrolyze linkages found in low molecular weight muropeptide fragments.[6] As mentioned previously, these peptidases can be specific for D,L-, L,D-, or D,D-linkages and can cleave peptides at a number of different positions in

peptidoglycan polymers. The D,D-endopeptidases function to specifically hydrolyze the cross-links between different glycan strands found in peptidoglycan.[6] This hydrolysis is the reverse reaction of the transpeptidation catalyzed by the high molecular weight PBPs during peptidoglycan synthesis. Perhaps as a result of this similarity, many D,D-endopeptidases are members of the low MW PBPs and are inhibited by β-lactams in the same manner as other PBPs.[6]

1.3.2 Muramidases and Glucosaminidases

Two main classes of enzymes are responsible for the cleavage of glycosidic bonds in both high and low molecular weight peptidoglycan, *N*-acetyl-β-D-muramidases (or muramidases) and *N*-acetylglucosaminidases.[6] Muramidases cleave β-(1→4)-glycosidic linkages between MurNAc and GlcNAc in peptidoglycan and its muropeptide subunits. The major type of muramidase responsible for peptidoglycan metabolism in bacteria is the lytic transglycosylase (LT). These enzymes cleave the β-(1→4)-glycosidic linkages between MurNAc and GlcNAc non-hydrolytically to generate a 1,6-anhydro-linkage at the terminal MurNAc residue (Figure 1.15).[6] A single catalytic glutamate residue is proposed to first protonate the glycosidic oxygen, promoting cleavage of the anomeric bond and formation of an oxocarbenium intermediate (Figure 1.15).[6] This oxocarbenium intermediate is stabilized by the formation of an intramolecular oxazolinium ion with the *N*-acetyl group at the C-2 position (Figure 1.16). The inhibition of a number of lytic transglycosylases by the compound *N*-acetylglucosamine thiazoline provides strong evidence for the existence of this oxazolinium-stabilized intermediate (Figure 1.16).[6] Upon formation of the oxocarbenium intermediate, the catalytic glutamate acts as a base to deprotonate the C-6 hydroxyl group of the MurNAc residue for intramolecular attack at the anomeric center. Lytic

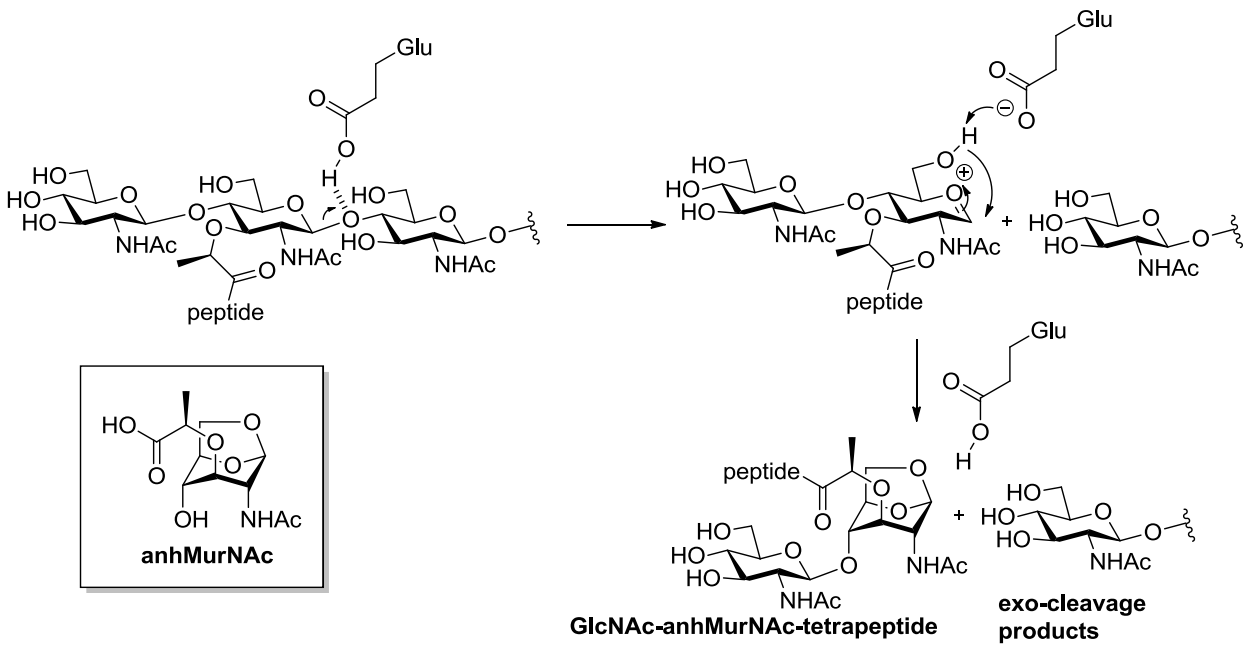

Figure 1.15 Mechanism of lytic transglycosylase-catalyzed cleavage of peptidoglycan. transglycosylases are generally exo-selective, cleaving glycosidic linkages at the terminal ends of glycan strands to produce GlcNAc-1,6-anhMurNAc disaccharides with attached peptides.[6]

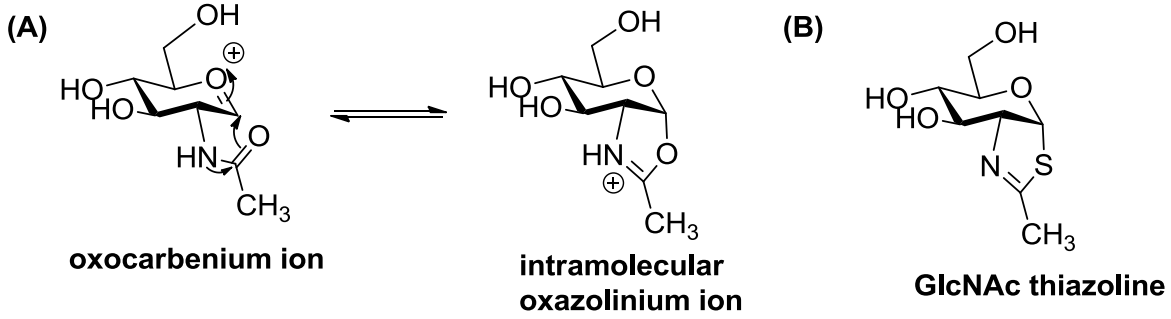

Figure 1.16 (A) Stabilization of the oxocarbenium ion through formation of an intramolecular oxazolinium ion. (B) Structure of the lytic transglycosylase inhibitor GlcNAc thiazoline.

N-Acetylglucosaminidases are enzymes that hydrolyze glycosidic bonds between GlcNAc and other monosaccharides in a number of different biological substrates. In

peptidoglycan, the glucosaminidases possess a cell wall-binding domain and cleave the β-(1→4)-linkage between GlcNAc and MurNAc, generating a product containing a GlcNAc reducing sugar at one end. This cleavage product is distinct from those produced by the lytic transglycosylases and gives bacteria an alternative way of breaking down their murein sacculus (Figure 1.17).[6] Furthermore, many of the *N*-acetylglucosaminidases found in bacteria have an endo-specificity and cleave glycosidic linkages at non-terminal positions in high molecular weight peptidoglycan substrates. This is in contrast with the exo-selectivity that is observed in most members of the other major type of glycan-cleaving enzymes, the lytic transglycosylases.[6]

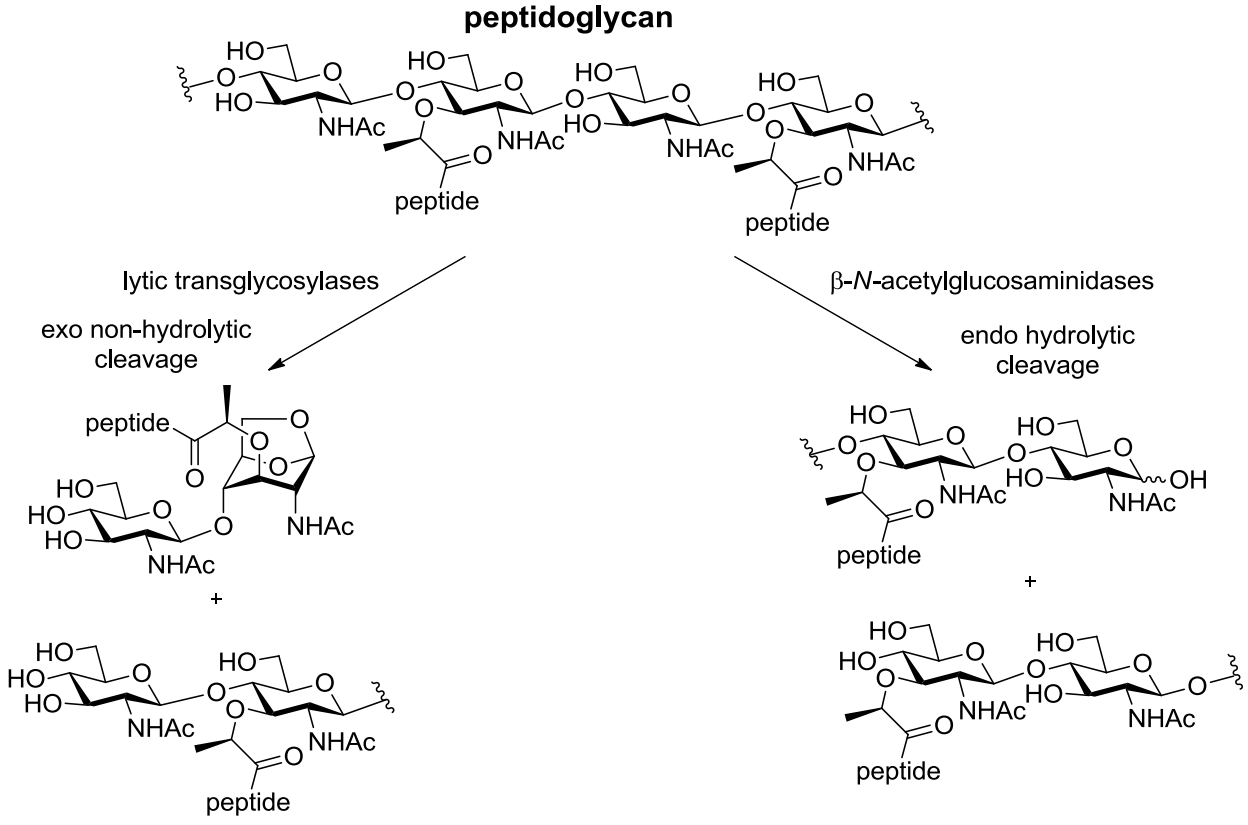

Figure 1.17 Peptidoglycan degradation products of lytic transglycosylases (left) and β-*N*-acetylglucosaminidases (right).

1.3.3 Peptidoglycan Recycling

Our present understanding of how certain Gram-negative bacteria such as *E. coli* recycle their peptidoglycan pales in comparison to the well-characterized process of peptidoglycan biosynthesis. Since peptidoglycan makes up only 2% of the total weight of a bacterial cell, it is not presumed to be a large nutrient source for bacteria.[7] However, when placed under stress, the peptidoglycan recycling pathway may play more of an important role in ensuring that there are enough nutrients available for survival. In *E. coli* there are over 10 enzymes and proteins that are produced solely for the recycling of peptidoglycan.[7] Characterization of these recycling pathway components reveals that they are not essential for viability, normal growth rate, proper cell morphology, and normal peptidoglycan structure. Nevertheless, it has been postulated that this recycling pathway may play a more crucial role in bacteria that colonize areas where the competition for nutrients is intense. For instance, Gram-negative bacteria that live in the colon all possess a full complement of peptidoglycan recycling enzymes while others often lack a complete set.[7] In this thesis, discussion of the peptidoglycan recycling pathway will focus on the enzymes and proteins found in *E. coli*.

As discussed in Section 1.3, *E. coli* hydrolyzes between 40-50% of their peptidoglycan per generation. Up to 90% of these turnover products however, are shuttled into the peptidoglycan recycling pathway where they are used to synthesize muropeptide precursors for incorporation into new strands of peptidoglycan.[7] A detailed analysis of the characteristics of each of the enzymes and proteins involved in the recycling process will not be presented here, but instead, this section will give an overview of the key recycling enzymes and the roles that they play.

The main turnover product that is released by the peptidoglycan hydrolases is GlcNAc-anhMurNAc-tetrapeptide (Figure 1.18). In bacteria that lack the enzymes responsible for peptidoglycan recycling this turnover product is simply released into the environment, but in *E. coli* this disaccharide product is imported into the cytoplasm.[7] The transport of peptidoglycan degradation products across the cytoplasmic membrane is facilitated by AmpG, a protein that is essential for peptidoglycan recycling (Figure 1.18). This protein possesses several membrane-spanning regions and transports GlcNAc-anhMurNAc peptides but not monosaccharide anhMurNAc peptides across the cytoplasmic membrane.[7] Once inside the cell, the product is degraded by a number of cytoplasmic peptidoglycan-recycling enzymes. These enzymes can be grouped into two major categories, those involved in the recycling of peptidoglycan amino acids and those involved in the recycling of peptidoglycan amino sugars.

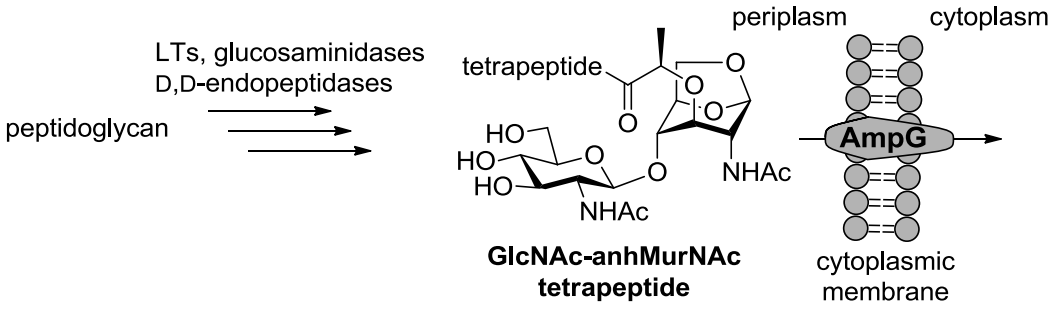

Figure 1.18 The major degradation product GlcNAc-anhMurNAc-tetrapeptide is imported into the cytoplasm by the membrane transporter AmpG.

1.3.3.1 Peptidoglycan Amino Acid-Recycling Enzymes

In *E. coli* a number of enzymes have been identified that participate in the recycling of the tetrapeptide side chain of MurNAc degradation products (Figure 1.19). As stated previously, the GlcNAc-anhMurNAc tetrapeptide is imported into the cytoplasm by the membrane transporter AmpG. Once inside the cytoplasm, the tetrapeptide side chain is first

separated from the anhMurNAc residue of the disaccharide degradation product by the anhydro-*N*-acetylmuramyl-L-alanine amidase, AmpD. This metalloenzyme contains a zinc ion that is essential for its catalytic activity. AmpD is specific for peptides attached to anhydro-MurNAc residues and is considerably less active on both MurNAc and UDP-MurNAc-linked peptide substrates.[7] This substrate specificity is extremely important, as the UDP-MurNAc precursors used in the biosynthesis of peptidoglycan are also found in the cytoplasm, and hydrolysis of their peptide side chains by recycling enzymes would be non-productive.

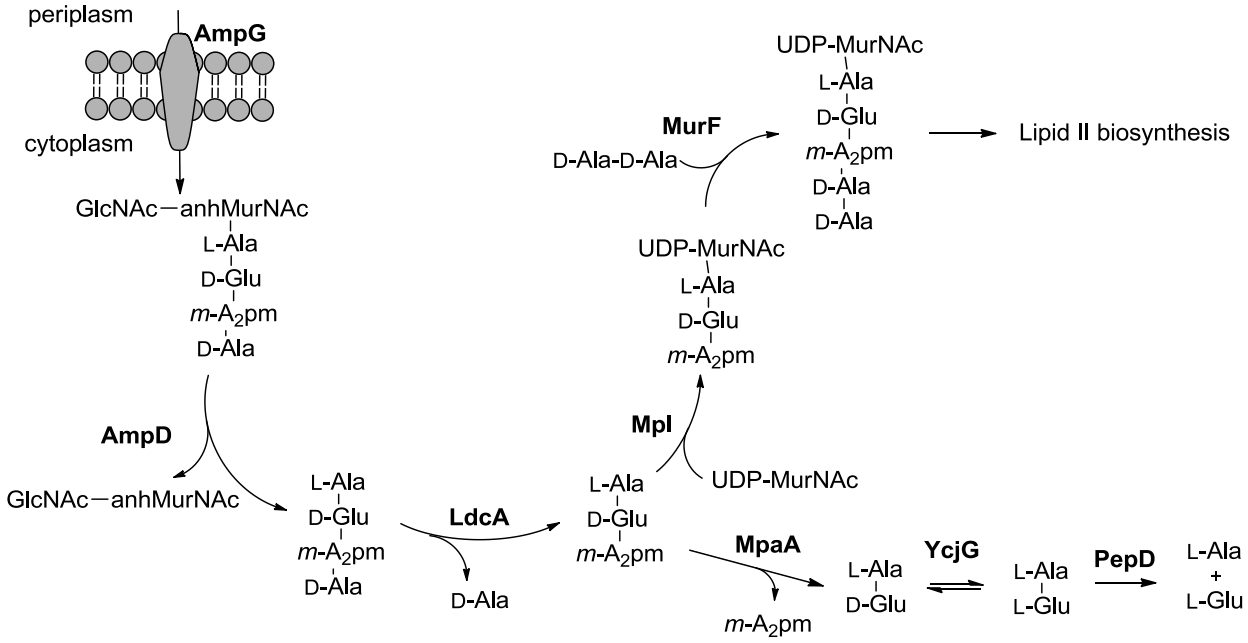

Figure 1.19 The peptidoglycan amino acid-recycling pathway.

The tetrapeptide side chain is a substrate for the L,D-carboxypeptidase LdcA. This enzyme removes the D-Ala residue from a variety of degradation products with attached tetrapeptides, generating the tripeptide L-Ala-γ-D-Glu-*m*-A_2pm (Figure 1.19).[7] These include the free tetrapeptide as well as those attached to anhMurNAc, GlcNAc-anhMurNAc

disaccharide, MurNAc, and UDP-MurNAc. Not surprisingly, LdcA is unable to cleave the terminal D,D-linkage on UDP-MurNAc-pentapeptide, preventing it from interfering in the synthetic pathway of muropeptide precursors.[7]

The major pathway for the reincorporation of amino acids from peptidoglycan degradation products is through the ligation of the tripeptide L-Ala-γ-D-Glu-*m*-A_2pm directly to UDP-MurNAc (Figure 1.19). This ligation is catalyzed by the enzyme murein peptide ligase (Mpl) that has 25.8% amino acid sequence identity to the MurC ligase responsible for the attachment of L-Ala to UDP-MurNAc. Mpl possesses flexible peptide substrate specificity and can ligate tri-, tetra-, and pentapeptides to UDP-MurNAc; it also tolerates the substitution of lysine for *meso*-DAP when catalyzing the ligation reaction.[7] The UDP-MurNAc-tripeptide product of this reaction can be subsequently used as a substrate for the MurF-catalyzed addition of D-Ala-D-Ala dipeptide to generate UDP-MurNAc-pentapeptide.[7]

The enzyme LdcA is unique in that it is the only member of the amino acid-recycling pathway whose deletion causes a phenotypic change in the bacterial cell. Deletion or inhibition of LdcA results in bacteria that grow as thick, oval cells and eventually results in cell lysis. Interestingly, the effects of deletion or inhibition are most pronounced when the bacteria is in the stationary phase of growth, providing support for the notion that peptidoglycan recycling plays an important role during this stage.[7] Since the Mpl ligase can attach a number of different peptide substrates to UDP-MurNAc, it is likely that the absence of LdcA results in the production of UDP-MurNAc-tetrapeptide (Figure 1.20). There is no enzyme available to ligate an additional D-Ala and to produce the desired UDP-MurNAc-pentapeptide, so the UDP-MurNAc-tetrapeptide accumulates. It is postulated that during periods of cellular growth where the recycling process plays a more crucial role these

tetrapeptide substrates are incorporated into new peptidoglycan strands. This will produce glycan strands that cannot act as peptide donors in the critical PBP-catalyzed transpeptidation reaction, resulting in a peptidoglycan sacculus with a lower degree of cross-linking.[7]

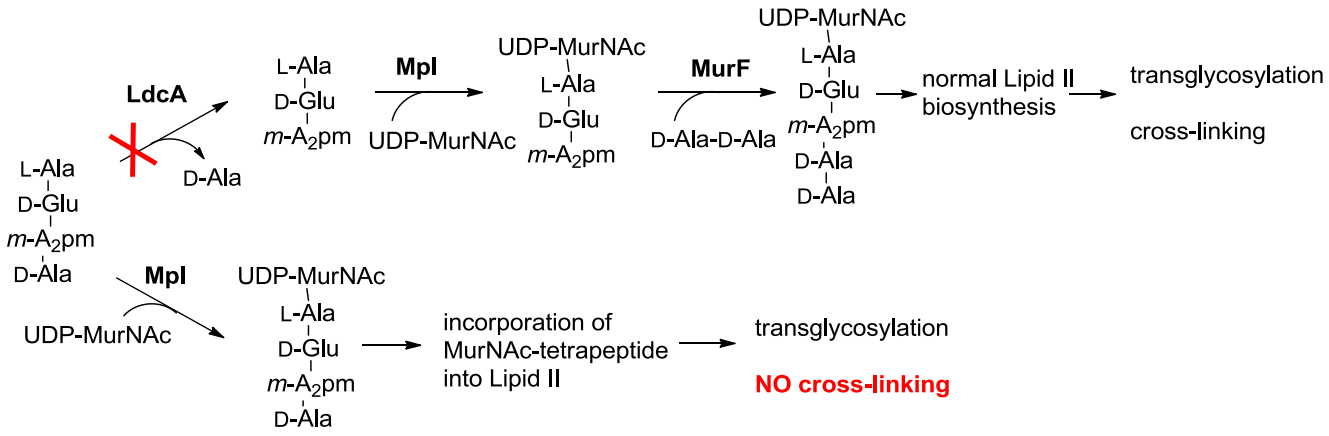

Figure 1.20 Deletion of LdcA causes alternative Lipid II production and impaired cross-linking of new peptidoglycan strands

The ligation of the tripeptide L-Ala-γ-D-Glu-*m*-A_2pm to UDP-MurNAc is the main pathway for peptidoglycan amino acid recycling in *E. coli*. However, there are a number of other enzymes that serve to cleave and recover the individual amino acids via an alternate pathway (Figure 1.19). The *meso*-DAP residue on the tripeptide can be cleaved by the enzyme MpaA, releasing *meso*-DAP and the dipeptide L-Ala-D-Glu.[7] This dipeptide is the substrate for the enzyme YcjG, an L-alanyl-D/L-glutamate epimerase that converts the L,D-dipeptide into the L,L-dipeptide.[7] The L,L-stereoisomer is the substrate for PepD, a dipeptidase with very broad substrate specificity that hydrolyzes the peptide bond and releases the individual amino acids. The significance of this alternative pathway for amino acid reutilization is not known, and it is generally thought that this pathway plays a very minor role in the recycling pathway.[7]

1.3.3.2 Peptidoglycan Amino Sugar-Recycling Enzymes

After the tetrapeptide side chain is cleaved from the imported GlcNAc-anhMurNAc degradation product by AmpD, the disaccharide is processed by a series of peptidoglycan amino sugar-recycling enzymes. These enzymes are ultimately responsible for the conversion of the disaccharide into UDP-GlcNAc, the basic building block of peptidoglycan synthesis (Figure 1.21). At the outset of the studies detailed in this dissertation, the pathway for reutilization of the GlcNAc component of the disaccharide degradation product was well characterized.[7] The pathway for the reutilization of anhMurNAc however, had not been fully

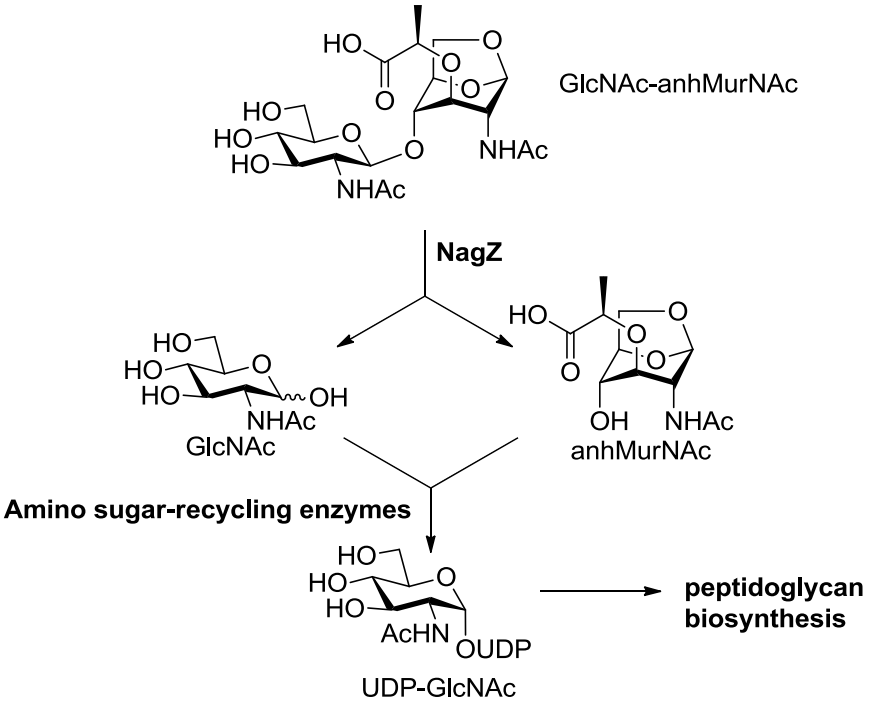

Figure 1.21 The degradation product GlcNAc-anhMurNAc is converted into UDP-GlcNAc for use in peptidoglycan biosynthesis.

characterized and the biochemical details of the mechanism through which it was converted to UDP-GlcNAc were still unknown. This section will summarize the roles of the enzymes

involved in the conversion of GlcNAc into UDP-GlcNAc as well as the point of entry of anhMurNAc into this metabolic pathway.

The first step in the recycling pathway of peptidoglycan amino sugars is the separation of the disaccharide into its constituents. This is accomplished by the enzyme NagZ, a β-*N*-acetylglucosaminidase that cleaves the glycosidic bond between the imported disaccharide peptidoglycan degradation products (Figure 1.22).[7] This cytoplasmic enzyme releases GlcNAc and anhMurNAc and is also active on substrates containing attached peptides as well as those containing MurNAc instead of anhMurNAc. The GlcNAc monosaccharide is subsequently regioselectively phosphorylated by the ATP-dependent kinase NagK, generating GlcNAc 6-phosphate.[7] This sugar phosphate is the substrate for the de-*N*-acetylase NagA, an enzyme that is essential for the recycling of peptidoglycan amino sugars. This enzyme removes the *N*-acetyl group from GlcNAc 6-phosphate to generate glucosamine (GlcN) 6-phosphate.[7] At this point the GlcN 6-phosphate intermediate can either be shuttled into the glycolysis pathway via conversion to fructose 6-phosphate by the enzyme NagB, or be isomerized to GlcN 1-phosphate by the enzyme GlmM.[7] GlcN 1-phosphate is acetylated to generate GlcNAc 1-phosphate by the bifunctional enzyme GlmU.[7] This enzyme also catalyzes the final conversion of GlcNAc 1-phosphate into the sugar nucleotide UDP-GlcNAc.[7]

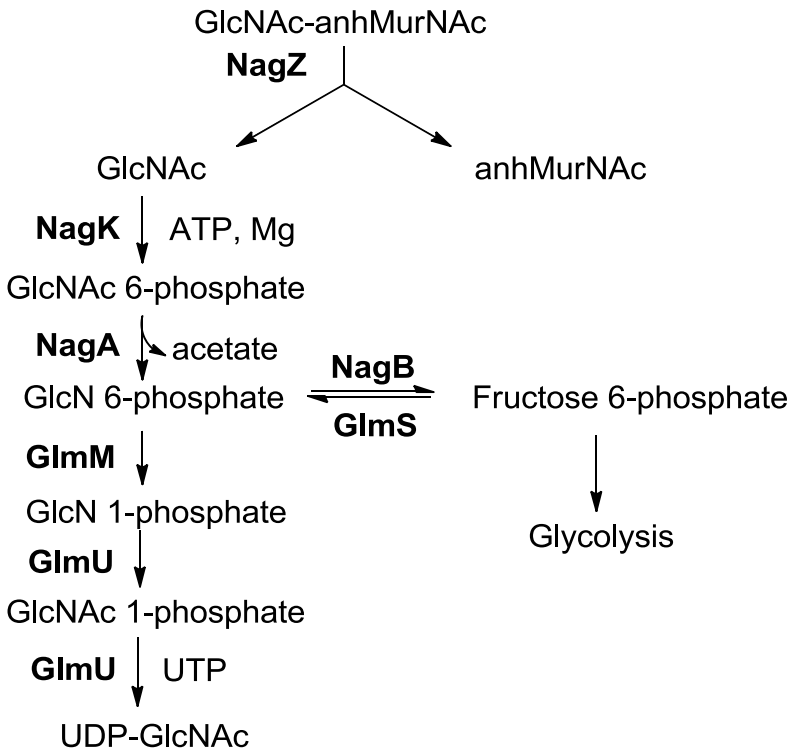

Figure 1.22 Conversion of GlcNAc to UDP-GlcNAc via the peptidoglycan recycling pathway.

Although the pathway for the reutilization of anhMurNAc was not fully characterized until recently, evidence for its conversion into an intermediate of the GlcNAc recycling pathway has existed for some time. The finding that *E. coli* cells could grow on MurNAc as the sole source of carbon, nitrogen and energy was first reported in 1983 by Parquet et al.[8] More recently, Dahl et al. reported findings indicating that the compound GlcNAc 6-phosphate was a critical intermediate in the pathway for MurNAc reutilization.[9] These results suggested that there should be a pathway for the conversion of anhMurNAc into GlcNAc 6-phosphate. The first step in this pathway is catalyzed by the enzyme anhydro-*N*-acetylmuramic acid kinase, AnmK (Figure 1.23).[10] This enzyme catalyzes the hydrolysis of the 1,6-anhydro linkage in anhMurNAc and the subsequent phosphorylation of the newly formed C-6 hydroxyl group to generate the compound MurNAc 6-phosphate. The

conversion of MurNAc 6-phosphate to the recycling intermediate GlcNAc 6-phosphate was proposed to be catalyzed by a hypothetical "etherase" that cleaves the C-3 lactyl ether on MurNAc 6-phosphate.[10] This etherase, MurQ, was identified in 2005 by Jaeger et al. and was shown to be essential for growth of *E. coli* on MurNAc as the sole source of carbon.[11] At the time, the mechanistic details of this reaction were still unknown and uncovering them became one of the goals of this thesis. Thus, two enzymes, AnmK and MurQ, are required for the recycling of the MurNAc residues in peptidoglycan through the conversion of anhMurNAc into GlcNAc 6-phosphate (Figure 1.23).

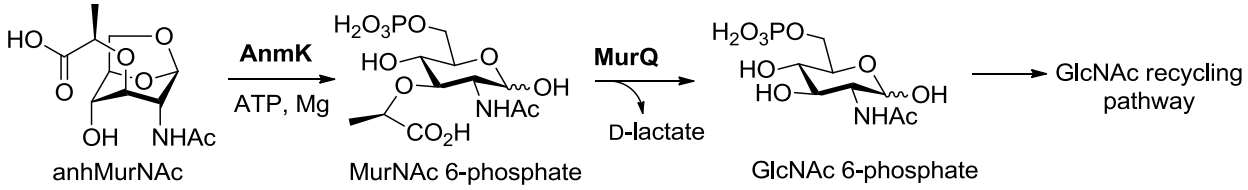

Figure 1.23 Conversion of anhMurNAc into GlcNAc 6-phosphate by AnmK and MurQ.

1.4 Lysozymes: Host Muramidases

Lysozymes are another type of enzyme that hydrolyzes the glycosidic linkages in peptidoglycan. These enzymes act exclusively on β-(1→4)-glycosidic linkages in nature, and are classified as muramidases when acting upon peptidoglycan because they cleave the linkages at the anomeric center of MurNAc residues.[6] Unlike the lytic transglycosylases however, they cleave these linkages hydrolytically, generating a MurNAc reducing sugar at one end of the cleavage product. Lysozymes are produced by a wide range of organisms including phages, fungi, vertebrates, and invertebrates.[6] Although some examples of bacterial lysozymes have been reported, the majority of identified lysozymes are thought to function as an initial host defensive response to bacterial infection. Through the release of

lysozymes, hosts disrupt the covalent linkages of the bacterial peptidoglycan that are important for cell integrity and eventually cause the bacterial cells to lyse.[6]

The mechanistic details of lysozyme-catalyzed reactions have been very well studied and characterized. A catalytic aspartate residue acts as a nucleophile, directly displacing the GlcNAc group at the anomeric position of MurNAc with inversion of configuration and subsequent formation of a covalent glycosyl-enzyme intermediate (Figure 1.24).[12] In a similar fashion to the lytic transglycosylases, a glutamate residue acts as an acid to protonate the oxygen at the C-4 position of the GlcNAc leaving group. The catalytic glutamate residue then acts as a base to activate a water molecule for nucleophilic attack on this glycosyl-enzyme intermediate. This results in another stereochemical inversion and an overall net retention of configuration for the entire enzyme-catalyzed reaction.[12] Lysozymes are endo-selective in general and possess a substrate binding pocket that is large enough to accommodate the multiple sugar residues present in the polymeric substrates that they act upon.[6]

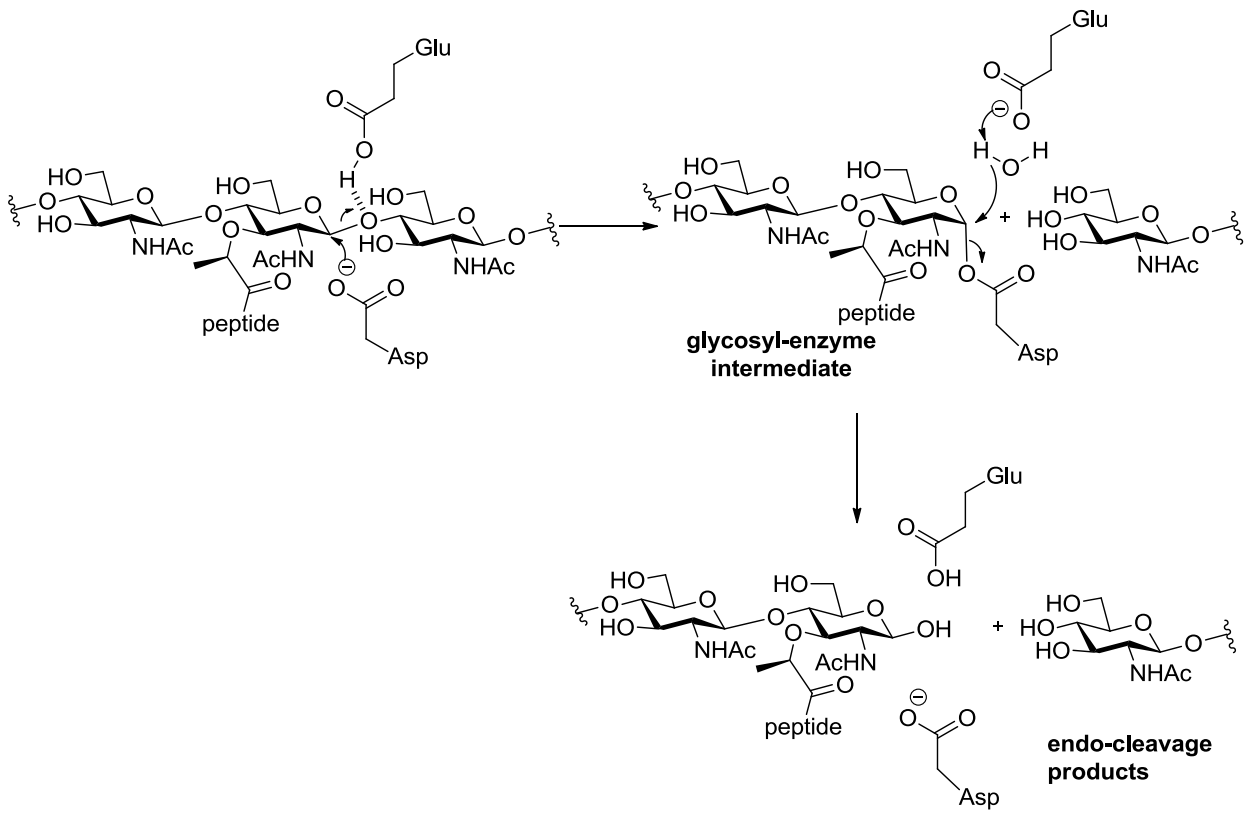

Figure 1.24 Mechanism of lysozyme-catalyzed hydrolysis of peptidoglycan.

Lysozymes are an important part of the immune response to bacterial infection in many types of host organisms. They not only target the cell wall of living bacteria but also play a key role in the removal of high molecular weight peptidoglycan fragments that remain after cell lysis. These fragments can often cause physiological problems in the host if they are allowed to persist within the cell, even after the majority of the viable bacteria have been destroyed.[6]

1.5 Glycan Modification in Peptidoglycan

There are no known examples of bacterial species that contain exclusively unmodified peptidoglycan polymerized from Lipid II.[13] A number of different modifications

are found in bacterial peptidoglycan and while their functional roles are often not completely clear, their presence often aids in the bacteria's resistance to lysozyme-catalyzed degradation. This finding is not surprising since bacteria are likely to encounter host lysozymes during infection, and resistance to these and other defense mechanisms is crucial for maintaining bacterial viability.

The de-*N*-acetylation of GlcNAc and MurNAc residues in peptidoglycan is a modification that is found in bacteria that are known to be resistant to the hydrolytic action of lysozymes (Figure 1.25).[13] This modification occurs outside of the cytoplasm on intact strands of peptidoglycan and is thought to prevent productive interactions in the binding pocket of lysozyme. In addition to conferring resistance to host lysozymes, the de-*N*-acetylation of the amino sugars of peptidoglycan is also believed to have effects related to the introduction of additional positive charges in the cell wall. This additional positive charge is thought to aid in the binding of cell-wall proteins or major virulence factors such as capsular polysaccharides, and is also suspected to reduce the permeability of antimicrobial peptides released by the host immune system.[13]

Another modification that is found in some species of bacteria is the *N*-glycolylation of muramic acid residues in peptidoglycan (Figure 1.25).[13] This introduces an additional hydroxyl group on the *N*-acetyl group of MurNAc and is catalyzed by a NADPH-dependent hydroxylase during the synthesis of UDP-MurNAc-pentapeptide. The role of this modification is unknown, but the additional hydroxyl group is thought to play a role in envelope stability as well as resistance to lysozymes and β-lactam antibiotics.[13] Other covalent modifications of peptidoglycan include the attachment of phosphate at the C-6 hydroxyl group, and the addition of surface polymers including teichoic acids, capsular

polysaccharides, and arabinogalactans via phosphodiester linkages (Figure 1.25).[13] These modifications introduce additional functional group complexity to the murein sacculus and play important roles in a number of key cellular processes.

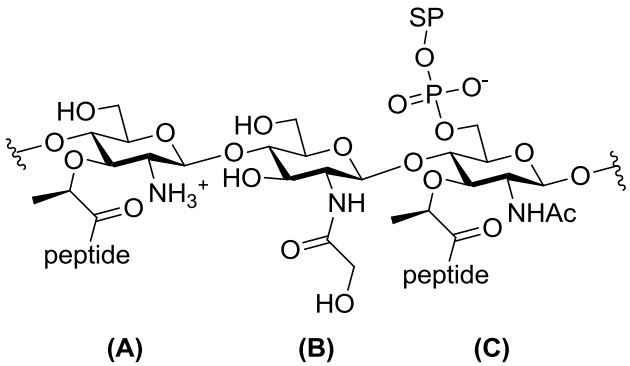

Figure 1.25 Covalent modifications of peptidoglycan. (A) de-*N*-acetylation, (B) *N*-glycolylation, (C) *O*-phosphorylation and attachment of surface polymers (SP).

1.5.1 *O*-Acetylation of Peptidoglycan

One of the most prevalent covalent modifications found in peptidoglycan is the *O*-acetylation of the C-6 hydroxyl group of MurNAc residues (Figure 1.26).[13, 14] This modification is found in many pathogenic bacteria including the Gram-positive *Bacillus cereus*, *Staphylococcus aureus*, *Enterococcus hirae*, and *Streptococcus pneumonia*, and the Gram-negative *Neisseria gonorrhoeae*, *Neisseria meningitides*, *Helicobacter pylori* and *Proteus mirabilis*.[1516] The extent of modification of MurNAc residues varies from species to species but is generally between 20-70%.[15]

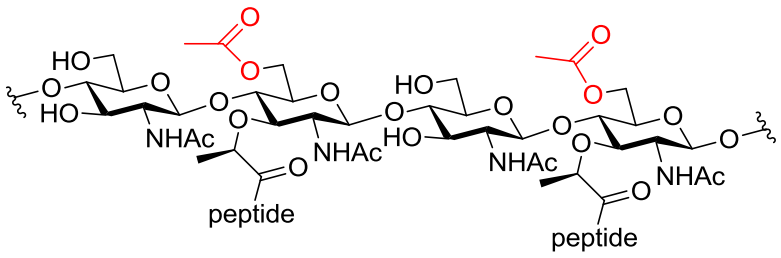

Figure 1.26 Peptidoglycan *O*-acetylation at the C-6 hydroxyl group of MurNAc residues.

Most muramidases that normally degrade peptidoglycan have either reduced or no activity against *O*-acetylated peptidoglycan.[14, 17] This includes lysozyme, for which a direct correlation has been demonstrated between the degree of *O*-acetylation of peptidoglycan and lysozyme-catalyzed hydrolysis.[17] In addition to increased resistance to lysozyme-catalyzed hydrolysis, a correlation between *O*-acetylation and pathogenicity was demonstrated in *Staphylococcus* species.[13] This modification also affects the clearance of high molecular weight fragments of peptidoglycan that remain after invading bacteria are destroyed by the immune system. By preventing the binding of these fragments to peptidoglycan-recognition proteins they increase their time of persistence within the host, causing complement activation, pyrogenicity, somnogenesis, and arthrogenicity.[13]

It is clear that the *O*-acetylation of peptidoglycan has many physiological consequences with regard to the bacterium/host interaction. But one of the most important consequences of peptidoglycan *O*-acetylation is this covalent modification's effect on the activity of bacterial lytic transglycosylases.[13, 15, 18] As detailed in Section 1.3.2, the lytic transglycosylases play an important role in the metabolism of peptidoglycan during cell growth and division, the proper functioning of bacterial secretion systems, and the insertion of bacterial appendages.[18] Their mechanism of action (Figure 1.15) has a strict requirement for a free C-6 hydroxyl group on the MurNAc residue in order to create the 1,6-anhydro

linkage, and the masking of this group as an acetyl ester completely prevents this reaction from occurring. Thus, bacteria that *O*-acetylate their peptidoglycan must possess a mechanism for the controlled addition and removal of this modification in order to both mask the cell from host defense mechanisms and allow for the continued autolytic activity of lytic transglycosylases (Figure 1.27).[15, 16] Indeed, there is speculation that the controlled addition and removal of *O*-acetyl groups from peptidoglycan functions as a spatial and temporal regulator of bacterial lytic transglycosylases.[13]

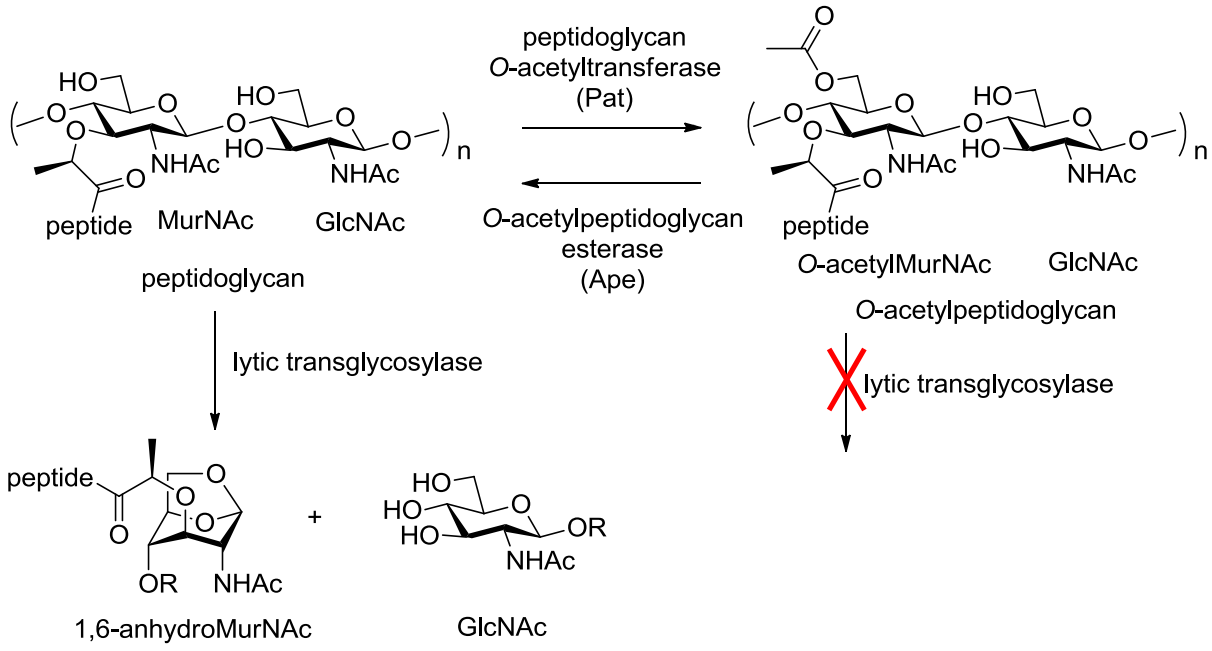

Figure 1.27 Peptidoglycan *O*-acetylation/deacetylation and the action of lytic transglycosylase.

1.5.1.1 Peptidoglycan *O*-Acetyltransferases

The addition of acetyl groups to the MurNAc residues in peptidoglycan most likely occurs after the insertion of Lipid II into the existing murein sacculus. This scenario is likely as there is no experimental evidence for the existence of *O*-acetylated muropeptide precursors such as Lipid II.[13] The source of the acetate required for these reactions varies

between species, but in most cases acetyl-CoA or acetyl phosphate are the likely donors for this covalent modification.[13] In certain bacteria there has been evidence reported that suggests that acetate is transferred from the *N*-acetyl groups of GlcNAc and MurNAc, but this link remains unproven as the proposed de-*N*-acetylated amino sugars have not been isolated.[13] There are two proposed mechanisms for the transfer of acetate onto the C-6 hydroxyl of MurNAc residues in peptidoglycan. The "one-component" mechanism proposes that a single protein functions to both transfer acetate through the cytoplasmic membrane and then to catalyze its transfer onto peptidoglycan (Figure 1.28). The "two-component" mechanism proposes that there are two proteins involved in this process; one that is responsible for transporting acetate across the cytoplasmic membrane and another that is responsible for transferring the translocated acetate onto peptidoglycan (Figure 1.28).[13]

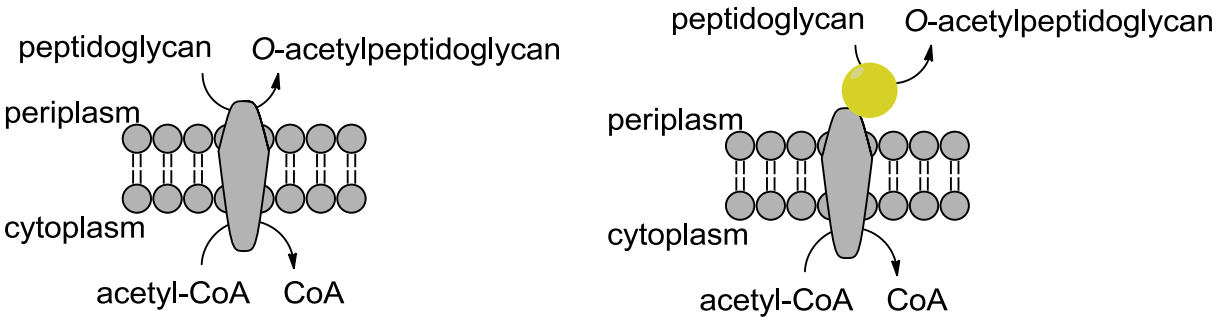

Figure 1.28 One-component (left) and two-component (right) models for peptidoglycan *O*-acetylation.

Analysis of the putative *poa* (peptidoglycan *O*-acetylation) gene clusters in many Gram-positive and Gram-negative bacteria reveals that different systems for the *O*-acetylation of peptidoglycan may be operative in these two classes of bacteria. A peptidoglycan *O*-acetyltransferase (Pat) of the one-component model has been identified in *S. aureus* and potential homologs of this enzyme have been identified in a number of other

Gram-positive bacteria.[13] However, it has been postulated that many Gram-negative bacteria *O*-acetylate their peptidoglycan via the two-component model.

Recently, the Clarke group at the University of Guelph identified part of the Pat system in the Gram-negative bacteria *N. gonorrhoeae*.[19] An enzyme, PatB, in the *poa* gene cluster that was thought to function as an *O*-acetylpeptidoglycan esterase (Ape) was cloned and expressed in *E. coli*. This enzyme did not function as an esterase however, and was actually found to increase the *O*-acetylation of peptidoglycan in *E. coli*, a Gram-negative bacterial species that normally lacks this covalent modification.[19] Analysis of the *poa* gene cluster in *N. gonorrhoeae* also revealed the presence of a predicted membrane-spanning protein (PatA) that is responsible for the translocation of acetate across the cytoplasmic membrane. The newly-discovered PatB peptidoglycan *O*-acetyltransferase was proposed to act in conjunction with PatA in a two-component model to *O*-acetylate peptidoglycan in *N. gonorrhoeae*.[19]

Since *E. coli* is one of the few pathogenic bacteria that does not *O*-acetylate its peptidoglycan, it does not contain a homolog of PatA. It does however possess an integrated cytoplasmic membrane protein (WecH) that plays a role in the *O*-acetylation of the enterobacterial common antigen. Clarke proposed that WecH functioned to transfer acetate across the cytoplasmic membrane, and that the expressed PatB used this acetate to acetylate MurNAc residues on peptidoglycan.[19] Indeed, when WecH was knocked out of *E. coli* cells transformed with PatB, no detectable *O*-acetylation of peptidoglycan was observed, providing further support for this hypothesis. These experiments provided the first biochemical evidence for a two-component system for peptidoglycan *O*-acetylation in *N. gonorrhoeae*.[19]

Interestingly, the low-level expression of PatB in *E. coli* cells that resulted in an increase (1.7%) in *O*-acetylation of peptidoglycan proved to be toxic to the cell and eventually resulted in cell death. *E. coli* lacks the machinery to remove this covalent modification and the consequences of its inability to properly metabolize even a small percentage of *O*-acetylated peptidoglycan highlight the importance of this modification in bacterial viability.[19]

1.5.1.2 *O*-Acetylpeptidoglycan Esterases

The uncontrolled *O*-acetylation of peptidoglycan undoubtedly has deleterious effects on normally viable bacterial cells. This is likely due to the inability of bacterial lytic transglycosylases that are important in many essential metabolic processes to cleave MurNAc residues containing this covalent modification (Section 1.3.2). The *poa* gene cluster identified in many bacteria that *O*-acetylate their peptidoglycan encodes for a number of enzymes believed to be involved in the addition and removal of *O*-acetyl groups to MurNAc residues.[16] In *N. gonorrhoeae* this includes the two-component *O*-acetyltransferase system (PatA and PatB) described in Section 1.5.1.1 as well as an esterase that functions to hydrolyze acetate from modified peptidoglycan residues.

This *O*-acetylpeptidoglycan esterase was first identified and characterized by Weadge and Clarke in *N. gonorrhoeae* and was named Ape1 (Figure 1.27).[15] The enzyme was cloned and expressed in *E. coli* and was produced as two *N*-terminally processed forms of the wild-type protein. These two forms were found to be localized to the periplasm and outer membrane, areas where the maintenance of peptidoglycan would be required. Sequence alignment studies with Ape1 and a known *O*-acetylxylan esterase helped to identify potential catalytic residues.[15, 20] Generation of a number of alanine-mutants of these suspected amino

acids by site-directed mutagenesis confirmed that Ape1 is a serine esterase belonging to the CE-3 family of carbohydrate esterases.[20]

Ape1's activity was demonstrated on suspensions of partially *O*-acetylated peptidoglycan samples isolated from bacteria as well as on a number of soluble, chromogenic substrates. The enzyme hydrolyzed acetate from *O*-acetylated peptidoglycan samples with a higher specific activity than from *O*-acetylated xylan, making this the first characterized *O*-acetylpeptidoglycan esterase.[15] Chromosomal deletion of Ape1 from *N. gonorrhoeae* resulted in nonviable bacteria, suggesting that Ape1 is an essential enzyme in bacteria that contain *O*-acetylated peptidoglycan.[15]

1.6 The Role of Peptidoglycan Metabolism in Physiological Processes

The importance of peptidoglycan metabolism in physiological processes is emphasized by the sheer volume of peptidoglycan-modifying enzymes that have been detailed in the previous sections. The assignment of specific roles to each of these enzymes is complicated by the fact that many of them have more than one function, and different enzymes often possess redundant activities. In *E. coli* for example, it is believed that 5 L-Ala-amidases, 6 lytic transglycosylases, and 3 endopeptidases are involved in the cleavage of the septum during cell division.[6] Thus, elimination of a single hydrolase involved will rarely result in the complete loss of physiological function.

Peptidoglycan hydrolases are involved in a host of processes that occur during the lifetime of a bacterial cell. The elongation and separation of the bacterial cell, the regulation of cell wall growth, the insertion of bacterial appendages, and the functioning of bacterial secretion systems are just a few of the processes that require peptidoglycan hydrolases.[6] In addition, modifications of the murein sacculus can greatly affect a bacterium's interaction

with host defenses and different types of antibiotics.[6] As was described with *O*-acetylation, these modifications can also affect the normal metabolism of peptidoglycan and if not properly regulated can result in cell death.[13, 15] Although some of these processes are more important than others for bacterial viability, disruption of even the non-essential activities will generally have a deleterious effect on the cell. For this reason, the study of both the mechanism of action and the functional role of peptidoglycan-modifying enzymes is critical towards the discovery of new methods of combating bacterial infection.

1.7 Thesis Aims

This thesis focuses on the study of two enzymes involved in the metabolism of peptidoglycan. Chapter 2 details research performed on the *O*-acetylpeptidoglycan esterase (Ape1) that plays an important role in the masking of peptidoglycan through covalent modification. This peptidoglycan hydrolase catalyzes the cleavage of *O*-acetate esters from the MurNAc residues of peptidoglycan in *N. gonorrhoeae* (Figure 1.29).[15] The modification of MurNAc residues with *O*-acetate esters has been shown to protect the bacterial cell wall from degradation by host lysozymes and plays an important role in bacterial virulence and toxicity. The Ape1-catalyzed hydrolysis of these esters is necessary for a number of bacterial processes to continue to occur, and previous studies have shown that this enzyme may be essential for viability in bacteria that *O*-acetylate their peptidoglycan. The design, synthesis, and testing of substrate analogues will be undertaken in order to explore the ability of Ape1 to catalyze the hydrolysis of *O*-acetyl esters on small molecule substrates. This is an important step towards validating this enzyme as a viable antibiotic target and lays the groundwork for the design of small molecule transition state inhibitors that can be used to inhibit the enzyme *in vitro* and *in vivo*. In addition, these substrate analogues will aid in the

elucidation of the molecular details of the enzyme active site and the molecular machinery involved in catalysis.

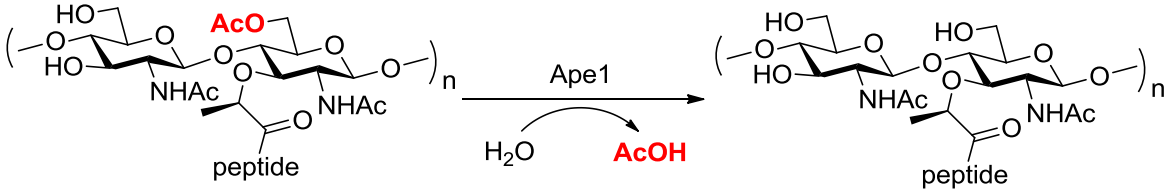

Figure 1.29 Hydrolysis of *O*-acetylated peptidoglycan by the *O*-acetylpeptidoglycan esterase, Ape1.

Chapter 3 contains details of the research performed on MurQ, a hydrolase (or etherase) that is involved in the recycling of MurNAc units of peptidoglycan. MurQ catalyzes the conversion of MurNAc 6-phosphate into GlcNAc 6-phosphate through scission of the C-3 lactyl ether (Figure 1.30).[11] This unusual transformation results in the cleavage of a very stable ether bond in the substrate and presents a very interesting target for study from a mechanistic standpoint. We plan to overexpress and purify a recombinant form of MurQ, and to generate a number of mutant enzymes using sequence alignment models to identify potential active site residues. The synthesis of both the natural substrate and product of the enzymatic reaction will be conducted so that these compounds may be used as mechanistic probes to monitor the reaction by ^{1}H NMR spectroscopy and mass spectrometry. A kinetic analysis of the reaction using either wild-type or mutant enzyme will be undertaken. Isotopically-labeled substrates will also be synthesized to further probe the mechanistic details of the reaction and to identify and characterize reaction intermediates. Finally, the role of MurQ in peptidoglycan metabolism and the potential use of inhibitors of the enzyme will be discussed.

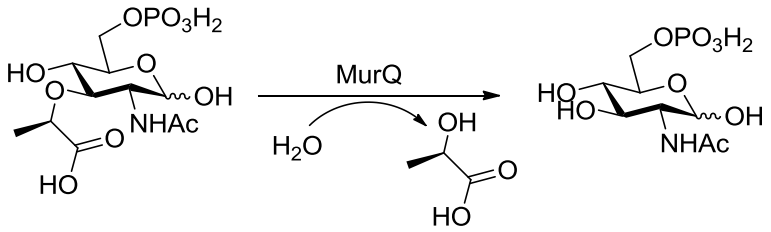

Figure 1.30 Conversion of MurNAc 6-phosphate to GlcNAc 6-phosphate by the MurNAc 6-phosphate hydrolase, MurQ.

Chapter 2: Substrate and Inhibitor Design for the Enzyme *O*-Acetylpeptidoglycan Esterase (Ape1) from *Neisseria gonorrhoeae*

As discussed in Section 1.5.1, the *O*-acetylation of peptidoglycan is an important covalent modification that helps to protect bacteria from attack and degradation by host lysozymes. However, this modification also prevents the action of lytic transglycosylases that play an important role in the metabolism of peptidoglycan. Because the action of lytic transglycosylases is required for normal cell growth and division, the function of bacterial secretion systems, and the insertion of bacterial appendages, a mechanism for the controlled addition and removal of *O*-acetyl groups on peptidoglycan must exist so that these activities may continue to occur.[15, 19]

Our collaborators in the Clarke group at the University of Guelph have used the Gram-negative bacterium *N. gonorrhoeae* to study the enzymes responsible for the addition (Pat's) and removal (Ape's) of this covalent modification.[15, 19, 20] The *poa* gene cluster found in *N. gonorrhoeae* encodes for a number of enzymes and proteins that have been shown to, or have been speculated to, play a role in peptidoglycan *O*-acetylation. These include the peptidoglycan *O*-acetyltransferases PatA and PatB described in Section 1.5.1.1,[19] and the *O*-acetylpeptidoglycan esterase Ape1 described in Section 1.5.1.2. The work described in this dissertation focuses on the study of the serine esterase Ape1, an enzyme believed to be essential in *N. gonorrhoeae* and other bacteria that *O*-acetylate their peptidoglycan.

Although Ape1 activity had previously been demonstrated by the Clarke group using *O*-acetylated peptidoglycan samples isolated from bacteria, these experiments were complicated by the fact that the substrate was an insoluble polymer that required sonication for even dispersal.[15] In order to obtain the kinetic parameters k_{cat} and K_M of Ape1, the highly

activated esters *p*-nitrophenyl (*p*-NP) acetate or α-naphthyl (α-NA) acetate were used as model substrates.[15] These substrates provided some sense of Ape1's catalytic efficiency, but because of their highly labile nature would also be expected to undergo non-specific hydrolysis by a number of different esterases.

In this chapter, we describe the design and synthesis of 6-*O*-acetylated monosaccharide and disaccharide peptidoglycan analogues that we predicted would serve as water-soluble substrates of Ape1. The testing of these compounds with Ape1 is also described and serves to provide more meaningful data regarding Ape1's activity against peptidoglycan substrates containing the 6-*O*-acetyl modification. Finally, the synthesis and testing of a potential inhibitor of the enzyme is presented as well as a discussion regarding future research that will explore Ape1's potential as an antibacterial target.

2.1 Catalytic Mechanism of Ape1

Ape1 belongs to the family 3 carbohydrate esterases (CE-3) according to the CAZy classification system. This family also includes a number of previously characterized *O*-acetylxylan esterases that are found to hydrolyze *O*-acetylated xylan in the cell wall of many different species of plants.[20] Through sequence alignment studies between Ape1 and other members of the CE-3 family, a number of invariant residues were identified that were proposed to play a crucial role in catalysis.[16, 20] Using site-directed mutagenesis, alanine mutants of Ser80, Asp366, and His369 were generated and their activity levels compared to that of wild-type enzyme. It was determined that the loss of enzymatic activity was greatest for the Ser80 mutant, then the His369 mutant and finally the Asp366 mutant.[20] These results are consistent with a model where these three residues form a catalytic triad that is characteristic of serine proteases and esterases. In this well-established model, a salt bridge

is formed between Asp366 and His369 and this bridge promotes the abstraction of the proton from the hydroxyl group of Ser80 by the imidazolium group of His369 (Figure 2.1). The alkoxide nucleophile of the serine residue then forms a tetrahedral oxyanion intermediate through attack of the carbonyl carbon of the targeted amide/ester bond of the substrate. This oxyanionic intermediate is stabilized by an "oxyanion hole" formed by backbone amides appropriately positioned in the active site of the enzyme, and subsequently collapses to generate an acylated-enzyme intermediate and the cleaved product. This acyl-enzyme intermediate is then hydrolyzed by water to regenerate the catalytic triad.[20]

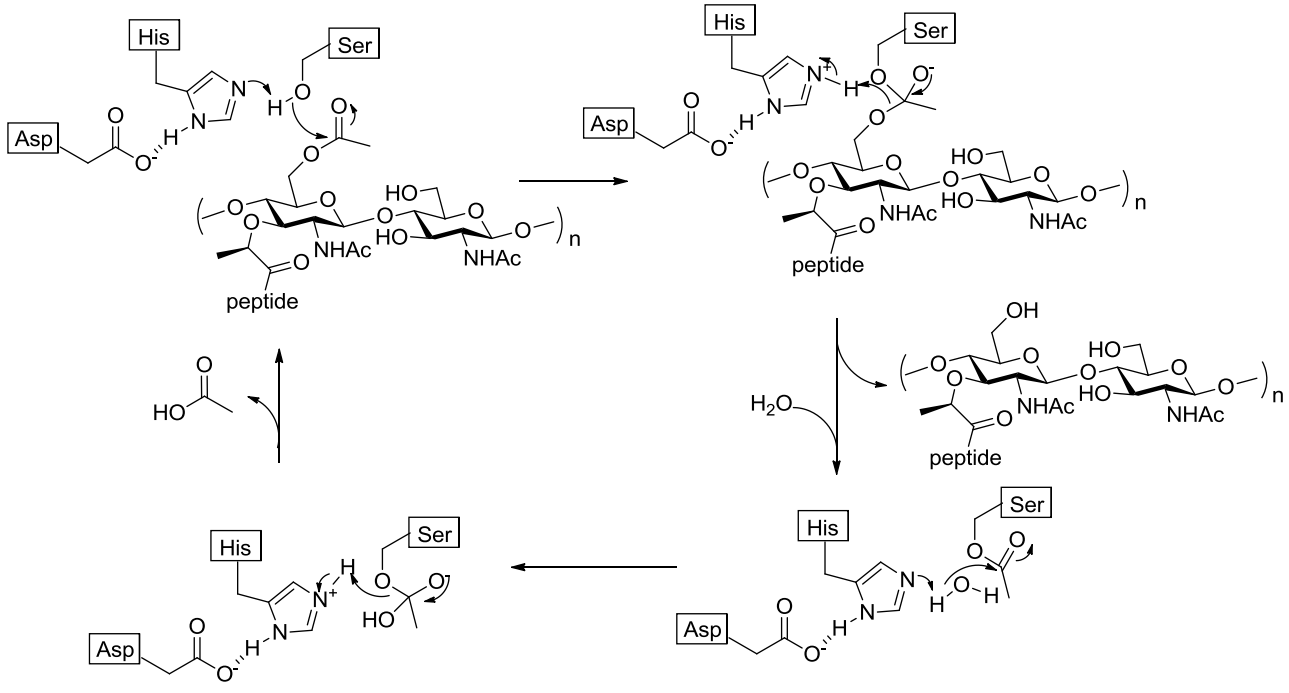

Figure 2.1 Proposed mechanism of Ape1-catalyzed hydrolysis of *O*-acetylated peptidoglycan.

2.2 Previous Attempts at Assaying Ape1 Enzymatic Activity

Since Ape1 belongs to the CE-3 family of enzymes that also includes the *O*-acetylxylan esterases, the substrate specificity of Ape1 was probed. A specific activity of

1.63 +/- 0.61 μmol·min^{-1}·mg protein^{-1} was reported for *O*-acetylated peptidoglycan as compared to 1.36 +/- 0.34 μmol·min^{-1}·mg protein^{-1} for *O*-acetylated xylan (Table 2.1).[15] Although Ape1's activity on *O*-acetylated peptidoglycan and *O*-acetylated xylan were

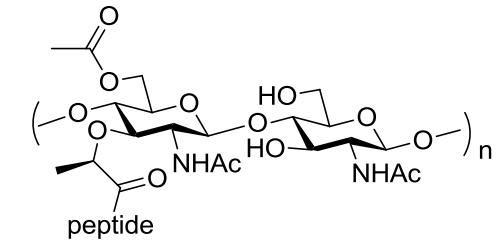

***O*-acetyl PG**

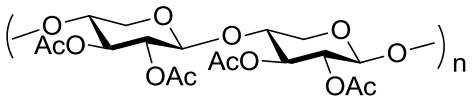

***O*-acetyl xylan**

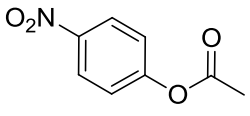

***p*-NP acetate**

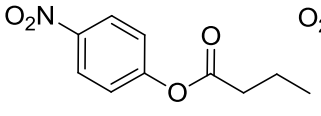

***p*-NP butyrate**

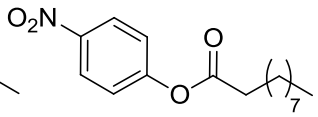

***p*-NP decanoate**

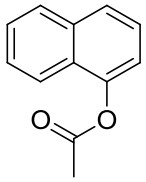

α-naphtyl acetate

Substrate	Specific Activity (μmol·min^{-1}·mg protein^{-1})
O-acetyl PG [a]	1.63 +/– 0.61
O-acetyl xylan [a]	1.36 +/– 0.34
p-NP acetate [b]	9.98 +/– 0.21
αNA acetate [b]	6.29 +/– 0.26
p-NP butyrate [b]	4.49 x 10^{-4} +/– 7.8 x 10^{-5}
p-NP decanoate [b]	6.93 x 10^{-4} +/– 9.8 x 10^{-5}

Table 2.1 Specific activity of Ape1-catalyzed hydrolysis of test substrates. [a]enzyme was incubated with a 5 mg/mL suspension of insoluble substrate. [b]enzyme was incubated with soluble substrate at a final substrate concentration of 2 mM.[15]

roughly the same, the finding that Ape1 was able to catalyze the hydrolysis of acetate from *O*-acetylated peptidoglycan was important as previously reported *O*-acetylxylan esterases were all devoid of activity on this alternate substrate. This result represented the first reported evidence for the existence of an esterase that displayed activity on samples of *O*-acetylated peptidoglycan. Unfortunately, these activity assays used *O*-acetylated peptidoglycan samples isolated from bacteria that were insoluble suspensions requiring sonication and the addition of detergents for even dispersal. Because of this the concentration of peptidoglycan samples could not be accurately measured, thus preventing the determination of the kinetic parameters k_{cat} and K_M for Ape1 with the natural substrate.

In addition to the insoluble *O*-acetylated peptidoglycan and xylan polymers, a number of other compounds were tested for activity with purified Ape1 (Table 2.1). These results include data for a number of compounds that yields additional information about the substrate specificity of the enzyme. To test the ability of Ape1 to catalyze the hydrolysis of esters containing an increased number of carbon units, the compounds *p*-NP butyrate and *p*-NP decanoate were tested as substrates. The specific activity of Ape1 on these non-acetate ester substrates was orders of magnitude lower than that of the corresponding *p*-NP acetate (Table 2.1).[15] This provided strong evidence that Ape1 is able to discriminate between ester substrates of differing chain length and confirmed that the enzyme was an *O*-acetyl esterase and not a lipase. In addition, Ape1 was unable to liberate acetate from samples of GlcNAc or chitin oligosaccharides, confirming that Ape1 does not function to deacetylate *N*-acetyl groups from 2-*N*-acetyl amino sugars.

To obtain the kinetic parameters k_{cat} and K_M for Ape1, Clarke and coworkers employed the water-soluble chromogenic substrates *p*-NP acetate and α-naphthyl acetate (α-

NA acetate). Using these two acetyl ester substrates, k_{cat}'s of 6.95 +/– 0.34 s^{-1} and 3.99 +/– 0.28 s^{-1} and K_M's of 0.53 +/– 0.12 mM and 0.27 +/– 0.08 mM were obtained, respectively.[15] These measurements provided some sense of Ape1's catalytic power, but because these soluble substrates form a relatively stable anionic species upon hydrolysis, they are not the best indicator of Ape1's ability to catalyze acetate hydrolysis on native substrates. Many other serine proteases and esterases including subtilisin and acetylcholine esterase have been found to catalyze the hydrolysis of acetate from these highly-activated substrates.[20]

2.3 Design and Synthesis of Peptidoglycan-Like Substrate Analogues of Ape1

Since Ape1 acts on a polymeric substrate, it is likely that both binding and catalysis are influenced by the number of sugar residues present in the substrate. Consequently, Ape1's ability to catalyze the de-*O*-acetylation of truncated fragments of *O*-acetylated peptidoglycan could be significantly impaired. A marked dependency on the rate of reaction as a function of the number of monomer units in the substrate has been reported for other deacetylases that operate on polysaccharides.[21] We designed the 6-*O*-acetylated disaccharide

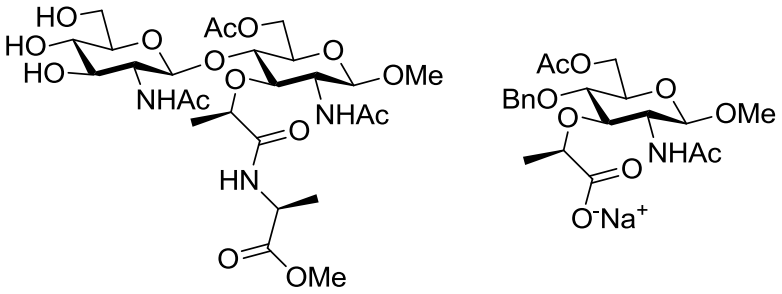

1 2

Figure 2.2 Proposed water-soluble disaccharide (1) and monosaccharide (2) substrates of Ape1.

and monosaccharide peptidoglycan analogues **1** and **2** that could potentially serve as water-soluble substrates of the Ape1. The synthesis and testing of both the mono- and disaccharide substrate analogues will serve to identify whether Ape1 is able to accept truncated substrates and if so, examine whether there is a strict requirement for the presence of the GlcNAc moiety. The kinetic characterization of Ape1 with these compounds will provide a better indication of the ability of the enzyme to catalyze the turnover of acetate esters on unactivated substrates. These substrates will also serve to validate the use of mono- and disaccharide fragments as the basic scaffold for the design of small-molecule transition state/intermediate analogues of Ape1, and act as benchmarks for future experiments involving the testing of these compounds as potential antibacterials.

We chose to start with the relatively complex disaccharide substrate **1** (Figure 2.2) in order to maximize our chances of observing a high level of activity with Ape1. This substrate was designed to serve as a benchmark to which other monosaccharide substrates could be compared. The core structure of **1** is a β-(1→4)-linked GlcNAc-MurNAc disaccharide that is elaborated with an *O*-acetyl ester at the C-6 position of the MurNAc moiety and an L-alanine methyl ester appended to the lactyl side chain. The β-methoxy group at the anomeric carbon of MurNAc was chosen to mimic the β-linkages found in peptidoglycan and it was anticipated that the three free hydroxyl groups on the GlcNAc residue would increase the water solubility of the final compound. It is important to note that the presence of the β-linked GlcNAc at the C-4 position of MurNAc also serves to prevent any potential migration of the 6-*O*-acetyl ester.[22]

The truncated monosaccharide substrate **2** (Figure 2.2) was designed to further examine the contributions of different structural elements towards binding. The GlcNAc

moiety at O-4 has been replaced by a hydrophobic *O*-benzyl ether that is designed to occupy the GlcNAc binding pocket in the enzyme active site, and also serves to prevent migration of the 6-*O*-acetyl ester.[22] In addition, the L-alanine moiety has been deleted from the lactyl side chain to test whether it is a critical recognition element for the enzyme. Because compound **2** lacks the free hydroxyl groups contained in the GlcNAc residue of disaccharide **1**, the lactate was left as a free carboxylate to confer greater water solubility. The testing of compounds **1** and **2**, both bearing an unactivated acetate ester at the C-6 position of the MurNAc residue, will provide valuable information with regard to the structural elements required for binding. The results of these tests will also shape future strategies in the design and synthesis of Ape1 substrates and inhibitors.

2.3.1 Synthesis of Disaccharide Substrate (1)

Oligosaccharide synthesis is generally accomplished through the coupling of appropriately designed glycosyl "donors" and "acceptors." The glycosyl donor typically contains a functional group at the anomeric center that, upon activation, leaves to produce an electrophilic oxocarbenium species (Figure 2.3).[23, 24] The glycosyl acceptor acts as a nucleophilic species in the glycosidic coupling reaction and is typically a sugar bearing a number of protecting groups such that only one hydroxyl group is left free to act as a nucleophile.

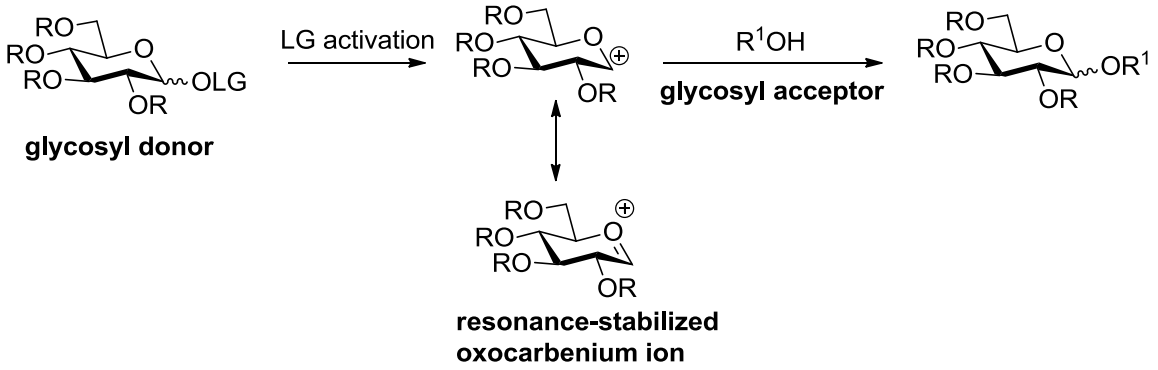

Figure 2.3 Glycosidic coupling reaction using a glycosyl donor and a glycosyl acceptor.

There are many different strategies that have been developed to perform glycosidic couplings, each possessing its own unique limitations. In general, each glycosylation method aims to address a specific set of requirements; a minimal amount of donor should be required for the coupling, the glycosylation step should be stereoselective and high-yielding, and the method should be applicable on a large scale.[24] Unfortunately, despite the immense interest in the development of new methods for oligosaccharide synthesis, a single all-encompassing protocol has yet to be developed, and the choice of glycosylation strategy is often dependent upon the target of interest.[24]

The synthesis of oligosaccharides containing D-glucosamine, and more commonly, its *N*-acetyl derivative GlcNAc, has been the subject of significant research effort as a result of their prevalence in glycoconjugates.[23] Peptidoglycan-like fragments present an especially challenging synthetic target because both the donors and acceptors required for oligosaccharide synthesis contain *N*-acetyl groups at the C-2 position. The *N*-acetyl group imposes a number of unique constraints for both oligosaccharide donors and acceptors; this is likely the reason that the volume of literature describing the synthesis of peptidoglycan-like oligosaccharides pales in comparison to that for the synthesis of other classes of oligosaccharides.[25]

Glycoside bond formation using GlcNAc donors is complicated by neighbouring-group participation of the 2-acetamido group in donor substrates. Upon leaving-group activation, an intramolecular oxazolinium ion intermediate is formed via nucleophilic attack of the carbonyl oxygen on the anomeric centre (Figure 2.4). The formation of this oxazolinium ion via neighbouring-group participation ensures the formation of the β-anomeric linkage in coupling reactions. However, this particular oxazolinium ion is also

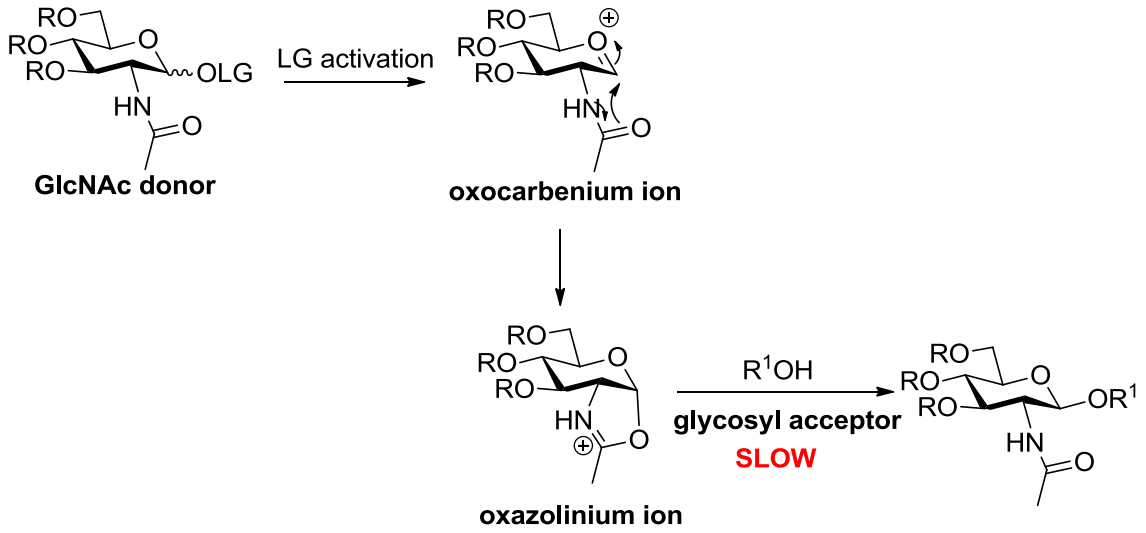

Figure 2.4 Formation of an oxazolinium intermediate in glycosidic coupling reactions using GlcNAc donors slows transfer to the glycosyl acceptor.

relatively stable, resulting in slow and inefficient reactions with glycosyl acceptors.[23, 26] Several methods have been developed to increase the electrophilicity of GlcNAc donors, while still preferentially forming the β-linkage in the coupled products. A few notable examples include the dimethylmaleoyl group, the phthalimido group, and the trichloroacetamido group (Figure 2.5).[26-28] These methods rely primarily on increasing the electron-withdrawing character of the *N*-acyl substituents. This serves to decrease the stability of the oxazolinium system and increases the rate of nucleophilic attack by a glycosyl acceptor.

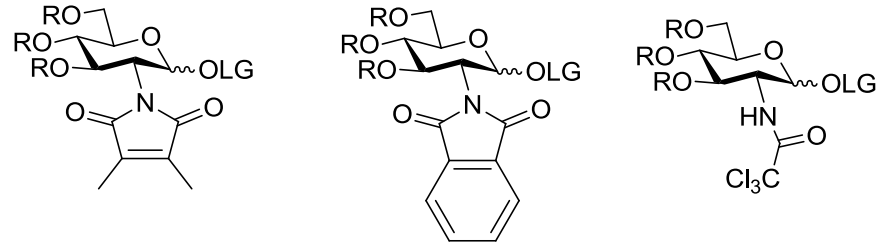

Figure 2.5 Functional groups used to increase the donor properties of 2-*N*-acetyl-containing monosaccharides in oligosaccharide synthesis.

For the synthesis of disaccharide **1**, we chose to mask the 2-acetamido group as a 2-trichloroacetamido group in our GlcNAc donor system (Compound **8**, Figure 2.6). The increased electron-withdrawing character of this amide will serve to increase the glycosyl donor properties of this compound and result in higher-yielding coupling reactions. This trichloroacetamido group can be easily reduced back to the corresponding acetamido group using tributyltin hydride and AIBN after the coupling has been completed.[26] Although the synthesis of related peptidoglycan fragments has been previously reported,[25] the requirement of the 6-*O*-acetate ester on the MurNAc moiety of disaccharide **1** necessitates a number of changes to our synthetic strategy, as *O*-acetate esters are traditionally employed as protecting groups in oligosaccharide synthesis. In order to selectively *O*-acetylate at the C-6 position on the MurNAc residue, the hydroxyl groups at C-3, C-4, and C-6 on the GlcNAc moiety must be masked until the *O*-acetate ester is installed. We chose to protect the three hydroxyl groups on the GlcNAc moiety as *O*-levulinate esters after coupling because they can be selectively removed in the presence of an *O*-acetate ester. The orthogonal protecting group strategy detailed within also allows for the installation of different functional groups at the C-6 position of MurNAc, a feature that is very attractive for the future development of small molecule inhibitors of Ape1.

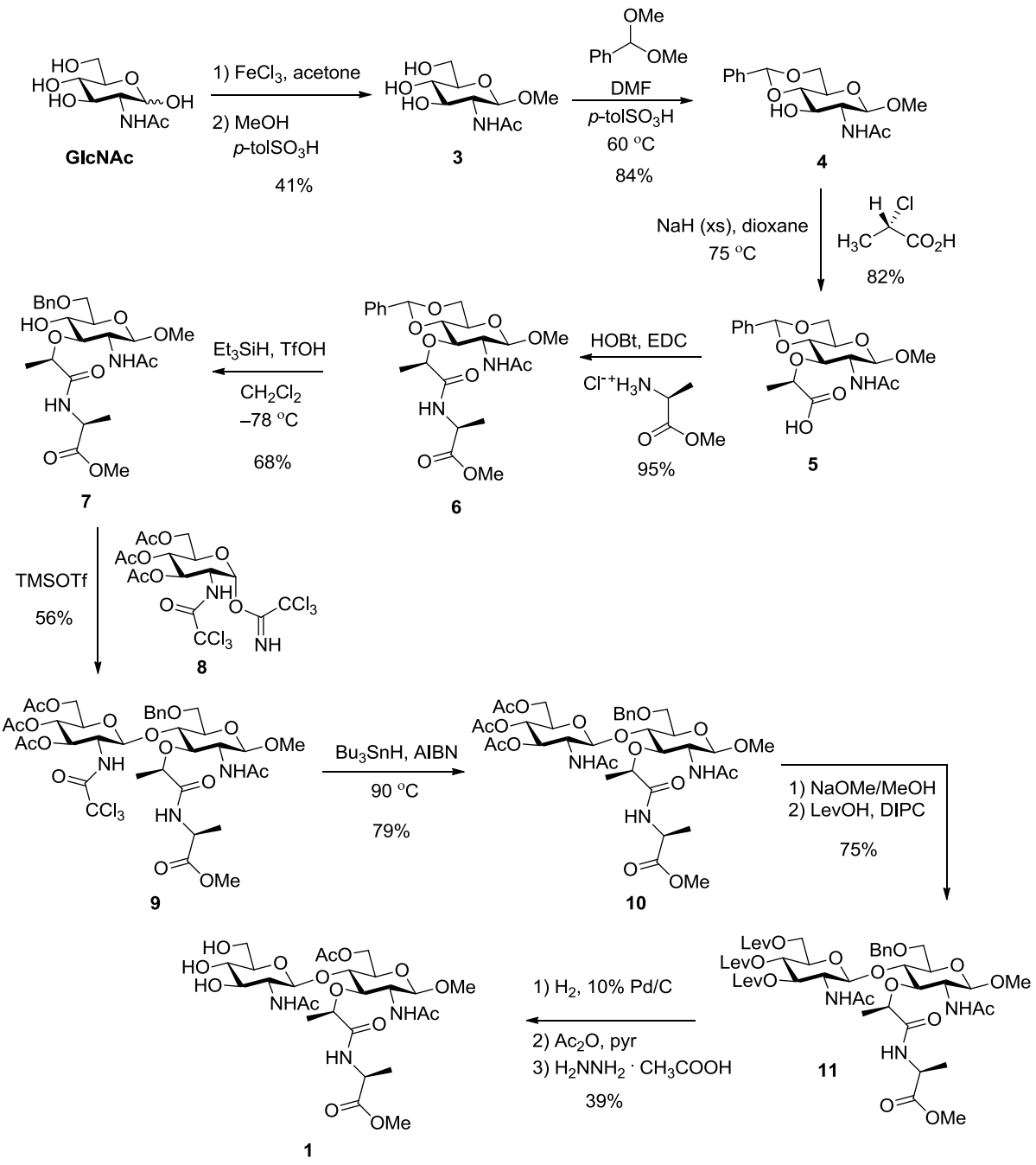

Figure 2.6 Synthesis of disaccharide substrate (1).

The methyl glycoside **3** was prepared from *N*-acetylglucosamine in two steps using a literature protocol (Figure 2.6).[29] Since peptidoglycan monomers are linked in a β-(1→4) manner, the methyl glycoside at C-1 was installed in the β-configuration. Compound **3** was

then reacted with benzaldehyde dimethyl acetal under acidic conditions to generate the known 4,6-*O*-benzylidene-protected compound **4**.[30] Installation of the D-lactyl ether at the C-3 position using (*S*)-2-chloropropionic acid gave the previously characterized MurNAc derivative **5** in 82% yield.[30] 1-Ethyl-3-(3-dimethylaminopropyl) carbodiimide (EDC) and 1-hydroxybenzotriazole-mediated (HOBt) coupling of the methyl ester of L-alanine to **5** gave compound **6** in good yield.

A reductive ring-opening of the benzylidene acetal with Et_3SiH and TfOH was then used to generate the 6-*O*-benzyl ether **7**.[31] The regioselectivity of this reaction was dictated by the choice of acid catalyst; the use of a protic acid such as TfOH gave the 6-*O*-benzyl ether while the use of a Lewis acid such as $PhBCl_2$ gave the 4-*O*-benzyl ether regioisomer.[31] This regioselectivity is presumably due to the selective interaction of the acid catalyst with either O-4 or O-6 of the benzylidene acetal. A sterically bulky Lewis acid such as $PhBCl_2$ will preferentially coordinate to the oxygen atom at the C-6 position, while a smaller protic acid coordinates to the oxygen atom at the C-4 position. The position of the free hydroxyl group was confirmed via NMR spectroscopy through analysis of the coupling pattern of the hydroxyl group proton. A COSY spectrum of compound **7** revealed that the hydroxyl group proton was coupled to the proton at the C-4 position and not to either of the protons at the C-6 position. The yield of this selective reduction was lower than expected, most likely due to the presence of the L-alanine attached to the C-3 lactate group and its interaction with TfOH. Reactions involving the selective reduction of the MurNAc derivatives lacking the L-alanine side chain gave significantly higher yields (data not shown).

The donor, **8**, was synthesized using literature methodology starting from D-glucosamine.[26] As discussed previously, the 2-trichloroacetamido group was incorporated in

order to mask the 2-acetamido moiety and to ensure successful coupling. The MurNAc acceptor **7** was coupled with donor **8** using TMSOTf as a promoter. The anomeric proton at the C-1 position of the donor monosaccharide was visualized as a doublet with a *J* value of 8.0 Hz due to coupling to the axial proton at the C-2 position. This large *J* value confirmed that the expected β-linkage was formed between the donor and acceptor monosaccharides during the coupling reaction. The modest yield of disaccharide **9** can be partially accounted for by the lack of nucleophilicity of the C-4 hydroxyl group in acceptors possessing an unmasked 2-acetamido group.[32] Significant concentration dependence has been previously observed on the chemical shift value of the amide N-H proton in GlcNAc derivatives with an unmasked hydroxyl group at the C-4 position. It was speculated that intermolecular hydrogen bonding (i.e. dimerization) was occurring between the amide N-H proton of one molecule and the oxygen at the C-4 position of another molecule and that this intermolecular interaction at least partially accounted for the decrease in nucleophilicity of the C-4 hydroxyl group observed in GlcNAc acceptors.[32] Although previous strategies involving masking of the 2-acetamido group in the acceptor have been reported,[25] we chose to leave the group intact in order to minimize the number of manipulations required after the disaccharide coupling step. The trichloroacetamido functionality of disaccharide **9** was then reduced with tributyltin hydride/AIBN in order to unmask the 2-acetamido group on the "GlcNAc" portion of disaccharide **10**.[26] In order to generate the final product **1**, a protecting group for the hydroxyl groups at C-3, C-4, and C-6 of the GlcNAc moiety that could be selectively cleaved in the presence of an *O*-acetate ester was required. Accordingly, the *O*-acetate groups on compound **10** were replaced with *O*-levulinate esters through a two-step procedure involving

deprotection with NaOMe, and a subsequent *N,N'*-diisopropylcarbodiimide-mediated (DIPC) coupling of the free hydroxyls with levulinic acid to give disaccharide **11**.

With the proper protecting groups now in place, the acetate ester was introduced selectively at the C-6 position of the MurNAc residue through the hydrogenolysis of the benzyl ether, and acetylation of the newly-formed primary hydroxyl group. Deprotection of the *O*-levulinate esters was accomplished selectively in the presence of the *O*-acetate ester with the use of hydrazine acetate, generating disaccharide substrate **1**. In this reaction, the hydrazine reagent nucleophilically attacks the more reactive ketone of the levulinate ester to first form a hydrazone (Figure 2.7). The remaining amino group of the hydrazone then undergoes an intramolecular cyclization with the ester carbonyl through a six-membered ring intermediate. The breakdown of the intermediate results in amide formation and cleavage of the levulinate group (Figure 2.7). Although hydrazine can also be used to remove acetate

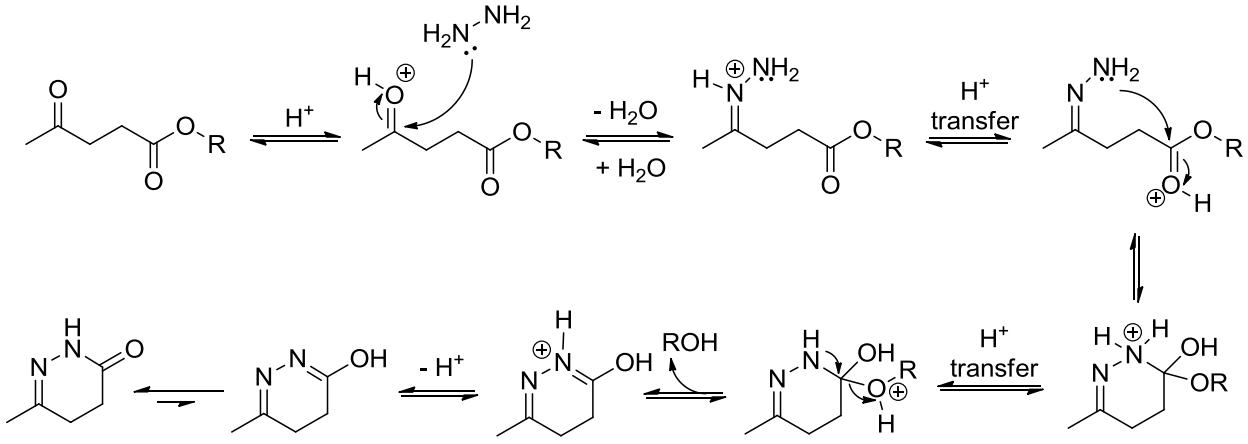

Figure 2.7 Mechanism of levulinate ester cleavage by hydrazine.

esters, the mechanism through which it catalyzes levulinate ester cleavage allows for the selective removal of this γ-keto ester protecting group in the presence of other esters. The

removal of the *O*-levulinate esters in compound **11** was complete almost immediately after addition of the hydrazine acetate, and no corresponding product lacking the C-6 *O*-acetyl ester was detected.

2.3.2 Synthesis of Monosaccharide Substrate (2)

The synthesis of monosaccharide substrate **2** was accomplished in three steps from the protected MurNAc derivative **12** (Figure 2.8).[33] The known compound **12** was prepared from compound **5** using TMS-diazomethane to protect the carboxylic acid as a methyl ester. The protection of the free carboxylate as a methyl ester was required to increase solubility in methylene chloride during the subsequent regioselective reductive ring-opening of the benzylidene acetal with Et_3SiH and $PhBCl_2$. 4-*O*-Benzyl ether **13** was generated in good yield (89%) leaving a primary hydroxyl at C-6 for further functionalization. The regioselectivity of this reduction was confirmed by NMR spectroscopy in a similar manner to compound **7** (Section 2.3.1). A COSY spectrum of compound **13** revealed that the hydroxyl group proton was coupled to the two protons at the C-6 position and not to the proton at the C-4 position. The methyl ester was hydrolyzed with LiOH in a mixture of MeOH and dioxane to give the free carboxylic acid and the crude compound was *O*-acetylated at the C-6 position. A subsequent exchange from the triethylamine salt to the sodium salt gave monosaccharide substrate **2** in a 63% yield.

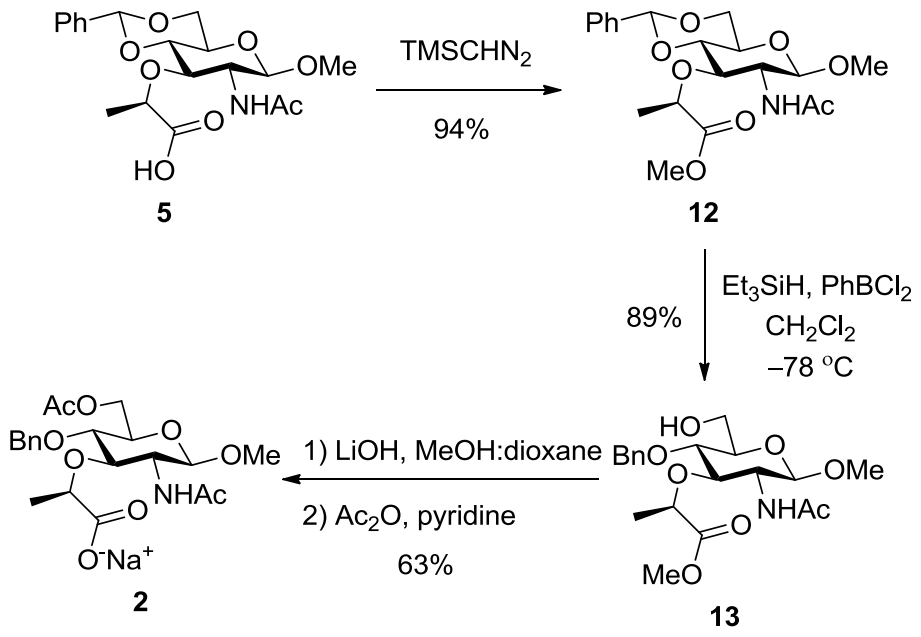

Figure 2.8 Synthesis of monosaccharide substrate (2).

2.4 Testing of Compounds 1 and 2 with Ape1

The testing of compounds **1** and **2** with Ape1 was performed by John M. Pfeffer at the University of Guelph. The esterase activity with the alternate substrates **1** and **2** was determined by incubating varying concentrations of the compounds with a truncated form of the Ape1 enzyme lacking the *N*-terminal signal peptide.[20] The enzymatic reactions were terminated with the addition of H_2SO_4, and the amount of acetate released was quantified using a coupled enzymatic assay. The initial velocity of Ape1-catalyzed acetate hydrolysis was measured at a series of substrate concentrations of **1** and **2** (Figures 2.9 and 2.10).

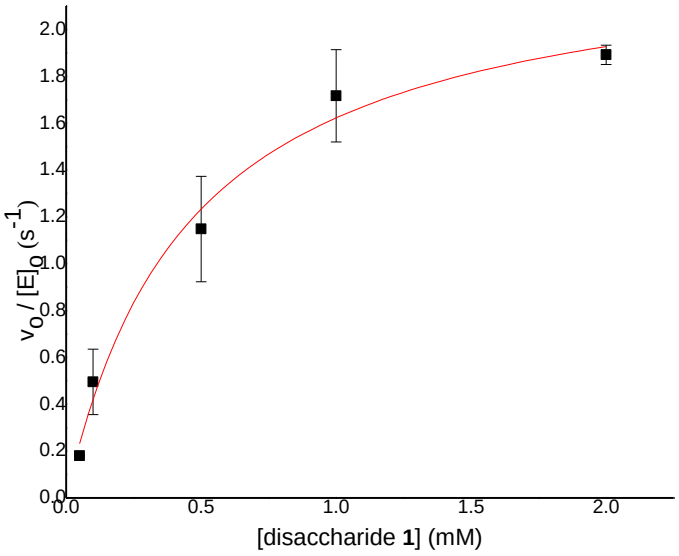

Figure 2.9 Plot of initial velocity vs. substrate concentration for Ape1's reaction with disaccharide substrate (1). Plotted data represent the average of three trials at each concentration point, and the error bars represent error associated with the rate measurement at each specific concentration.

It was determined that Ape1 follows Michaelis-Menten kinetics when acting on both the mono- and disaccharide substrates. The parameters k_{cat}, K_M, and k_{cat}/K_M were determined for both substrates and the results are outlined in Table 2.2. The kinetic parameters k_{cat} and K_M, and their associated errors, were determined by fitting the initial velocity data to the Michaelis-Menten equation using non-linear regression.

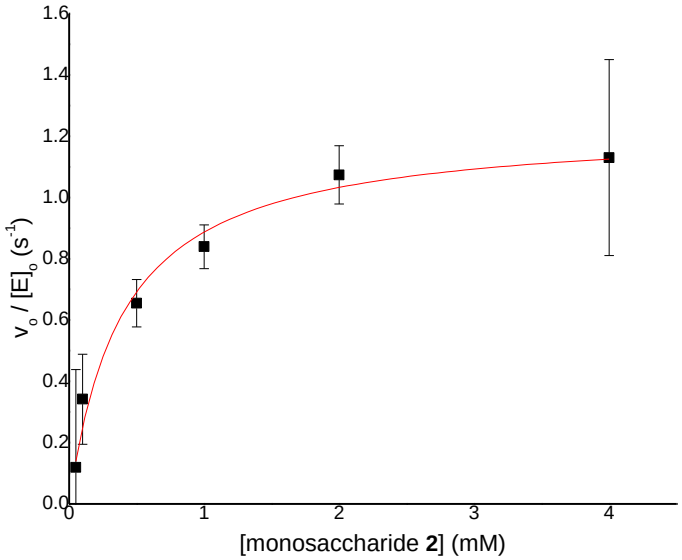

Figure 2.10 Plot of initial velocity vs. substrate concentration for Ape1's reaction with monosaccharide substrate (2). Plotted data represent the average of three trials at each concentration point, and the error bars represent error associated with the rate measurement at each specific concentration.

Both **1** and **2** served as substrates of Ape1, and their k_{cat}/K_M values were on the same order of magnitude as those previously reported for the highly-activated *p*-NP acetate (k_{cat} = 6.95 +/– 0.34 s^{-1}, k_{cat}/K_M = 1.31 x 10^4 $M^{-1}s^{-1}$).[20] Each substrate analogue bears an unactivated acetate ester at the C-6 position of the MurNAc residue, and their acceptance as substrates of Ape1 demonstrates that binding to a polymeric substrate is not a strict requirement for enzymatic activity. The disaccharide, **1**, possesses a β-(1→4)-linked GlcNAc moiety, as well as a methyl ester-protected L-alanine appended to its lactyl side chain. Its more complex design, with the inclusion of these recognition elements, was pursued with the goal of obtaining a substrate with a high level of activity. Indeed, compound **1** served as a slightly better substrate than **2**, but the small magnitude of this difference was perhaps the more

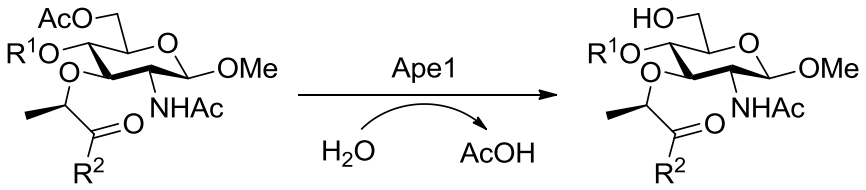

1: R^1 = GlcNAc, R^2 = L-Ala methyl ester
2: R^1 = Bn, R^2 = O^-Na^+

Substrate	k_{cat} (s^{-1})	K_M (mM)	k_{cat}/K_M ($M^{-1}s^{-1}$)
1	2.36 +/– 0.18	0.46 +/– 0.10	(5.1 +/– 1.7) x 10^3
2	1.24 +/– 0.07	0.39 +/– 0.08	(3.1 +/– 0.8) x 10^3

Table 2.2 Kinetic parameters for the Ape1-catalyzed hydrolysis of synthetic substrates 1 and 2.

interesting finding. Because Ape1 acts on polymeric *O*-acetylated peptidoglycan, it is not unreasonable to assume that disaccharide substrates would bind more tightly in the Ape1 active site than the corresponding monosaccharide units. Replacing the GlcNAc moiety with an *O*-benzyl ether at the C-4 position of MurNAc however, results in only a minimal decrease in the rate of Ape1 hydrolysis of the acetate ester. It is likely that the movement of the benzyl group from bulk water into the relatively hydrophobic pocket of the GlcNAc binding site is favored by the hydrophobic effect. This entropic driving force could compensate for any loss of enthalpic interactions due to the lack of the GlcNAc moiety. Compound **2** also lacks the L-alanine that was appended to the lactyl side chain in compound **1**. The small decrease in activity with this substrate also suggests that the peptides normally attached to the lactyl moiety are not required for binding in the Ape1 active site. These findings provide important information regarding the recognition elements required for productive binding, and bode well for the future development of substrates and inhibitors of

Ape1. The synthesis of monosaccharide **2** is more efficient and requires fewer synthetic transformations than that of disaccharide **1**, so the future development of Ape1 inhibitors will focus on monosaccharide scaffolds.

2.5 Synthesis of Phosphate Inhibitor (15) and Testing with Ape1

Following the design, synthesis, and testing of compounds **1** and **2** with Ape1, we began work on the development of small-molecule inhibitors of the enzyme. Because previous experiments have suggested that Ape1 is an essential enzyme in bacteria that contain *O*-acetylated peptidoglycan and because of the enzyme's periplasmic localization outside of the cytoplasm, inhibitors of Ape1 present attractive antibiotic candidates.[15, 20] As monosaccharide compound **2** possessed a similar level of activity as a substrate of Ape1 when compared to disaccharide compound **1**, we chose to approach the design and synthesis of inhibitors using the monosaccharide scaffolds due to their ease of synthesis.

We chose the phosphate-containing compound **15** (Figure 2.11) as our first target because our existing methodology can easily be adapted for its synthesis. Compound **15** contains a free phosphate group at the C-6 position on the MurNAc monosaccharide scaffold in place of the *O*-acetyl ester that is normally found in *O*-acetylated peptidoglycan. This phosphate group contains a negative charge at a tetrahedral center and we predicted that this would serve to mimic the negative charge found in the oxyanionic intermediate of the enzyme-catalyzed acetate hydrolysis reaction. We hoped that this tetrahedral negative charge would serve to capture some of the transition-state/intermediate binding energy and would make a good reversible non-covalent inhibitor of the enzyme. Although it is conceivable that compound **15** could act as a substrate for Ape1 through the transfer of the phosphate group

onto the nucleophilic serine residue, such a process would likely be very slow due to the poor electrophilicity of an anionic phosphate.

The synthesis of compound **15** began with the intermediate **13** used in the synthesis of monosaccharide substrate **2** (Figure 2.11). The hydroxyl group of the monosaccharide was phosphorylated using a phosphoramidite coupling reagent and subsequently oxidized using H_2O_2 to generate the phosphate ester **14** in 80% yield. The benzyl groups on the phosphate ester were then removed via hydrogenolysis using 10% Pd/C as catalyst. The removal of the phosphate benzyl groups was easily accomplished in the presence of the less labile *O*-benzyl ether at the C-4 position through the use of mild hydrogenolysis conditions (1 atm H_2, rt, 5 min reaction time). After hydrogenolysis of the benzyl groups was finished, the crude product was purified using a column of AG-1X8 resin (formate form) and subsequently exchanged into the sodium salt using Amberlite IRC-50 (sodium form). The solution was frozen and lyophilized to give the sodium salt of compound **15** in 75% yield.

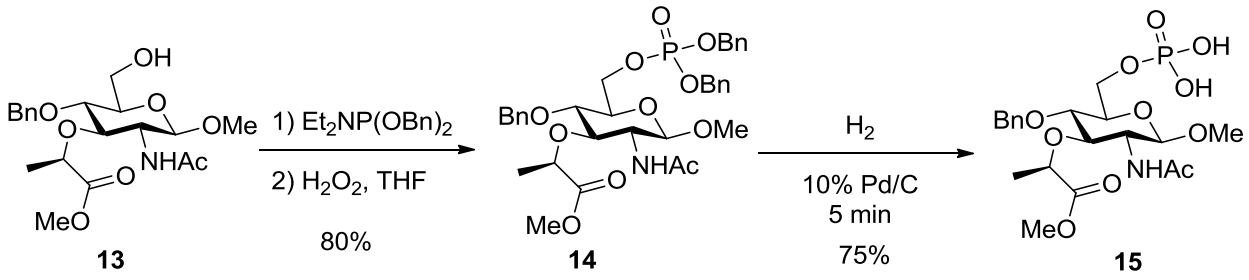

Figure 2.11 Synthesis of monosaccharide phosphate (15).

Compound **15** was tested as an inhibitor of Ape1 by John M. Pfeffer at the University of Guelph. The water-soluble chromogenic compound *p*-NP acetate was used as the test substrate for these reactions and compound **15** was added at varying concentrations to determine its effect on Ape1-catalyzed acetate hydrolysis. At a substrate concentration of 0.5

mM (near K_M) the concentration of inhibitor **15** required to reduce the rate of enzyme-catalyzed acetate hydrolysis by 50% (IC_{50}) was 0.2 mM. Since the concentration of **15** required to reduce Ape1 activity was very similar to the K_M of Ape1 substrates, we can conclude that compound **15** was not a very effective inhibitor of the enzyme.

Potent inhibitors of enzymes are typically effective at concentrations that are orders of magnitude smaller than that of the natural substrate. This is because inhibitors typically mimic the properties of the transition-state/intermediate of the enzymatic reaction and are consequently bound tightly in the enzyme active site. Although compound **15** contains a negative charge at a tetrahedral center that serves to mimic the oxyanionic intermediate in the Ape1-catalyzed reaction, it is likely that the significant steric bulk introduced by the phosphate group interferes with the serine hydroxyl of the catalytic triad and prevents the proper positioning of this functional group within the active site.

2.6 Summary

In this chapter, we have detailed the design, synthesis, and testing of the water-soluble 6-*O*-acetylated peptidoglycan substrate analogues **1** and **2** of the *O*-acetylpeptidoglycan esterase Ape1. Both **1** and **2** served as substrates of Ape1, and interestingly, the substitution of the GlcNAc residue for an *O*-benzyl ether at the C-4 position of MurNAc did not greatly affect the Ape1 activity on monosaccharide substrate **2**. In addition, the removal of the L-Ala residue attached to the D-lactyl ether on MurNAc did not result in a significant decrease in Ape1 activity, indicating that the peptide side chain of peptidoglycan may not play a crucial role in substrate binding and recognition. These results validate the use of both MurNAc monosaccharides, and MurNAc-GlcNAc disaccharides as templates for Ape1 substrate and inhibitor design. This is an important finding as it

demonstrates that the catalytic prowess of Ape1 is not dependent on its binding to a polymeric substrate. This ensures that small molecule transition state/intermediate analogues can also capture the transition state binding energy of Ape1 and potentially serve as potent inhibitors. The ability of Ape1 to catalyze acetate hydrolysis of monosaccharide substrates at roughly the same rate as disaccharide substrates bodes well for inhibitor design; the synthesis of disaccharide inhibitors is significantly more complex, challenging, and costly than the synthesis of their monosaccharide counterparts, and presents a serious obstacle in the development of potential antibacterials.

Initial efforts towards the synthesis of monosaccharide inhibitors of Ape1 have also been detailed in this chapter. The 6-*O*-phosphorylated monosaccharide **15** was synthesized using methods adapted from our synthesis of monosaccharide substrate **2**. This compound however, did not serve as a strong inhibitor of Ape1 when tested using *in vitro* assays for enzymatic acetate hydrolysis. This indicates that the phosphate functionality is not a good mimic of the tetrahedral intermediate being formed during catalysis.

2.7 Future Directions

Future work regarding Ape1 will focus upon the design and synthesis of potential inhibitors of the enzyme. This undertaking will be aided by the abundance of literature available outlining mechanism-based strategies for the inhibition of serine proteases and esterases. The conserved catalytic triad of Asp-His-Ser found in this class of enzymes provides a target that has a very well-characterized mechanism of action. Our synthetic route to monosaccharide substrate **2** and phosphate inhibitor **15** introduces the acetate or phosphate group, respectively, during the late stages of the synthesis and can be easily adapted towards the installation of a variety of different functional groups at the C-6 position. Therefore, the

synthesis of a wide variety of potential inhibitors of Ape1 could be easily accomplished using this synthetic scheme.

Initial targets will attempt to employ functional groups that have been shown to act as potent reversible covalent inhibitors of serine proteases and esterases.[34, 35] The potential inhibitors **16** and **17** contain aldehyde and boronic acid functional groups, respectively, in the place of the normal acetate ester (Figure 2.12). Upon binding to the Ape1 active site, the serine nucleophile will be poised to form a covalent bond to the aldehyde carbonyl (compound **16**) or the vacant orbital on boron (compound **17**). The formation of this

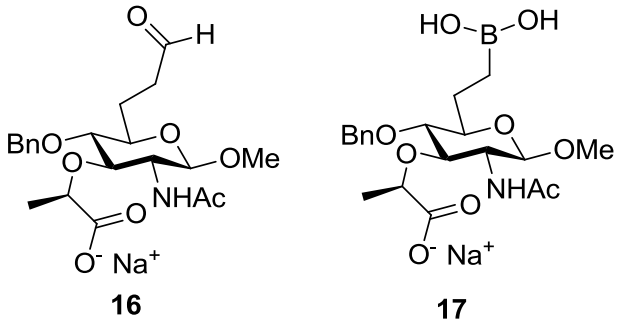

Figure 2.12 Potential reversible covalent inhibitors of Ape1.

covalent bond will generate a negative charge on the carbonyl oxygen or boron atom of the inhibitors that will mimic the tetrahedral oxyanion intermediate formed during catalysis (Figure 2.13). Although the formation of this covalent bond is reversible, the use of these functional groups as inhibitors of serine proteases has ample literature precedence and represents an excellent potential strategy for mechanism-based inhibition of the Ape1 enzyme. Once targets are validated as potent Ape1 inhibitors using *in vitro* assays, they will be tested for bacteriocidal activity against *N. gonorrhoeae* and other pathogenic bacteria that

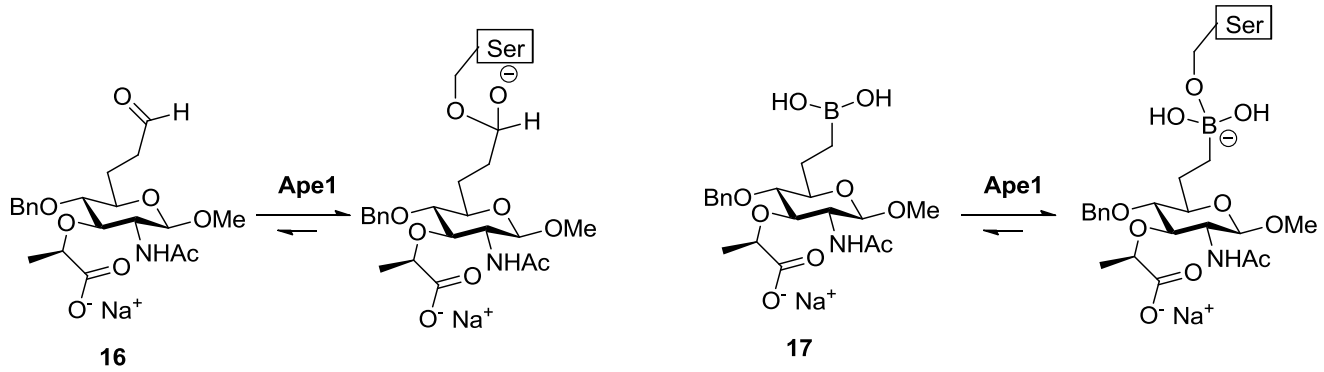

Figure 2.13 Proposed mode of action of reversible covalent Ape1 inhibitors (16) and (17).

are known to *O*-acetylate their peptidoglycan. These results will eventually serve to determine Ape1's viability as an antibacterial target.

Potent inhibitors of Ape1 could also be used in the future as aids in the structural characterization of Ape1. No crystal structure of Ape1 is currently available, hampering detailed analysis of the enzyme active site. A crystal structure of Ape1 with a bound substrate analogue or inhibitor would enable the definitive assignment of active site acid/base residues involved in catalysis. In addition, the analysis of the substrate binding pocket of the enzyme would provide a clearer picture of the elements that are most important for substrate recognition and greatly facilitate the design of future inhibitors.

2.8 Experimental Procedures

2.8.1 Materials and General Methods

Chemicals and resins were purchased from Alfa Aesar or Sigma-Aldrich and used without further purification unless otherwise noted. Silica gel chromatography was performed using Silica Gel SiliaFlash F60 (230-400 mesh, Silicycle). Pyridine, triethylamine,

methylene chloride, and methanol were distilled over CaH_2 under an atmosphere of N_2. AG-1X8 resin (100-200 mesh, formate form) was purchased from Bio-Rad Laboratories.

^1H NMR spectra were obtained on Bruker AV300 or AV400 NMR spectrometers at field strengths of 300 or 400 MHz, respectively. ^{13}C NMR spectra were obtained on Bruker AV300 or AV400 NMR spectrometers at field strengths of 75 or 100 MHz, respectively. Proton-decoupled ^{31}P NMR spectra were obtained on Bruker AV300 or AV400 NMR spectrometers at field strengths 121.5 or 162 MHz, respectively. High resolution mass spectrometry was performed by electrospray ionization (ESI-MS) using an Esquire LC mass spectrometer at the UBC Mass Spectrometry Facility. Neutral compounds were detected as positive ions, and negatively charged compounds were detected as negative ions.

2.8.2 Synthesis of Disaccharide (1)

2.8.2.1 Methyl 2-acetamido-2-deoxy-β-D-glucopyranoside (3)

The conversion of GlcNAc into the β-methyl glycoside **3** was accomplished in two steps using a literature procedure.[29] A suspension of GlcNAc (15.3 g, 69.2 mmol) in 500 mL of acetone was prepared by first partially drying the acetone over K_2CO_3 and the filtering it into a flame-dried flask containing the GlcNAc. $FeCl_3$ (22.25 g, 137.2 mmol) was added, and the mixture was refluxed for 45 min at 75 ^oC under an argon atmosphere. The reaction mixture was cooled in an ice bath and a mixture of acetone (200 mL) and diethylamine (54 mL) was added. A solution of Na_2CO_3 (32.0 g) in H_2O was added slowly via addition funnel and the mixture was vigourously stirred to prevent solidification. The brown sludge was transferred to a separatory funnel and extracted three times with Et_2O. The ethereal layers were pooled, dried over $MgSO_4$, and filtered. The solvents were removed *in vacuo* to give the slightly crude oxazoline as a brown syrup (8.9 g). ^1H NMR spectroscopy and MS data of

this compound matched literature values and the crude compound was used without further purification.

The crude oxazoline was dissolved in anhydrous MeOH and *p*-toluenesulfonic acid (1.86 g, 10.8 mmol) was added, and the resultant mixture stirred overnight at rt. After TLC analysis (6:3:1 EtOAc:MeOH:H_2O) showed the consumption of starting material, the reaction was neutralized with NEt_3, and the solvents removed *in vacuo*. The residue was washed multiple times with CH_2Cl_2 and filtered to give compound **3** as an off-white solid (6.6 g, 41%). ^{1}H NMR spectroscopy and MS data were identical to that previously reported in the literature.[29]

2.8.2.2 Methyl 2-acetamido-4,6-*O*-benzylidene-2-deoxy-β-D-glucopyranoside (4)

To a solution of **3** (4.28 g, 18.2 mmol) in DMF was added benzaldehyde dimethyl acetal (8.2 mL, 54.6 mmol), and *p*-toluenesulfonic acid monohydrate (1.73 g, 9.1 mmol). The mixture was heated at 55 ^{o}C under vacuum produced by a water aspirator for 1 h before another 0.9 g of *p*-toluenesulfonic acid monohydrate was added. The reaction was stirred for an additional 50 min, after which TLC analysis (9:1 CH_2Cl_2:MeOH) confirmed the disappearance of starting material. The reaction was cooled down to rt and quenched with 2.5 mL NEt_3. The solvents were removed *in vacuo* and the residue was stirred vigorously as a suspension in equal volumes of hexanes and MeOH. The suspension was filtered and the solid washed with boiling hexanes:CH_2Cl_2:Et_2O (10:1:2) to give the known compound **4** as a white solid (4.96 g, 84%). ^{1}H NMR spectroscopy and MS data were identical to that previously reported in the literature.[30]

2.8.2.3 Methyl 2-acetamido-4,6-*O*-benzylidene-2-deoxy-3-*O*-((*R*)-1-carboxyethyl)-β-D-glucopyranoside (5)

To a solution of **4** (3.88 g, 12.0 mmol) in dioxane was added 2.15 g of sodium hydride (60% dispersion in mineral oil), and the mixture stirred under argon atmosphere at 95 °C for 1 h with a water-cooled condenser. The solution was cooled to 65 °C and (*S*)-2-chloropropionic acid (5.13 mL, 60 mmol) was added. Stirring was continued for 30 min before an additional 1.9 g of sodium hydride (60% dispersion in mineral oil) was added. Additional dioxane was also added to facilitate stirring and the temperature was increased to 75 °C and the reaction left to stir overnight under an argon atmosphere. After TLC analysis (9:1 CH_2Cl_2:MeOH) confirmed the consumption of starting material, the solution was cooled to rt after which H_2O (300 mL) was added and the majority of the dioxane was removed *in vacuo*. The aqueous solution was acidified with concentrated HCl and then extracted three times with $CHCl_3$. A small amount of methanol was added to facilitate dissolving before the organic extracts were pooled, dried over Na_2SO_4, and filtered. The solvents were removed *in vacuo* and the residual solid was rinsed with hexanes and subsequently recrystallized in two batches with hot MeOH to give the known compound **5** (3.93 g, 82%) as a white solid. ^{1}H NMR spectroscopy and MS data were identical to that previously reported in the literature.[30]

2.8.2.4 Methyl 4,6-*O*-benzylidene-β-D-*N*-acetylmuramylpyranoside-L-alanine methyl ester (6)

Compound **5** (2.9 g, 7.34 mmol) was dissolved in 160 mL anhydrous DMF, and HOBt (1.35 g, 8.81 mmol), EDC (1.69 g, 8.81 mmol), and 1.25 mL NEt_3 were added. The resultant mixture was allowed to stir for 5 min at rt before L-alanine methyl ester hydrochloride (1.23 g, 8.81 mmol) and an additional 1.25 mL of NEt_3 were added. The

reaction was allowed to stir overnight at room temperature under an argon atmosphere, after which it was judged complete by TLC analysis (9:1 CH_2Cl_2:MeOH). The mixture was diluted with CH_2Cl_2, and washed consecutively with 5% $KHSO_4$, sat. $NaHCO_3$, sat. NaCl, and H_2O. The organic layer was separated, dried over $MgSO_4$, and filtered. The solvents were removed *in vacuo* and the solid purified via silica gel chromatography (40:1 CH_2Cl_2:MeOH) to give product **6** (3.37 g, 7.02 mmol, 95%) as a white solid. ^{1}H NMR (400 MHz, $CDCl_3$) δ ppm 7.48-7.34 (m, 5H), 7.18 (d, 1H, J = 6.8 Hz), 6.09 (d, 1H, J = 8.0 Hz), 5.55 (s, 1H), 4.78 (d, 1H, J = 8.0 Hz), 4.47 (qd, 1H, J = 7.2 Hz), 4.36 (dd, 1H, J = 4.8 Hz, 10.4 Hz), 4.19 (q, 1H, J = 6.8 Hz), 4.13 (dd, 1H, J = 9.2 Hz), 3.79 (dd, 1H, J = 10.4 Hz), 3.76 (s, 3H), 3.61 (dd, 1H, J = 9.2 Hz), 3.54-3.47 (m, 5H), 1.99 (s, 3H), 1.43 (d, 3H, J = 7.2 Hz), 1.39 (d, 3H, J = 6.4 Hz); ^{13}C NMR (100 MHz, $CDCl_3$) δ ppm 173.7, 173.1, 171.3, 137.2, 129.3, 128.5 (2 x C), 126.1 (2 x C), 101.6, 101.5, 82.0, 78.6, 78.2, 68.9, 66.0, 57.7, 57.2, 52.7, 48.2, 23.9, 19.6, 18.3; HRMS (ESI) *m/z* calcd for $[C_{23}H_{32}N_2O_9Na]^+$, 503.2006, found 503.1994.

2.8.2.5 Methyl 6-*O*-benzyl-β-D-*N*-acetylmuramylpyranoside-L-alanine methyl ester (7)

Molecular sieves (4 Å) were added to a solution of compound **6** (247 mg, 0.514 mmol) in 40 mL of distilled CH_2Cl_2 and the mixture stirred under an argon atmosphere for 1 h. The reaction flask was cooled to −78 ^{o}C and Et_3SiH (0.25 mL, 1.54 mmol) was added, followed 5 min later by TfOH (0.15 mL, 1.75 mmol). The mixture was maintained at −78 ^{o}C while stirring and was judged complete after 1.5 h by TLC analysis (9:1 CH_2Cl_2:MeOH). NEt_3 (2 mL) and MeOH (2 mL) were added and the solution diluted with $CHCl_3$ and filtered through a pad of Celite. The filtrate was washed consecutively with sat. $NaHCO_3$, sat. NaCl,

and H_2O. The organic layer was dried over $MgSO_4$, filtered, and the solvents removed *in vacuo*. The residue was purified via silica gel chromatography (CH_2Cl_2, then 39:1 CH_2Cl_2:MeOH, then 9:1 CH_2Cl_2:MeOH) to give compound **7** (170 mg, 0.353 mmol, 68%) as a white foam. ^{1}H NMR (400 MHz, $CDCl_3$) δ ppm 7.38-7.24 (m, 5H), 6.90 (d, 1H, J = 8.8 Hz), 4.61-4.53 (m, 2H), 4.46-4.37 (m, 2H), 4.25 (q, 1H, J = 6.8 Hz), 3.86-3.70 (m, 4H), 3.70 (s, 3H), 3.66-3.46 (m, 3H), 3.43 (s, 3H), 2.64 (br s, 1H), 1.94 (s, 3H), 1.42 (d, 3H, J = 6.8 Hz), 1.38 (d, 3H, J = 6.8 Hz); ^{13}C NMR (100 MHz, $CDCl_3$) δ ppm 173.9(6), 173.5(3), 171.5, 138.0, 128.6 (2 x C), 127.9(3), 127.8(7) (2 x C), 101.9, 82.2, 77.0, 74.6, 73.8, 71.5, 70.5, 56.7, 54.8, 52.6, 48.3, 23.6, 19.6, 17.6; HRMS (ESI) *m/z* calcd for $[C_{23}H_{34}N_2O_9Na]^+$, 505.2162, found 505.2166.

2.8.2.6 Methyl 3,4,6-tri-*O*-acetyl-2-deoxy-2-trichloroacetamido-β-D-glucopyranosyl-(1→4)-6-*O*-benzyl-β-D-*N*-acetylmuramylpyranoside-L-alanine methyl ester (9)

To a solution of acceptor **7** (330 mg, 0.684 mmol) and donor **8** (666 mg, 1.13 mmol) in 20 mL distilled CH_2Cl_2 was added 4 Å molecular sieves and the resultant mixture stirred under argon atmosphere for 1 h. The mixture was cooled to 0 ^{o}C, and TMSOTf (0.19 mL, 1.03 mmol) was added. After stirring for 1 h at 0 ^{o}C, the ice bath was removed and the mixture warmed to rt. The reaction was judged complete by monitoring the disappearance of acceptor **7** by TLC analysis (EtOAc), and was subsequently quenched with 0.4 mL NEt_3. The mixture was diluted with CH_2Cl_2, filtered through a pad of Celite and the solvents removed *in vacuo*, leaving a dark brown foam. Silica gel chromatography (EtOAc, then 9:1 EtOAc:MeOH) gave compound **9** (355 mg, 0.388 mmol, 56% based on acceptor) as a white solid. ^{1}H NMR (400 MHz, MeOD) δ ppm 7.44-7.28 (m, 5H), 5.40 (dd, 1H, J = 9.2 Hz, 10.4

Hz), 4.98 (dd, 1H, *J* = 9.6 Hz), 4.86 (obscured by solvent, 1H), 4.67 (dd, 1H, *J* = 11.6 Hz), 4.64 (dd, 1H, *J* = 11.6 Hz), 4.39 (q, 1H, *J* = 7.2 Hz), 4.33 (dd, 1H, *J* = 4.0 Hz, 12.4 Hz), 4.27 (d, 1H, *J* = 8.4 Hz), 4.23 (q, 1H, *J* = 6.8 Hz), 4.02-3.94 (m, 2H), 3.89-3.76 (m, 4H), 3.73 (s, 3H), 3.58-3.45 (m, 3H), 3.43 (s, 3H), 2.02-1.96 (m, 9H), 1.92 (s, 3H), 1.46-1.41 (m, 6H); ^{13}C NMR (100 MHz, MeOD) δ ppm 174.1, 173.2, 172.2, 170.9, 170.3, 170.0, 163.0, 138.5, 128.2 (2 x C), 127.6(4) (2 x C), 127.5(7), 102.1, 98.6, 92.5, 79.5, 78.0, 75.0, 74.4, 73.0, 71.5, 71.4, 68.8, 68.3, 61.4, 56.5, 55.7, 54.8, 51.6, 48.0, 21.8, 19.5, 19.3 (2 x C), 17.8, 16.3; HRMS (ESI) *m/z* calcd for $[C_{37}H_{50}N_3Cl_3O_{17}Na]^+$, 936.2104, found 936.2111.

2.8.2.7 Methyl 3,4,6-tri-*O*-acetyl-2-acetamido-2-deoxy-β-D-glucopyranosyl-(1→4)-6-*O*-benzyl-β-D-*N*-acetylmuramylpyranoside-L-alanine methyl ester (10)

Disaccharide **9** (270 mg, 0.295 mmol) and AIBN (10 mg, 0.059 mmol) were dissolved in 10 mL DMA and the resultant solution stirred at 90 ^{o}C for 1 h with argon gas bubbling directly through the mixture. Tributyltin hydride (0.63 mL, 2.36 mmol) and additional AIBN (3 mg, 0.0183 mmol) were added to the reaction mixture and the stirring was continued at 90 ^{o}C. The reaction progress was monitored for the disappearance of starting material by TLC analysis (9:1 CH_2Cl_2:MeOH), and was judged complete after approximately 2 h. The solvents were removed *in vacuo* and the residue purified by silica gel chromatography (EtOAc, then 19:1 EtOAc:MeOH, then 9:1 EtOAc:MeOH) to give compound **10** (190 mg, 0.234 mmol, 79%) as a white solid. ^{1}H NMR (400 MHz, MeOD) δ ppm 7.45-7.29 (m, 5H), 5.20 (dd, 1H, *J* = 9.2 Hz, 10.4 Hz), 4.94 (dd, 1H, *J* = 9.6 Hz), 4.73-4.59 (m, 3H), 4.40 (q, 1H, *J* = 7.2 Hz), 4.32-4.20 (m, 3H), 4.00-3.90 (m, 2H), 3.88-3.79 (m, 4H), 3.73 (s, 3H), 3.53-3.40 (m, 3H), 3.44 (s, 3H), 2.01-1.96 (m, 9H), 1.93 (s, 3H), 1.91 (s, 3H), 1.44-1.39 (m, 6H); ^{13}C NMR (100 MHz, MeOD) δ ppm 174.2, 173.3, 172.4, 172.2,

170.9(7), 170.5(2), 170.0(0), 138.5, 128.3 (2 x C), 127.7(1) (2 x C), 127.6(3), 102.3, 99.5, 79.3, 77.7, 75.1, 74.7, 73.0, 72.4, 71.4, 68.8(2), 68.4(7), 61.5, 55.7, 54.6(9), 54.5(5), 51.7, 48.0, 21.8(5), 21.6(2), 19.5(0), 19.3(3), 19.2(9), 17.7, 16.3; HRMS (ESI) *m/z* calcd for $[C_{37}H_{54}N_3O_{17}]^+$, 812.3453 , found 812.3436.

2.8.2.8 Methyl 2-acetamido-2-deoxy-3,4,6-tri-*O*-levulinoyl-β-D-glucopyranosyl-(1→4)-6-*O*-benzyl-β-D-*N*-acetylmuramylpyranoside-L-alanine methyl ester (11)

Disaccharide **10** (42 mg, 0.052 mmol) was dissolved in 10 mL distilled MeOH in a flame-dried round-bottom flask and NaOMe was added (108 mg, 2.0 mmol). The reaction mixture was stirred at rt under an argon atmosphere for 20 min, after which it was judged complete by TLC analysis (9:1 CH_2Cl_2:MeOH). The reaction was neutralized with Amberlite IR-120(H^+), filtered, and concentrated *in vacuo*. The residue was dissolved in 9:1 CH_2Cl_2:MeOH, filtered through a silica gel plug, and concentrated *in vacuo* to give the deacetylated product (30 mg) that was used without further purification.

Levulinic acid (0.015 mL, 0.144 mmol), and DMAP (17 mg, 1.38 mmol) were dissolved in 5 mL of distilled CH_2Cl_2, and the mixture was cooled to 0 ^oC under an argon atmosphere. DIPC (0.023 mL, 0.144 mmol) was added and the mixture stirred for 5 min before a solution of the deacetylated disaccharide (30 mg) in 2 mL CH_2Cl_2 was added. The mixture was allowed to warm to rt and was stirred overnight under an argon atmosphere, after which TLC analysis (9:1 CH_2Cl_2:MeOH) confirmed the disappearance of the starting material. The solution was diluted with EtOAc and filtered through a plug of silica; the plug was then flushed with 200 mL of 9:1 CH_2Cl_2:MeOH, and the eluent concentrated *in vacuo*. The residue was subjected to silica gel chromatography (40:1 CH_2Cl_2:MeOH then 20:1 CH_2Cl_2:MeOH) to give the levulinate-protected disaccharide **11** (37.8 mg, 0.0386 mmol,

75%) as a white solid. ^{1}H NMR (400 MHz, MeOD) δ ppm 7.44-7.29 (m, 5H), 5.21 (dd, 1H, *J* = 9.2 Hz, 10.4 Hz), 4.92 (dd, 1H, *J* = 9.2 Hz, 10.4 Hz), 4.71-4.58 (m, 3H), 4.41 (q, 1H, *J* = 7.2 Hz), 4.28-4.19 (m, 3H), 4.01 (dd, 1H, *J* = 1.6 Hz, 12 Hz), 3.93 (dd, 1H, *J* = 8.4 Hz), 3.88-3.78 (m, 4H), 3.73 (s, 3H), 3.52-3.42 (m, 3H), 3.43 (s, 3H), 2.84-2.66 (m, 6H), 2.58-2.42 (m, 6H), 2.16-2.12 (m, 9H), 1.93 (s, 3H), 1.92 (s, 3H), 1.43-1.37 (m, 6H); ^{13}C NMR (100 MHz, MeOD) δ ppm 207.8, 207.6, 207.5, 174.1, 173.3, 172.6, 172.4(6), 172.4(1), 172.1, 171.9, 138.5, 128.3 (2 x C), 127.8 (2 x C), 127.6, 102.3, 99.6, 79.0, 77.4, 75.3, 74.7, 73.2, 72.3, 71.7, 69.1, 68.9, 62.1, 55.6, 54.7, 54.2, 51.6, 48.0, 47.7, 37.5, 37.2(8), 37.2(4), 28.4, 28.2, 27.7(8), 27.7(2), 27.6(8), 21.7(7), 21.7(2), 17.8, 16.3; HRMS (ESI) *m/z* calcd for $[C_{46}H_{65}N_3O_{20}Na]^+$, 1002.4059, found 1002.4034.

2.8.2.9 Methyl 2-acetamido-2-deoxy-β-D-glucopyranosyl-(1→4)-6-*O*-acetyl-β-D-*N*-acetylmuramylpyranoside-L-alanine methyl ester (1)

Disaccharide **11** (22 mg, 0.022 mmol) was dissolved in 10 mL distilled MeOH and 10% Pd/C (20 mg) was added. The reaction flask was placed under a H_2 atmosphere (1 atm) and the reaction stirred at rt until TLC analysis (9:1 CH_2Cl_2:MeOH) indicated that the starting material was completely consumed and the hydrogenolysis was complete. The mixture was filtered through a pad of Celite and the solvents removed *in vacuo*. The crude residue was carried on without further purification.

The crude debenzylated disaccharide was dissolved in 5 mL of distilled pyridine and cooled to 0 °C before acetic anhydride (0.5 mL, 5.3 mmol) was added. The reaction mixture was allowed to warm to rt and was stirred under a blanket of argon. After 2.5 h, TLC analysis (9:1 CH_2Cl_2:MeOH) showed the disappearance of the starting material and the appearance of a new spot at a higher R_f. Toluene was added and the mixture co-evaporated

in vacuo; this procedure was repeated three times to ensure all of the residual pyridine was removed from the reaction mixture. Acetylation of the disaccharide was confirmed by MS and ^{1}H NMR spectroscopy (data not shown) and the crude product was used without further purification.

The crude 6-*O*-acetylated disaccharide was dissolved in 5 mL of distilled pyridine and hydrazine acetate (12 mg, 0.13 mmol) was added. The reaction mixture was monitored by TLC analysis (9:1 CH_2Cl_2:MeOH) for the disappearance of starting material and was judged complete after 10 min. The reaction was diluted with toluene and the mixture co-evaporated to remove any residual pyridine. Silica gel chromatography (20:1 CH_2Cl_2:MeOH then 9:1 CH_2Cl_2:MeOH) gave compound **1**, which was dissolved in water, frozen, and lyophilized to produce a white solid (5.6 mg, 0.0088 mmol, 39%). ^{1}H NMR (400 MHz, D_2O) δ ppm 4.55 (m, 1H), 4.48-4.35 (m, 4H), 4.19 (dd, 1H, J = 5.2 Hz, 12.0 Hz), 3.98-3.92 (m, 2H), 3.84-3.72 (m, 4H), 3.79 (s, 3H), 3.64-3.52 (m, 2H), 3.48 (s, 3H), 3.44-3.38 (m, 2H), 2.17 (s, 3H), 2.06 (s, 3H), 1.98 (s, 3H), 1.46 (d, 3H, J = 6.8 Hz), 1.41 (d, 3H, J = 6.8 Hz); ^{13}C NMR (100 MHz, D_2O) δ ppm 175.3, 175.1, 174.8, 174.4, 173.9, 102.0, 100.5, 79.4, 78.3, 76.4, 74.9, 73.6, 72.8, 70.4, 62.8, 61.3, 57.2, 56.1, 54.6, 53.2, 48.7, 22.3(7), 22.3(0), 20.4, 18.3, 16.1; HRMS (ESI) *m/z* calcd for $[C_{26}H_{43}N_3O_{15}Na]^+$, 660.2592, found 660.2582.

2.8.3 Synthesis of Monosaccharide (2)

2.8.3.1 Methyl 2-acetamido-4,6-*O*-benzylidene-2-deoxy-3-*O*-((*R*)-1-(methoxycarbonyl)ethyl)-β-D-glucopyranoside (12)

Compound **5** (138 mg, 0.349 mmol) was dissolved in 72 mL of an 8:1 mixture of MeOH:toluene. TMS-diazomethane (2M solution in diethyl ether) was added dropwise to the reaction mixture until the yellow colour in the solution persisted. The solution was

stirred at rt for 1.5 h, after which the reaction was judged complete by TLC analysis (6:3:1 EtOAc:MeOH:H_2O). The solvents were removed *in vacuo* and the crude methyl ester subjected to silica gel chromatography (CH_2Cl_2 then 9:1 CH_2Cl_2: MeOH), affording compound **12** as a white solid (134 mg, 0.328 mmol, 94%). MS and ^{1}H NMR spectroscopy were used to confirm the identity of the known compound.[33]

2.8.3.2 Methyl 2-acetamido-4-*O*-benzyl-2-deoxy-3-*O*-((*R*)-1-(methoxycarbonyl)ethyl)-β-D-glucopyranoside (13)

The known methyl ester-protected MurNAc derivative **12** (170 mg, 0.415 mmol) was dissolved in distilled CH_2Cl_2 and 4 Å molecular sieves were added. The resultant mixture was stirred under an argon atmosphere for 1 h and was subsequently cooled to −78 ^{o}C. Et_3SiH (0.33 mL, 2.08 mmol) was first added, followed 5 min later by $PhBCl_2$ (0.27 mL, 2.08 mmol) and the reaction was stirred at −78 ^{o}C. The reaction was monitored for the disappearance of starting material by TLC analysis (9:1 CH_2Cl_2: MeOH) and was quenched with 1 mL each of NEt_3 and MeOH after it was judged complete. The mixture was then diluted with $CHCl_3$ and washed with saturated $NaHCO_3$. The organics were dried over $MgSO_4$, filtered, and then concentrated *in vacuo*. The crude product was purified via silica gel chromatography (40:1 CH_2Cl_2:MeOH) to give compound **13** (152 mg, 0.37 mmol, 89%) as a white solid. ^{1}H NMR (400 MHz, $CDCl_3$) δ ppm 7.38-7.28 (m, 5H), 6.93 (d, 1H, J = 5.6 Hz), 4.71 (m, 2H), 4.57 (q, 1H, J = 6.8 Hz), 4.41 (d, 1H, J = 7.2 Hz), 3.87 (m, 1H), 3.76-3.59 (m, 4H), 3.71 (s, 3H), 3.48 (s, 3H), 3.37-3.31 (m, 1H), 2.32 (br s, 1H), 2.02 (s, 3H), 1.35 (d, 3H, J = 6.8 Hz); ^{13}C NMR (100 MHz, $CDCl_3$) δ ppm 175.2, 171.9, 137.7, 128.7(7) (2 x C), 128.2(2), 127.9(8) (2 x C), 103.0, 79.4(0), 79.2(0), 75.5 (2 x C), 75.1, 61.6, 57.1, 55.7, 52.2, 23.7, 19.3; HRMS (ESI) *m/z* calcd for $[C_{20}H_{29}NO_8Na]^+$, 434.1791, found 434.1782.

2.8.3.3 Methyl 2-acetamido-6-*O*-acetyl-4-*O*-benzyl-3-*O*-((*R*)-1-carboxyethyl)-2-deoxy-β-D-glucopyranoside monosodium salt (2)

Compound **13** (152 mg, 0.369 mmol) was dissolved in 25 mL (1:1 dioxane:MeOH) and 1M LiOH was added until the solution reached a pH of 10. The reaction mixture was left to stir overnight at rt, after which it was judged complete by TLC analysis (6:3:1 EtOAc:MeOH:H_2O). The mixture was neutralized by the addition of Amberlite IR-120(H^+), filtered, and then concentrated *in vacuo*. The crude solid was re-dissolved in H_2O, washed with CH_2Cl_2, and the aqueous layer concentrated *in vacuo* and used without further purification.

The crude carboxylic acid was dissolved in 20 mL distilled pyridine and the resulting solution cooled to 0 °C. Acetic anhydride (1.0 mL, 10.6 mmol) was added and the mixture was allowed to warm to rt before being left to stir overnight under an argon atmosphere. After TLC analysis of the reaction mixture (6:3:1 EtOAc:MeOH:H_2O) confirmed the disappearance of starting material, toluene was added and the solvents co-evaporated *in vacuo*. The addition of toluene and its removal *in vacuo* was repeated several times to ensure the removal of all residual pyridine. The residue was re-dissolved in CH_2Cl_2, excess NEt_3 was added, and the resultant solution evaporated *in vacuo*. This procedure was repeated twice to generate the triethylammonium salt of the 6-*O*-acetylated ester and was confirmed by ^{1}H NMR spectroscopy (data not shown). The triethylammonium salt was dissolved in H_2O and passed through a 10 mL column of Amberlite IR-120(Na^+); fractions containing product were pooled, frozen, and lyophilized to generate the sodium salt **2** as a white, fluffy solid (108 mg, 0.234 mmol, 63%). ^{1}H NMR (400 MHz, MeOD) δ ppm 7.37-7.26 (m, 5H), 4.83 (d, 1H, J = 10.8 Hz), 4.61 (d, 1H, J = 10.8 Hz), 4.42 (q, 1H, J = 6.8 Hz), 4.38-4.28 (m,

2H), 4.16 (dd, 1H, J = 3.2 Hz, 11.6 Hz), 3.74-3.48 (m, 4H), 3.41 (s, 3H), 2.03 (s, 3H), 1.98 (s, 3H), 1.37 (d, 3H, J = 6.8 Hz); ^{13}C NMR (100 MHz, MeOD) δ ppm 176.8, 172.9, 171.3, 138.0, 128.3 (2 x C), 127.7(7) (2 x C), 127.7(1), 102.8, 80.8, 78.8, 77.2, 74.7, 73.1, 62.8, 55.7(7), 55.2(4), 22.0, 19.5, 18.6; HRMS (ESI) *m/z* calcd for $[C_{21}H_{28}NO_9]^-$, 438.1764, found 438.1773.

2.8.4 Synthesis of Monosaccharide Phosphate Inhibitor (15)

2.8.4.1 Methyl 2-acetamido-4-*O*-benzyl-2-deoxy-6-*O*-dibenzylphosphoryl-3-*O*-((*R*)-1-(methoxycarbonyl)ethyl)-β-D-glucopyranoside (14)

Compound **13** (77 mg, 0.187 mmol) was dissolved in 20 mL of distilled CH_2Cl_2 under an argon atmosphere. Triazole (65 mg, 0.936 mmol) and dibenzyl *N,N*-diethylphosphoramidite (85%, 0.33 mL, 0.936 mmol) were added, and the resultant mixture was stirred at rt for 4 h. After TLC analysis (9:1 CH_2Cl_2:MeOH) confirmed the disappearance of starting material, the reaction mixture was concentrated *in vacuo*.

The residue was re-dissolved in 20 mL of THF and the solution was subsequently cooled to −78 ^{o}C before 30% H_2O_2 (1.3 mL) was added. The reaction mixture was allowed to warm to rt before being diluted with Et_2O and washed with sat. NaCl. The organics were dried over $MgSO_4$, filtered, and then concentrated *in vacuo*. The crude product was purified via silica gel chromatography (EtOAc) to give compound **14** as a colourless oil (101 mg, 0.150 mmol, 80%). ^{1}H NMR (300 MHz, $CDCl_3$) δ ppm 7.40-7.25 (m, 15H), 6.73 (d, 1H, J = 5.7 Hz), 5.106 (d, 2H, J = 5.1 Hz), 5.079 (d, 2H, J = 5.1 Hz), 4.68-4.51 (m, 3H), 4.44-4.39 (m, 1H), 4.37-4.29 (m, 1H), 4.24-4.16 (m, 1H), 3.74 (s, 3H), 3.69-3.50 (m, 3H), 3.49-3.42 (m, 4H), 2.05 (s, 3H), 1.39 (d, 3H, J = 6.9 Hz); ^{13}C NMR (75 MHz, $CDCl_3$) δ ppm 175.0,

171.8, 137.4, 135.9(8), 135.8(9), 128.8 – 127.9(7) (15 x C), 102.7, 79.4, 79.0, 75.5, 75.0, 73.8 (d), 69.5 (2 x C, d), 66.1 (d), 56.8, 55.6, 52.3, 23.7, 19.3; $^{31}P\{^{1}H\}$ NMR (300 MHz, $CDCl_3$) δ ppm -1.36 (s); HRMS (ESI) *m/z* calcd for $[C_{34}H_{42}NO_{11}PNa]^+$, 694.2393, found 694.2377.

2.8.4.2 Methyl 2-acetamido-4-*O*-benzyl-2-deoxy-3-*O*-((*R*)-1-(methoxycarbonyl)ethyl)-β-D-glucopyranoside 6-dihydrogen phosphate (15)

Compound **14** (60 mg, 0.089 mmol) was dissolved in 10 mL distilled MeOH and 10% Pd/C (15 mg) was added. The reaction mixture was placed under vacuum and then blanketed with H_2 (1 atm). This sequence was repeated twice to ensure the reaction was blanketed with H_2. The reaction mixture was stirred for 5 min at which point TLC analysis (6:3:1 EtOAc:MeOH:H_2O) indicated the disappearance of starting material. The mixture was filtered through a pad of Celite and concentrated *in vacuo*. The crude product was dissolved in H_2O and loaded onto a 10 mL column of AG-1X8 resin (formate form). The column was washed successively with 50 mL H_2O, 100 mL 2.4N formic acid, 250 mL 4.8N formic acid, and 50 mL 5.8N formic acid. Fractions were analyzed for the presence of product by ESI-MS and fractions found to contain compound **15** were pooled and the volume reduced *in vacuo*. Distilled H_2O was added and the remaining solution concentrated *in vacuo*; this procedure was repeated multiple times to remove any residual formic acid in the mixture. The product was dissolved in 10 mL distilled H_2O and stirred with Amberlite IRC-50 (sodium form) resin until the pH of the solution reached 7.0. The solution was then filtered, frozen, and lyophilized to give the monosodium salt of compound **15** as an off-white solid (34.4 mg, 0.067 mmol, 75%). ^{1}H NMR (400 MHz, D_2O) δ ppm 7.44-7.29 (m, 5H), 4.79 (d, 1H, J = 8.0 Hz), 4.68 (obscured by solvent, 1H), 4.35-4.28 (m, 2H), 4.11-4.05 (m, 1H), 3.98-

3.92 (m, 1H), 3.70-3.59 (m, 5H), 3.53-3.44 (m, 2H), 3.41 (s, 3H), 1.90 (s, 3H), 1.25 (d, 3H, *J* = 6.8 Hz); ^{13}C NMR (100 MHz, D_2O) δ ppm 175.2, 174.4, 136.9, 129.2 (2 x C), 128.9 (2 x C), 128.7, 102.0, 82.0, 77.8, 77.4, 75.5, 74.4(6) (d), 62.6(6) (d), 57.5, 55.2, 52.7, 22.4, 18.6; ^{31}P{^{1}H} NMR (400 MHz, D_2O) δ ppm 4.03 (s); HRMS (ESI) *m/z* calcd for $[C_{20}H_{29}NO_{11}P]^-$, 490.1478, found 490.1482.

2.8.5 Ape1 Enzyme Production and Enzymatic Activity Assays

2.8.5.1 Bacterial Strains and Growth Media

The sources of plasmids and bacterial strains used in this study are listed with their respective genotypic descriptions in Table 2.3. *Escherichia coli* Rosetta^{TM}(λDE3)pLysS, used for protein expression, was maintained on LB agar containing 35 μg/mL chloramphenicol. For expression of high levels of Ape1 (previously Ape1a),[20] cells were always freshly transformed with pACJW16 using standard procedures and grown in SuperBroth (5 g NaCl, 20 g yeast extract and 32 g tryptone/L) containing 35 μg/mL chloramphenicol and 50 μg/mL kanamycin at 37 ^{o}C with agitation. All reagents were from Sigma unless otherwise noted.

Strain or Plasmid	Genotype or relevant characteristic	Reference or source
Strains		
E. coli Rosetta^{TM}(λDE3)pLysS	F$^-$ *ompT hsdS*$_B$(r_B^- m_B^-) *gal dcm* (λDE3) pLysSRARE(Cm^R)	Novagen
Plasmids		
pACJW16	pET28a(+) truncated derivative of *ape1a* from *N. gonorrhoeae* lacking N-terminal signal sequence on a *Nco*I/*Hind*III fragment; Kan^R	(1)

Cm^R, chloramphenicol resistance; Kan^R, kanamycin resistance

(1) Weadge, J. T.; Clarke, A. J. *Biochemistry* **2006***, 45*, 839-851.

Table 2.3 Bacterial strains and plasmids used in this study.

2.8.5.2 Production and Purification of Ape1

For the overexpression of Ape1, *E. coli* Rosetta^{TM}(λDE3)pLysS cells transformed with pACJW16 were grown in SuperBroth at 37 ^oC to an OD_{600} of ~0.6 and then induced for a minimum of 3 h at 18 ^oC with the addition of IPTG to a final concentration of 1 mM. Cells were isolated by centrifugation (5,000*g*, 15 min, 4 ^oC) and pellets stored at –20 ^oC until needed.

To purify His_6-Ape1, cell pellets were thawed and resuspended in a minimal volume of lysis buffer [50 mM $NaPO_4$ and 500 mM NaCl (pH 8.0)]. Lysozyme (1 mg/mL), RNase A (10 mg/mL) and DNase I (5 mg/mL) were added to aid in lysis and EDTA-free protease inhibitor tablets (1 per 15 mL of suspension) were added to prevent protein degradation. The suspension was incubated at 4 ^oC for 1 h before being subjected to lysis in a French pressure cell (four passes at 18,000 psi). The resulting cell lysates were clarified by centrifugation (20,000*g*, 20 min, 4 ^oC) and 1 mL of Ni^{2+}NTA-agarose was added for every 10 mL of

cleared lysate. The mixture was incubated overnight at 4 ^{o}C with shaking before being applied to a 15 mL disposable plastic column. Unbound proteins were allowed to flow through and the matrix was washed with approximately 30 column volumes of lysis buffer. The matrix was subsequently washed with approximately 20 column volumes of wash buffer containing 20 mM imidazole and a further 10 column volumes of wash buffer containing 30 mM imidazole. Bound Ape1 was recovered by batch elution in 10 mL of wash buffer containing 150 mM imidazole. The eluted protein was then dialyzed for 16 h against 2 x 4 L of 25 mM sodium phosphate buffer (pH 7.0).

His_6-tagged Ape1 was further purified by cation-exchange chromatography on MonoS. Protein was applied to the column following its equilibration in running buffer (25 mM $NaPO_4$, pH 7.0) at a flow rate of 0.7 mL/min. Elution of protein from the column was accomplished by increasing the ionic strength of the running buffer using a linear gradient of 0-1 M NaCl over 30 min. Eluted Ape1 was then collected and dialyzed against 6 L of 50 mM sodium phosphate buffer, pH 7.0 for 16 h at 4 ^{o}C.

2.8.5.3 Enzyme Assays

For the routine detection of acetyl esterase activity, 2 mM *p*-nitrophenyl acetate (*p*-NP acetate) in 50 mM sodium phosphate buffer (pH 6.5) was used as a substrate in a 96-well microtiter plate as previously described.[15, 20]

The Michaelis-Menten parameters of Ape1 were determined for **1** and **2** using concentrations ranging from 0.05 to 4 mM in 50 mM sodium phosphate buffer pH 6.5. Reaction mixtures, performed in triplicate, were initiated by the addition of substrate and incubated at 25 ^{o}C. Reactions were terminated by acidifying with H_2SO_4 to a final concentration of 60 mM. Samples of substrate incubated in the absence of enzyme were used

as controls for the spontaneous release of any acetate. Quantification of released acetate was performed using the Megazyme Acetic Acid Assay kit (Megazyme International Ireland, Ltd., Wicklow, Ireland). Plots of initial reaction velocities as a function of substrate concentration were analyzed by nonlinear regression using Microcal Origin 7.5, assuming a one-site binding model.

Chapter 3: Mechanistic Studies on *N*-Acetylmuramic Acid 6-Phosphate Hydrolase (MurQ) from *Escherichia coli*

The complementary processes of peptidoglycan biosynthesis and peptidoglycan turnover are extremely important during the bacterial life cycle. These two processes must be carefully regulated in order to maintain cell wall integrity, particularly during periods of growth and division. *E. coli*, amongst other bacteria, possesses a complex system of enzymes and proteins that functions to breakdown peptidoglycan, import the degradation products into the cytoplasm, and recycle these components into building blocks for use in future peptidoglycan biosynthesis or other basic metabolic pathways. This recycling system is speculated to play an important role during periods of bacterial stress or when nutrients from the surrounding host environment are scarce.

The function of many of the enzymes and proteins involved in this recycling pathway have been described previously and are summarized in Section 1.3. The pathway of MurNAc reutilization is unusual in that it is first converted into a 1,6-anhydro sugar via the action of the lytic transglycosylases. This 1,6-anhydro-MurNAc (anhMurNAc) sugar is converted into MurNAc 6-phosphate by the bifunctional enzyme AnmK. This enzyme hydrolytically cleaves the 1,6-anhydro linkage of the substrate and subsequently phosphorylates the newly-formed C-6 hydroxyl group using ATP (Figure 3.1).[10] The newly-generated MurNAc 6-phosphate is the substrate for the enzyme MurQ, a *N*-acetylmuramic acid 6-phosphate hydrolase that has also been previously called an etherase or lyase.[11] MurQ converts MurNAc 6-phosphate into GlcNAc 6-phosphate and D-lactic acid, an enzymatic reaction that results in the cleavage of an ether bond. The ability of MurQ to act as an

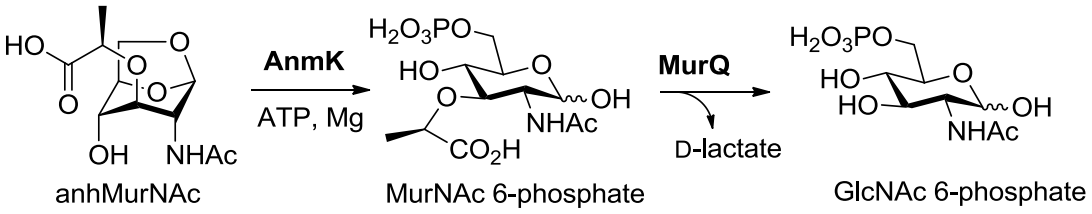

Figure 3.1 Conversion of anhMurNAc to GlcNAc 6-phosphate by AnmK and MurQ.

"etherase" in this reaction is particularly interesting from a mechanistic point of view as ether bonds are normally very stable to hydrolysis.[36]

This chapter details our mechanistic studies on the reaction catalyzed by MurQ. We first present a brief overview of previous experiments that have been performed towards the identification and characterization of MurQ. A proposed mechanism for the MurQ-catalyzed conversion of MurNAc 6-phosphate to GlcNAc 6-phosphate is then presented and discussed in the context of other enzyme-catalyzed elimination and addition reactions. Through the synthesis of the enzyme substrate and a number of substrate analogues, the molecular details of the enzymatic reaction are examined using ^{1}H NMR spectroscopy and mass spectrometry. A continuous coupled assay is developed to measure the rate of reaction, and the kinetic constants k_{cat} and K_M of the enzyme are determined. Reaction intermediates are isolated and characterized and the stereochemistry of the enzymatic elimination and addition is addressed. A structural model of MurQ is constructed and used to identify potential active site acid/base residues involved in catalysis. Site-directed mutagenesis is used to explore and assign more specific roles to these identified residues, and an overview of the updated mechanism of MurQ action is presented. Finally, the chapter is concluded with a discussion regarding the design and synthesis of potential inhibitors of MurQ, and more specifically, their use as tools in probing the residues involved in catalysis.

3.1 Previous Characterization of MurQ

The first reported identification of the enzymes involved in the recycling pathway of anhMurNAc in *E. coli* came from the Park lab in 2005.[10] They were able to partially isolate two different enzymes from crude cell extracts that were responsible for the conversion of anhMurNAc to GlcNAc 6-phosphate. The first enzyme, AnmK, converted anhMurNAc to MurNAc 6-phosphate using ATP and $MgCl_2$. The second enzyme was a hypothetical "etherase", eventually named MurQ, that was responsible for the conversion of MurNAc 6-phosphate to GlcNAc 6-phosphate. They were able to show that MurQ could convert a phosphorylated GlcNAc species into a phosphorylated MurNAc species, but were unable to conclusively determine the position of the phosphate groups on these monosaccharides.[10]

Shortly after the initial identification of AnmK and MurQ by Park and coworkers, the Mayer lab at the University of Konstanz reported the isolation and identification of MurQ.[11] A recombinant form of *E. coli* MurQ bearing a C-terminal hexahistidine tag was purified from *E. coli*. This purification procedure was complicated by the presence of seven cysteine residues within the enzyme that appeared to be sensitive to oxidation. Because of this sensitivity, either 2-mercaptoethanol or DTT were used as supplements during the reported purification procedures. Even with the addition of these reducing agents, it was found that purified enzyme was only active for a few days when stored at 4 ^{o}C. When stored at –20 ^{o}C as a solution with glycerol and DTT, the enzyme preparation was found to be stable for a period of several weeks.[11]

During previous studies examining the metabolism of amino sugars it was shown that certain *E. coli* strains could survive using MurNAc as the sole source of carbon, nitrogen, and energy.[8] It was determined that the phosphotransferase MurP served to both import MurNAc

into the cytoplasm as well as phosphorylate the imported monosaccharide at the C-6 position, generating MurNAc 6-phosphate.[9] Deletion of this phosphotransferase halted the importation of MurNAc as well as its conversion into MurNAc 6-phosphate and resulted in bacteria unable to survive on MurNAc alone.[9] Interestingly, chromosomal deletion of MurQ in *E. coli* resulted in mutant bacteria that were also unable to survive on MurNAc as the sole source of carbon, nitrogen and energy. The growth of these deletion mutants was successfully rescued when they were transformed with MurQ-containing plasmids, indicating that MurQ is essential for the metabolism of MurNAc.[11] During these experiments it was found that a compound accumulated when the mutants were grown in a rich medium supplemented with MurNAc. This compound was determined to be MurNAc 6-phosphate when analyzed by TLC and mass spectrometry and compared to a MurNAc 6-phosphate sample prepared using the phosphotransferase MurP. In order to obtain samples of MurNAc 6-phosphate for future experiments, MurQ deletion mutants were cultured in the presence of MurNAc and the accumulation product, MurNAc 6-phosphate, was isolated and purified.[11]

With the enzyme and substrate in hand, the Mayer group performed a number of experiments to further characterize the MurQ reaction. By monitoring the reaction progress of MurQ with MurNAc 6-phosphate by TLC and MS they found that MurQ catalyzed the conversion of MurNAc 6-phosphate into GlcNAc 6-phosphate. No similar loss of lactate was observed when MurQ was incubated with the closely related sugars MurNAc, anhMurNAc, or muramic acid. The reaction was also conducted in ^{18}O-labelled water and an increase of 2 amu was observed in mass spectra of the GlcNAc 6-phosphate product, corresponding to the incorporation of a single ^{18}O atom during the reaction.[11]

The MurQ-catalyzed reaction also produced lactic acid in addition to GlcNAc 6-phosphate. The D-lactate stereoisomer was exclusively generated during the reaction and no L-lactate could be detected using a series of coupled assays designed to measure D- and L-lactate. This result confirmed that the displacement of the D-lactyl ether from MurNAc 6-phosphate proceeds with retention of stereochemistry at the stereogenic center of the lactate leaving group.[11]

Interestingly, the Mayer group found that a chromogenic compound was also generated when MurNAc 6-phosphate was incubated with MurQ. This chromogenic compound was not detected in the absence of MurQ or when MurNAc 6-phosphate was incubated with inactivated enzyme preparations. The chromogenic compound exhibited an absorption maximum of 235 nm and decoloured bromine water, indicating the presence of a carbon-carbon double bond. This compound was postulated to be a 2,3-unsaturated sugar resulting from deprotonation at the C-2 position and elimination of lactate from MurNAc 6-phosphate. Mass spectrometric analysis of this compound revealed the presence of a peak displaying the expected mass of such an elimination product, but this analysis was complicated by the presence of this peak in pure samples of MurNAc 6-phosphate, presumably as a fragmentation product of the molecular ion.[11]

In order to determine whether this chromogenic compound was in fact a 2,3-unsaturated sugar, Mayer and coworkers employed a literature-known assay used to detect the presence of 2-*N*-acetylated amino sugars.[37, 38] Under the normal assay conditions, 2-*N*-acetylated amino sugars are heated under basic conditions in borate buffer to generate 2,3-unsaturated elimination products. A mixture of *p*-dimethylaminobenzaldehyde, acetic acid, and concentrated HCl, collectively known as Ehrlich's reagent, is then added to the sample

and the mixture is heated at 37 °C (Figure 3.2). Under the conditions of this assay, the 2,3-unsaturated pyranose product can be interconverted into the furanose form. This type of unsaturated sugar has been termed a Morgan-Elson chromogen I and can undergo a further dehydration reaction to generate the aromatic Morgan-Elson chromogen III (Figure 3.2). Morgan-Elson chromogen III then condenses with *p*-dimethylaminobenzaldehyde to form a product that is a red/violet colour in solution and strongly absorbs at 585 nm.[37]

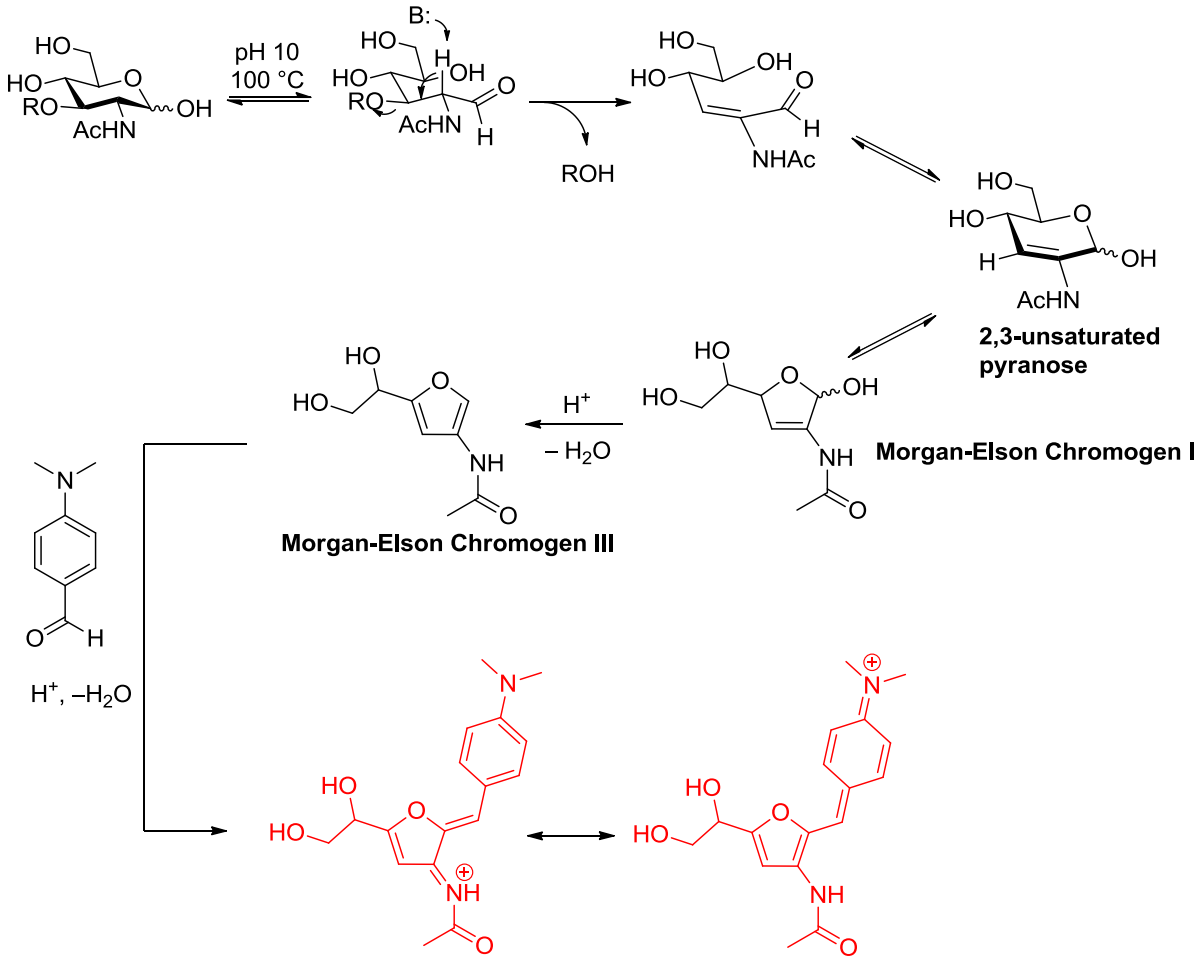

Figure 3.2 Assay for the detection of 2-*N*-acetylated amino sugars using Ehrlich's reagent.

Interestingly, when aliquots of the reaction mixture of MurNAc 6-phosphate with MurQ were tested with Ehrlich's reagent, a purple solution was produced indicating the

presence of a Morgan-Elson chromogen. This chromogen was generated without heating of the reaction mixture under basic conditions, indicating that its formation was catalyzed by MurQ (Figure 3.3). The presence of this chromogen was also detected when samples of MurQ incubated with GlcNAc 6-phosphate were tested with Ehrlich's reagent. Thus, MurQ was found to catalyze the formation of an intermediate that is likely Δ2,3-GlcNAc 6-phosphate when incubated with either MurNAc 6-phosphate or GlcNAc 6-phosphate. Because of the results of this assay, it was predicted that a high steady-state level of this unsaturated intermediate was generated by the enzyme, and that hydration of this compound to form GlcNAc 6-phosphate was rate-limiting.[11]

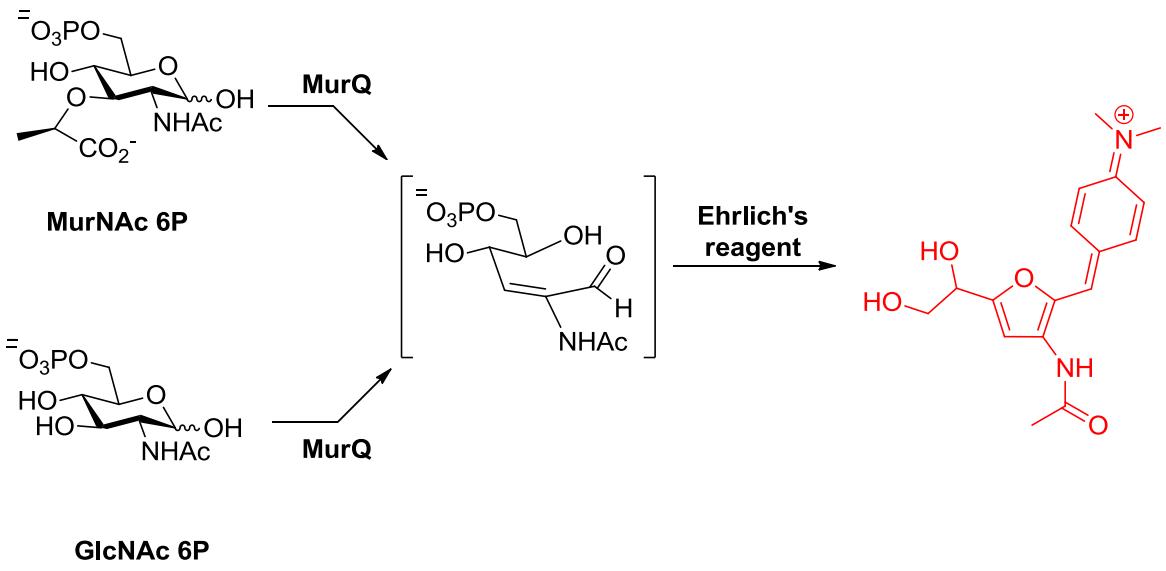

Figure 3.3 Incubation of MurQ with MurNAc 6-phosphate or GlcNAc 6-phosphate produces a compound that reacts with Ehrlich's reagent.

Based on its amino acid sequence, MurQ was assigned to the sugar phosphate isomerase/sugar phosphate-binding (SIS) protein family. MurQ showed significant sequence similarity (33% identity) to one of the SIS domains of the glucosamine 6-phosphate synthase, GlmS.[11] GlmS catalyzes the conversion of fructose 6-phosphate into glucosamine 6-

phosphate (GlcN 6-phosphate) with glutamine acting as a source of ammonia (Figure 3.4).[39] This enzymatic conversion is an important step in the pathway for the synthesis of UDP-GlcNAc.

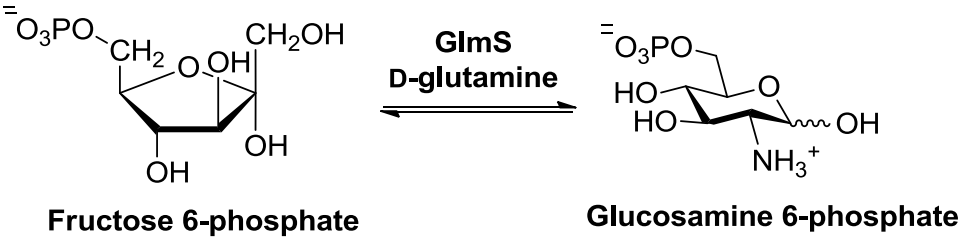

Figure 3.4 The reaction catalyzed by glucosamine 6-phosphate synthase, GlmS.

In addition to the SIS domain that possesses significant similarity to MurQ, GlmS also possesses a glutaminase domain that uses glutamine to generate the ammonia needed for the synthesis of the amino sugar GlcN 6-phosphate. Although the synthesis of GlcN 6-phosphate is the primary function of GlmS, it can also catalyze an alternate reaction in the absence of glutamine. With no source of ammonia, GlmS catalyzes the isomerization of fructose 6-phosphate into glucose 6-phosphate. This reaction can also be catalyzed by the SIS domain in the absence of the glutaminase domain.[39, 40] The mechanism through which GlmS catalyzes the formation of glucose 6-phosphate and glucosamine 6-phosphate is of interest as it likely shares similar features with the mechanism employed by MurQ.

Fructose 6-phosphate is first bound in the active site of GlmS in its closed chain furanose form. An active site histidine residue (His604) is positioned to catalyze ring-opening and produces the 2-keto form of the sugar (Figure 3.5). A Schiff base is subsequently formed between the ketone at C-2 and the ε-amino group of a lysine residue (Lys603) within the active site.[41] At this point, the reaction can proceed towards the synthesis of either glucose 6-phosphate or glucosamine 6-phosphate. In the presence of

glutamine and an active glutaminase domain, ammonia is channeled to the active site and displaces the Schiff base at the C-2 position. Deprotonation of the *pro*-R hydrogen at the C-1 position by Glu488 then produces a *cis*-enolamine intermediate. This intermediate can then be protonated at the C-2 position by Glu488 to generate the product glucosamine 6-phosphate. In the absence of glutamine, the reaction proceeds via a similar mechanism except that the Schiff base enzyme-adduct is proposed to be hydrolyzed to regenerate the ketone at the C-2 position. The *pro*-R hydrogen at the C-1 position is deprotonated by Glu488 to generate an anionic enediol intermediate, which is then protonated at the C-2 position by Glu488 to generate the isomerized product, glucose 6-phosphate (Figure 3.5).[39]

The formation of a Schiff base between fructose 6-phosphate and Lys603 is still a matter of debate. Although an intermediate trapping experiment showed the presence of a Schiff base between Lys603 and a competitive inhibitor of the reaction, a separate mutagenesis experiment revealed that the mutation of lysine to arginine only slightly impaired catalytic activity. Because the reaction mechanism proposed in Figure 3.5 does not invoke a Schiff base to activate the *pro*-R hydrogen on C-1 for deprotonation it is reasonable to question the need for such an intermediate to exist during catalysis.

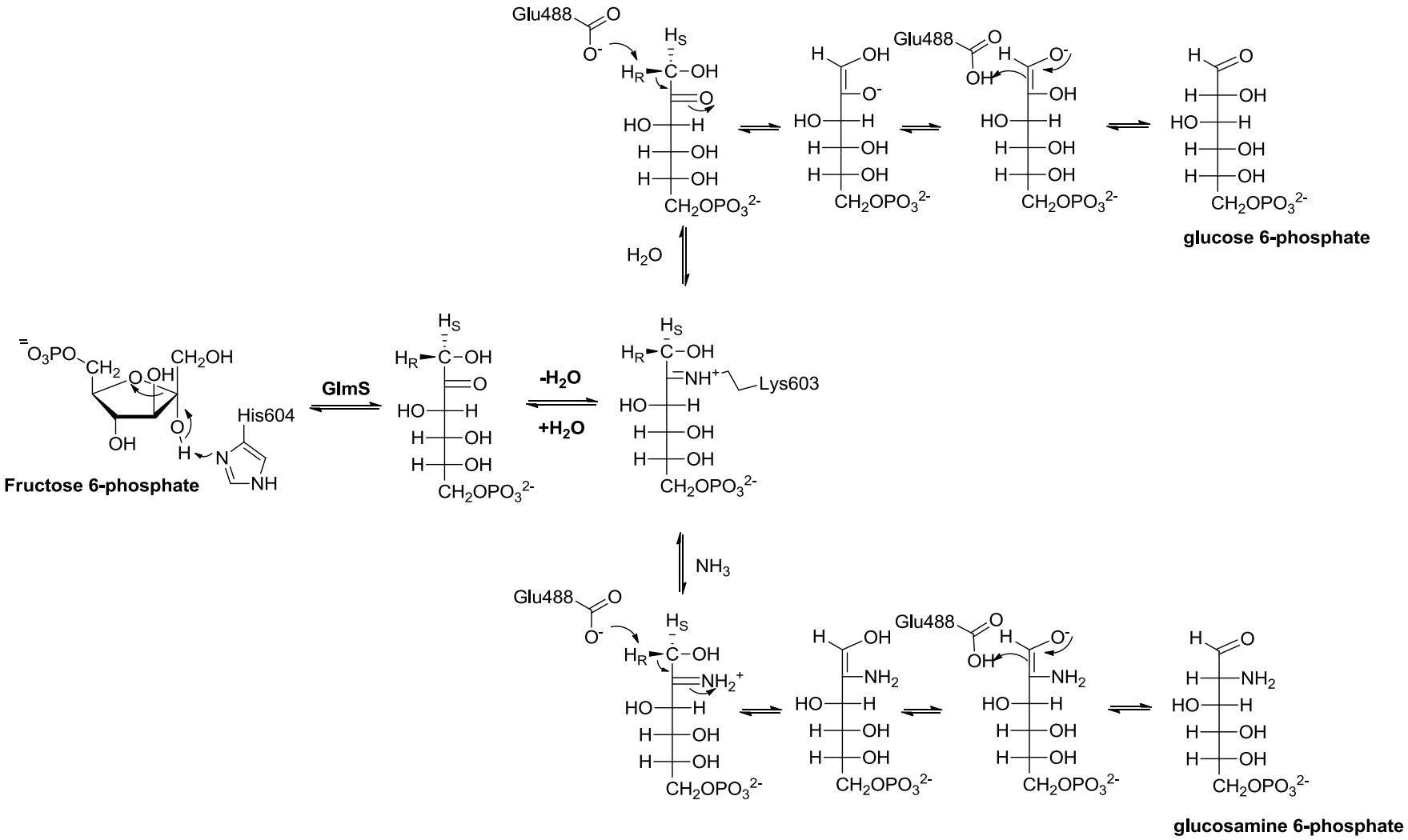

Figure 3.5 Mechanism of glucose 6-phosphate synthesis and glucosamine 6-phosphate synthesis by GlmS.

3.2 Proposed Mechanism of MurQ Action

The MurQ-catalyzed conversion of MurNAc 6-phosphate into GlcNAc 6-phosphate and D-lactate presents an interesting target for mechanistic analysis. The results of previous experiments have helped to significantly narrow the possibilities through which enzymatic action can occur. Although an alkoxide anion is a poor leaving group, nucleophilic displacement of the lactyl ether at the C-3 position could conceivably occur if aided by enzyme active site acid/base residues. Such a mechanism can be ruled out however, as the resultant product would be of inverted stereochemistry at the C-3 position. Nucleophilic displacement at the stereogenic center of the lactate group can also be ruled out, as this would result in the production of the L-lactate stereoisomer during the reaction, and no ^{18}O isotope incorporation into GlcNAc 6-phosphate.

The detection of a species suspected to be a 2,3-unsaturated sugar suggests that the enzyme may function via an elimination/addition pathway.[42] Enzyme-catalyzed eliminations generally proceed with a leaving group located at a position β- to a suitable activating group. These activating groups serve to acidify a proton that is found α- to the functional group and are often species such as aldehydes, ketones, iminium ions, or esters. Enzymes can employ cofactors such as NAD^+ to catalyze an oxidation and create a carbonyl activating group so that an elimination reaction can occur. They can also use divalent metal cations to improve the ability of the leaving group to depart.[42] MurQ however, does not employ any cofactors or require a divalent metal cation for catalysis to occur. The substrate of the reaction, MurNAc 6-phosphate, does not require oxidation to form an activating group since an aldehyde is unveiled at the C-1 position upon ring-opening. In this open chain form, the acidity of the α-proton at the C-2 position is significantly increased and the D-lactyl ether is

positioned β- to the aldehyde functionality. Elimination of the lactyl ether and the subsequent addition of water to the alkene intermediate are likely accomplished with the aid of a number of active site acid/base residues that catalyze proton transfers and stabilize anionic intermediates.

The proposed mechanism of MurQ action starts with a ring-opening reaction of the substrate MurNAc 6-phosphate, that is likely enzyme-catalyzed, to generate a free aldehyde at the C-1 position (Figure 3.6). The presence of this aldehyde serves to acidify the proton at the C-2 position and allows deprotonation by a catalytic active site base (B_1, Figure 3.6) to generate a resonance-stabilized enolate anion. The loss of lactate is then proposed to occur with the aid of a second catalytic active site acidic residue (B_2, Figure 3.6) that protonates the departing oxygen. The presence of B_2 to protonate the departing oxygen anion is likely important as the alkoxide anion of the lactate leaving group is highly basic. The elimination of lactate generates an α,β-unsaturated aldehyde intermediate of unknown stereochemistry. This elimination is presumed to be essentially irreversible under most reaction conditions as the concentration of the departing lactate will generally be orders of magnitude smaller than that of water. To generate the GlcNAc 6-phosphate product of the enzymatic reaction, the same two catalytic bases B_1 and B_2 are used to catalyze the conjugate addition of water onto the α,β-unsaturated aldehyde intermediate in a manner that mirrors the elimination of lactate. The residue B_2 that is responsible for protonating the lactate leaving group would be appropriately positioned to deprotonate a water molecule for attack at the C-3 position of the unsaturated intermediate. This generates a resonance-stabilized enolate anion intermediate that can subsequently be protonated at the C-2 position by the appropriately positioned

catalytic residue, B_1. Ring-closure of this compound to give GlcNAc 6-phosphate could occur spontaneously in solution or be enzyme-catalyzed.

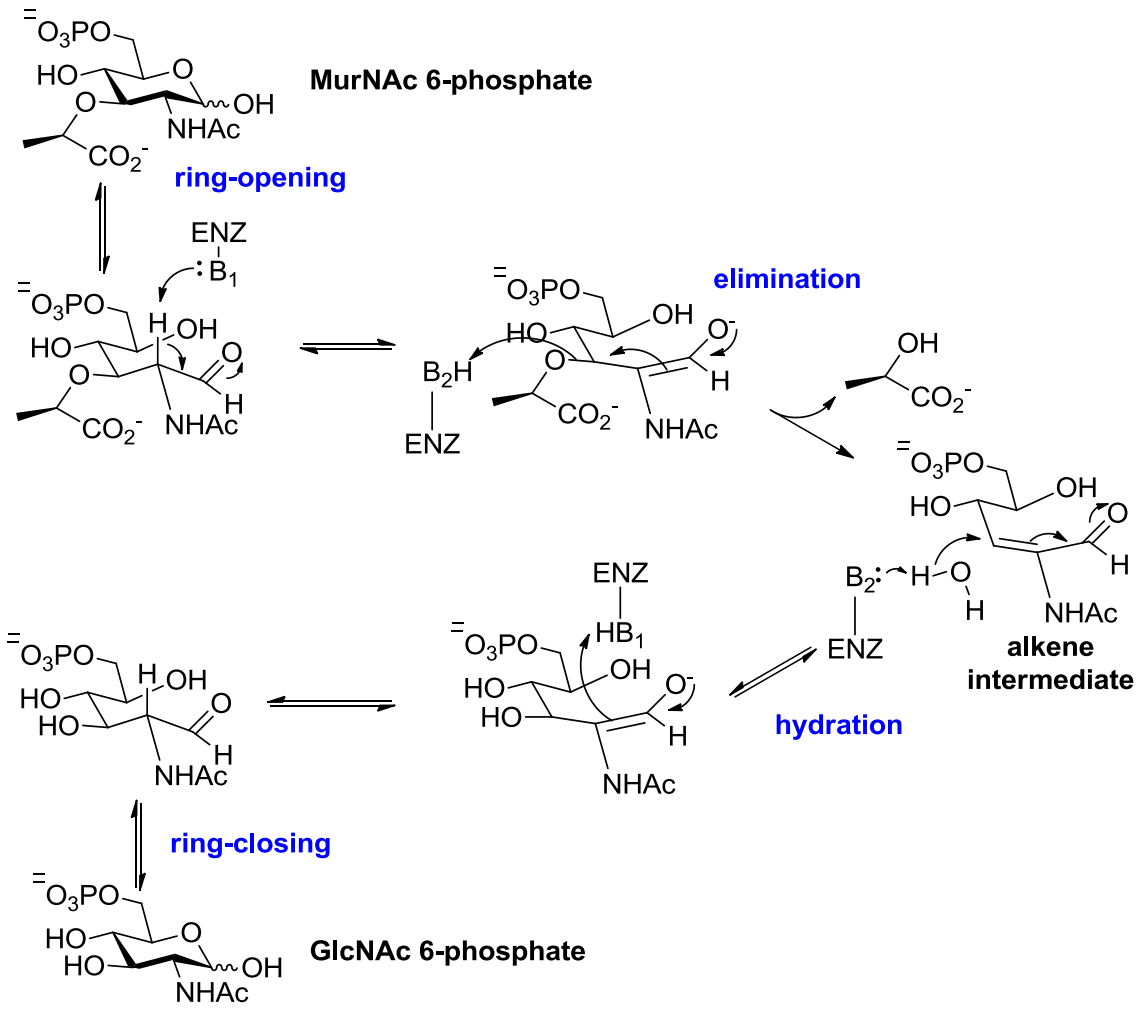

Figure 3.6 Proposed mechanism of MurQ catalysis.

This proposed mechanism is completely consistent with results obtained during past work on the mechanism of MurQ.[10, 11] The incorporation of a single ^{18}O label into GlcNAc 6-phosphate when the reaction was conducted in $H_2{}^{18}O$ indicates that a molecule of water has been added to the sugar moiety during the reaction. The detection of a putative 2,3-unsaturated aldehyde upon incubation of MurQ with either MurNAc 6-phosphate or GlcNAc 6-phosphate is consistent with the formation of the alkene intermediate shown in Figure

3.6.[11] The proposed existence of an enolate anion in both the formation of the alkene intermediate and the hydration of this intermediate to produce product is also supported by MurQ's assignment to the SIS family of proteins and its significant sequence similarity to the enzyme GlmS. Members of the SIS family, including GlmS, catalyze sugar phosphate isomerizations using enolate-based mechanisms (Figure 3.5) very similar to that proposed for MurQ (Figure 3.6). The studies outlined in this chapter provide further evidence in support of an enolate-based elimination/addition mechanism. The numerous intermediates and active-site acid/base residues proposed in Figure 3.6 provide the basis for the design of many of the experiments detailed in the following sections.

3.3 Synthesis of the Substrate and Product of the MurQ Reaction

3.3.1 Synthesis of MurNAc 6-Phosphate

Previous studies on MurQ were hampered by a lack of access to sufficient quantities of the enzyme's substrate, MurNAc 6-phosphate. During their studies, our collaborators in the Mayer group isolated MurNAc 6-phosphate from incubations of MurQ deletion mutants grown in the presence of MurNAc.[11] Unfortunately, this method of substrate production only gave them access to microgram quantities of MurNAc 6-phosphate. To overcome this hurdle, we set out to develop a chemical synthesis of MurNAc 6-phosphate (Figure 3.7).

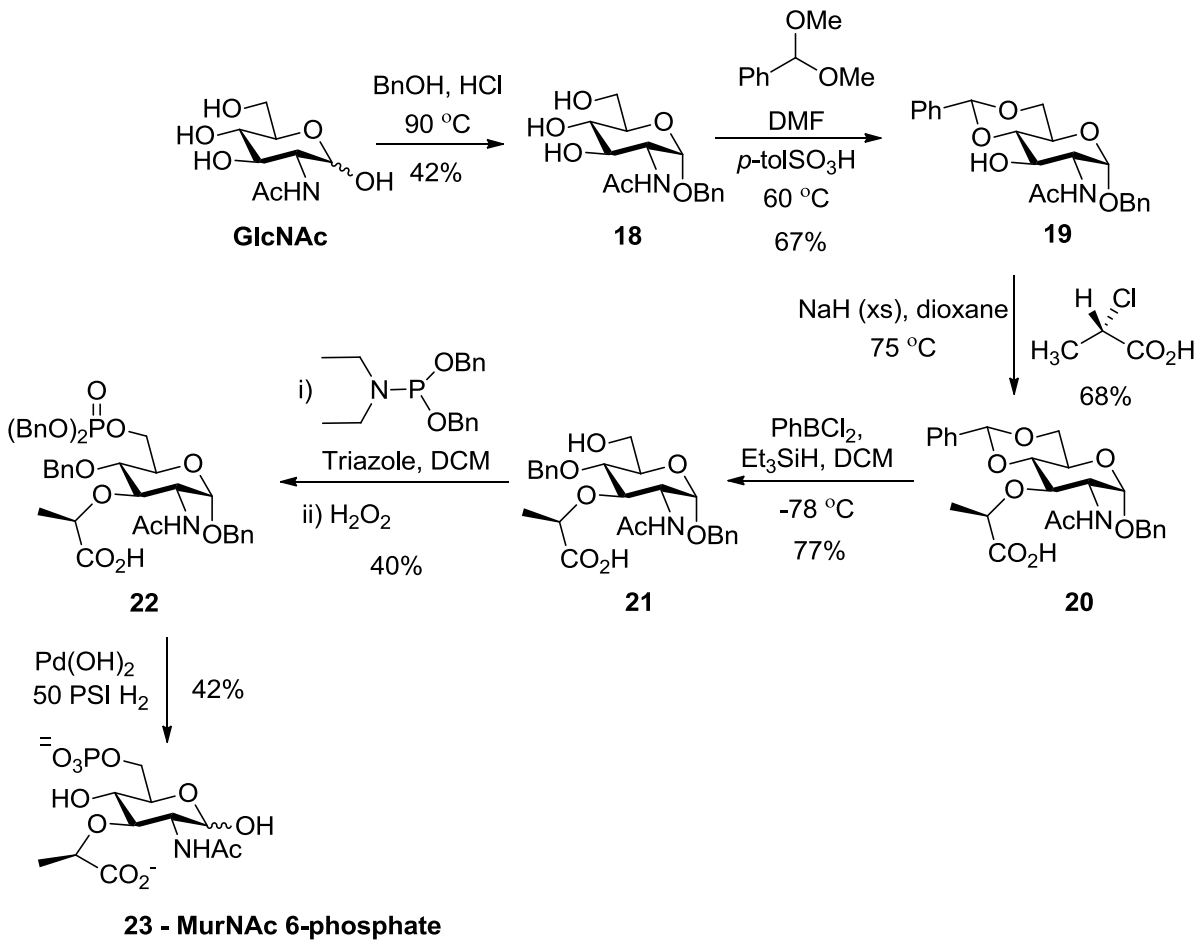

Figure 3.7 Chemical synthesis of MurNAc 6-phosphate.

Starting from the commercially available amino sugar GlcNAc, a benzyl ether was introduced at the anomeric position under acidic conditions using literature methodology.[43] The benzyl glycoside was generated as an α/β mixture and the α-anomer, compound **18**, was isolated from this mixture in 42% overall yield. In order to enable the selective functionalization of the C-3 hydroxyl group, compound **18** was reacted with benzaldehyde dimethyl acetal to generate the known 4,6-*O*-benzylidene derivative **19** using adapted literature methodology.[44, 45] The D-lactyl ether was introduced at the C-3 position of compound **19** through a substitution reaction under basic conditions with (*S*)-2-chloropropionic acid to generate the literature-known MurNAc derivative **20** in modest

yield.[46, 47] The 4,6-*O*-benzylidene-containing compound **20** was subjected to a regioselective reductive ring-opening using dichlorophenylborane ($PhBCl_2$) and triethylsilane (Et_3SiH) to generate compound **21** with a free C-6 hydroxyl group in 77% yield.[31] The phosphate ester **22** was generated by reaction of **21** with a phosphoramidite coupling reagent and subsequent oxidation of the dibenzyl phosphite into the dibenzyl phosphate.[48] Global deprotection of the benzyl groups via hydrogenolysis using palladium hydroxide as catalyst gave compound **23** (MurNAc 6-phosphate) in 42% yield. Our synthetic scheme enabled us to generate MurNAc 6-phosphate quickly and efficiently on a 100 mg scale.

3.3.2 Synthesis of GlcNAc 6-Phosphate

In order to have access to sufficient quantities of the product of the MurQ reaction for our mechanistic studies, the chemical synthesis of the known compound GlcNAc 6-phosphate was undertaken (Figure 3.8). The α-benzyl glycoside **18** was selectively phosphorylated at the C-6 hydroxyl using diphenylchlorophosphate to give compound **24** in 63% yield.[49, 50] This compound was then subjected to hydrogenolysis using 10% Pd/C and then PtO_2 as catalysts to generate compound **25** (GlcNAc 6-phosphate) expeditiously on a 100 mg scale.[50]

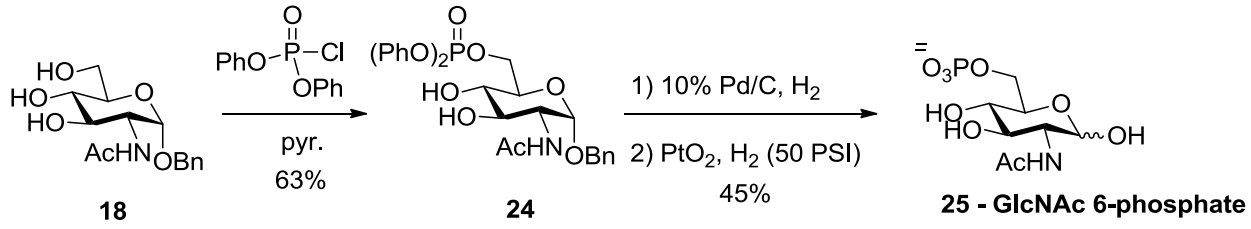

Figure 3.8 Chemical synthesis of GlcNAc 6-phosphate.

3.3.3 Synthesis of [2-^{2}H]MurNAc 6-Phosphate

The synthesis of an isotopically-labeled analogue of MurNAc 6-phosphate was undertaken in order to test for a potential kinetic isotope effect on the MurQ-catalyzed reaction. A single deuterium atom was introduced into MurNAc 6-phosphate at the C-2 position to give the labeled compound [2-^{2}H]MurNAc 6-phosphate. According to our proposed mechanism of MurQ action, the C-2H bond is broken during catalysis to form a resonance-stabilized enolate intermediate. The replacement of the hydrogen at C-2 with a deuterium in [2-^{2}H]MurNAc 6-phosphate should enable us to determine if there is any kinetic isotope effect occurring as a result of this bond breaking during catalysis.

In order to obtain the labeled substrate, [2-^{2}H]GlcNAc was first prepared from GlcNAc according to previous reported procedures (Figure 3.9).[51, 52] This isotopically-labeled compound was then converted into [2-^{2}H]MurNAc 6-phosphate (**26**) using synthetic procedures identical to those described in Section 3.3.1 for the synthesis of MurNAc 6-phosphate (**23**). ^{1}H NMR spectra of the isotopically-labeled synthetic intermediates were identical to the corresponding unlabeled compounds with the following exceptions: the signal due to the anomeric proton appeared as a singlet instead of a doublet, and the signal due to the proton at the C-2 position was absent. Both of these observations are consistent with the incorporation of a single deuterium atom at the C-2 position. ^{1}H NMR spectroscopy and MS analysis of the final compound confirmed the extent of deuterium incorporation at the C-2 position of MurNAc 6-phosphate to be > 95%.

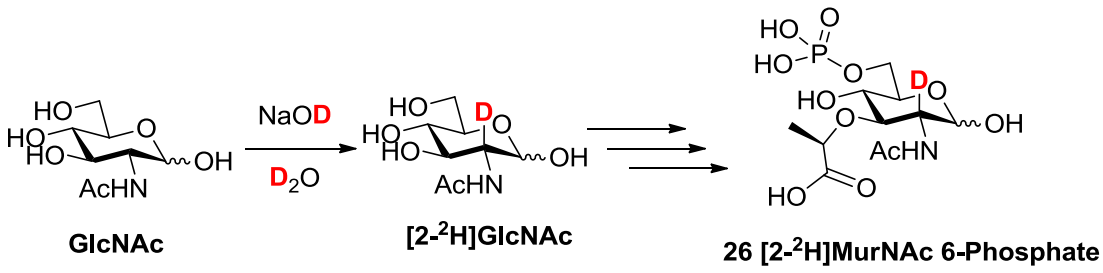

Figure 3.9 Chemical synthesis of [2-^{2}H]MurNAc 6-phosphate.

3.4 Kinetic Studies on Wild-Type MurQ

A detailed kinetic analysis of the reaction catalyzed by MurQ, including the experimental determination of the kinetic parameters k_{cat} and K_M, had yet to be performed at the outset of these studies due to a lack of access to the substrate MurNAc 6-phosphate. The chemical synthesis of MurNAc 6-phosphate described in Section 3.3.1 allowed us to overcome this hurdle and proceed with the assaying of MurQ enzymatic activity.

The enzyme used in these studies was a recombinant form of the MurQ enzyme from *E. coli* that contained a C-terminal hexahistidine tag. A plasmid containing the MurQ gene along with the C-terminal hexahistidine tag was transformed into chemically competent *E. coli* BL-21 cells as described previously.[11] The recombinant enzyme was then expressed and purified using metal ion affinity chromatography (Figure 3.10). Due to the sensitivity of the purified enzyme toward freezing and prolonged storage, frozen cell pellets were stored at −78 ^{o}C and fresh enzyme was purified each day immediately prior to use. Enzyme purified in this manner could be kept in solution at 4 ^{o}C for several hours without any detectable loss of activity.

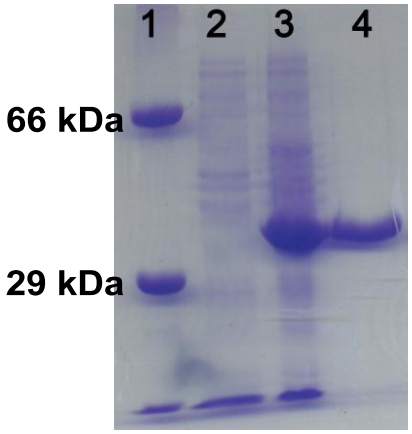

Figure 3.10 SDS-PAGE gel showing the purification of MurQ. Lane 1: molecular weight standards of 66 kDa (bovine serum albumin) and 29 kDa (carbonic anhydrase); Lane 2: crude cell extract before induction; Lane 3: crude cell extract after induction with IPTG; Lane 4: purified MurQ.

In order to measure the kinetic constants for MurQ, we developed a continuous coupled assay for D-lactate using the enzyme D-lactate dehydrogenase and the cofactor NAD^+. The D-lactate released during the enzymatic reaction is oxidized to pyruvate with the concomitant reduction of NAD^+ to NADH by the enzyme D-lactate dehydrogenase. To ensure the irreversibility of our assay, the production of NADH was coupled to the reduction of *p*-iodonitrotetrazolium violet (INT) using the enzyme diaphorase (Figure 3.11).[53] This coupling enzyme serves to regenerate NAD^+ in situ and also produces the reduced form of INT that absorbs strongly at 500 nm and appears red in solution.

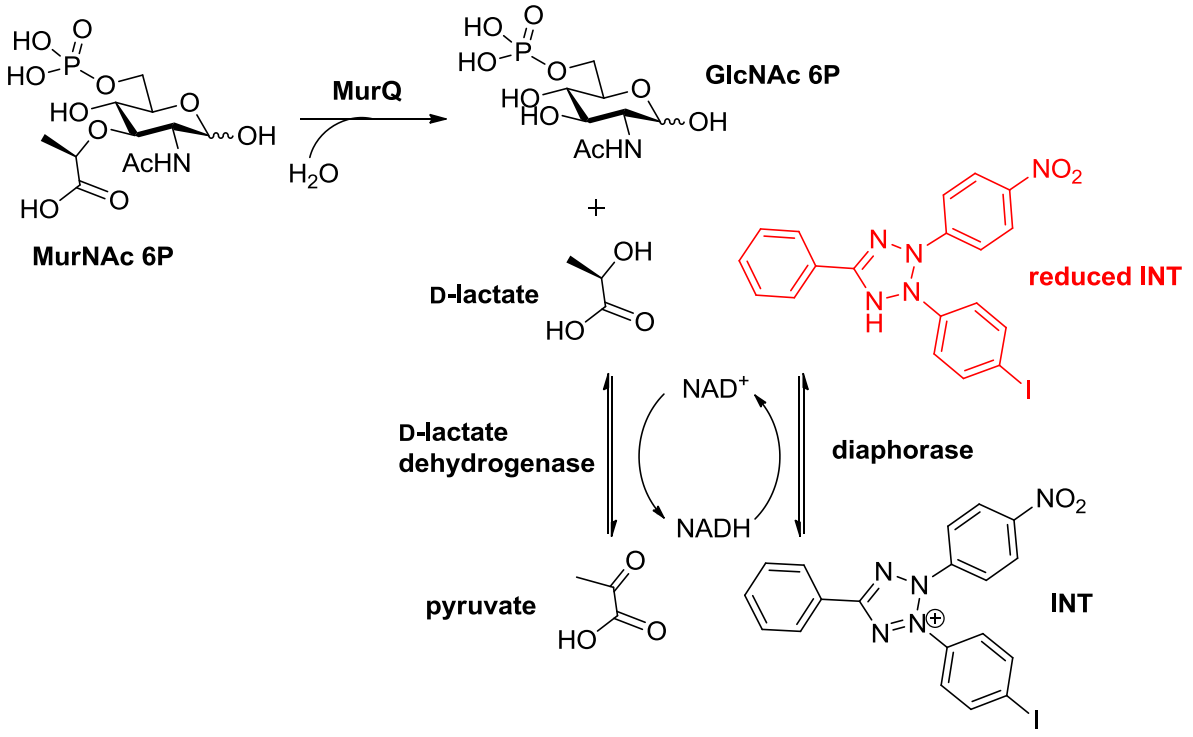

Figure 3.11 Continuous coupled assay measuring the release of D-lactate by MurQ.

The rate of D-lactate release was measured by monitoring the increase in absorbance at 500 nm due to the formation of reduced INT. The initial rate of product formation was measured at varying concentrations of MurNAc 6-phosphate and is plotted in Figure 3.12. It was found that the MurQ-catalyzed reaction follows Michaelis-Menten kinetics with the following kinetic parameters: k_{cat} = 5.7 +/– 0.1 s^{-1}, K_M = 1.20 +/– 0.07 mM, and k_{cat}/K_M = 4.8 x 10^3 $M^{-1}s^{-1}$. The kinetic parameters k_{cat} and K_M, and their associated errors, were determined by fitting the initial velocity data to the Michaelis-Menten equation using non-linear regression. Data obtained on different days with different batches of purified enzyme could result in kinetic parameters that differed from those reported above by up to 25%. The addition of 5 mM EDTA to the assay resulted in a relatively small reduction in rate (25%), indicating that the enzyme does not require metal ions for catalysis.

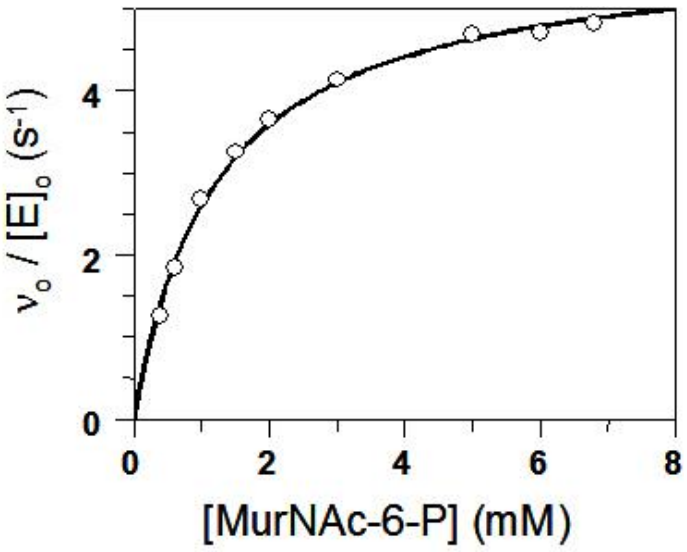

Figure 3.12 Plot of initial velocity vs. MurNAc 6-phosphate concentration for the wild-type MurQ reaction.

3.4.1 Kinetic Isotope Effect Measurement on the Wild-Type MurQ Reaction

With the development of our kinetic assay measuring the release of D-lactate it was possible to measure a kinetic isotope effect (KIE) for the reaction using our isotopically-labeled substrate [2-^{2}H]MurNAc 6-phosphate (**26**). KIE experiments provide a method of probing for bonding changes that occur at a specific site during a chemical reaction.[54] This involves a comparison of the rates of reaction of unlabeled and isotopically-labeled substrates. Important information can be obtained if bonding changes occur at, or near the site of substitution are involved in a rate-determining step of the reaction.

When a hydrogen atom is substituted for a deuterium atom, the KIE for the reaction is generally represented as the ratio k_H/k_D, where k_H is the rate of reaction with protiated substrate and k_D is the rate of reaction with deuterated substrate. KIEs can be generally classified as either primary or secondary, although only the former is pertinent to this discussion. Primary deuterium kinetic isotope effects are observed when the hydrogen/deuterium bond is broken during the rate-determining step of catalysis.[54] The

carbon-deuterium bond possesses a lower vibrational zero-point energy than the corresponding carbon-hydrogen bond due to the increase in the reduced mass of the two atoms. This decrease in the vibrational zero-point energy results in a higher activation energy barrier for the cleavage of the carbon-deuterium bond. Typical primary KIEs for the cleavage of a carbon-hydrogen bond in enzymatic reactions will generally range from 2-4.[54] Depending on the mechanism of reaction however, primary enzymatic KIEs can be masked by a number of other isotopically-insensitive steps.[54]

The rate of the MurQ-catalyzed formation of D-lactate was measured using the labeled substrate [2-^{2}H]MurNAc 6-phosphate and compared to the rate of catalysis measured for unlabeled substrate (Figure 3.13). It is apparent from this plot of initial velocity vs. substrate concentration that the reaction of MurQ with the labeled substrate [2-^{2}H]MurNAc 6-phosphate proceeds slower than the corresponding reaction with unlabeled substrate. From this data, the kinetic parameter k_{cat} was determined to be 2.40 +/– 0.17 s^{-1} for [2-^{2}H]MurNAc 6-phosphate and 4.40 +/– 0.80 s^{-1} for MurNAc 6-phosphate. The kinetic parameters k_{cat} and K_M, and their associated errors, were determined by fitting the initial velocity data to the Michaelis-Menten equation using non-linear regression. A KIE of 1.8 +/– 0.2 on the value of k_{cat} was observed using our coupled assay. The error associated with this KIE measurement was derived from the fractional errors associated with the measurement of k_{cat} for labeled and unlabeled substrate. A KIE of this magnitude can be interpreted as a primary KIE on a partially rate-limiting step of catalysis. This result strongly supports a mechanism involving cleavage of the C-H bond at the C-2 position of MurNAc 6-phosphate during catalysis. Other steps such as the ring-opening of substrate, loss of lactate, or addition of water could

also be partially rate-determining and account for an observed KIE value that is lower than its instrinsic value.

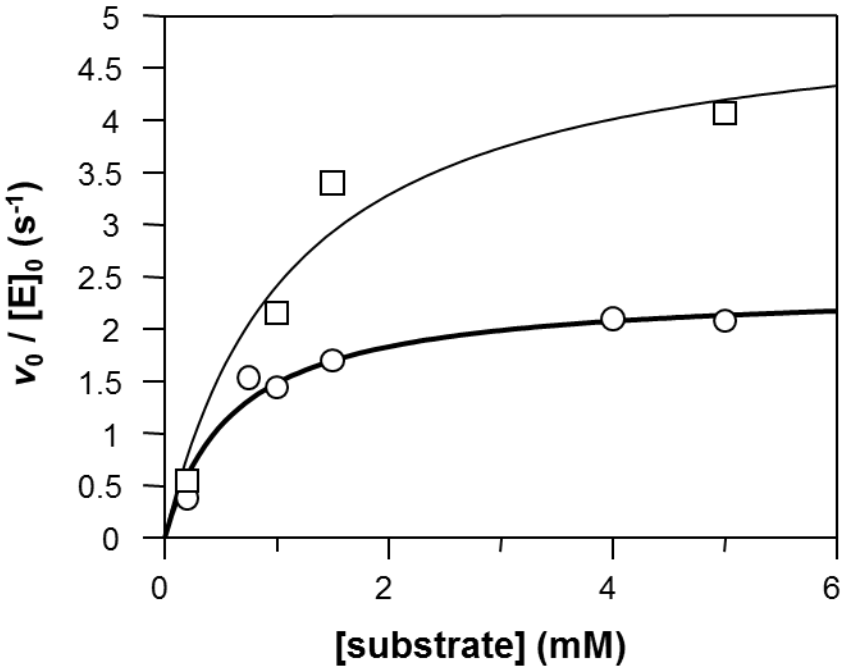

Figure 3.13 Plot of initial velocity vs. substrate concentration for the wild-type MurQ reaction with [2-^{2}H]MurNAc 6-phosphate (circles) and MurNAc 6-phosphate (squares).

3.5 Monitoring the MurQ Reaction by ^{1}H NMR Spectroscopy and Mass Spectrometry: Solvent Deuterium Incorporation and Intermediate Release

To gather more information regarding the molecular details of the MurQ-catalyzed reaction, we conducted the reaction in buffer prepared from D_2O and monitored its progress via ^{1}H NMR spectroscopy and MS. This experiment enabled us to determine whether any solvent-derived deuterium was incorporated at the C-2 position of either the substrate or product during the course of the reaction. We also envisioned that by monitoring the reaction by ^{1}H NMR spectroscopy, we would be able to observe the formation of the previously reported α,β-unsaturated reaction intermediate and garner additional information regarding its chemical structure.

The ^{1}H NMR spectrum of MurNAc 6-phosphate in deuterated phosphate buffer at pH 7.5 showed an equilibrium mixture of 70% α-anomer to 30% β-anomer (Figure 3.14, top). The anomeric proton of the α-anomer of MurNAc 6-phosphate is seen as a doublet at 5.59 ppm while the signal due to the anomeric proton of the β-anomer of MurNAc 6-phosphate is partially obscured by the signal of residual HDO solvent. This anomeric signal is visualized as a doublet due to coupling to the axial proton at the C-2 position. The methyl groups on the lactate side chains of the two anomers of MurNAc 6-phosphate are visualized as two slightly overlapping doublets at 1.38 and 1.41 ppm.

A number of changes to the ^{1}H NMR spectrum of the reaction were observed after the addition of MurQ to the mixture and incubation for 20 min at 37 ^{o}C (Figure 3.14, bottom). The two overlapping doublets at 1.38 and 1.41 ppm were converted into a single doublet at 1.36 ppm corresponding to the methyl group of free D-lactic acid. Interestingly, the singlet at 2.09 ppm due to the *N*-acetamido functional group of both anomers of MurNAc 6-phosphate displayed no observable change after the conversion into GlcNAc 6-phosphate. The signal due to the anomeric proton of the α-anomer of MurNAc 6-phosphate was cleanly converted into a new signal at 5.23 ppm that corresponds to the α-anomeric proton of the product GlcNAc 6-phosphate. This new peak at 5.23 ppm was visualized as a singlet, indicating that a deuterium atom had been incorporated into the C-2 position of the product during catalysis. Indeed, mass spectral analysis of the product confirmed that a single nonexchangeable deuterium had been incorporated into GlcNAc 6-phosphate.

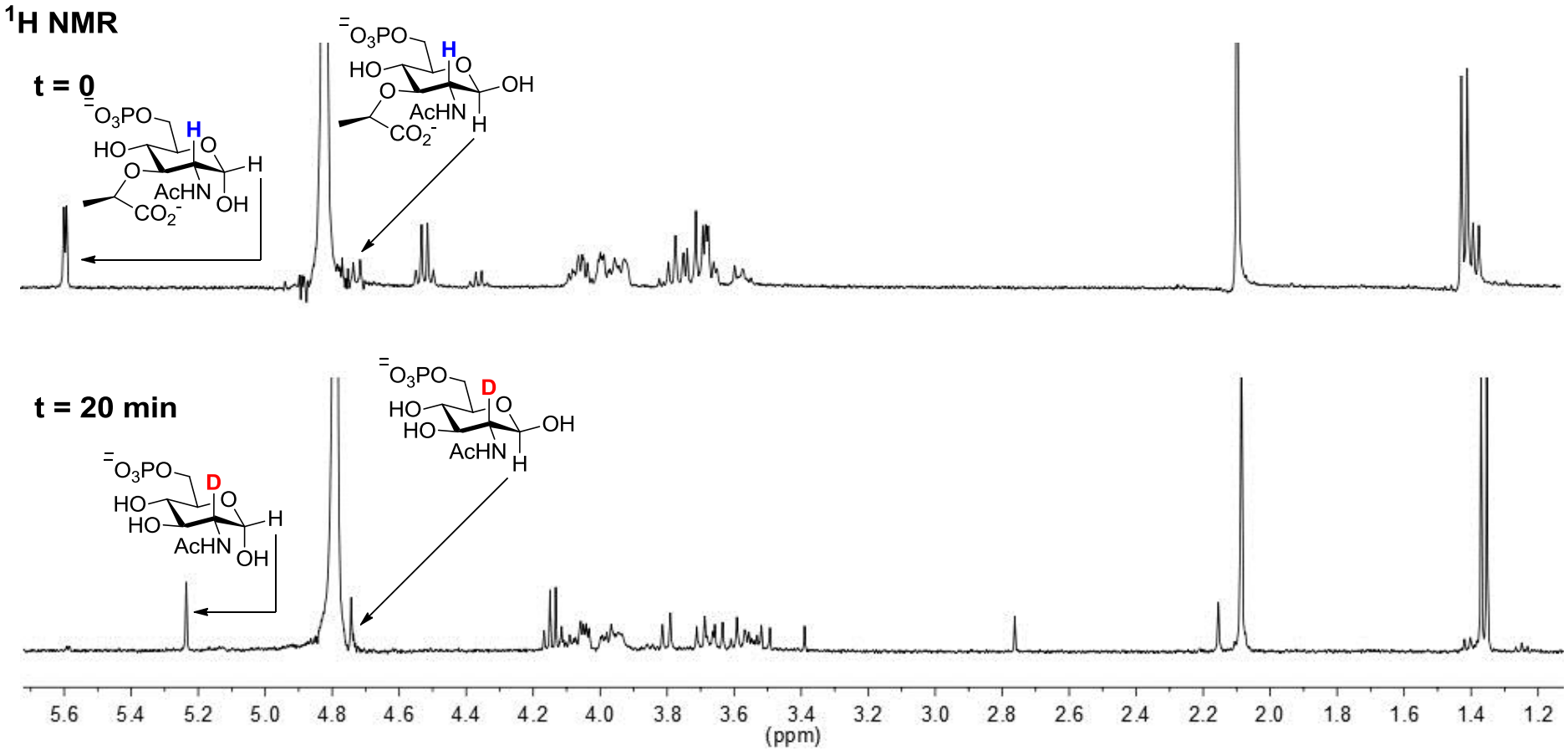

Figure 3.14 ^{1}H NMR (D_2O, 400 MHz) spectra of the MurQ reaction with MurNAc 6-phosphate. (Top) Spectrum of MurNAc 6-phosphate before addition of MurQ. (Bottom) Spectrum of reaction mixture showing conversion of MurNAc 6-phosphate to GlcNAc 6-phosphate after addition of MurQ and incubation for 20 min at 37 ^{o}C.

The spectral changes described above were useful markers for monitoring the progress of the enzymatic reaction, and the incorporation of a deuterium atom at the C-2 position of GlcNAc 6-phosphate lends support for the proposed mechanism of enzymatic action (Figure 3.6). This result indicates that the proton that is removed from the C-2 position during the elimination of the C-3 lactyl ether exchanges with solvent during the lifetime of the α,β-unsaturated intermediate. Spectra taken at early stages of the conversion showed that complete solvent deuterium incorporation occurred with each turnover and that the loss of the C-2 proton was not simply a result of the reversible dehydration/rehydration of the product. By monitoring the anomeric signal of residual pools of MurNAc 6-phosphate during the course of the reaction we were also able to test whether incorporation of solvent-derived deuterium at the C-2 position of MurNAc 6-phosphate was occurring. The anomeric signal remained a doublet even at very late stages of the reaction, indicating that deuterium incorporation into the C-2 position of residual starting material was not occurring at any significant rate. This result indicates that after deprotonation of MurNAc 6-phosphate occurs, the enolate-anion intermediate will partition towards the reaction product rather than back to starting material. An alternative explanation is that the proton removed from the C-2 position is unable to exchange with bulk solvent during the lifetime of the enolate.

Interestingly, after further incubation of the reaction mixture, a set of new signals were observed that were tentatively assigned to the α,β-unsaturated sugar intermediate of the MurQ-catalyzed reaction. A new singlet peak at 2.16 ppm was observed due to the *N*-acetyl group of the unsaturated intermediate (visible in Figure 3.14, bottom), and four new peaks also accumulated in the downfield region of the spectrum between 6.0 and 6.3 ppm (the downfield region is shown in Figure 3.15). Mass spectral analysis of the reaction mixture

showed a significant signal due to a species that has the same mass as the proposed α,β-unsaturated alkene intermediate. This result however, is complicated by the observation of the same signal, albeit of smaller magnitude, in spectra taken of pure samples of MurNAc 6-

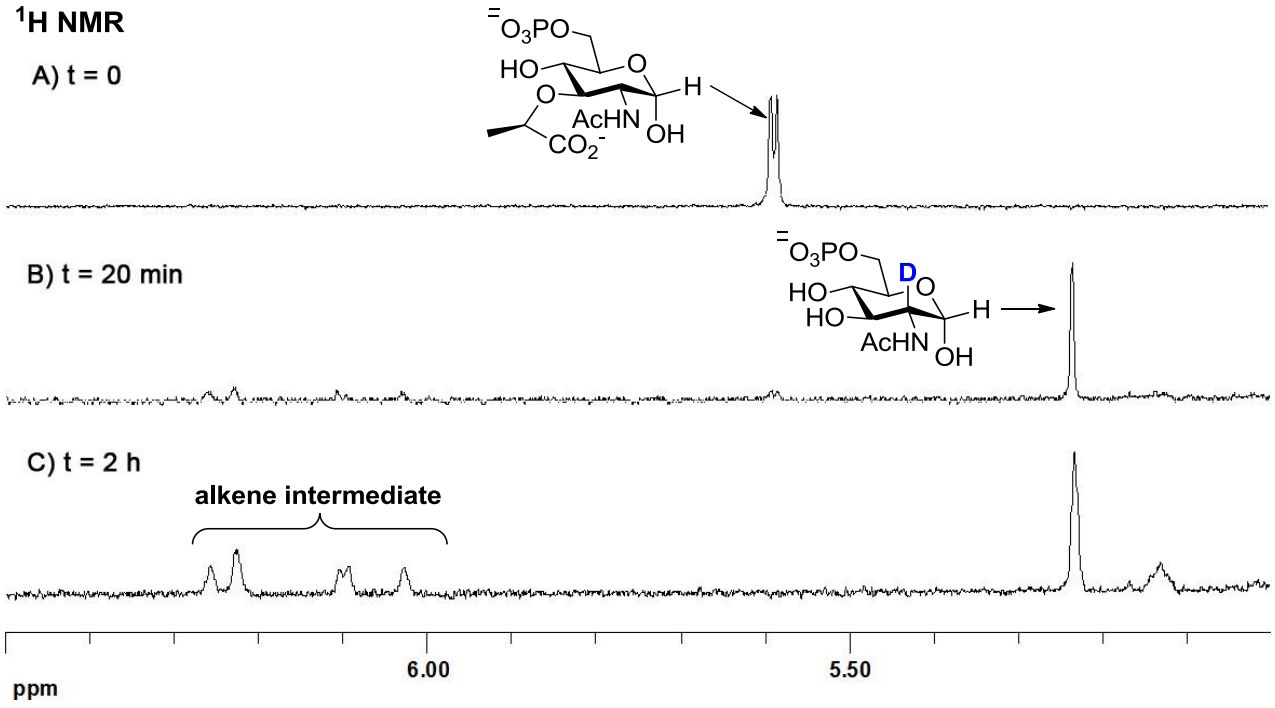

Figure 3.15 ^{1}H NMR spectra from monitoring the reaction of MurNAc 6-phosphate with MurQ in buffered D_2O. (A) Spectrum taken before the addition of enzyme. (B) Spectrum taken after 20 min showing [2-^{2}H]GlcNAc 6-phosphate as the sole product. (C) Spectrum taken after incubation for 2 h showing the appearance of peaks due to the alkene intermediate.

phosphate and GlcNAc 6-phosphate; the peaks in this case are not due to the presence of intermediate but are likely fragmentation products of the molecular ion. After extended incubations, a 1:2 equilibrium ratio of alkene intermediate to GlcNAc 6-phosphate product is eventually reached. This same equilibrium ratio of alkene intermediate to GlcNAc 6-phosphate was obtained when MurQ was incubated with pure GlcNAc 6-phosphate.

The timing of formation of the α,β-unsaturated intermediate during the reaction is interesting because the appearance of an "intermediate" of a reaction generally occurs before

complete conversion of starting material to product. In the case of the MurQ-catalyzed reaction however, MurNAc 6-phosphate is converted rapidly by the enzyme into GlcNAc 6-phosphate and only after extended incubation of the product with MurQ is the reaction intermediate observed (Figure 3.16). These experimental observations indicate that GlcNAc 6-phosphate is the kinetic product of the MurQ-catalyzed enzymatic reaction and likely the only relevant product under *in vivo* conditions. Since newly-formed GlcNAc 6-phosphate is shuttled into the GlcNAc recycling pathway (outlined in Section 1.3.3.2), buildup of this MurQ product in properly functioning bacterial cells is unlikely to occur. However, when GlcNAc 6-phosphate is allowed to accumulate and is left to incubate with MurQ *in vitro*, the reversible elimination of water occurs, and occasionally, the α,β-unsaturated intermediate is released into solution where it remains until an equilibrium ratio of intermediate to GlcNAc 6-phosphate is reached (Figure 3.16). This enzyme-catalyzed reversible elimination of water from GlcNAc 6-phosphate is further supported by the observation that a solvent-derived deuterium atom is incorporated into the C-2 position of pure GlcNAc 6-phosphate when it is left to incubate with MurQ in deuterated buffer.

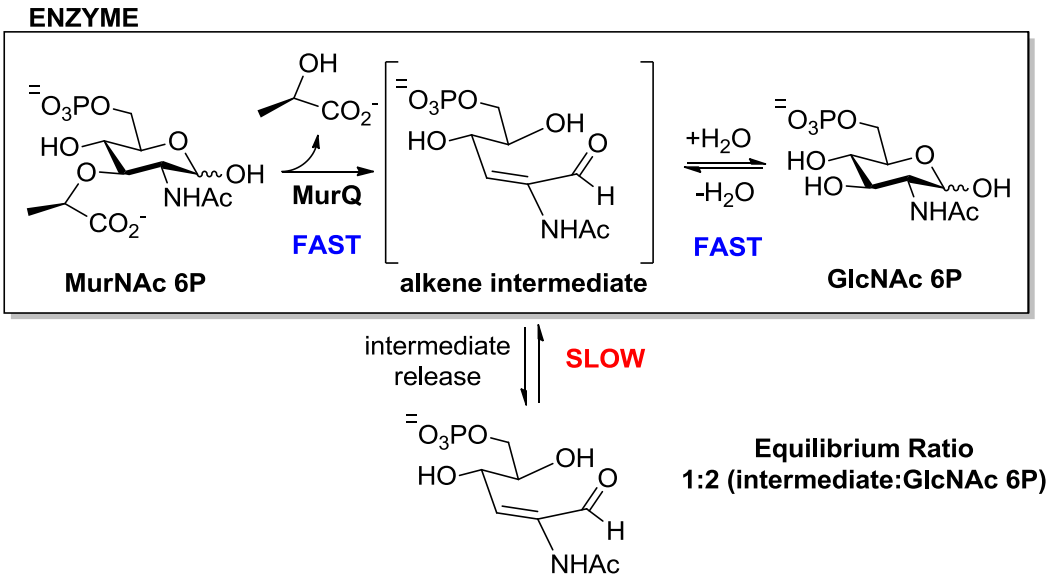

Figure 3.16 An equilibrium ratio of alkene intermediate and GlcNAc 6-phosphate is formed through the reversible dehydration of GlcNAc 6-phosphate by MurQ and occasional release of the alkene intermediate into solution. Boxed compounds represent enzyme-bound species.

3.6 Determination of the Nature of the Unsaturated Sugar Intermediate

The release of the α,β-unsaturated aldehyde intermediate into solution following prolonged incubations of substrate or product with MurQ allows for the determination of its chemical structure. Once determined, the structure of the intermediate will allow us to directly address the stereochemistry of the elimination occurring during the enzymatic reaction. The elimination of lactate (or water) proceeds via the formation of an enolate anion and can occur in either a *syn* or *anti* fashion. If *syn* eliminations are involved then the unsaturated intermediate would be an (*E*)-alkene, and if *anti* eliminations are involved then the unsaturated intermediate would be a (*Z*)-alkene.

When inside the active site of MurQ, the α,β-unsaturated aldehyde intermediate must exist in an unhydrated open chain form in order for the reaction to proceed. The presence of an unhydrated aldehyde at the C-1 position is required for the formation of the enolate

intermediate by the conjugate addition of water at the C-3 position. Once released from the active site however, the α,β-unsaturated aldehyde intermediate species could adopt several alternate forms (Figure 3.17). If an (*E*)-alkene is being formed via a *syn* elimination, the intermediate could exist in an open chain form as either a hydrated or unhydrated aldehyde. Due to the conjugation between the carbonyl and the alkene, it is likely that the unhydrated form of the aldehyde is preferred. In addition, the (*E*)-alkene intermediate species could also exist in either the furanose or pyranose closed chain forms, each of which would give rise to two distinct anomers. If a (*Z*)-alkene is being formed via an *anti*-elimination, the geometry of the (*Z*)-alkene would preclude cyclization into a pyranose or furanose form due to the high level of ring strain that would be generated. Consequently, the α,β-unsaturated aldehyde intermediate could only adopt the open chain hydrated and unhydrated forms.

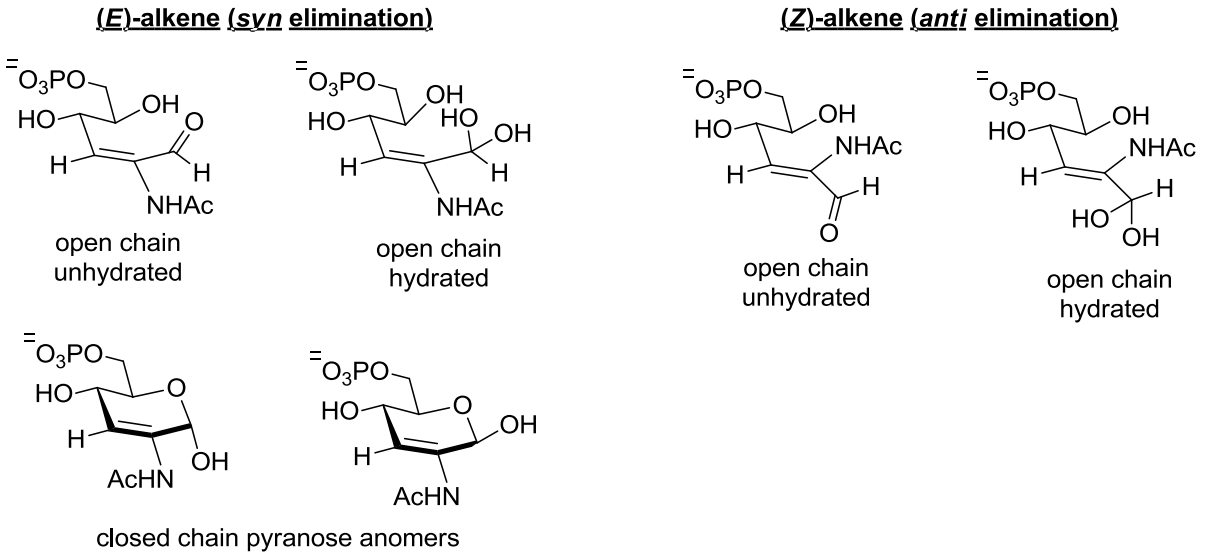

Figure 3.17 Possible structures of the alkene intermediate of the MurQ reaction following its release from the active site into solution. Possible (*E*)-alkene structures resulting from *syn* elimination are shown on the left, while possible (*Z*)-alkene structures resulting from *anti* elimination are shown on the right.

Analysis of the downfield region of the ^{1}H NMR spectrum of the α,β-unsaturated aldehyde intermediate reveals that no signals are present above 7.0 ppm that would indicate the presence of an open chain unhydrated aldehyde. From this information alone we can deduce that the stereochemistry of the intermediate is either (*E*)- or that there is a mixture of stereoisomers since the (*Z*)-open chain hydrated alkene would not give such a complex spectrum. For the ease of interpretation, the four signals in the downfield region of the spectrum have been labeled from 1 through 4 (Figure 3.18). A long-range COSY experiment on the alkene mixture, designed to allow for the observation of coupling through multiple bonds, revealed the presence of cross-peaks between signals 1 and 4, and between signals 2 and 3. The results of this NMR experiment strongly indicated that the four signals were derived from two distinct species in solution. An HMQC NMR experiment, designed to allow for the observation of one bond coupling between carbon and hydrogen, revealed that peaks 3 and 4 were coupled to carbon atoms with chemical shift values of around 100 ppm, and peaks 1 and 2 were coupled to carbon atoms with chemical shift values of 111 and 110 ppm, respectively. The results of this HMQC NMR experiment helped to further assign the two downfield signals (peaks 1 and 2) as hemiacetal protons and the two upfield signals (peaks 3 and 4) as alkene protons. In order to test whether these two species shared a common alkene geometry, the intermediate mixture was treated with sodium borohydride and analyzed by ^{1}H NMR spectroscopy. The mild reducing conditions employed during this experiment were designed to result in the reduction of any aldehydic species in solution while leaving the alkene functional groups intact. As can be seen in the ^{1}H NMR spectra displayed in Figure 3.18, the addition of sodium borohydride to the intermediate mixture

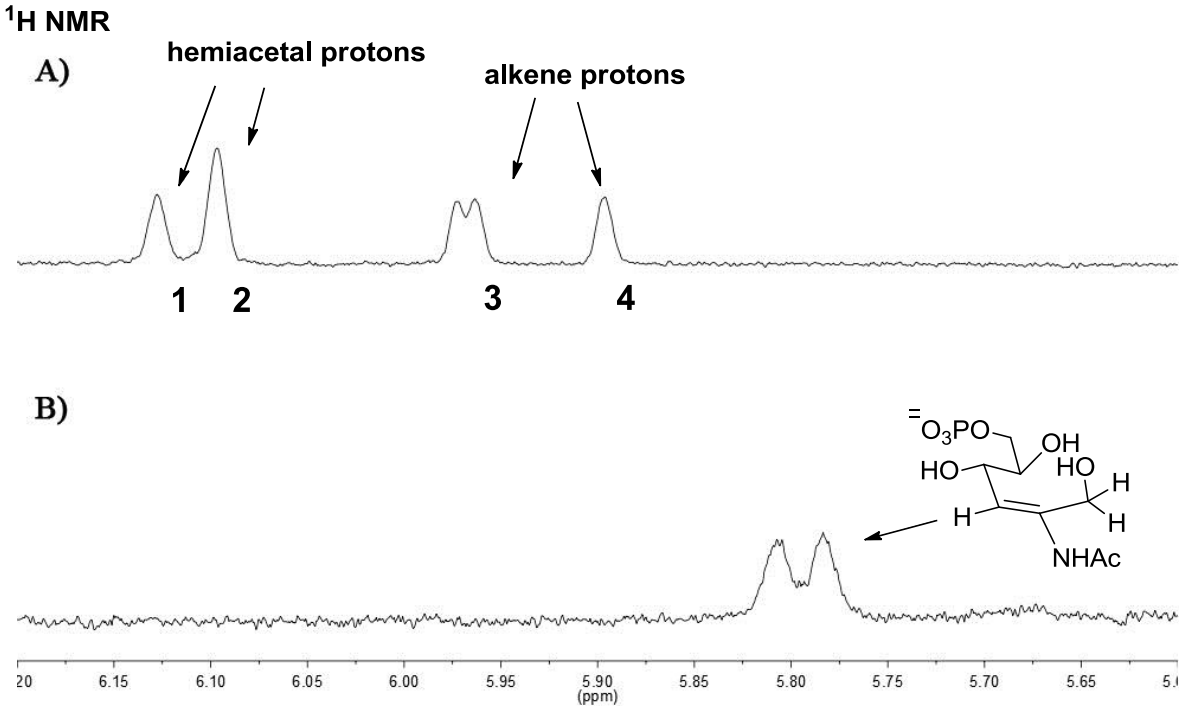

Figure 3.18 ^{1}H NMR spectra of the α,β-unsaturated aldehyde intermediate before (A) and after (B) reduction with $NaBH_4$.

results in the formation of a single alkene signal at 5.79 ppm. This indicates that the two unsaturated alkene species share a common geometry.

Taken together, these experimental results indicate that the α,β-unsaturated aldehyde intermediate of the MurQ reaction exists as two closed chain anomers of the (*E*)-alkene in solution (Figure 3.19). These two closed chain forms could exist as either furanose or pyranose rings in solution, but it is likely that the pyranose form is the dominant species due to the strain produced by an alkene in a five-membered ring species.[55] The assignment of the α,β-unsaturated aldehyde intermediate as the two pyranose anomers of the (*E*)-alkene indicates that the MurQ reaction proceeds via *syn* elimination of D-lactate from MurNAc 6-

phosphate followed by *syn* addition of water to the (*E*)-alkene intermediate to form GlcNAc 6-phosphate.

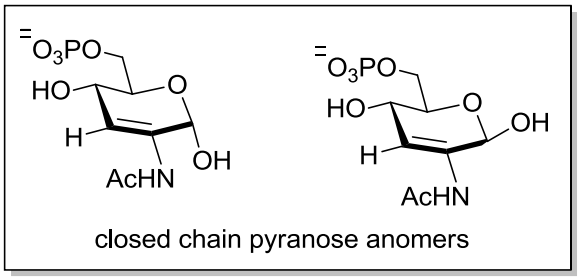

Figure 3.19 Favored structures of the (*E*)-α,β-unsaturated aldehyde intermediate of the MurQ reaction.

3.7 Studies with 3-Chloro-3-Deoxy-*N*-Acetylglucosamine 6-Phosphate

In order to further probe the proposed elimination mechanism of the MurQ reaction, the synthesis of 3-chloro-3-deoxy-*N*-acetylglucosamine 6-phosphate (3-chloro-3-deoxy-GlcNAc 6-phosphate) was undertaken to explore its ability to act as an alternate substrate of the enzyme. It was envisioned that the replacement of the D-lactyl ether at the C-3 position with a chlorine atom would still allow for a normal enzyme-catalyzed elimination reaction to occur. Deprotonation at the C-2 position by an active site base (B_1, Figure 3.6) to form the enolate anion intermediate would then result in the elimination of HCl (acidic catalysis by B_2 would not be required for a chloride leaving group) and formation of the (*E*)-alkene intermediate (Figure 3.20). The MurQ-catalyzed conjugate addition of water to the intermediate would then proceed as normal and GlcNAc 6-phosphate would be formed.

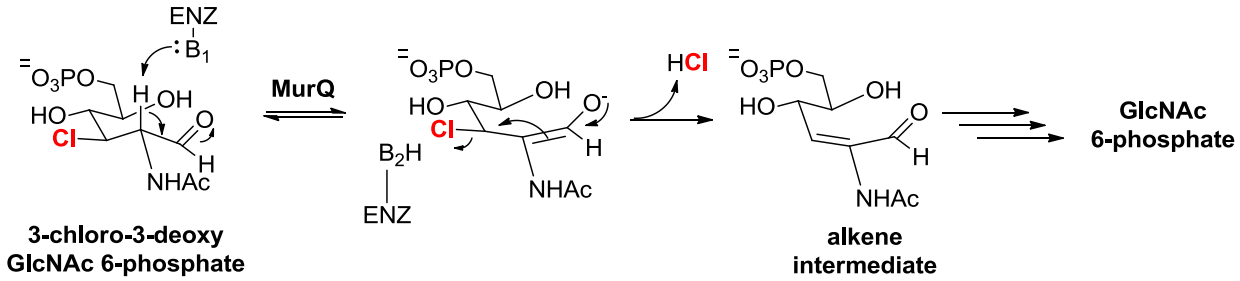

Figure 3.20 Proposed mechanism for the reaction of the alternate substrate 3-chloro-3-deoxy-GlcNAc 6-phosphate with MurQ.

The compound 3-chloro-3-deoxy-GlcNAc 6-phosphate could potentially be a very useful tool for the identification of active site residues involved in catalysis. Because of the stability of the chloride anion, and consequently its effective leaving group ability, the elimination of chloride does not require the assistance of an acid catalyst. It is conceivable then, that a mutant enzyme with an impaired ability to protonate the lactate leaving group (B_2 in Figure 3.6) could still catalyze the conversion of 3-chloro-3-deoxy-GlcNAc 6-phosphate into the (*E*)-alkene.

3.7.1 Synthesis of 3-Chloro-3-Deoxy-GlcNAc 6-Phosphate

A synthesis was designed to obtain 3-chloro-3-deoxy-GlcNAc 6-phosphate starting from commercially available D-glucosamine hydrochloride (Figure 3.21). A protected version of 3-chloro-3-deoxy-GlcNAc (compound **30**) was known,[56, 57] and served as an excellent starting point from which to selectively install a phosphate group at the C-6 position. To prepare compound **30**, the known compound **27** was first prepared from D-glucosamine hydrochloride using adapted literature procedures that involved functionalization of the amino group,[58] followed by anomeric benzylation,[43] and introduction of a 4,6-*O*-benzylidene acetal.[44] The free hydroxyl group at the C-3 position was tosylated using *p*-toluenesulfonyl chloride to generate compound **28** in modest yield.[56] The benzoyl

amide protecting group at the C-2 position was removed using sodium isopropoxide, and the resultant amide anion displaced the tosyl group at the C-3 position to generate an aziridine ring between C-2 and C-3. The crude aziridine was subjected to an unusual, yet precedented, diequatorial ring-opening reaction with ammonium chloride to give compound **29** in 34% yield as the *gluco*-configured amino sugar with a chlorine substituent at the C-3 position.[56]

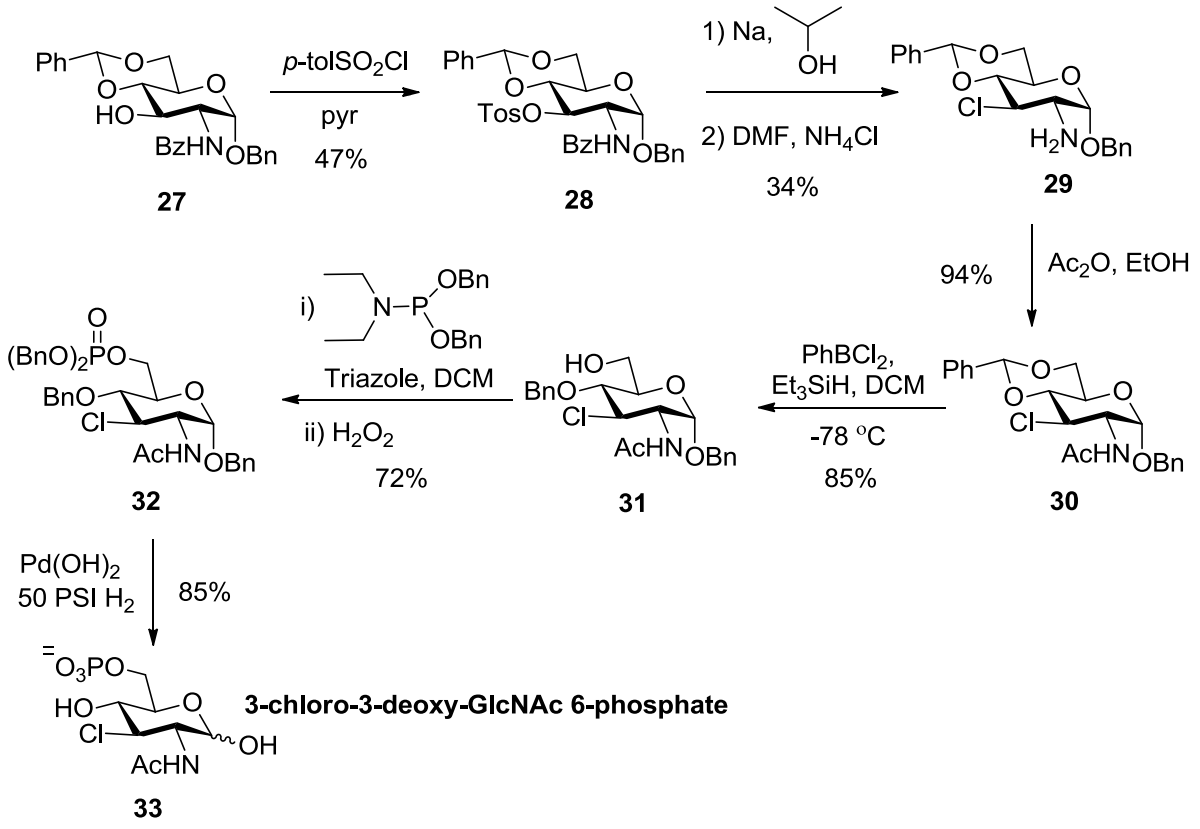

Figure 3.21 Synthesis of 3-chloro-3-deoxy-GlcNAc 6-phosphate.

Compound **29** was subsequently acetylated using acetic anhydride to give the known compound **30** in 94% yield.[56, 57] The subsequent transformations were performed in a manner identical to that used for the synthesis of MurNAc 6-phosphate (compound **23**). Compound **30** was subjected to a regioselective reductive ring-opening reaction using dichlorophenylborane and triethylsilane to give compound **31** with a free hydroxyl group at

the C-6 position in excellent yield.[31] The free hydroxyl group was converted into a phosphate ester by reaction of **31** with a phosphoramidite coupling reagent followed by oxidation with H_2O_2 to give the phosphorylated compound **32** in 72% yield.[48] Global deprotection of the benzyl protecting groups via hydrogenolysis using palladium hydroxide as catalyst gave compound **33** (3-chloro-3-deoxy-GlcNAc 6-phosphate) in 85% yield.

3.7.2 Studies with 3-Chloro-3-Deoxy-GlcNAc 6-Phosphate

Because of the presence of the relatively good chloride leaving group at the C-3 position of compound **33**, the stability of this compound in solution was examined before testing it as an alternate substrate of MurQ. To test for non-enzymatic decomposition of compound **33**, its stability in solution was examined at a higher buffer concentration and incubation temperature than those used for normal enzymatic incubation experiments. Gauging the stability of compound **33** under these harsher conditions would enable us to determine whether non-enzymatic decomposition would be a problem when assaying the compound for activity with MurQ. A sample of pure 3-chloro-3-deoxy-GlcNAc 6-phosphate was dissolved in 50 mM deuterated phosphate buffer (pD 7.9) and transferred to a NMR tube. A spectrum was acquired and the mixture was then incubated in a water bath at 42 °C. Surprisingly, the compound was relatively stable under the conditions of this experiment despite the substitution of the labile chloride leaving group at the C-3 position. Elimination products were only observed after several hours of incubation at 42 °C and complete elimination of chloride from compound **33** took several days.

In addition to addressing the stability of this potential MurQ substrate, monitoring the non-enzymatic decomposition of 3-chloro-3-deoxy-GlcNAc 6-phosphate by ^{1}H NMR spectroscopy yielded important information regarding the stereochemistry and structure of

the α,β-unsaturated aldehyde intermediate of the MurQ reaction (Figure 3.22). The first elimination product to appear displayed a singlet at 9.28 ppm and a doublet at 6.71 ppm corresponding to an aldehydic proton and alkene proton, respectively. These peaks were assigned to the unhydrated (*Z*)-α,β-unsaturated aldehyde that is formed as a result of *anti*-elimination of HCl from compound **33**. Because of the geometry of this (*Z*)-alkene, this aldehydic compound can only exist in an open chain form due to the ring-strain that would result from a closed chain species. After further incubation, signals began to appear between 5.9 and 6.2 ppm that corresponded to the hemiacetal and alkene protons of the two anomers of the (*E*)-α,β-unsaturated aldehyde. These peaks were identical to those obtained upon extended incubation of MurNAc 6-phosphate or GlcNAc 6-phosphate with MurQ. Eventually, the peaks corresponding to the (*E*)-alkene dominated the spectrum while those attributed to the (*Z*)-alkene disappeared. To account for these observations, it was proposed that the (*Z*)-α,β-unsaturated aldehyde was the first-formed kinetic product of the elimination reaction, and that this species gradually isomerized to the (*E*)-α,β-unsaturated aldehyde that is the more stable, thermodynamic product.

The observation of peaks corresponding to the (*Z*)-alkene by ^{1}H NMR spectroscopy during this decomposition experiment indicates that this species has a significant lifetime in solution (Figure 3.22, B). The complete absence of any aldehydic peaks corresponding to the (*Z*)-alkene species during extended incubations of either MurNAc 6-phosphate or GlcNAc 6-phosphate with MurQ indicate that the (*E*)-alkene is produced exclusively by the enzyme. This rules out the possibility that the previously observed (*E*)-alkene was simply an isomerization product of an enzyme-generated (*Z*)-alkene intermediate. It was also possible

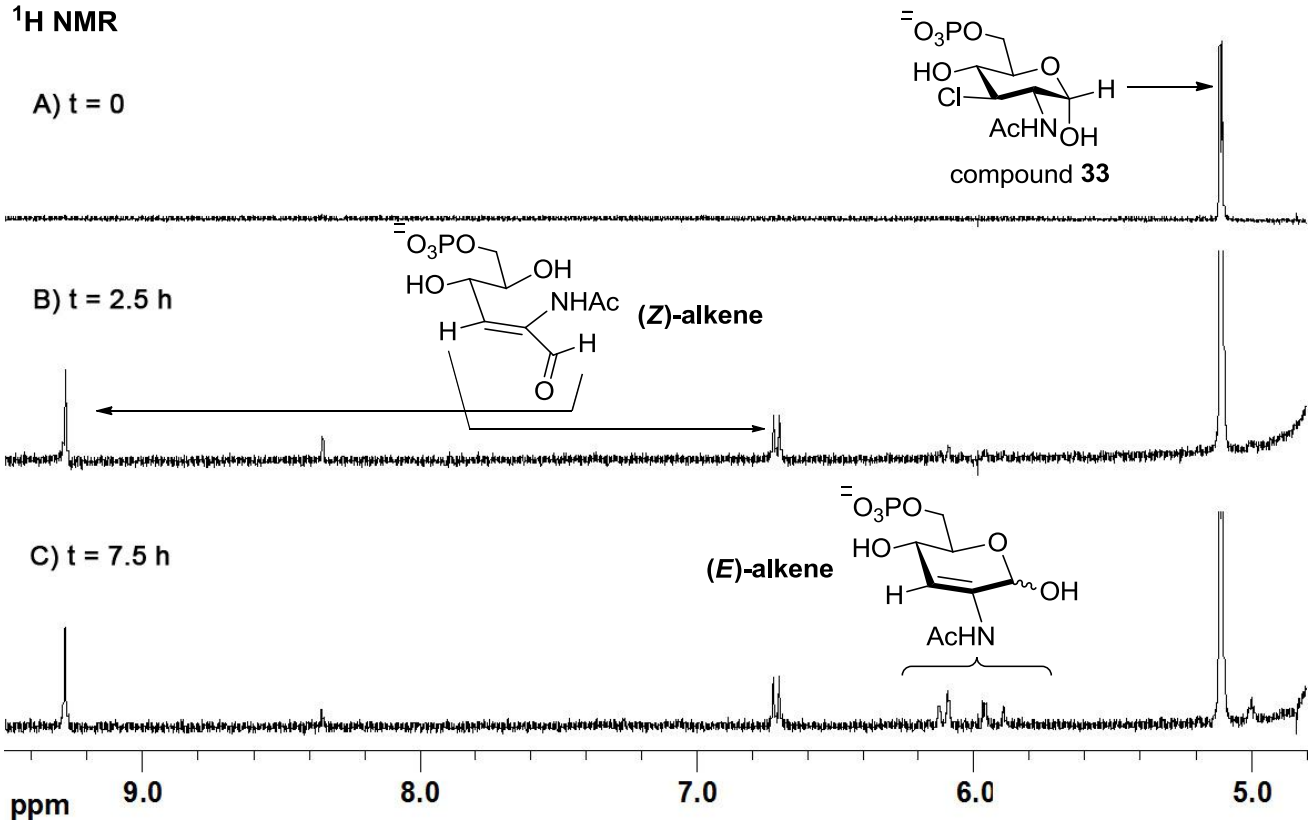

Figure 3.22 ^{1}H NMR spectra showing the decomposition of 3-chloro-3-deoxy-GlcNAc 6-phosphate (33) when incubated at 42 °C in deuterated phosphate buffer (50 mM, pD 7.9). (A) Before incubation at 42 °C. (B) After 2.5 h at 42 °C. (C) After 7.5 h at 42 °C.

to prepare an authentic sample of the (*E*)-α,β-unsaturated aldehyde intermediate; this was accomplished through the non-enzymatic elimination of HCl from 3-chloro-3-deoxy-GlcNAc 6-phosphate and subsequent incubation of the reaction mixture to allow for complete isomerization to occur (Figure 3.23). This sample was shown to be catalytically competent and was hydrated by MurQ to give the same equilibrium ratio of 1:2 (*E*)-α,β-unsaturated aldehyde intermediate to GlcNAc 6-phosphate seen previously (Figure 3.23).

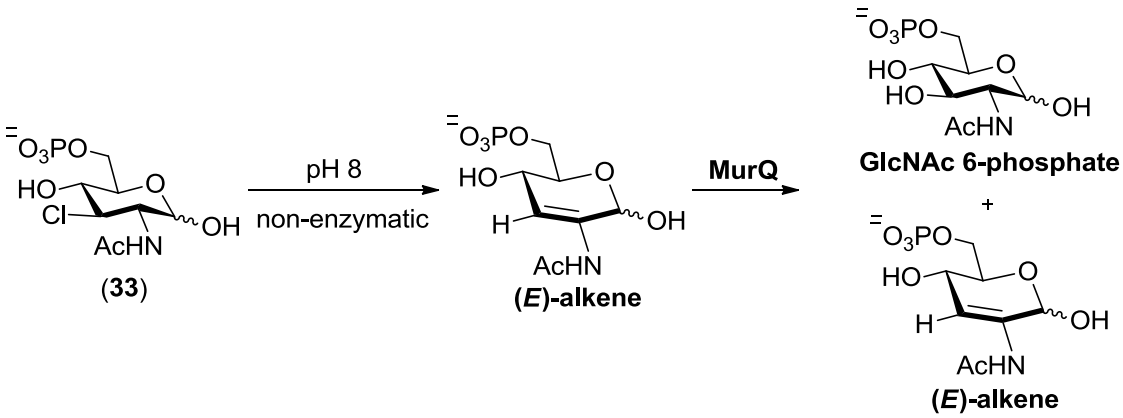

Figure 3.23 Incubation of (*E*)-alkene intermediate (produced non-enzymatically) with MurQ to test for catalytic competence.

3.7.3 Testing of 3-Chloro-3-Deoxy-GlcNAc 6-Phosphate as a Substrate of MurQ

A pure sample of 3-chloro-3-deoxy-GlcNAc 6-phosphate was tested as an alternate substrate for MurQ. Since this alternate substrate lacks the D-lactyl ether at the C-3 position, our coupled-assay measuring the release of lactate could not be used to measure the rate of enzyme-catalyzed reaction. Instead, the rate of reaction was estimated based on the conversion of the alternate substrate into the (*E*)-α,β-unsaturated aldehyde intermediate and product GlcNAc 6-phosphate as observed by ^{1}H NMR spectroscopy. The reaction progress could be monitored through observation of the peaks between 1.90 and 2.05 ppm due to the *N*-acetamido groups of 3-chloro-3-deoxy-GlcNAc 6-phosphate, GlcNAc 6-phosphate, and the (*E*)-α,β-unsaturated aldehyde intermediate (Figure 3.24). A very slow conversion of 3-chloro-3-deoxy-GlcNAc 6-phosphate into an equilibrium mixture of alkene intermediate and GlcNAc 6-phosphate was observed upon incubation with MurQ. Comparable incubations of MurNAc 6-phosphate with MurQ resulted in the consumption of substrate almost immediately after the addition of enzyme and it was estimated that MurQ activity with the alternate 3-chloro substrate was less than 2% of that observed for MurNAc 6-phosphate.

Because of the slow nature of this conversion, control experiments were performed in the absence of enzyme and confirmed that the process was indeed enzyme-catalyzed. Based on these experiments it was determined that 3-chloro-3-deoxy-GlcNAc 6-phosphate acts as an alternate substrate for the MurQ enzyme, albeit a poor one. It is likely that the replacement of the D-lactyl ether (or hydroxyl group in GlcNAc 6-phosphate) with a chlorine alters key interactions in the enzyme active site and results in a dramatic decrease in activity.

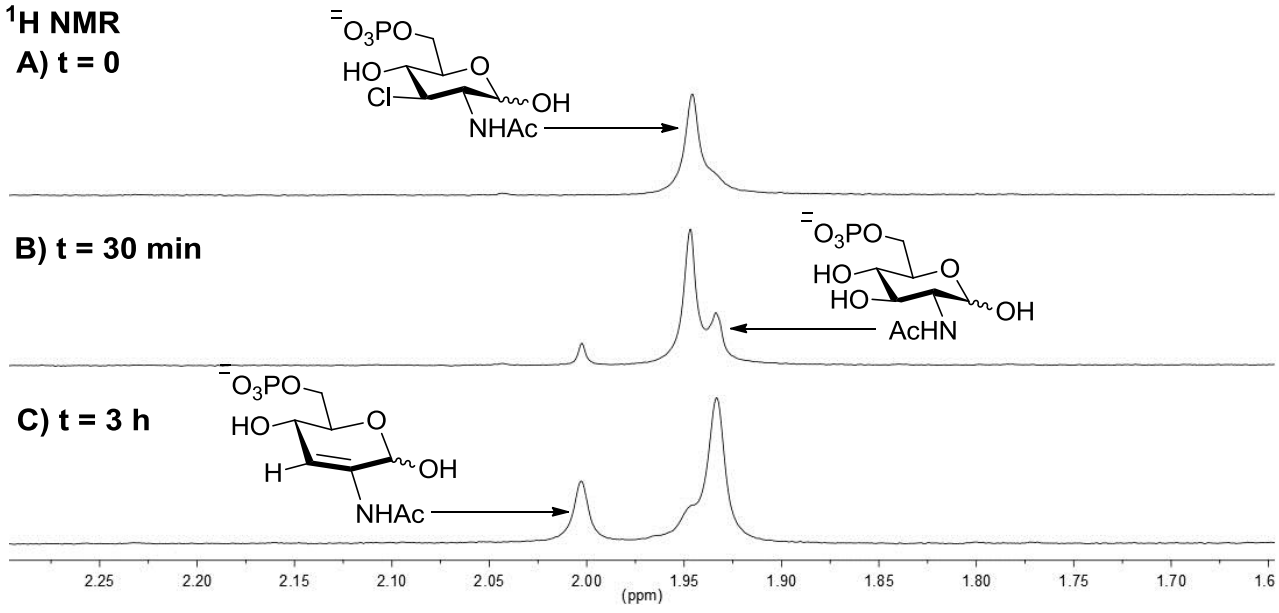

Figure 3.24 ^{1}H NMR spectra from monitoring the conversion of 3-chloro-3-deoxy-GlcNAc 6-phosphate into an equilibrium mixture of alkene intermediate and GlcNAc 6-phosphate. (A) Before enzyme addition. (B) After 30 min incubation with MurQ. (C) After 3 h incubation with MurQ.

3.8 Solvent-Derived ^{18}O Isotope Incorporation Catalyzed by MurQ

During previous studies on MurQ, the enzymatic reaction was performed in buffer prepared from ^{18}O-labelled water in order to determine if a solvent-derived oxygen was being incorporated into the product GlcNAc 6-phosphate.[11] Incubation of MurNAc 6-phosphate

with MurQ under these conditions resulted in the incorporation of 1 equivalent of ^{18}O isotope into the GlcNAc 6-phosphate product. It was reasonably assumed that the incorporation of this ^{18}O isotope had occurred at the C-3 position of the product, but this study did not rule out isotopic incorporation at the C-1 position. It is also conceivable that solvent isotope incorporation was occurring at both C-1 and C-3, but that the C-1 isotope readily exchanged with bulk solvent during the analysis procedures. Such results would be expected if MurQ were to employ a Schiff base mechanism involving a covalent imine linkage between the aldehyde at the C-1 position and an active site lysine residue. Formation of a Schiff base during catalysis, and hydrolysis of this intermediate to give the corresponding aldehyde, would result in the incorporation of ^{18}O solvent isotope into the sugar if the reaction was conducted in ^{18}O-labelled water. The enzyme glucosamine 6-phosphate synthase (GlmS), detailed in Section 3.1, has been proposed to catalyze the conversion of fructose 6-phosphate to glucosamine 6-phosphate through the formation of a Schiff base intermediate.[59] Because of the notable similarities between GlmS and MurQ, a mechanism involving a Schiff base intermediate is a distinct possibility for MurQ and should be addressed accordingly.

In order to examine the possibility of a Schiff base intermediate in the MurQ reaction, we chose to exploit the reversible nature of the elimination of water from the product of the reaction, GlcNAc 6-phosphate. To generate an isotopically-labeled analogue of GlcNAc 6-phosphate containing an ^{18}O-label at the C-1 position, a sample of GlcNAc 6-phosphate (synthesis detailed in Section 3.3.2) was dissolved in $H_2{}^{18}O$ and the solution was heated at 60 °C in a sealed glass tube for 5 h. Analysis of the reaction mixture by ESI-MS indicated that > 95% of the sugar had been converted into an isotopically-labeled analogue containing one ^{18}O-label. This labeled sample of GlcNAc 6-phosphate was incubated with MurQ in buffer

prepared from 50% $H_2{}^{18}O$ and 50% $H_2{}^{16}O$, and the reaction was monitored by mass spectrometry. Four isotopically-labeled forms of GlcNAc 6-phosphate could conceivably be observed during this experiment: a product with no ^{18}O label, two singly labeled products, and a doubly labeled product (Figure 3.25). The presence, or absence, of these products in the reaction mixture can be used to determine whether or not the MurQ-catalyzed reaction proceeds through the formation of a Schiff base intermediate.

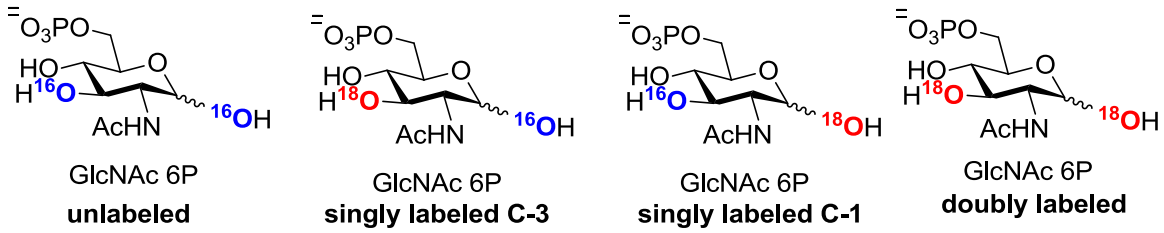

Figure 3.25 Possible isotopically-labeled forms of GlcNAc 6-phosphate that could be formed when [1-^{18}O]GlcNAc 6-phosphate is incubated with MurQ in 50:50 $H_2{}^{18}O$:$H_2{}^{16}O$.

An initial mass spectrum taken of [1-^{18}O]GlcNAc 6-phosphate in a 50:50 mixture of $H_2{}^{18}O$ and $H_2{}^{16}O$ displayed a single signal at *m*/*z* 302 (Figure 3.26, top). After the addition of MurQ to this mixture, this peak was gradually converted into an approximately 50:50 mixture of two signals at *m*/*z* 302 (singly labeled) and *m*/*z* 304 (doubly labeled) over time (Figure 3.26, bottom). The appearance of a peak corresponding to a doubly labeled species indicates that a solvent-derived ^{18}O isotope was being incorporated into the C-3 position via reversible dehydration of GlcNAc 6-phosphate. Mass spectra of the products derived from experiments conducted in the absence of enzyme displayed no peaks corresponding to unlabeled or doubly labeled GlcNAc 6-phosphate. These findings are completely consistent with the proposed mechanism of MurQ action as well as the results reported in previous experiments. The absence of a species containing no ^{18}O-isotope indicates that the label at

the C-1 position was not washed out (either enzymatically or non-enzymatically) during incubation of the compound with MurQ under these reaction conditions. Thus, we can conclude that a Schiff base intermediate is not being formed during catalysis.

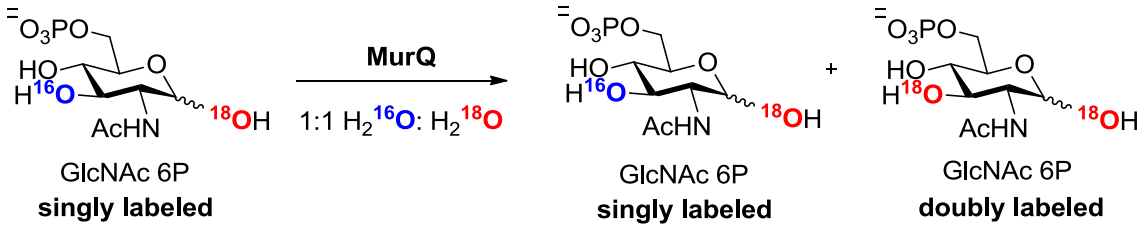

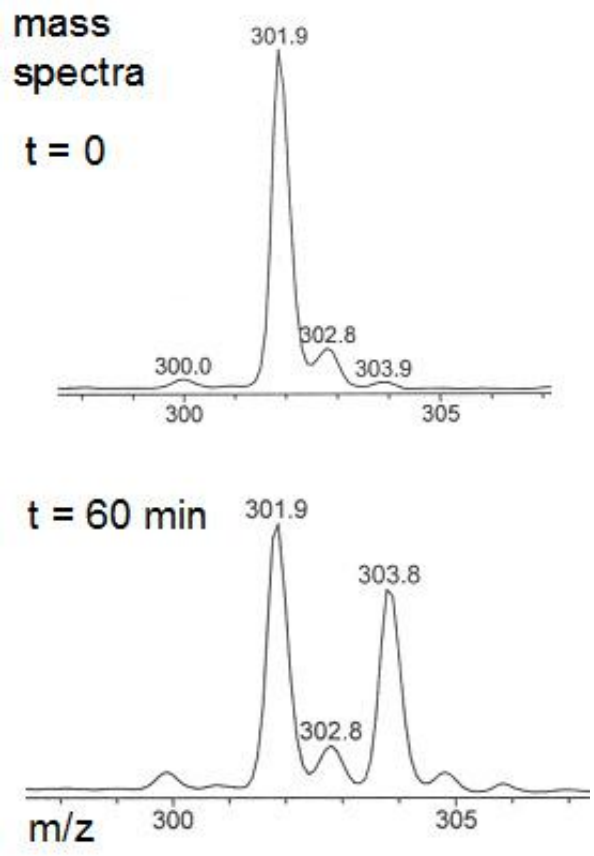

Figure 3.26 Mass spectra showing the reaction of [1-^{18}O]GlcNAc 6-phosphate with MurQ in a buffer prepared from a 50:50 mixture of $H_2{}^{18}O$ and $H_2{}^{16}O$: (top) spectrum taken before the addition of enzyme and (bottom) spectrum taken after incubation with MurQ for 60 min.

3.9 Comparison of a Structural Model of MurQ with GlmS and Identification of Potential Active Site Residues

In order to identify potential residues that could be playing important roles during catalysis, a structural model for the *E. coli* MurQ enzyme was developed. More specifically, it was envisioned that this model would allow for the identification of the acid/base catalysts that were playing the roles of B_1 and B_2 in the proposed mechanism of action (Figure 3.6). Work on the development of this model and the identification of potential active-site acid/base residues was performed at the University of Konstanz by Ulrike Dahl and Christoph Mayer.

A model was developed that was based upon the structure of a protein from *Haemophilus influenzae* that was very similar to *E. coli* MurQ.[60] This protein of unknown function, identified as HI0754, possessed an amino acid sequence that was 55% identical to that of *E. coli* MurQ and contained roughly the same number of residues (303 for HI0754 and 298 for MurQ). Because of the high level of sequence identity between HI0754 and MurQ, it is likely that HI0754 also functions as a MurNAc 6-phosphate etherase in *H. influenzae*. A structure of HI0754 was solved and reported as part of a structural genomics initiative (PDB entry 1NRI) and provided a basis for the *E. coli* MurQ etherase model that will be described herein.

As described in Section 3.1, MurQ and GlmS both belong to the SIS domain family of proteins. SIS domain proteins can be divided into two general classes: mono-SIS domain proteins and double-SIS domain proteins. Each SIS domain is characterized by the presence of five parallel β-sheets sandwiched by α-helices on either side.[60, 61] Reported crystal structures of proteins belonging to either of these two classes indicate that mono-SIS domain

proteins exist predominately as homo-dimers, while the two domains of double-SIS domain proteins come into close contact to form the active site.[60, 61]

MurQ belongs to the mono-SIS domain family and forms stable dimers as seen by gel filtration and dynamic light scattering. Its structure is proposed to contain additional α-helices at both the N- and C-termini that play important roles in dimer formation and catalysis.[60] Using the reported structure of HI0754, MurQ was modeled as a homodimer that contained two putative active sites. This homodimeric model of MurQ closely resembled the crystal structure of the isomerase module of GlmS (Figure 3.27). Unlike the modeled structure of MurQ, the isomerase module of GlmS forms a pseudodimer that consists of two SIS domains on a single polypeptide strand. Despite these differences however, a significant amount of structural and sequence overlap exists between the SIS domain of MurQ and one of the SIS domains of GlmS.

By using the structural model of MurQ, along with the crystal structure of GlmS and multiple-sequence alignments, three conserved amino acid residues were implicated as key active site residues of putative etherases (Figure 3.28). These residues, Glu83, Glu114, and Asp115, were examined in detail in order to probe their potential roles in catalysis. Glu83 is located at the end of helix 1 (H1) that connects β-strands 1 and 2 (S1 and S2) in the α–β–α sandwich fold of the SIS domain.[60] The positioning of this residue in the MurQ model is very similar to that of a key acid/base residue involved in GlmS catalysis, Glu488. Glu114 and Asp 115 of MurQ were found to be located on an α-helix and were positioned very similarly to His504 of GlmS that is thought to be involved in catalyzing ring opening of sugar substrates during catalysis. Interestingly, the lysine residue (Lys603) in GlmS that is proposed to form a Schiff base intermediate with the ketone of fructose 6-phosphate is not

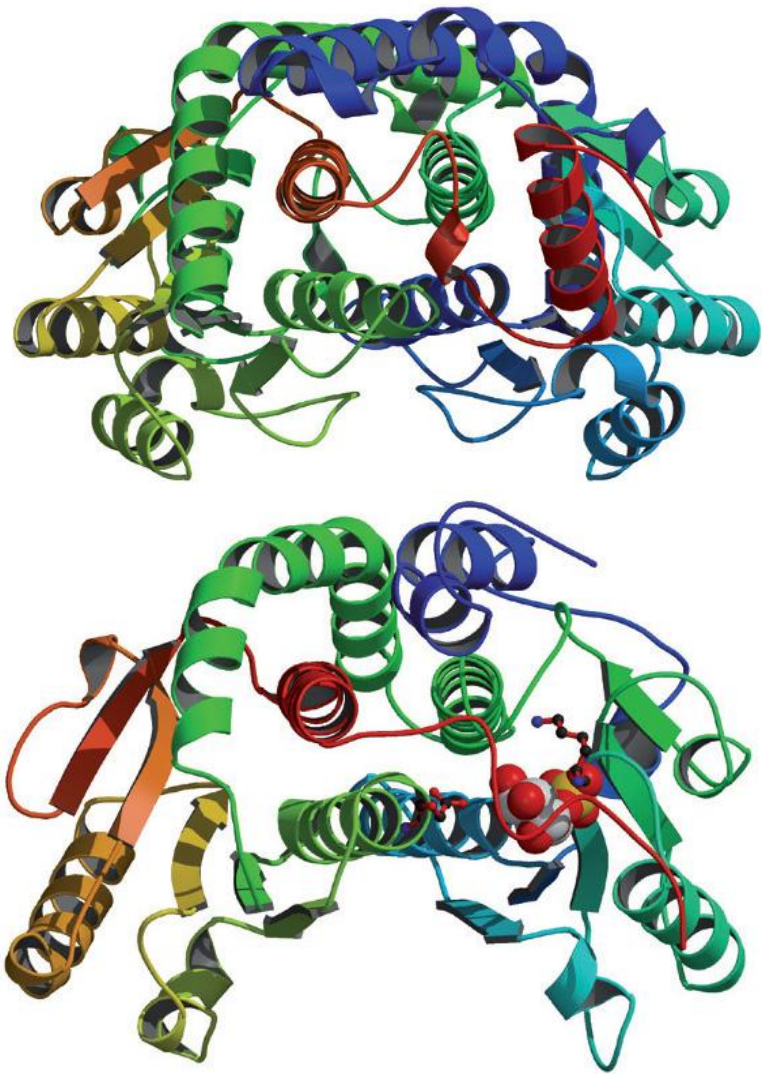

Figure 3.27 Structural model of MurQ modeled as a homodimer (top) and structure of the isomerase module of GlmS (PDB code: 1MOR). In the GlmS structure, the proposed catalytic residues Glu488 (left) and Lys603 (right) are shown as ball and sticks, and glucose 6-phosphate is shown as a space-filling model in the active site. Diagrams obtained from T. Jaeger and C. Mayer.[60]

conserved within any of the etherases that were subjected to multiple sequence alignment.[60] This is a strong indication that although MurQ and other etherases bear significant similarity to GlmS, they are unlikely to employ a mechanism involving the formation of a Schiff base. The lack of a Schiff base intermediate during MurQ catalysis is further supported by our

experiments examining solvent isotope incorporation with [1-^{18}O]GlcNAc 6-phosphate (detailed in Section 3.8).

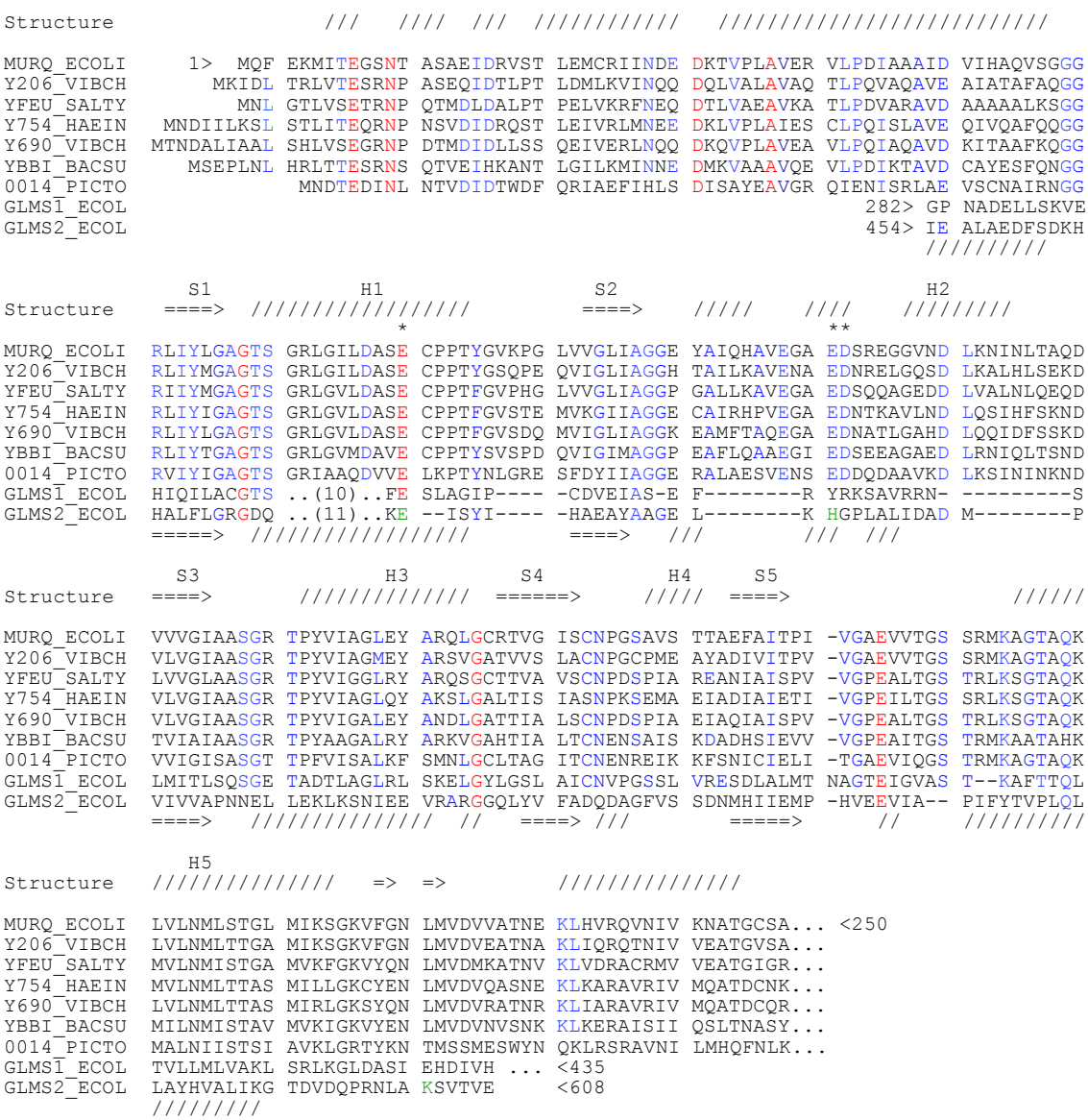

Figure 3.28 Identification of putative active site residues using a multiple sequence alignment and the structural model of *E. coli* MurQ. The amino acid sequences of the sugar phosphate isomerase/ sugar phosphate binding protein (SIS) domains of MurQ of *E. coli* (MURQ_ECOLI) and selected putative MurNAc etherases (*Vibrio cholerae*, Y206_VIBCH and Y690_VICH; *Salmonella thyphi*, YFEU_SALTY; *Haemophilus influenzae*, Y754_HAEIN; *Bacillus subtilis*, YBBI_BACSU; *Picrophilus torridus*, 0014_PICTO) are shown along with the two SIS domains of GlmS, the glucosamine-6-

phosphate synthase of *E. coli* (GLMS1_ECOLI and GLMS2_ECOLI). Conserved amino acid residues are shown in red, and residues that are conserved only within the etherase sequences are shown in blue. The active site residues Glu488, His504, and Lys603 of GlmS are shown in green. The structural motifs (helices, =>; sheets, ////) of the SIS domain fold (a five stranded parallel beta sheet flanked by five alpha helices) are shown and numbered according to their appearance in the amino acid sequence. Residues Glu83, Glu114, Asp115 (*E. coli* MurQ numbering) are marked (*).

3.9.1 Construction and Kinetic Characterization of MurQ Mutants

In order to probe the catalytic roles of the amino acid residues that were identified using our MurQ structural model, four *E. coli* MurQ mutants were generated: Glu83Gln, Glu83Ala, Glu114Gln, and Asp115Asn. The conversion of glutamic acid to glutamine and aspartic acid to asparagine was designed to minimize the structural differences between the mutant and wild type enzymes while at the same time greatly affecting the ability of the residues to act as an acid/base catalyst (Figure 3.29). The conversion of glutamic acid to an alanine residue is a much less conservative mutation, but was undertaken for reasons that will be described in the following section.

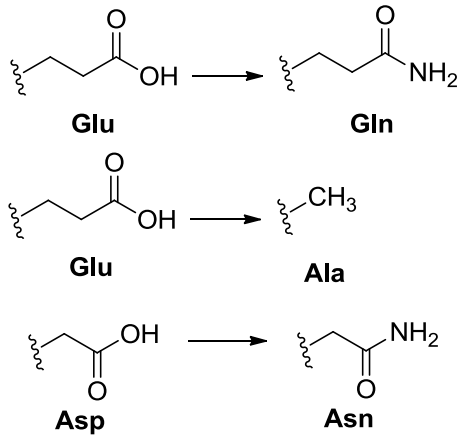

Figure 3.29 Structural changes of mutated residues for the Glu83Gln, Glu83Ala, Glu114Gln, and Asp115Asn MurQ mutant enzymes.

All four of the MurQ mutants were kinetically characterized with MurNAc 6-phosphate as a substrate using the continuously coupled assay for lactate release detailed in

Section 3.4. Although detailed analysis of the stability of these four MurQ mutants was not conducted, it was assumed that the mutant enzymes shared similar properties in this regard to the wild type *E. coli* MurQ enzyme. Accordingly, mutant enzyme was freshly purified each day immediately prior to use from frozen cell pellets stored at –78 °C. The Glu83Gln mutant was completely devoid of activity using MurNAc 6-phosphate as a substrate; interestingly however, the Glu83Ala mutant bearing a structurally more dramatic modification showed an extremely low, but measurable, level of activity (Figure 3.30). Similar plots of the rate of D-lactate release at varying concentrations of MurNAc 6-phosphate were constructed from data obtained with the Glu114Gln and Asp115Asn mutants (Figures 3.31 and 3.32).

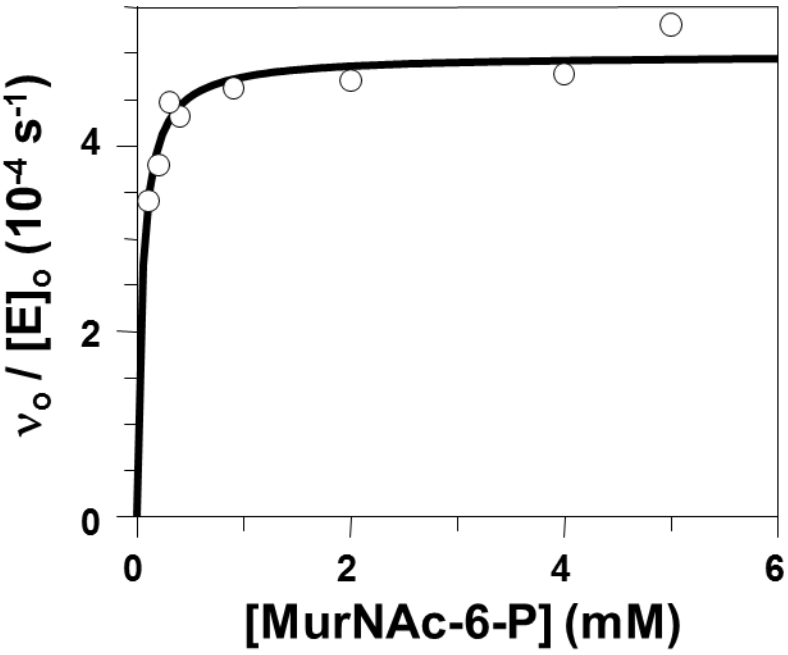

Figure 3.30 Plot of initial velocity vs. MurNAc 6-phosphate concentration for the Glu83Ala MurQ mutant.

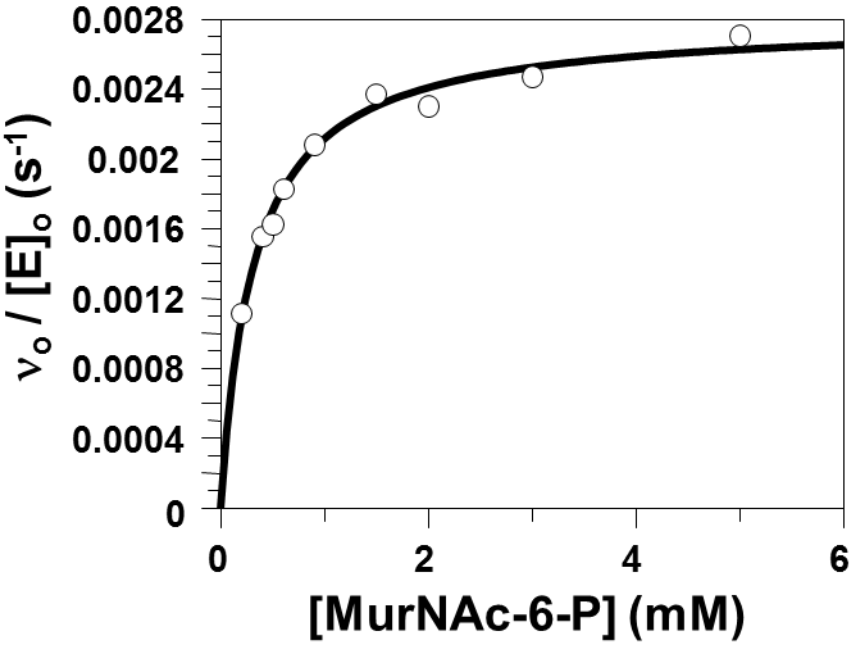

Figure 3.31 Plot of initial velocity vs. MurNAc 6-phosphate concentration for the Glu114Gln MurQ mutant.

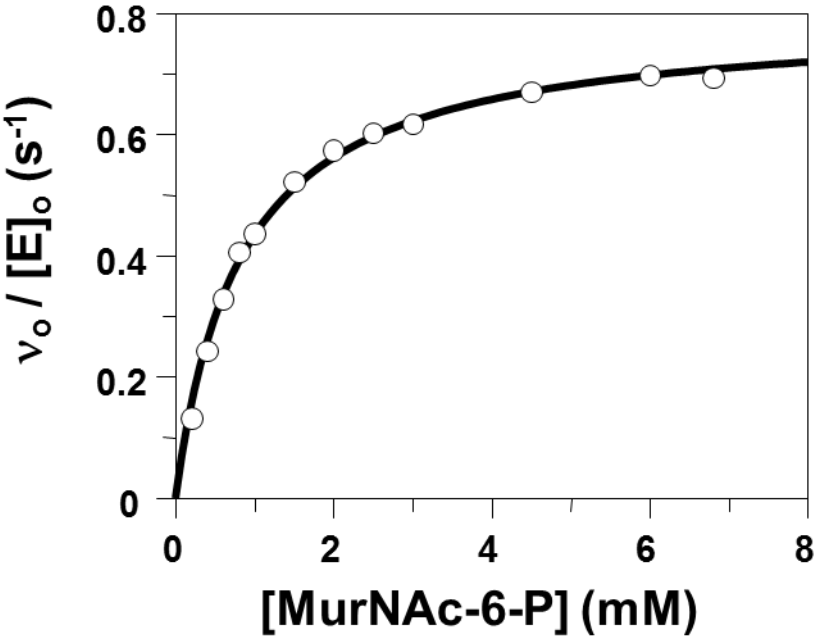

Figure 3.32 Plot of initial velocity vs. MurNAc 6-phosphate concentration for the Asp114Asn MurQ mutant.

The kinetic parameters k_{cat}, K_M, and k_{cat}/K_M, were determined for the Glu83Ala, Glu114Gln, and Asp115Asn mutants and are shown in Table 3.1. The kinetic parameters k_{cat} and K_M, and their associated errors, were determined by fitting the initial velocity data to the Michaelis-Menten equation using non-linear regression. Data obtained on different days with different batches of purified mutant enzyme could result in kinetic parameters that differed from those reported above by up to 25%. The Glu83Ala mutation had the greatest effect on enzyme activity with a greater than 10,000-fold reduction in k_{cat} as compared to wild type enzyme. The activity of this mutant on MurNAc 6-phosphate was so low that an accurate determination of K_M could not be performed. The Glu114Gln mutant also displayed a significant reduction in the value of k_{cat} (2,000-fold) and a more modest decrease in the value of K_M (4-fold). Kinetic data obtained for the Asp115Asn mutant showed that the transformation of aspartic acid to asparagine resulted in only a 7-fold reduction in the value of k_{cat}, indicating that this residue is unlikely to play an important role as an acid/base during catalysis. The identification of two residues whose mutation severely impairs the catalytic ability of the enzyme serves to further validate our structural model of MurQ and its comparison to GlmS. These findings also implicate Glu83 and Glu114 as reasonable candidates to act as B_1 and B_2 in the proposed mechanism of MurQ action (Figure 3.6).

enzyme	k_{cat} (s^{-1})	K_M (mM)	k_{cat}/K_M ($M^{-1}s^{-1}$)
WT MurQ	5.7 ± 0.1	1.20 ± 0.07	4.8 X 10^3
Glu83Ala	0.0005 ± 0.0001	---	---
Glu114Gln	0.0028 ± 0.0002	0.32 ± 0.03	8.8
Asp115Asn	0.79 ± 0.01	0.83 ± 0.04	9.5 X 10^2

Table 3.1 Kinetic constants for the reactions catalyzed by MurQ and its mutants. The kinetic parameters k_{cat} and K_M, and their associated errors, were determined by fitting the initial velocity data to the Michaelis-Menten equation using non-linear regression. Data obtained on different days with different batches of enzyme could result in kinetic constants that differed from those reported above by up to 25%.

3.9.2 Monitoring the MurQ Mutant Reactions by ^{1}H NMR Spectroscopy and Mass Spectrometry

Because kinetic characterization of the three MurQ mutants using our coupled assay only provides a measurement of the enzyme's ability to catalyze the liberation of D-lactate from MurNAc 6-phosphate, a number of enzymatic reactions with MurQ mutants were carried out in buffer prepared from D_2O. These MurQ mutant reactions were monitored by ^{1}H NMR spectroscopy and mass spectrometry, and the results were compared to those obtained during the reaction with wild type enzyme. In this manner, changes in the partitioning of the enzymatic reaction toward the α,β-unsaturated aldehyde intermediate, GlcNAc 6-phosphate product, or back to the MurNAc 6-phosphate substrate could be easily monitored along the reaction coordinate.

Although the Asp115Asn mutant did not show any significant decrease in its ability to catalyze the liberation of D-lactate from MurNAc 6-phosphate, it was still incubated with MurNAc 6-phosphate and GlcNAc 6-phosphate in deuterated buffer and monitored by ^{1}H NMR spectroscopy. Expectedly, no dramatic differences were observed when the

Asp115Asn mutant reaction was compared to similar incubations conducted with the wild type enzyme. It was concluded that although Asp115 is conserved throughout the etherases analyzed by our sequence alignment, it is unlikely to play a key role during catalysis.

3.9.2.1 Reaction of MurNAc 6-Phosphate with the Glu83Ala MurQ Mutant

When the reaction with MurNAc 6-phosphate and the Glu83Ala mutant was carried out in buffered D_2O and monitored by ^1H NMR spectroscopy a number of interesting observations were made. As expected from the kinetic results, the turnover of MurNAc 6-phosphate into GlcNAc 6-phosphate product was extremely slow. In fact, no peaks corresponding to GlcNAc 6-phosphate or the (*E*)-α,β-unsaturated aldehyde intermediate were observed during the normal time course of the enzymatic reaction. A change was observed however, in the anomeric signal at 5.59 ppm corresponding to the α-anomer of MurNAc 6-phosphate (Figure 3.33). This peak normally appears a doublet due to the coupling between the anomeric proton and the axial proton at the C-2 position. After incubation of MurNAc 6-phosphate with the Glu83Ala MurQ mutant however, this doublet was observed to collapse into a singlet over time (Figure 3.33). This change was attributed to the wash-in of solvent-derived deuterium at the C-2 position of MurNAc 6-phosphate and was found to occur much more rapidly than turnover to product. The incorporation of a single non-exchangeable deuterium atom into MurNAc 6-phosphate was also confirmed through mass spectral analysis of the reaction mixture.

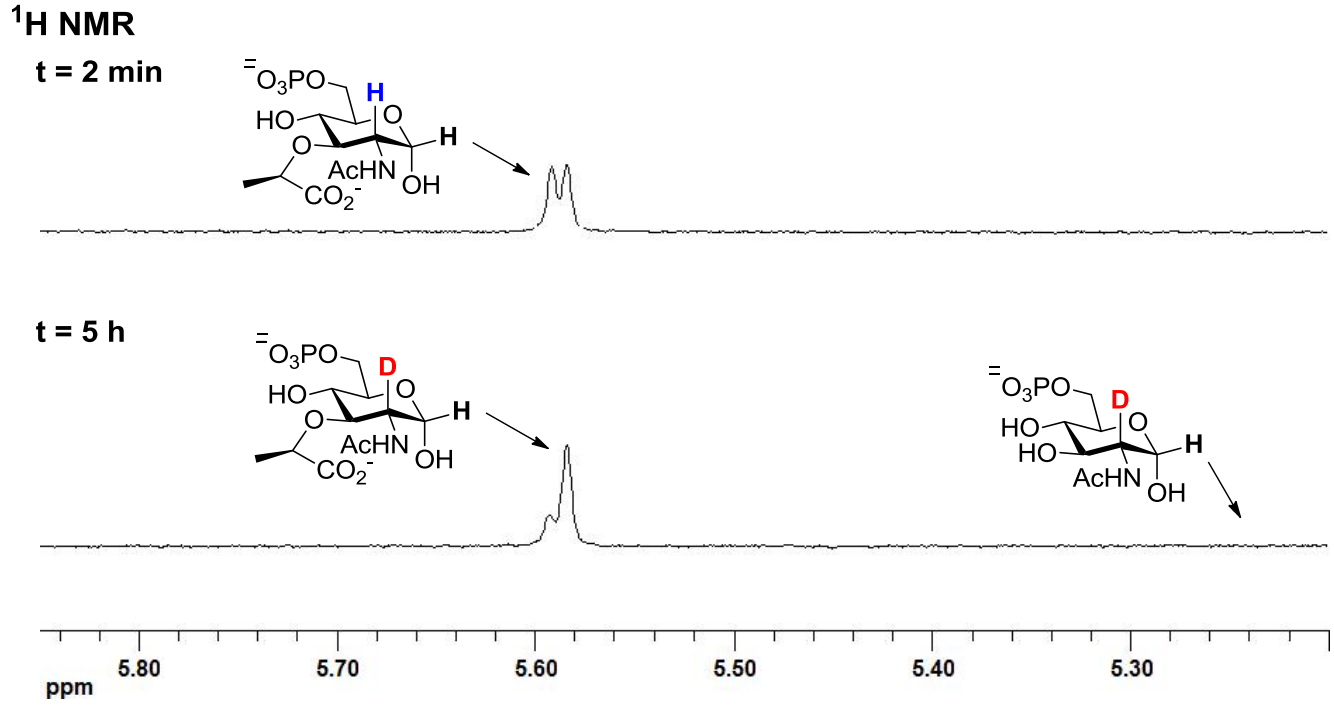

Figure 3.33 ^{1}H NMR spectra from monitoring the reaction of MurNAc 6-phosphate with the Glu83Ala mutant in deuterated buffer. (Top) Spectrum taken after incubation for 2 min with the mutant showing unlabeled MurNAc 6-phosphate. (Bottom) Spectrum taken after incubation for 5 h with the mutant showing the formation of [2-^{2}H]MurNAc 6-phosphate before any GlcNAc 6-phosphate is generated.

The formation of [2-^{2}H]MurNAc 6-phosphate during incubation with the Glu83Ala mutant differed significantly from what was observed during the wild-type enzymatic reaction. No deuterium incorporation into the residual pool of starting material could be detected by either ^{1}H NMR spectroscopy or mass spectrometry during the wild-type MurQ reaction, even after 80% of the MurNAc 6-phosphate substrate had been turned over to the product, GlcNAc 6-phosphate. This indicates that during the wild-type reaction the partitioning of the deprotonated enolate anion proceeds forward towards product much more rapidly than exchange of the C-2 proton with bulk solvent. In the MurQ Glu83Ala reaction

however, the conversion of substrate to product is slow enough to allow reprotonation of the enolate anion intermediate with a solvent-derived deuterium and partitioning of the reaction backwards to give [2-^{2}H]MurNAc 6-phosphate (Figure 3.34).

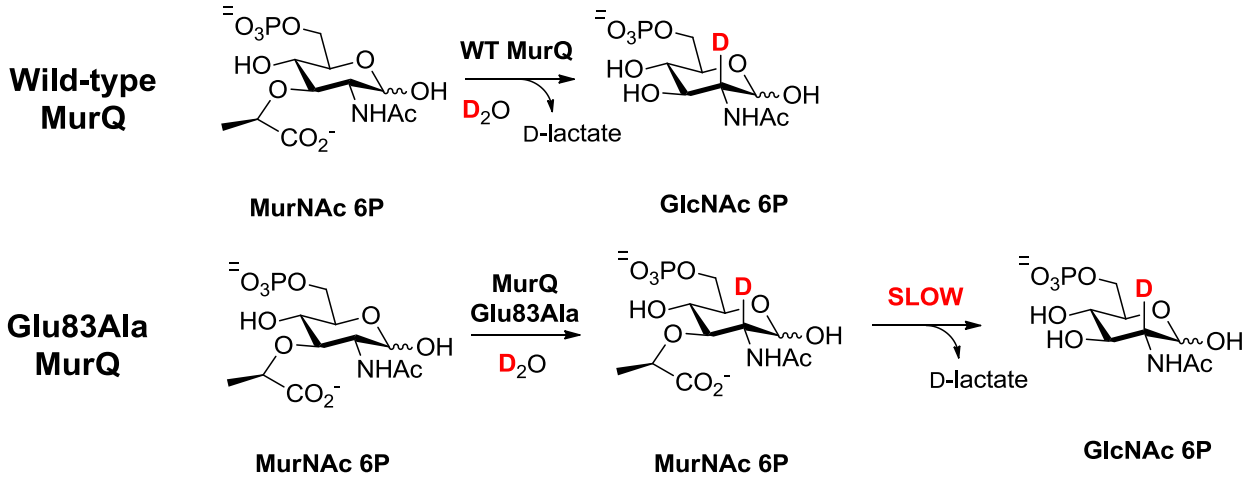

Figure 3.34 Schematic of the reactions catalyzed by wild-type (top) and Glu83Ala MurQ (bottom). The slow elimination of D-lactate by the mutant enzyme allows for exchange of solvent-derived deuterium at the C-2 position of MurNAc 6-phosphate via the enolate anion intermediate.

The incorporation of a solvent-derived deuterium at the C-2 position of MurNAc 6-phosphate during incubation with the Glu83Ala mutant but not with the wild-type enzyme suggests that Glu83 is a reasonable candidate to serve as B_2 in catalysis. If Glu83 is responsible for protonating the departuring lactate (or hydroxyl) group at the C-3 position, then the Glu83Ala mutant would still have a properly functioning amino acid acid/base (B_1) capable of removing the proton at the C-2 position to form the enolate anion intermediate (Figure 3.35). Since the subsequent elimination of lactate from this enolate anion is significantly impaired, the proton removed from the C-2 position will have sufficient time to exchange with bulk solvent before it is returned to give isotopically-labeled starting material.

The assignment of Glu83 as B_2 in our catalytic mechanism of MurQ could also explain the 10,000-fold reduction in k_{cat} for the Glu83Ala mutant.

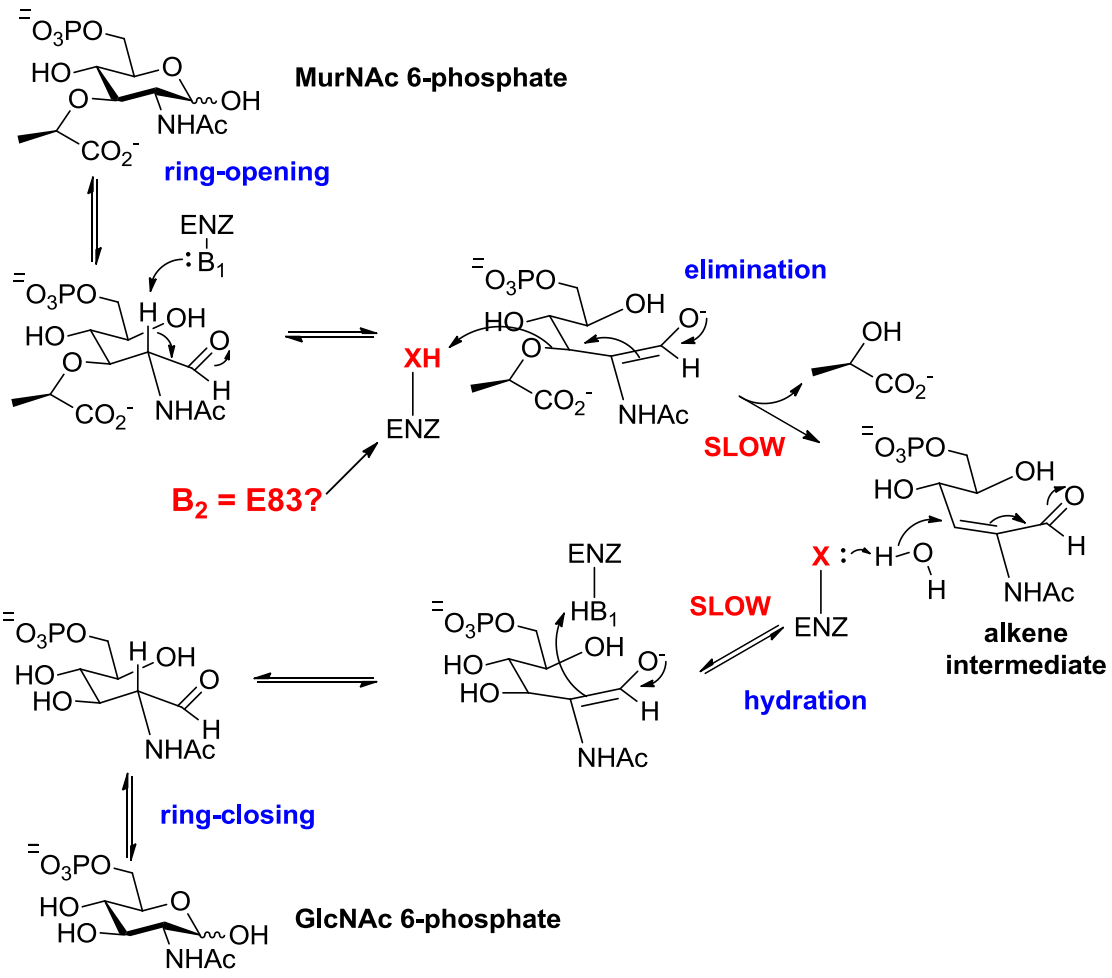

Figure 3.35 Proposed catalytic mechanism of MurQ with Glu83 playing the role of B_2. Mutagenesis of Glu83 to an alanine prevents the protonation of lactate and results in a dramatic decrease in catalytic activity. WT XH = CH_2CH_2COOH, Glu83Ala mutant XH = CH_3.

3.9.2.2 Reaction of MurNAc 6-Phosphate with the Glu114Gln MurQ Mutant

When monitored by ^{1}H NMR spectroscopy, the Glu114Gln mutant reaction also showed significant differences as compared to the wild-type MurQ reaction. As discussed in Section 3.5, when MurNAc 6-phosphate was incubated with wild-type MurQ the first formed product was GlcNAc 6-phosphate. After extended incubations with enzyme however, a 1:2

equilibrium ratio of (*E*)-α,β-unsaturated aldehyde intermediate to GlcNAc 6-phosphate was produced. In the case of the Glu114Gln mutant reaction, the first formed product was not GlcNAc 6-phosphate, but the (*E*)-α,β-unsaturated aldehyde intermediate. This result is clearly shown in Figure 3.36, where the signals between 6.0 and 6.3 ppm corresponding to the anomeric and alkene protons of the (*E*)-α,β-unsaturated aldehyde intermediate are clearly present before the appearance of the singlet at 5.23 ppm corresponding to the α-anomeric proton of GlcNAc 6-phosphate.

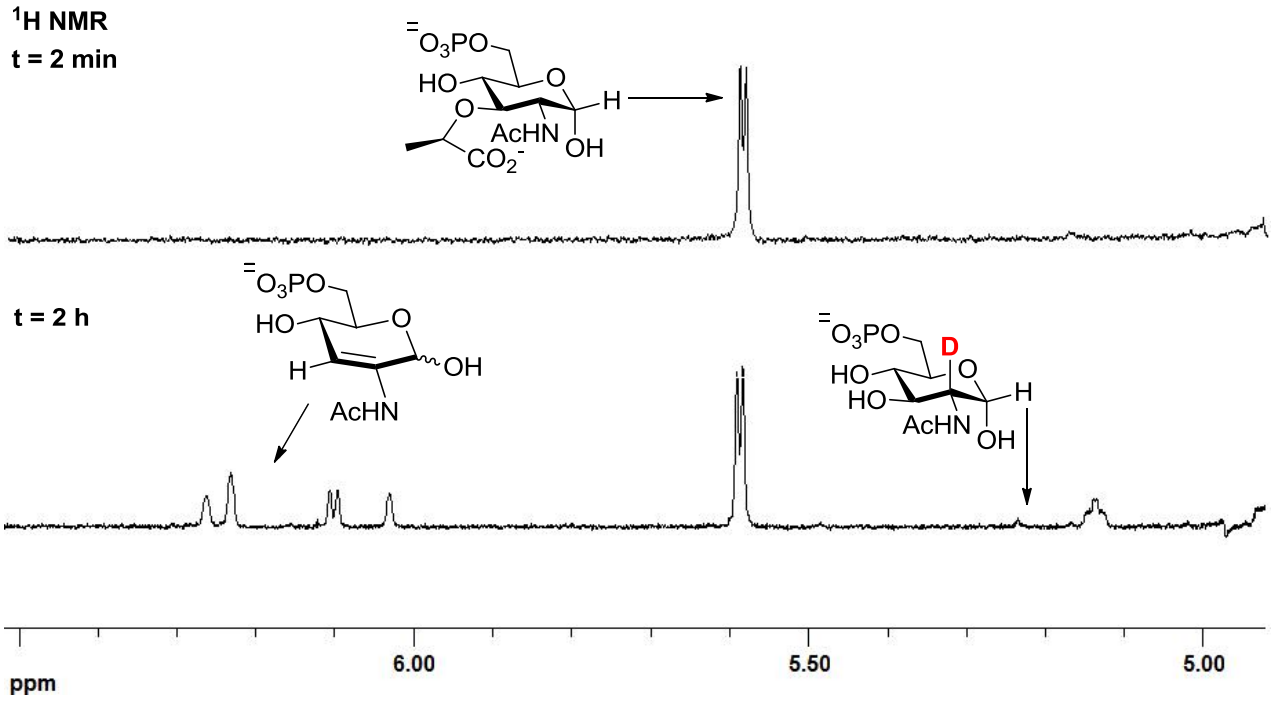

Figure 3.36 ^{1}H NMR spectra monitoring the reaction of MurNAc 6-phosphate with the Glu114Gln MurQ mutant in deuterated buffer. (Top) Spectrum taken after incubation for 2 min with the mutant enzyme showing MurNAc 6-phosphate. (Bottom) Spectrum taken after incubation for 2 h with the mutant enzyme showing the appearance of the alkene intermediate before significant formation of GlcNAc 6-phosphate.

The fact that intermediate release is faster than conversion of MurNAc 6-phosphate into GlcNAc 6-phosphate with the Glu114Gln mutant is consistent with the notion that

Glu114 plays a critical role in the hydration of the intermediate to produce product, or is important for binding of the intermediate in the active site. The 2,000-fold reduction in k_{cat} (Table 3.1) also shows that the elimination of lactate is compromised by the disruption of the Glu114 residue. Taken together, a scenario emerges where D-lactate is first eliminated very slowly from MurNAc 6-phosphate by the Glu114Gln mutant to generate the enzyme-bound (*E*)-α,β-unsaturated aldehyde intermediate (Figure 3.37). Because of the impaired ability of the mutant enzyme to catalyze the hydration of the alkene to form GlcNAc 6-phosphate however, the intermediate is released from the active site and accumulates in solution. In the wild-type enzyme, D-lactate is eliminated from MurNAc 6-phosphate to generate the (*E*)-α,β-unsaturated aldehyde intermediate, but this intermediate is rapidly hydrated to form GlcNAc 6-phosphate before any significant release from the active site occurs (Figure 3.37).

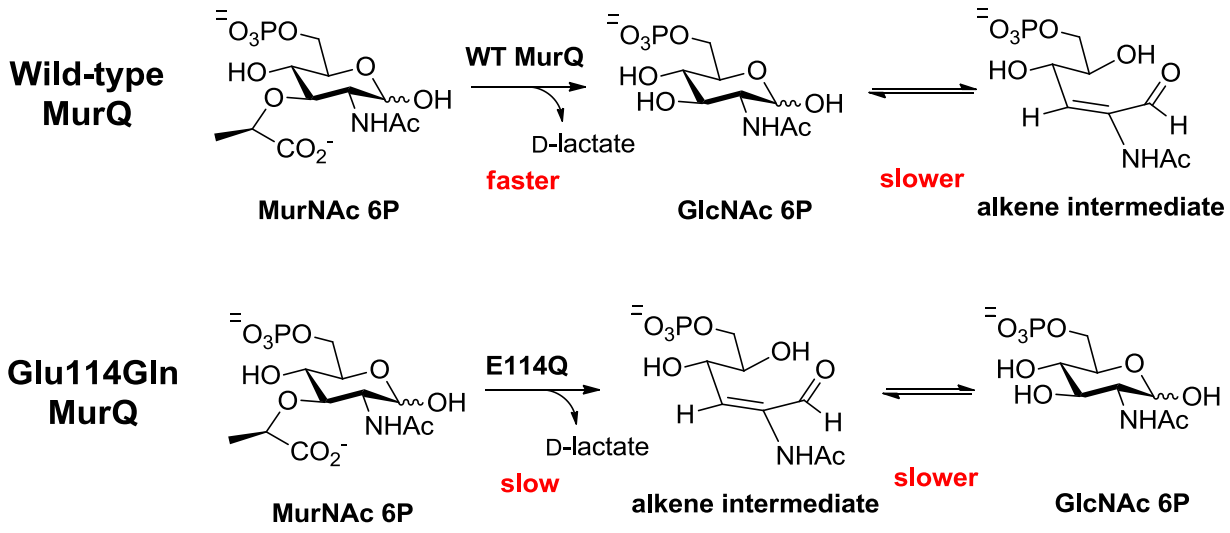

Figure 3.37 Schematic of the reactions catalyzed by wild-type (top) and Glu114Gln MurQ (bottom). The impaired ability of the Glu114Gln mutant to hydrate the alkene intermediate results in release of the intermediate into solution before conversion to GlcNAc 6-phosphate can occur.

Unlike the Glu83Ala mutant, no incorporation of solvent-derived deuterium into residual pools of MurNAc 6-phosphate was observed upon incubation with the Glu114Gln mutant. As can be seen in Figure 3.36, the doublet at 5.59 ppm due to the α-anomeric proton of MurNAc 6-phosphate is not converted to a singlet during the incubation. It is possible given the results of these experiments that Glu114 could be playing the role of B_1 in the MurQ catalytic mechanism (Figure 3.38). B_1 is proposed to be involved in deprotonation at the C-2 position to form the enolate anion intermediate as well as reprotonation of the enolate anion intermediate formed after the conjugate addition of water to the alkene intermediate. If the deprotonation of MurNAc 6-phosphate to form the enolate anion intermediate were impaired through the mutation of the catalytic base, the elimination of D-lactate would undoubtedly be slowed. In this scenario, another amino acid residue could be positioned in close enough proximity to act as a surrogate B_1 to allow for formation of the first enolate anion intermediate. Once formed, the enolate anion would presumably be able to rapidly eliminate D-lactate to give the (*E*)-α,β-unsaturated aldehyde intermediate with the assistance of an intact catalytic B_2. The conjugate addition of water to this intermediate would then occur normally to generate a second enolate anion intermediate, but the protonation of this species to generate GlcNAc 6-phosphate would be slowed due to the mutation of B_1 (Figure 3.38). Unable to partition forward to product, the enolate would exist in equilibrium with the alkene intermediate, increasing the likelihood that the alkene intermediate could be released from the active site into solution.

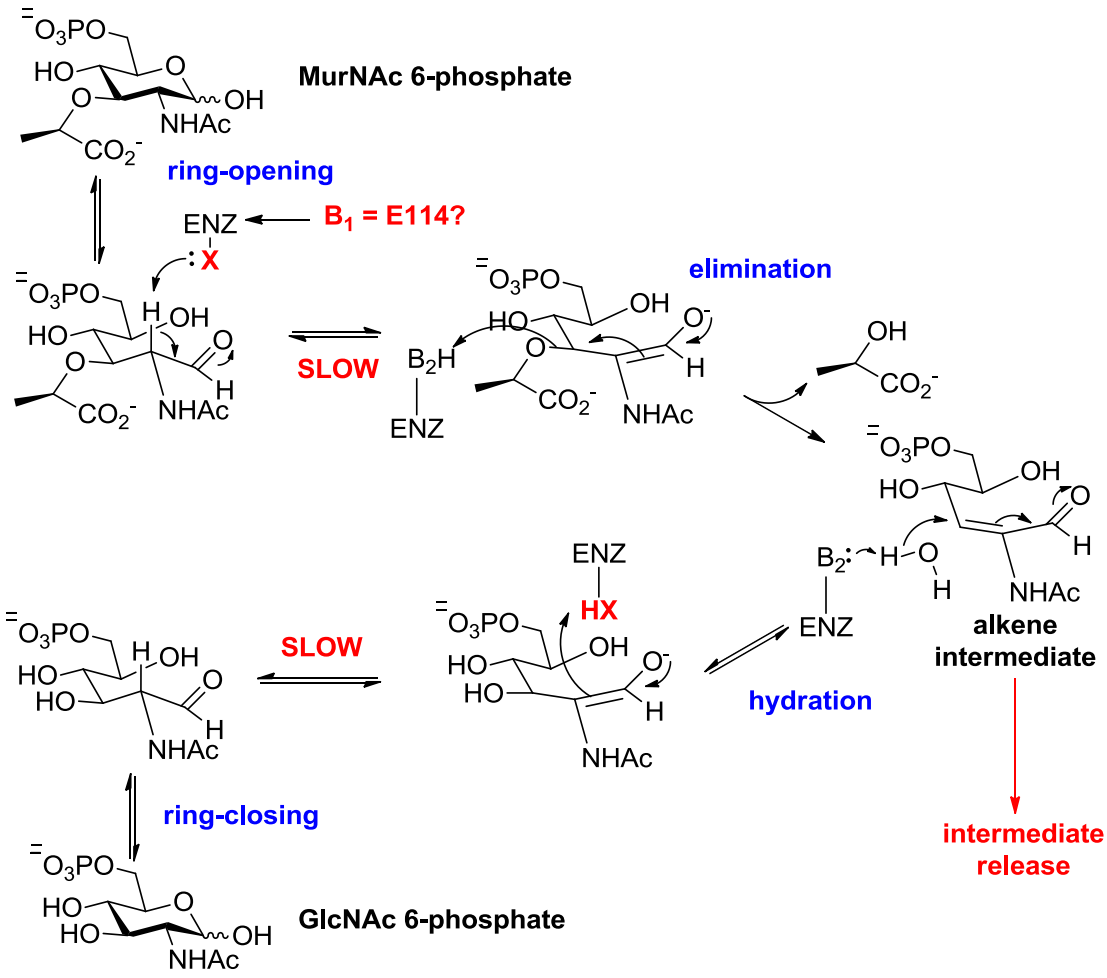

Figure 3.38 Proposed catalytic mechanism of MurQ with Glu114 playing the role of B_1. Mutagenesis of Glu114 to a glutamine prevents deprotonation at the C-2 position and slows the formation of the enolate anion intermediate. Protonation of the hydrated alkene intermediate is also impaired and results in the release of alkene intermediate into solution before turnover to GlcNAc 6-phosphate. WT X = $CH_2CH_2CO_2^-$, Glu114Gln mutant X = $CH_2CH_2CONH_2$.

3.9.3 Testing of Glu114Gln and Glu83Ala MurQ Mutants with Alternate Substrates

To obtain further information with respect to their catalytic roles, the Glu114Gln and Glu83Ala mutants were tested for their ability to accept 3-chloro-3-deoxy-GlcNAc 6-phosphate as an alternate substrate. Unlike lactate, the chloride leaving group does not require acid catalysis for elimination to occur, and consequently, a mutant without a properly functioning B_2 could catalyze the turnover 3-chloro-3-deoxy-GlcNAc 6-phosphate at a rate

similar to that of wild-type enzyme. If either Glu114 or Glu83 was playing the role of B_2 during catalysis, one would expect that a mutant lacking this base would still be able to promote the elimination of HCl from this alternate substrate.

3-Chloro-3-deoxy-GlcNAc 6-phosphate was incubated in buffered D_2O with either the Glu114Gln or Glu83Ala MurQ mutant enzymes. The reaction progress was monitored by ^1H NMR spectroscopy for the appearance of peaks corresponding to either GlcNAc 6-phosphate or the (*E*)-α,β-unsaturated aldehyde intermediate. Interestingly, even after extended incubations, no enzyme-catalyzed elimination products could be detected with either of the mutants. Thus, these experiments did not provide any additional evidence for the assignment of the residue that acts as B_2 in catalysis. Since 3-chloro-3-deoxy-GlcNAc 6-phosphate was a very poor substrate for the wild-type MurQ enzyme, it is clear that the introduction of a chlorine atom at the C-3 position has a detrimental effect on enzyme catalysis. The Glu83Ala and Glu114Gln mutants were already found to catalyze lactate release from MurNAc 6-phosphate at rates much slower (10,000-fold and 2,000-fold, respectively) than that of wild-type enzyme. The introduction of a chlorine atom at the C-3 position in this alternate substrate could presumably be magnifying the impaired ability of these mutants to catalyze elimination reactions even further, slowing any enzyme-catalyzed turnover to the point where it would be unobservable.

3.10 Summary

In this chapter we have detailed studies toward the characterization of the mechanism of the *N*-acetylmuramic acid 6-phosphate hydrolase, MurQ. The results that we have obtained are in full agreement with the proposed mechanism of MurQ action (Figure 3.6) and have also shed new light on the chemical intermediates and catalytic residues involved. A

chemical synthesis of the substrate of the reaction, MurNAc 6-phosphate, greatly facilitated the detailed analysis of the reaction intermediates and products. Through the development of a continuous coupled assay quantifying the release of D-lactate, kinetic constants for the enzyme were determined and a KIE was measured on the isotopically-labeled substrate analogue [2-^{2}H]MurNAc 6-phosphate. A primary KIE on k_{cat} of 1.8 +/– 0.2 was observed and, taken together with the incorporation of a solvent-derived deuterium atom at the C-2 position of the product GlcNAc 6-phosphate, indicated that cleavage of the C-2H bond accompanies catalysis. Our experiments using the isotopically-labeled [1-^{18}O]GlcNAc 6-phosphate in a mixture of $H_2{}^{18}O$ and $H_2{}^{16}O$ confirmed that a solvent-derived ^{18}O-isotope is incorporated at the C-3 position but not at the C-1 position. This indicates that the C-3 C-O bond is cleaved during the course of catalysis and argues strongly against a mechanism invoking the formation of a Schiff base between the carbonyl at C-1 and an active site lysine residue.

Extended incubations of either MurNAc 6-phosphate or GlcNAc 6-phosphate with MurQ produced an equilibrium ratio containing a species that was identified as the alkene intermediate as well as GlcNAc 6-phosphate. Spectroscopic analysis of this compound helped to identify this species as the two anomers of the (*E*)-α,β-unsaturated aldehyde intermediate formed as a result of the *syn* elimination of D-lactate. Decomposition experiments with the alternate substrate 3-chloro-3-deoxy-GlcNAc 6-phosphate provided further evidence that the enzymatic reaction intermediate is exclusively the *syn* elimination product and that no enzyme-catalyzed *anti* elimination was occurring. Furthermore, a synthetic sample of the (*E*)-2,3-alkene was hydrated by MurQ to form GlcNAc 6-phosphate,

proving that the compound is a catalytically competent species and the true reaction intermediate.

Taken together, these studies lend support to a catalytic mechanism that proceeds through a *syn* elimination of D-lactate to form an (*E*)-α,β-unsaturated aldehyde intermediate, followed by the *syn* addition of water to this intermediate to form GlcNAc 6-phosphate. When divided into two half reactions, the elimination of D-lactate from MurNAc 6-phosphate and the conjugate addition of water to an α,β-unsaturated aldehyde intermediate each possesses ample precedence in the literature.[62, 63] However, the overall hydrolysis of the lactyl ether of MurNAc 6-phosphate via an E1cB-like elimination and hydration mechanism is relatively rare in enzymology.[36] The mechanism through which the family 4 glycosidase BglT from *Thermotoga maritima* catalyzes glycoside hydrolysis provides perhaps the closest precedence for the MurQ mechanism (Figure 3.39).[64] BglT uses a NAD^+ cofactor to transiently oxidize the C-3 hydroxyl group of its substrate and generate a ketone activating group. This serves to acidify the proton at the C-2 position and elimination of the anomeric group then occurs through abstraction of this proton by an enzyme active-site base, and generates a 1,2-unsaturated ketone intermediate. Leaving group departure at the anomeric position is aided by an active-site acid/base residue, which then is positioned properly to deprotonate a water molecule for conjugate addition to this unsaturated intermediate. Protonation at the C-2 position by an enzyme active-site acid/base residue and reduction of the ketone at the C-3 position by NADH regenerates the cofactor NAD^+ and gives the hydrolyzed product. Both the elimination of the anomeric group and the subsequent addition of water to the 1,2-unsaturated intermediate occur in a *syn* fashion. Although MurQ does not require an enzyme cofactor to catalyze a transient oxidation and create an activating group,

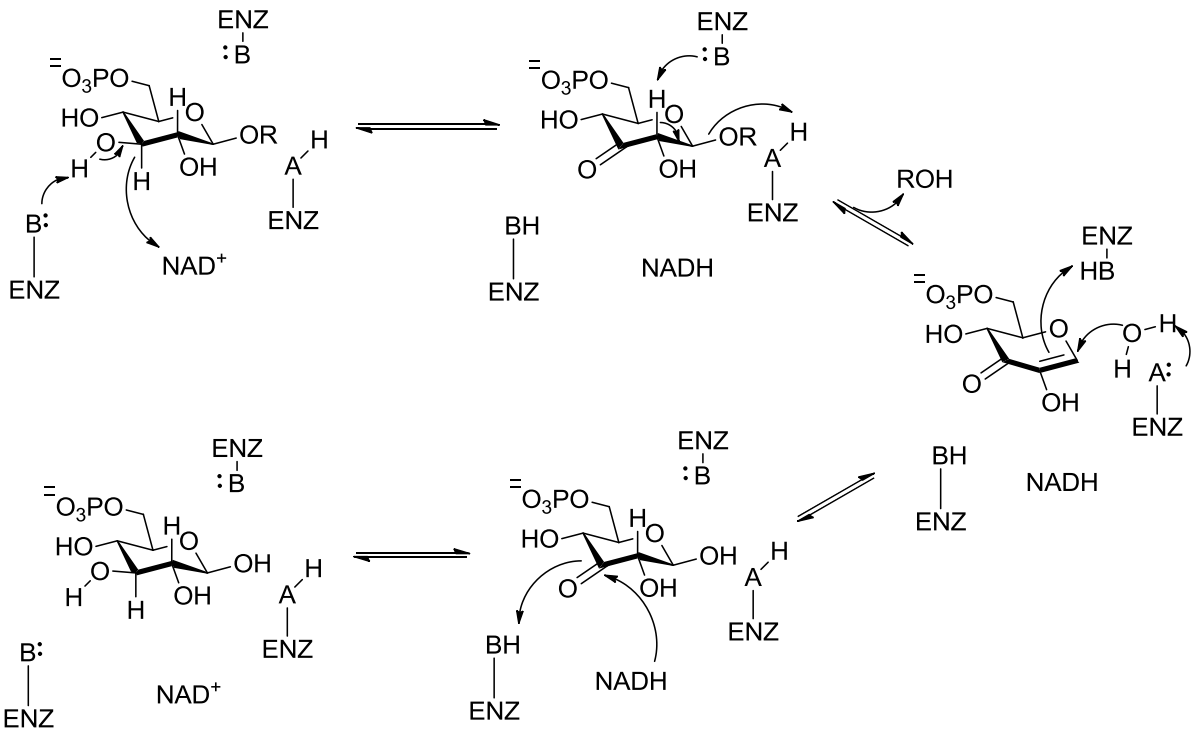

Figure 3.39 Mechanism of glycoside hydrolysis catalyzed by the Family 4 glycosidase BglT.

the remaining steps of the BglT reaction share significant similarity to the eliminations and additions catalyzed by MurQ.

MurQ's assignment to the sugar phosphate isomerase/sugar phosphate binding protein family also is supportive of our proposed mechanism of action.[61] Many enzymes belonging to the SIS family operate through mechanisms that involve carbanionic intermediates and deprotonations adjacent to activating functional groups such as carbonyls or iminium ions. The high sequence identity between MurQ and the *H. influenzae* HI0754 protein of known structure enabled the construction of a structural model of MurQ.[60] It was found that when this structure was modeled as a homodimer, it resembled the pseudodimeric structure of GlmS. Through sequence alignment of GlmS with MurQ etherase homologs from different bacterial species, a number of conserved residues were identified. Kinetic

analysis of MurQ mutants constructed via site-directed mutagenesis served to identify Glu83 and Glu114 as key catalytic residues in the MurQ reaction.

The assignment of catalytic roles to Glu83 and Glu114 could not be solely accomplished through the direct comparison to the corresponding residues in the enzyme GlmS. Although MurQ shares sequence similarity with the SIS domain of GlmS, its sequence identity when compared to the entire GlmS enzyme is relatively low. In addition, the reactions catalyzed by MurQ and GlmS are quite different, increasing the likelihood that key active site residues are playing different roles in their respective reactions. Through structural comparison and sequence alignments, Glu83 of MurQ was thought to be playing the role of Glu488 in GlmS.[39, 59] Glu488 is responsible for deprotonation to form an anionic intermediate in the GlmS reaction, and it was thought that Glu83 plays a similar role in MurQ catalysis. The observation that a Glu83Ala MurQ mutant was essentially devoid of hydrolase activity but was still able to catalyze the exchange of a solvent-derived deuterium into the C-2 position of MurNAc 6-phosphate does not support this line of thinking. It is more likely that Glu83 plays the role of B_2 in our catalytic mechanism (Figure 3.6), and assists in lactate departure and the addition of water to the (*E*)-α,β-unsaturated aldehyde intermediate. The role of Glu114 is not as clear from our studies as that of Glu83. Experiments with the Glu114Gln mutant showed that the rate of lactate release slowed considerably and the mutant enzyme released the (*E*)-α,β-unsaturated aldehyde intermediate into solution before hydration could take place. In addition, no incorporation of solvent-derived deuterium into residual pools of MurNAc 6-phosphate was observed during extended incubations with this mutant enzyme. These results suggest that Glu114 plays a key role in the elimination and hydration steps of the reaction and could be responsible for deprotonation

at the C-2 position (B_1 in Figure 3.6). However, further evidence is required to confirm the exact nature of the role of Glu114 during catalysis.

3.11 Future Work

Future work on MurQ will focus on further characterizing the roles of the active site acid/base residues responsible for catalysis. Although Glu83 and Glu114 have been shown to be important in MurQ catalysis, the definitive assignment of a specific catalytic role, particularly for Glu114, has yet to be accomplished. Future mutagenesis studies will also be performed to identify candidate residues that assist in sugar ring-opening. The comparison of our structural model of MurQ with the known GlmS structure has enabled the identification of a number of putative active site residues involved in catalysis, but without a crystal structure of MurQ in complex with an inhibitor or substrate analogue, the assignment of specific catalytic roles to these residues remains tenuous. Such a structure would greatly assist in the identification of important active site residues as well as the assignment of their catalytic roles. The reported stability issues of the *E. coli* MurQ enzyme make it less attractive for crystallographic studies, but the *H. influenzae* protein HI0754 may present a viable alternative. A detailed description of the structural determination of the protein HI0754 was recently published, and the enzyme was renamed YfeU and predicted to serve the same role as MurQ in *E. coli*.[65] The cloning and expression of YfeU in *E. coli* are currently underway in our laboratory with experiments towards the characterization of YfeU as a MurNAc 6-phosphate hydrolase to follow. Crystallization studies with YfeU and potential substrate and intermediate analogues could allow for the detailed examination of the active site of the enzyme including the proximity of active site residues to the bound substrates and intermediates of the reaction. Since YfeU has 55% sequence identity to

MurQ, the correlation of residues between the two enzymes should be relatively straightforward.[65] Information gathered from the crystal structure of YfeU can potentially be used to confirm the catalytic roles of Glu83 and Glu114 in MurQ as well as to identify any other residues playing key roles during catalysis.

Although MurQ is not an essential enzyme in *E. coli*, it has been speculated to play a more important role during periods of bacterial stress. The design and testing of compounds that could act as inhibitors of MurQ could be used to help elucidate the role of MurQ when bacteria are subjected to different environmental stressors. Three compounds that could be tested as inhibitors of MurQ are shown in Figure 3.40. The compounds mimic the open chain form of the alkene intermediate, substrate, and product of the reaction, but are reduced

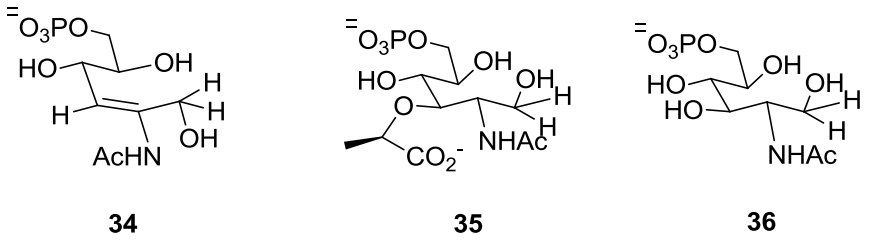

34 **35** **36**

Figure 3.40 Structures of potential reversible non-covalent inhibitors of MurQ.

at the C-1 position. The lack of an aldehyde functional group in these compounds significantly lowers the acidity of the proton at the C-2 position and prevents MurQ catalysis from occurring. Since each of these compounds closely resembles an intermediate in the MurQ reaction pathway but are unable to act as substrates for MurQ, they are predicted to act as potent reversible, non-covalent inhibitors of the enzyme.

An undergraduate summer student in our lab, Yi Han, has aided in the preparation of the reduced substrate analogue **35** and preliminary studies with MurQ have been conducted. Although the kinetic data obtained from these experiments is incomplete and requires

repetition, an estimated K_I value of 130 +/– 70 μM was calculated from equation 1, below. The preliminary observation that compound **35** acts as a competitive inhibitor of MurQ bodes

Equation 1: $K_{Mapp} = K_M (1 + [I]/K_I)$

well for the future development of MurQ inhibitors. Compound **34** in particular should function as a potent inhibitor of the enzyme as it closely mimics the natural (*E*)-alkene intermediate of the MurQ reaction. In addition to inhibiting the enzymatic reaction, these compounds could be used in crystallographic studies with MurQ as they would occupy the active site of the enzyme and provide a snapshot of the residues involved during catalysis.

3.12 Experimental Procedures

3.12.1 Materials and General Methods

Chemicals and resins were purchased from Alfa Aesar or Sigma-Aldrich and used without further purification unless otherwise noted. Silica gel chromatography was performed using Silica Gel SiliaFlash F60 (230-400 mesh, Silicycle). Pyridine, triethylamine, methylene chloride, and methanol were distilled over CaH_2 under an atmosphere of N_2. AG-1X8 resin (100-200 mesh, formate form) was purchased from Bio-Rad Laboratories.

^{1}H NMR spectra were obtained on Bruker AV300 or AV400 NMR spectrometers at field strengths of 300 or 400 MHz, respectively. Proton-decoupled ^{31}P NMR spectra were obtained on Bruker AV300 or AV400 NMR spectrometers at field strengths 121.5 or 162 MHz, respectively. Mass spectrometry was performed by electrospray ionization (ESI-MS) using an Esquire LC mass spectrometer at the UBC Mass Spectrometry Facility. Neutral compounds were detected as positive ions, and negatively charged compounds were detected

as negative ions. Protein concentrations were determined by the method of Bradford using bovine serum albumin as standard.[66]

3.12.2 Synthesis of MurNAc 6-Phosphate (23)

3.12.2.1 Benzyl 2-acetamido-2-deoxy-α-D-glucopyranoside (18)

Compound **18** was prepared from *N*-acetyl-D-glucosamine using a literature procedure.[43] In brief, GlcNAc (6.0 g, 27.1 mmol) was suspended in benzyl alcohol (50 mL) and concentrated HCl (2.9 mL) was added. The reaction mixture was heated at 90 °C for 3 h after which TLC analysis (3:1 EtOAc:MeOH) showed the disappearance of starting material. The reaction was cooled to rt and was subsequently poured into 500 mL of Et_2O and stored overnight at – 20 °C. The suspension was filtered and the off-white solid rinsed with hexanes and Et_2O. The crude product was purified via silica gel chromatography (9:1 CH_2Cl_2:MeOH) to give compound **18** (3.56 g, 42%) as a white solid. ^{1}H NMR and ESI-MS data were identical to those reported in the literature.[43]

3.12.2.2 Benzyl 2-acetamido-4,6-*O*-benzylidene-2-deoxy-α-D-glucopyranoside (19)

Compound **18** (1.12 g, 3.6 mmol) was dissolved in 30 mL anhydrous DMF, and benzaldehyde dimethyl acetal (1.62 mL, 10.8 mmol) and *p*-toluenesulfonic acid monohydrate (0.41 g, 2.2 mmol) were added. The solution was heated to 50 °C under a water aspirator and stirred for 2.5 h. An additional portion of *p*-toluenesulfonic acid (0.30 g, 1.6 mmol) was added and the solution was left to stir for 1 h, at which point the reaction was judged complete by TLC analysis (9:1 CH_2Cl_2:MeOH). The reaction was cooled down to rt and quenched with 2 mL NEt_3. The solvents were removed *in vacuo* and the residue was stirred vigorously as a suspension in equal volumes of hexanes and MeOH. The suspension was

filtered and the solid washed with boiling hexanes:CH_2Cl_2:Et_2O (10:1:2) to give the known compound **19** as a white solid (0.96 g, 67%). ^{1}H NMR (400 MHz, DMSO-d_6) δ ppm 8.01 (d, 1H, *J* = 8.3 Hz), 7.48-7.27 (m, 10H), 5.62 (s, 1H), 5.20 (d, 1H, *J* = 12.8 Hz), 4.79 (d, 1H, *J* = 3.6 Hz), 4.70 (d, 1H, *J* = 12.4 Hz), 4.49 (d, 1H, *J* = 12.4 Hz), 4.16-4.11 (m, 1H), 3.85 (ddd, 1H, *J* = 3.6 Hz, 8.3 Hz, 10.4 Hz), 3.77-3.65 (m, 3H), 3.51 (dd, 1H, *J* = 9.2 Hz, 8.8 Hz), 1.85 (s, 3H). ESI-MS *m/z* 422.1 $[M + Na]^+$.

3.12.2.3 Benzyl 2-acetamido-4,6-*O*-benzylidene-2-deoxy-3-*O*-[(*R*)-1-carboxyethyl]-α-D-glucopyranoside (20)

To a solution of **19** (840 mg, 2.1 mmol) in dioxane (50 mL) was added 500 mg of sodium hydride (60% dispersion in mineral oil), and the mixture stirred under argon atmosphere at 95 °C for 1 h with a water-cooled condenser. The solution was cooled to 65 °C and (*S*)-2-chloropropionic acid (0.90 mL, 10.5 mmol) was added. Stirring was continued for 1 h before an additional 600 mg of sodium hydride (60% dispersion in mineral oil) was added. The temperature was increased to 75 °C and the reaction left to stir overnight under an argon atmosphere. The solution was cooled to rt after which H_2O (50 mL) was added and the majority of the dioxane was removed *in vacuo*. The aqueous solution was acidified with concentrated HCl and then extracted three times with $CHCl_3$. The organic extracts were pooled, dried over $MgSO_4$, and filtered. The solvents were removed *in vacuo* and the residual solid was rinsed with hexanes and subsequently recrystallized in two batches with hot MeOH to give the known compound **20** (675 mg, 68%) as a white solid. ^{1}H NMR (400 MHz, DMSO-d_6) δ ppm 8.00 (m, 1H), 7.47-7.28 (m, 10H), 5.70 (s, 1H), 5.03 (d, 1H, *J* = 3.2 Hz), 4.70 (d, 1H, *J* = 12.4 Hz), 4.49 (d, 1H, *J* = 12.4 Hz), 4.28 (q. 1H, *J* = 6.8 Hz), 4.15 (m, 1H), 3.84-3.65 (m, 5H), 1.85 (s, 3H), 1.27 (d, 3H, *J* = 6.8 Hz). ESI-MS *m/z* 470.3 $[M - H]^-$.

3.12.2.4 Benzyl 2-acetamido-4-*O*-benzyl-3-*O*-[(*R*)-1-carboxyethyl]-2-deoxy-α-D-glucopyranoside (21)

The procedure for the regioselective ring-opening of compound **20** was adapted from existing literature methodology.[31] Compound **20** (666 mg, 1.41 mmol) was dissolved in 50 mL distilled CH_2Cl_2 and the solution was stirred for 1 h under an argon atmosphere in the presence of 4 Å molecular sieves. The reaction was cooled to –78 °C and triethylsilane was added (1.35 mL, 8.48 mmol). After 5 min, dichlorophenylborane (1.11 mL, 8.48 mmol) was added to the reaction mixture, and the stirring was continued at –78 °C. The reaction progress was monitored for the disappearance of starting material by TLC analysis (4:1 CH_2Cl_2:MeOH), and was judged complete after 2 h. The reaction was quenched at –78 °C with 1.25 mL NEt_3 and 1.25 mL MeOH, and was allowed to warm to rt. The solution was diluted with 25 mL CH_2Cl_2, washed twice with 75 mL cold H_2O, and once with 50 mL of saturated NaCl. The aqueous washes were combined and acidified with concentrated HCl and subsequently extracted multiple times with CH_2Cl_2. All organic extracts were pooled and dried over $MgSO_4$ before being concentrated *in vacuo*. Silica gel chromatography (9:1 CH_2Cl_2:MeOH, then 4:1 CH_2Cl_2:MeOH) gave compound **21** (520 mg, 77%). ^{1}H NMR (400 MHz, MeOD) δ ppm 7.32-7.20 (m, 10H), 5.13 (d, 1H, J = 2.4 Hz), 4.75-4.61 (m, 3H), 4.48-4.39 (m, 2H), 3.80-3.52 (m, 6H), 1.91 (s, 3H), 1.30 (d, 3H, J = 6.8 Hz). ESI-MS *m/z* 472.3 $[M - H]^-$.

3.12.2.5 Benzyl 2-acetamido-4-*O*-benzyl-3-*O*-[(*R*)-1-carboxyethyl]-2-deoxy-6-*O*-dibenzylphosphoryl-α-D-glucopyranoside (22)

To a solution of compound **21** (520 mg, 1.10 mmol) in 50 mL distilled CH_2Cl_2 under argon atmosphere, was added triazole (0.304 g, 4.40 mmol). To this mixture, dibenzyl *N,N*-

diethylphosphoramidite (85%, 1.00 g, 2.68 mmol) was added, and the reaction was stirred at room temperature for 3 h. The reaction was diluted with 200 mL Et_2O and washed with 150 mL each of H_2O and saturated NaCl. The organic layer was dried over $MgSO_4$ and concentrated *in vacuo* to generate the crude phosphite sugar. The crude phosphite sugar residue was dissolved in 30 mL THF and cooled down to –78 °C before 5 mL of 30% H_2O_2 was added. The reaction was allowed to warm to rt and subsequently poured into 120 mL Et_2O and washed successively with 3 x 50 mL ice-cold H_2O and 1 x 60 mL saturated NaCl. The aqueous washes were pooled and acidified with conc. HCl, and extracted with CH_2Cl_2. The combined organic extracts were dried over $MgSO_4$, filtered, and the solvents concentrated *in vacuo*. Silica gel chromatography (CH_2Cl_2, then 9:1 CH_2Cl_2:MeOH, then 4:1 CH_2Cl_2:MeOH) afforded compound **22** (322 mg, 39.9%). ^{1}H NMR (400 MHz, MeOD) δ ppm 7.37-7.20 (m, 20H), 5.12-5.02 (m, 5H), 4.69-4.53 (m, 3H), 4.50-4.39 (m, 2H), 4.16-4.07 (m, 2H), 3.78-3.68 (m, 3H), 3.46 (dd, 1H, *J* = 8.8 Hz, *J* = 9.2 Hz), 1.93 (s, 3H), 1.34 (d, 3H, *J* = 6.8 Hz). ESI-MS *m/z* 732.7 $[M - H]^-$.

3.12.2.6 2-Acetamido-3-*O*-[(*R*)-1-carboxyethyl]-2-deoxy-α,β-D-glucose 6-dihydrogen phosphate (23 - MurNAc 6-phosphate)

Compound **22** (410 mg, 0.56 mmol) was hydrogenated (50 psi) over $Pd(OH)_2$ in distilled MeOH with a catalytic amount of acetic acid (60 μL). When the reaction was judged complete by mass spectral analysis, the mixture was filtered through a pad of Celite and the filtrate concentrated *in vacuo*. The residue was dissolved in a minimal amount of MeOH, toluene was added, and the mixture concentrated to remove any residual amounts of acetic acid. The residue was dissolved in H_2O and loaded onto a 10 mL column of AG-1X8 resin (formate form). The column was washed with 50 mL each of H_2O, 1.4N, 2.8N, 4.2N,

and 5.6N formic acid, and each of the fractions was analyzed by ESI-MS for the presence of MurNAc 6-phosphate. Fractions found to contain product (collected between 4.2N and 5.6N formic acid) were pooled and the volume was reduced on a rotary evaporator. Distilled H_2O was added and the remaining solvent evaporated; this procedure was repeated multiple times in order to remove any remaining formic acid, and gave 90 mg (42%) of MurNAc 6-phosphate. The phosphate sugar was dissolved in 10 mL H_2O and carefully titrated to pH 7.5 with NaOH. The resulting solution was frozen and lyophilized to give the disodium salt of MurNAc 6-phosphate as a white solid. α-anomer ^{1}H NMR (400 MHz, D_2O) δ ppm 5.54 (d, 1H, J = 2.8 Hz), 4.47 (q, 1H, J = 6.8 Hz), 4.04-3.84 (m, 2H), 3.75-3.46 (m, 3H), 2.04 (s, 3H), 1.36 (d, 3H, J = 6.8 Hz). β-anomer ^{1}H NMR (400 MHz, D_2O) δ ppm 4.67 (d, 1H, J = 8.4 Hz), 4.30 (q, 1H, J = 6.8 Hz), 4.04-3.84 (m, 2H), 3.75-3.46 (m, 3H), 2.04 (s, 3H), 1.33 (d, 3H, J = 6.8 Hz). ESI-MS *m/z* 372.3 $[M - H]^-$.

3.12.3 Synthesis of GlcNAc 6-Phosphate

3.12.3.1 Benzyl 2-acetamido-2-deoxy-6-*O*-diphenylphosphoryl-α-D-glucopyranoside (24)

Compound **18** (1.00 g, 3.21 mmol) was dissolved in 25 mL of freshly distilled pyridine and the solution cooled to 0 °C. A solution of diphenylchlorophosphate (0.80 mL, 3.86 mmol) in pyridine was added dropwise and the resultant mixture stirred overnight at rt. After the reaction was judged complete by TLC analysis (9:1 EtOAc:MeOH), 0.5 mL H_2O was added and the solvents were removed *in vacuo*. The orange syrup was purified by silica gel chromatography (EtOAc, then 9:1 EtOAc:MeOH) to give compound **24** (1.10 g, 63%).

^{1}H NMR (400 MHz, MeOD) δ ppm 7.40-7.18 (m, 15H), 4.79 (d, 1H, J = 3.6 Hz), 4.61 (d, 1H, J = 12 Hz), 4.57-4.51 (m, 1H), 4.47-4.39 (m, 1H), 4.397 (d, 1H, J = 12 Hz), 3.88

(dd, 1H, J = 10.8 Hz, J = 3.6 Hz), 3.86-3.81 (m, 1H), 3.69 (dd, 1H, J = 8.4 Hz, J = 10.4 Hz), 3.37 (dd, 1H, J = 8.7 Hz, J = 10 Hz), 1.93 (s, 3H). ESI-MS *m/z* 566.1 $[M + Na]^+$.

3.12.3.2 2-Acetamido-2-deoxy-α,β-D-glucose 6-dihydrogen phosphate (25 - GlcNAc 6-phosphate)

Compound **24** (1.10 g, 2.02 mmol) was hydrogenated (50 PSI) over $Pd(OH)_2$ (500 mg) in distilled MeOH. When the reaction was judged complete by TLC analysis (9:1 EtOAc:MeOH) the mixture was filtered through a pad of Celite and the filtrate was used without further purification. PtO_2 (100 mg) was added and the mixture was shaken under a hydrogen atmosphere (50 PSI). After the reaction was judged complete by mass spectral analysis, the mixture was filtered through a pad of Celite and the solvents were removed *in vacuo*. The off-white foam was dissolved in H_2O and loaded onto a 10 mL column of AG-1X8 resin (formate form). The column was washed with 50 mL each of H_2O, 1.4N, 2.8N, 4.2N, and 5.6N formic acid, and each of the fractions were analyzed by ESI-MS for the presence of the phosphate sugar, **25**. Fractions found to contain compound **25** were pooled and the volume was reduced on a rotary evaporator. Distilled H_2O was added and the remaining solvents evaporated; this procedure was repeated multiple times in order to remove any remaining formic acid, and finally gave compound **25** (260 mg, 43%) as a white solid. The sugar phosphate was dissolved in H_2O and carefully titrated to pH 7.6 with NaOH. The resultant solution was frozen and lyophilized to give the sodium salt of **25** as a white solid. α-anomer ^{1}H NMR (400 MHz, D_2O) δ ppm 5.14 (d, 1H, J = 3.6 Hz), 4.04-3.82 (m, 3H), 3.73-3.43 (m, 3H), 1.98 (s, 3H). β-anomer ^{1}H NMR (400 MHz, D_2O) δ ppm 4.64 (d, 1H, J = 8.4 Hz), 4.04-3.82 (m, 3H), 3.73-3.43 (m, 3H), 1.98 (s, 3H). ESI-MS *m/z* 300.3 $[M - H]^-$.

3.12.4 Synthesis of [2-^{2}H]MurNAc 6-Phosphate (26)

The synthesis of isotopically-labeled MurNAc 6-phosphate was carried out in an identical manner to that of MurNAc 6-phosphate except that the known compound [2-^{2}H]GlcNAc was used as the starting monosaccharide instead of GlcNAc. [2-^{2}H]GlcNAc was prepared according to literature procedures from GlcNAc and analysis of the ^{1}H NMR spectroscopy and mass spectrum of the product confirmed the incorporation of a single non-exchangeable deuterium at the C-2 position.[51, 52] This isotopically-labeled compound was transformed into [2-^{2}H]MurNAc 6-phosphate (**26**) using the experimental methods outlined in Section 3.12.2. ^{1}H NMR spectra of the isotopically-labeled synthetic intermediates were identical to the corresponding unlabeled compounds with the following exceptions: the signal due to the anomeric proton appeared as a singlet instead of a doublet, and the signal due to the proton at the C-2 position was absent. ^{1}H NMR spectroscopy and MS analysis of the the final compound confirmed the extent of deuterium incorporation at the C-2 position of MurNAc 6-phosphate to be > 95% (ESI-MS *m/z* 373.1 $[M - H]^-$).

3.12.5 Overexpression and Purification of Wild-Type *E. coli* MurQ

Recombinant C-terminal hexahistidine-tagged MurQ was prepared using the plasmid pUB9 that has been described previously.[11] pUB9 was transformed into chemically competent *E. coli* BL21, which were incubated overnight in 5 mL Luria-Bertani (LB) medium containing 50 μg/mL ampicillin at 37 °C with shaking at 225 rpm. The overnight cultures were poured into 500 mL LB medium containing 50 μg/mL ampicillin and incubated at 37 °C with shaking at 225 rpm until an OD_{600} of 0.6-0.8 was reached. Isopropyl 1-thio-β-D-galactopyranoside (IPTG) was added to induce overexpression (0.3 mM) and the cultures were allowed to continue to incubate at 37 °C with shaking at 225 rpm for an additional 4 h.

The cells were harvested at 5,000 rpm (3,800 X g) for 30 min and the pellets snap frozen in liquid nitrogen and stored at –80 °C. Because of the reported instability of *E. coli* MurQ, the purified enzyme was not stored for any prolonged period of time, but instead prepared freshly before each use according to the following protocol.

For each experiment, a frozen cell pellet was resuspended in 10 mL of lysis buffer (30 mM Na_2HPO_4, 300 mM NaCl, 3 mM DTT, pH 7.5) and lysed three times at 20,000 psi using an ice-cooled French Pressure Cell. The cell lysate was centrifuged at 5,000 rpm (3,800 X g) for 20 min and subsequently passed through a 0.45 μm and a 0.22 μm filter before affinity chromatography. A 10 mL column containing Chelating Sepharose – Fast Flow (GE Healthcare) was charged with 2 column volumes (CV) of 100 mM $NiSO_4$, followed by 2 CV of H_2O, and then 3 CV of running buffer containing 5 mM imidazole (20 mM Na_2HPO_4, 300 mM NaCl, pH 7.5). The filtered cell lysate was loaded onto the column and 50 mL of running buffer containing 5 mM imidazole was passed through, followed by 50 mL of running buffer containing 125 mM imidazole. The hexahistidine-tagged etherase, MurQ, was subsequently eluted with running buffer containing 500 mM imidazole. The enzyme was concentrated by passing it through an Amicon Ultra-4 (Millipore, 10,000 MWCO) membrane filter at 5,000 rpm (3,800 X g). The concentrated enzyme was exchanged into the appropriate buffer by spinning three times through an Amicon Ultra-4 (Millipore, 10,000 MWCO) membrane filter at 5,000 rpm (3,800 X g) with 1 mL of the appropriate buffer. Enzyme purified in this fashion was stored on ice and used for the appropriate experiments within 5 h of purification.

3.12.6 Coupled Kinetic Assay for MurQ Activity

The elimination of D-lactate from *N*-acetylmuramic acid 6-phosphate by MurQ was monitored using a coupled spectrophotometric assay that employs D-lactate dehydrogenase and NAD^+. In order to ensure the coupling reactions are thermodynamically favorable, the production of NADH was coupled to the reduction of *p*-iodonitrotetrazolium violet (INT) using the enzyme diaphorase. The rate of D-lactate elimination was followed by monitoring the increase in absorbance at 500 nm (reduced INT) using a Cary 4000 UV-Vis spectrophotometer. All kinetic assays were performed at 30 °C in 60 mM trien-HCl buffer, pH 8, containing 0.65 mM INT, 5 mM NAD^+, 10 units diaphorase, 30 units D-lactate dehydrogenase, a variable concentration of *N*-acetylmuramic acid 6-phosphate, and a fixed amount of MurQ (1 mL total volume). MurQ dilutions were stabilized by the addition of 5% v/v of a 10 mg/mL BSA solution in H_2O and kept on ice before use. Assay mixtures were pre-incubated at 30 °C for 5 min and then initiated by the addition of a fixed amount of MurQ. A non-linear lag associated with the coupled assay was observed and initial velocities were therefore calculated based on the linear slope between 10 and 15 minutes after initiation using a least squares analysis with Cary 3 software. Under these conditions, the observed rates changed in direct proportion to the amount of MurQ added and were unaffected by changes in the amount of added coupling enzymes. The extinction coefficient of reduced *p*-iodonitrotetrazolium violet at 500 nm was determined to be 10,250 M^{-1} cm^{-1} by adding stock solutions of NADH to the assay mixture and measuring the final absorbance changes. The initial rates were fit to the Michaelis-Menten equation using the program GraFit, version 4.0, and the kinetic parameters were determined based on this fit.

3.12.7 Monitoring the MurQ reaction in D_2O using ^1H NMR spectroscopy

A solution of sodium phosphate buffer prepared with D_2O (25 mM, pD 7.9, 600 μL) and containing MurNAc 6-phosphate (3.75 mM) was placed in an NMR tube and an initial ^1H NMR spectrum was taken. To this solution was added freshly purified MurQ (40 μg that had been exchanged into 15 μL of the same deuterated buffer using an Ultrafree - 0.5 centrifugal filter device (Millipore, 10,000 MWCO)) and the reaction was incubated at 37 °C. ^1H NMR spectra were acquired at 30 min intervals to monitor the progress of the enzymatic reaction. Spectra taken of control reactions lacking MurQ showed no change over the course of several days. Incubations with *N*-acetylglucosamine 6-phosphate and 3-chloro-3-deoxy-*N*-acetylglucosamine 6-phosphate were performed in an identical manner, however; additional MurQ was required in the latter case (40 μg in 15 μL of the same buffer).

3.12.8 Reduction of the unsaturated intermediate with $NaBH_4$

N-Acetylglucosamine 6-phosphate (10 mg) was dissolved in 500 μL of 10 mM phosphate buffer prepared using D_2O, pD 7.9, and WT MurQ (150 μg) was added. The enzymatic mixture was transferred to an NMR tube and incubated at 37 °C for 12 h until equilibrium had been reached. The enzyme was removed by filtration through an Ultrafree – 0.5 centrifugal filter device (Millipore, 10,000 MWCO) and the filtrate frozen and lyophilized. The residue was dissolved in 1.5 mL D_2O, $NaBH_4$ (10 mg) was added, and the resulting solution was heated at 37 °C in a 15 mL Falcon tube. After 3 h, the solution was transferred to an NMR tube and a ^1H NMR spectrum was acquired.

3.12.9 Synthesis of 3-Chloro-3-Deoxy-GlcNAc 6-Phosphate

3.12.9.1 Benzyl 2-benzamido-4,6-*O*-benzylidene-2-deoxy-6-*O*-toluene-*p*-sulfonyl-α-D-glucopyranoside (28)

Compound **27** (4.20 g, 9.1 mmol) was dissolved in distilled pyridine in a flame-dried flask under an argon atmosphere, and the solution was cooled down to 0 °C. *p*-Toluenesulfonyl chloride (6.07 g, 31.84 mmol) was dissolved in distilled pyridine and was added to the solution containing compound **27**. This mixture was allowed to stir for 4 d at rt, after which the reaction was poured into an ice/H_2O mixture. The white precipitate was filtered and rinsed multiple times with H_2O and the solid was air-dried and purified via silica gel chromatography (3:1 $CHCl_3$:Et_2O) to give the known compound **28** (2.66 g, 47%). ^1H NMR (400 MHz, $CDCl_3$) δ ppm 7.81 (d, 2H, *J* = 6.8 Hz), 7.63 (d, 2H, *J* = 8.4 Hz), 7.54-7.17 (m, 13H), 6.902 (d, 2H, *J* =8.4 Hz), 6.77 (d, 1H, *J* = 8.8 Hz), 5.38 (s, 1H), 5.18 (d, 1H, *J* = 3.6 Hz), 5.02 (dd, 1H, *J* = 10 Hz, 10 Hz), 4.703, (d, 1H, *J* = 12 Hz), 4.58 (ddd, 1H, *J* = 3.6 Hz, 10.4 Hz, 8.8 Hz), 4.52 (d, 1H, *J* = 12 Hz), 4.21 (dd, 1H, *J* = 4.8 Hz, 10.4 Hz), 3.92 (ddd, 1H, *J* = 4.8 Hz, 10 Hz, 10 Hz), 3.73 (dd, 2H), *J* = 10 Hz, 10.4 Hz), 2.21 (s, 3H). ESI-MS *m/z* 638.3 $[M + Na]^+$.

3.12.9.2 Benzyl 2-amino-4,6-*O*-benzylidene-3-chloro-2,3-dideoxy-α-D-glucopyranoside (29)

800 mg of sodium metal was added to 275 mL isopropanol and the mixture stirred for 20 min at rt. A suspension of compound **28** (2.66 g, 4.32 mmol) in isopropanol was added and the mixture refluxed at 105 °C for 90 min. The reaction mixture was allowed to cool down and the solvents were evaporated. The residue was taken up in a $CHCl_3$/H_2O mixture

and the organic layer separated. The aqueous layer was washed with $CHCl_3$ and the organics were pooled and washed three times with H_2O and subsequently dried over Na_2SO_4. The solution was filtered and the solvents removed *in vacuo* to give benzyl 2,3-aziridine-4,6-*O*-benzylidine-2,3-dideoxy-α-D-glucopyranoside (1.31 g, 89%) with minor impurities. The crude aziridine was used without further purification.

Ammonium chloride (413 mg, 7.73 mmol) was added to a solution of the crude aziridine (1.31 g, 3.86 mmol) in DMF and the mixture refluxed at 170 °C for 75 min. After TLC analysis (3:1 $CHCl_3$:Et_2O) indicated that the starting material was consumed, the solvents were evaporated *in vacuo* and the resulting reddish-brown syrup dissolved in MeOH and filtered through a small column of Amberjet 4400 OH^- resin. A white precipitate formed in the filtrate and was filtered out before concentrating the solution. The crude product was purified via silica gel chromatography (3:1 $CHCl_3$: Et_2O) to give the known compound **29** (547 mg, 38%). ^{1}H NMR (400 MHz, $CDCl_3$) δ ppm 7.48-7.20 (m, 10H), 5.52 (s, 1H), 4.98 (d, 1H, *J* = 3.2 Hz), 4.71 (d, 1H, *J* = 11.6 Hz), 4.51 (d, 1H, *J* = 11.6 Hz), 4.21 (dd, 1H, *J* = 4.8 Hz, 10.4 Hz), 4.00 (dd, 1H, *J* = 10 Hz, 10 Hz), 3.88 (ddd, 1H, *J* = 4.8 Hz, 10 Hz, 14.4 Hz), 3.70 (dd, 1H, *J* = 10 Hz, 10 Hz), 3.55 (dd, 1H, *J* = 9.6 Hz, 9.6 Hz), 2.95 (dd, 1H, *J* = 3.6 Hz, 9.6 Hz). ESI-MS *m/z* 376.3 $[M + H]^+$.

3.12.9.3 Benzyl 2-acetamido-4,6-*O*-benzylidene-3-chloro-2,3-dideoxy-α-D-glucopyranoside (30)

Compound **29** (306 mg, 0.82 mmol) was suspended in EtOH, and acetic anhydride was added to the mixture (0.32 mL, 3.43 mmol). The reaction mixture was stirred for 30 min at rt, during which time it became a thick white suspension. The solvents were removed *in vacuo* to give the known compound **30** (322 mg, 94%) that was carried forward without

further purification. ^{1}H NMR (400 MHz, $CDCl_3$) δ ppm 7.53-7.49 (m, 2H), 7.41-7.29 (m, 8H), 5.67 (d, 1H, *J* = 9.6 Hz), 5.59 (s, 1H), 4.92 (d, 1H, *J* = 3.6 Hz), 4.74 (d, 1H, *J* = 11.6 Hz), 4.53-4.45 (m, 2H), 4.26 (dd, 1H, *J* = 4.8 Hz, 10.4 Hz), 4.09 (dd, 1H, *J* = 10.4 Hz, 10.8 Hz), 3.92 (ddd, 1H, *J* = 4.8 Hz, 9.6 Hz, 14.4 Hz), 3.80-3.67 (m, 2H), 2.00 (s, 3H). ESI-MS *m/z* 440.2 $[M + Na]^+$.

3.12.9.4 Benzyl 2-acetamido-4-*O*-benzyl-3-chloro-2,3-dideoxy-α-D-glucopyranoside (31)

The procedure for the regioselective ring-opening of known compound **30** was adapted from existing literature methodology.[31] Compound **30** (322 mg, 0.77 mmol) was dissolved in distilled CH_2Cl_2 and stirred under an argon atmosphere in the presence of 4 Å molecular sieves for 1 h. The mixture was cooled to –78 °C and triethylsilane (0.370 mL, 2.32 mmol) was added and the reaction stirred for 5 min before the addition of dichlorophenylborane (0.34 mL, 2.63 mmol). The reaction was judged complete by TLC analysis (3:1 $CHCl_3$:Et_2O) after 1 h and was quenched with NEt_3 (1 mL) and MeOH (3 mL). The mixture was allowed to warm to rt and was then filtered through a pad of Celite, and subsequently washed with H_2O and saturated NaCl. The organic layer was dried over Na_2SO_4, filtered, and then concentrated *in vacuo*. The crude product was purified by silica gel chromatography (3:1 $CHCl_3$:Et_2O, then 9:1 $CHCl_3$:Et_2O) to give compound **31** (275 mg, 85%). ^{1}H NMR (400 MHz, $CDCl_3$) δ ppm 7.41-7.26 (m, 10H), 5.63 (d, 1H, *J* = 9.2 Hz), 4.99 (d, 1H, *J* = 10.4 Hz), 4.91 (d, 1H, *J* = 3.2 Hz), 4.71-4.65 (m, 2H), 4.48-4.36 (m, 2H), 4.13 (dd, 1H, *J* = 8.4 Hz, *J* = 11.2 Hz), 3.82-3.68 (m, 4H), 2.01 (s, 3H), 1.76 (dd, 1H, *J* = 5.6 Hz, *J* = 7.6 Hz). ESI-MS *m/z* 442.2 $[M + Na]^+$.

3.12.9.5 Benzyl 2-acetamido-4-*O*-benzyl-3-chloro-6-*O*-dibenzylphosphoryl-2,3-dideoxy-α-D-glucopyranoside (32)

Compound **31** (275 mg, 0.66 mmol), triazole (181 mg, 2.63 mmol), and dibenzyl *N,N*-diethylphosphoramidite (85%, 0.92 mL, 2.63 mmol) were dissolved in distilled CH_2Cl_2 and stirred at rt under an argon atmosphere. After 3.5 h the reaction was judged complete by TLC analysis (3:1 $CHCl_3$:Et_2O) and was diluted with Et_2O. The organic layer was washed successively with ice cold saturated $NaHCO_3$, saturated NaCl and H_2O, and then dried over Na_2SO_4. The mixture was filtered, and the organic solvents were concentrated *in vacuo*. The crude phosphite was immediately dissolved in THF and the solution cooled to –78 °C before the addition of 30% H_2O_2 (4 mL). The reaction was stirred at –78 °C for 20 min before being allowed to warm to room temperature. The mixture was diluted with Et_2O and washed successively with ice cold saturated $Na_2S_2O_3$, saturated $NaHCO_3$, saturated NaCl, and H_2O, before being dried over Na_2SO_4, filtered, and concentrated *in vacuo*. The crude phosphorylated sugar was purified by silica gel chromatography (4:1 Et_2O:hexanes, then Et_2O, then EtOAc) to give compound **32** (325 mg, 72%). ^{1}H NMR (400 MHz, $CDCl_3$) δ ppm 7.21-7.03 (m, 20H), 5.47 (d, 1H, J = 10 Hz), 4.95-4.85 (m, 4H), 4.70 (d, 1H, J = 10 Hz), 4.66 (d, 1H, J = 3.6 Hz), 4.45-4.35 (m, 2H), 4.24-4.16 (m, 2H), 4.10-3.98 (m, 2H), 3.89 (dd, 1H, J = 9.6 Hz, J = 11.6 Hz), 3.59-3.54 (m, 1H), 3.39 (dd, 1H, J = 9.6 Hz, J = 10 Hz), 1.82 (s, 3H). ESI-MS *m/z* 702.4 $[M + Na]^+$.

3.12.9.6 2-Acetamido-3-chloro-2,3-dideoxy-α,β-D-glucose 6-(dihydrogen phosphate) (33)

Compound **32** (235 mg, 0.35 mmol) was hydrogenated (50 PSI) over $Pd(OH)_2$ (200 mg) in distilled MeOH and a catalytic amount of glacial acetic acid (60 μL). After TLC analysis (EtOAc) revealed the consumption of starting material, the reaction was filtered through a pad of Celite and concentrated *in vacuo* to give the crude debenzylated product **33** (125 mg). The crude sugar was re-dissolved in H_2O and loaded onto a 10 mL column of AG-1X8 resin (formate form). The column was washed successively with 50 mL each of H_2O, 1.4N, 2.8N, 4.2N, and 5.6N formic acid, and each of the fractions were analyzed by ESI-MS for the presence of the 3-chloro sugar phosphate, **33**. Fractions found to contain compound **33** were pooled and the volume was reduced on a rotary evaporator. Distilled H_2O was added and the remaining solvent evaporated; this procedure was repeated multiple times in order to remove any remaining formic acid. The sugar was dissolved in H_2O and titrated to pH 7.55 with 0.1 N NaOH. The resulting solution was frozen and lyophilized to give the sodium salt of **33** (100 mg, approx. 85% based on MW of monosodium salt of **33**) as a white solid. α-anomer ^{1}H NMR (400 MHz, D_2O) δ ppm 5.11 (d, 1H, J = 2.8 Hz), 4.11-3.81 (m, 5H), 3.76-3.70 (m, 1H), 1.98 (s, 3H). β-anomer ^{1}H NMR (400 MHz, D_2O) δ ppm 4.64 (d, 1H, Obscured by HDO peak), 4.11-3.81 (m, 4H), 3.74-3.67 (m, 1H), 3.52-3.46 (m, 1H), 1.98 (s, 3H). ESI-MS *m/z* 317.9 $[M - H]^-$.

3.12.10 Non-Enzymatic Production of Alkene Intermediate from 3-Chloro-3-Deoxy-GlcNAc 6-Phosphate

A sample of trien-HCl buffer (200 mM, pH 8) was evaporated to dryness and reconstituted with an equal volume of D_2O. This procedure was repeated 4 times to ensure

that all residual H_2O was removed. A solution of 3-chloro GlcNAc 6-phosphate (6.0 mM, 1.2 mL) was prepared in the resulting buffer and incubated at 42 °C. The reaction was monitored periodically by ^1H NMR spectroscopy for the appearance of characteristic intermediate alkene peaks. After 5 days, the conversion of 3-chloro GlcNAc 6-phosphate to alkene intermediate was judged to be complete. The solution of intermediate was used without further purification to test its catalytic competence with both WT MurQ and MurQ mutants.

3.12.11 ^{18}O-Isotope Incorporation Experiment

N-Acetylglucosamine 6-phosphate (17 mg) was dissolved in 500 μL $H_2{}^{18}O$ (97%, Cambridge Isotope Laboratories) and the solution sealed in a glass tube. The mixture was heated at 60 °C for 5 h, after which analysis by ESI-MS indicated that > 95% of the sugar contained one equivalent of ^{18}O-isotope. The solution was snap frozen in liquid N_2 and lyophilized to dryness. Analysis of the [1-^{18}O]-*N*-acetylglucosamine 6-phosphate by ^1H NMR spectroscopy (D_2O, 400 MHz) gave an identical spectrum to that of unlabeled sample, and it was used for subsequent enzymatic experiments without further purification. A solution of sodium phosphate buffer (20 mM, pH 7.5, 500 μL) containing [1-^{18}O]-*N*-acetylglucosamine 6-phosphate (2.5 mM) was prepared and diluted with $H_2{}^{18}O$ (97%, 500 μL). A sample of MurQ (1.6 mg in 25 μL of the sodium phosphate buffer) was added and the resulting solution was incubated at 37 °C and monitored for ^{18}O-incorporation/washout by ESI-MS.

3.12.12 Structural Modeling of *E. coli* MurQ and Multiple Sequence Alignment

The structure of the MurQ homolog, *Haemophilus influenzae* HI0754, was elucidated as part of a structural genomic project (P. Kim, P. Quartey, R. Ng, T.I. Zarembinski, A. Joachimiak, unpublished results; structure code: 1NRI, posted to the database January, 24st., 2003). The *E. coli* MurQ structure was modeled using the coordinates of 1NRI (1.90 Å resolution) with SWISS-MODEL 8.05.[67] The structural model was refined using the programs MolProbity[68] and Coot[69]; the coordinates as Protein Data Bank files are available on request. MurQ forms stable dimers as seen by gel filtration and dynamic light-scattering (T. Jaeger, unpublished results). Accordingly, MurQ was modeled as a homodimer. The putative active site residues of MurQ were identified by comparing the homodimer model with crystal structures of the GlmS isomerase with phosphosugars bound to the active site (structural codes 1MOQ, 1MOR, 1MOS) and by multiple sequence alignment of etherases and the sugar-phosphate isomerase/sugar phosphate binding (SIS)-domains of GlmS using ClustalW.

3.12.13 Preparation and Expression of Mutant MurQ Plasmids

Site-directed mutagenesis was carried out essentially as described for the QuikChange kit from Strategene (La Jolla, CA). In brief, to introduce the point mutations Glu83Ala and Asp115Asn, a pair of complementary oligonucleotides was ordered from MWG Biotech (Ebersber, Germany) that encoded a modified codon at the desired position (Glu83(GAA)-> Ala83(GCC), Asp115(GAT)-> Asn115(AAT); for Glu83Ala: CTGGGGATTCTGGATGCTAGCGCCTGTCCGCCCACCTACG (non-matching nucleotides are underlined, introduction of a silent mutation "T" introduced an additional NheI site), for Asp115Asn:

GCCATTCAGCACGCGGTGGAAGGCGCCGAAAATAGCCGGGAAGGCGGTG (non-matching nucleotides are underlined, introduction of a silent mutation "C" introduced an additional KasI/NarI site). The oligonucleotides were used as primers for 18 cycles of in vivo DNA replication of the entire plasmid pUB9 with Pwo polymerase (pQLab, Erlangen, Germany). Subsequently, methylated template DNA was removed with DpnI restriction, and the entire mixture was transformed into competent DH5α cells. To confirm the introduction of the mutation, the plasmid DNA was controlled for cleavage of the restriction site that had been introduced by the mutagenesis primers, and subsequently the mutagenized region was sequenced. The MurQ mutants Glu83Gln and Glu114Gln were constructed in a similar fashion, but without the incorporation of a restriction site, using the oligonucleotide primers listed below (mutated nucleotides underlined). Oligonucleotide primers for the Glu83Gln mutant were as follows: 5' – CTGGATGCCAGCCAGTGTCCGCCCACCTACG – 3' (forward) and 5' – CGTAGGTGGGCGGACACTGGCTGGCATCCAG – 3' (reverse). Primers for the Glu114Gln mutant were as follows: 5' – GGTGGAAGGCGCGCAGGATAGCCGGGAAG – 3' (forward) and 5' – CTTCCCGGCTATCCTGCGCGCCTTCCACC – 3' (reverse). The Glu83Gln and Glu114Gln gene sequences were confirmed through DNA sequencing of the entire gene. Expression of the mutated plasmids and purification of the resulting MurQ mutants was carried out in an identical fashion to that of the wild type enzyme.

3.12.14 Solvent-Derived Deuterium Incorporation into MurNAc 6-Phosphate with Wild-Type and Glu83Ala MurQ

A solution of *N*-acetylmuramic acid 6-phosphate (6.9 mM) in sodium phosphate buffer prepared with D_2O (25 mM, pD 7.9, 1.60 mL) was divided into two aliquots. To one

aliquot was added WT MurQ (5 μg) and to the other was added E83A (40 μg). The samples were transferred to NMR tubes and incubated at 37 °C. The reactions were monitored periodically by NMR spectroscopy to observe any wash-in of deuterium at C-2 as evidenced by the collapse of the H-1 doublet to a singlet. At each time point, a small aliquot was removed from the reaction and diluted into MeOH for analysis by ESI-MS.

References

(1) Park, J. T. In *The Murein Sacculus;* Neidhardt, F. C., Curtis, R., III, Ingraham, J. L., Lin, E. C. C., Low, K. B., Magasanik, B., Resnikoff, W. S., Riley, M., Schaechter, M. and and Umbarger, H. E., Eds.; Escherichia coli and Salmonella: Cellular and Molecular Biology; American Society for Microbiology: Washington, DC, 1996; pp 48-57.

(2) Vollmer, W.; Blanot, D.; De Pedro, M. A. *FEMS Microbiol. Rev.* **2008***, 32*, 149-167.

(3) Holtje, J. V. *Microbiology and Molecular Biology Reviews* **1998***, 62*, 181-203.

(4) van Heijenoort, J. In *Murein Synthesis;* Neidhardt, F. C., Curtis, R., III, Ingraham, J. L., Lin, E. C. C., Low, K. B., Magasanik, B., Resnikoff, W. S., Riley, M., Schaechter, M. and and Umbarger, H. E., Eds.; Escherichia coli and Salmonella: Cellular and Molecular Biology; American Society for Microbiology: Washington, DC, 1996; pp 1025-1034.

(5) Zapun, A.; Contreras-Martel, C.; Vernet, T. *FEMS Microbiol. Rev.* **2008***, 32*, 361-385.

(6) Vollmer, W.; Joris, B.; Charlier, P.; Foster, S. *FEMS Microbiol. Rev.* **2008***, 32*, 259-286.

(7) Park, J. T.; Uehara, T. *Microbiology and Molecular Biology Reviews* **2008***, 72*, 211.

(8) Parquet, C.; Flouret, B.; Leduc, M.; Hirota, Y.; van Heijenoort, J. *European Journal of Biochemistry* **1983***, 133*, 371-377.

(9) Dahl, U.; Jaeger, T.; Nguyen, B. T.; Sattler, J. M.; Mayer, C. *J. Bacteriol.* **2004***, 186*, 2385-2392.

(10) Uehara, T.; Suefuji, K.; Valbuena, N.; Meehan, B.; Donegan, M.; Park, J. T. *J. Bacteriol.* **2005***, 187*, 3643-3649.

(11) Jaeger, T.; Arsic, M.; Mayer, C. *J. Biol. Chem.* **2005***, 280*, 30100-30106.

(12) Vocadlo, D. J.; Davies, G. J.; Laine, R.; Withers, S. G. *Nature* **2001***, 412*, 835-838.

(13) Vollmer, W. *FEMS Microbiol. Rev.* **2008***, 32*, 287-306.

(14) Clarke, A. J.; Dupont, C. *Can. J. Microbiol.* **1992***, 38*, 85-91.

(15) Weadge, J. T.; Clarke, A. J. *Biochemistry* **2006***, 45*, 839-851.

(16) Weadge, J. T.; Pfeffer, J. M.; Clarke, A. J. *BMC Microbiol.* **2005***, 5*, 49.

(17) Dupont, C.; Clarke, A. J. *European Journal of Biochemistry* **1991***, 195*, 763-769.

(18) Koraimann, G. *Cellular and Molecular Life Sciences* **2003***, 60*, 2371-2388.

(19) Moynihan, P. J.; Clarke, A. J. *J. Biol. Chem.* **2010***, 285*, 13264-13273.

(20) Weadge, J. T.; Clarke, A. J. *Biochemistry* **2007***, 46*, 4932-4941.

(21) Hekmat, O.; Tokuyasu, K.; Withers, S. G. *Biochem. J.* **2003***, 374*, 369-380.

(22) Chang, K. Y.; Wu, S. H.; Wang, K. T. *Carbohydr. Res.* **1991***, 222*, 121-129.

(23) Schmidt, R. R. *Angew. Chem., Int. Ed.* **1986***, 25*, 212-235.

(24) Zhu, X.; Schmidt, R. R. *Angew. Chem. Int. Ed.* **2009***, 48*, 1900-1934.

(25) Hesek, D.; Lee, M.; Morio, K.; Mobashery, S. *J. Org. Chem.* **2004***, 69*, 2137-2146.

(26) Blatter, G.; Beau, J. M.; Jacquinet, J. C. *Carbohydr. Res.* **1994***, 260*, 189-202.

(27) Aly, M. R. E.; Castro-Palomino, J. C.; Ibrahim, E. S. I.; El-Ashry, E. S. H.; Schmidt, R. R. *European Journal of Organic Chemistry* **1998***, 1998*, 2305-2316.

(28) Dullenkopf, W.; Castro-Palomino, J. C.; Manzoni, L.; Schmidt, R. R. *Carbohydr. Res.* **1996***, 296*, 135-147.

(29) Cai, Y.; Ling, C. C.; Bundle, D. R. *Org. Lett.* **2005***, 7*, 4021-4024.

(30) Hesek, D.; Suvorov, M.; Morio, K.; Lee, M.; Brown, S.; Vakulenko, S. B.; Mobashery, S. *J. Org. Chem.* **2004***, 69*, 778-784.

(31) Sakagami, M.; Hamana, H. *Tetrahedron Lett.* **2000***, 41*, 5547-5551.

(32) Crich, D.; Dudkin, V. *J. Am. Chem. Soc.* **2001***, 123*, 6819-6825.

(33) Jeanloz, R. W.; Walker, E.; Sinaĸ, P. *Carbohydr. Res.* **1968***, 6*, 184-196.

(34) Higaki, J. N.; Chakravarty, S.; Bryant, C. M.; Cowart, L. R.; Harden, P.; Scardina, J. M.; Mavunkel, B.; Luedtke, G. R.; Cordell, B. *J. Med. Chem.* **1999***, 42*, 3889-3898.

(35) Skordalakes, E.; Elgendy, S.; Goodwin, C. A.; Green, D.; Scully, M. F.; Kakkar, V. V.; Freyssinet, J. M.; Dodson, G.; Deadman, J. J. *Biochemistry* **1998***, 37*, 14420-14427.

(36) White, G. F.; Russell, N. J.; Tidswell, E. C. *Microbiol. Rev.* **1996***, 60*, 216-232.

(37) Reissig, J. L.; Strominger, J. L.; Leloir, L. F. *J. Biol. Chem.* **1955***, 217*, 959-966.

(38) Tipper, D. J. *Biochemistry* **1968***, 7*, 1441-1449.

(39) Teplyakov, A.; Obmolova, G.; Badet-Denisot, M. A.; Badet, B. *Protein Science* **1999***, 8*, 596-602.

(40) Leriche, C.; Badet-Denisot, M. A.; Badet, B. *J. Am. Chem. Soc.* **1996***, 118*, 1797-1798.

(41) Golinelli-Pimpaneau, B.; Badet, B. *Eur. J. Biochem.* **1991***, 201*, 175-182.

(42) Frey, P. A.; Hegeman, A. D. In *Addition and Elimination;* Enzymatic Reaction Mechanisms; Oxford University Press: New York, NY, 2007; pp 433-467.

(43) Yeager, A. R.; Finney, N. S. *J. Org. Chem.* **2005***, 70*, 1269-1275.

(44) Nóbrega, C.; Vázquez, J. T. *Tetrahedron: Asymmetry* **2003***, 14*, 2793-2801.

(45) Berger, I.; Nazarov, A. A.; Hartinger, C. G.; Groessl, M.; Valiahdi, S. M.; Jakupec, M. A.; Keppler, B. K. *ChemMedChem* **2007***, 2*, 505-514.

(46) Flowers, H. M.; Jeanloz, R. W. *J. Org. Chem.* **1963***, 28*, 2983-2986.

(47) Osawa, T.; Jeanloz, R. W. *J. Org. Chem.* **1965***, 30*, 448-450.

(48) Sim, M. M.; Kondo, H.; Wong, C. H. *J. Am. Chem. Soc.* **1993***, 115*, 2260-2267.

(49) Cawley, T. N.; Letters, R. *Carbohydr. Res.* **1971***, 19*, 373-382.

(50) Szabó, P. *J. Chem. Soc., Perkin Trans. 1* **1989**, 919-924.

(51) Hanchak, M.; Korynyk, W. *Carbohydr. Res.* **1976***, 52*, 219-222.

(52) Salo, W.; Hamari, M.; Hallcher, L. *Carbohydr. Res.* **1976***, 50*, 287-291.

(53) Rej, R. *Anal. Biochem.* **1982***, 119*, 205-210.

(54) Frey, P. A.; Hegeman, A. D. In *Kinetics of Enzymatic Reactions;* Enzymatic Reaction Mechanisms; Oxford University Press: New York, NY, 2007; pp 91-101.

(55) Wiberg, K. B. *Angew. Chem. , Int. Ed.* **1986***, 25*, 312-322.

(56) Ali, Y.; Richardson, A. C.; Gibbs, C. F.; Hough, L. *Carbohydr. Res.* **1968***, 7*, 255-271.

(57) Spohr, U.; zu Reckendorf, W. M. *Liebigs Ann. Chem.* **1982***, 7*, 1375-1383.

(58) Murakami, T.; Taguchi, K. *Tetrahedron* **1999***, 55*, 989-1004.

(59) Durand, P.; Golinelli-Pimpaneau, B.; Mouilleron, S.; Badet, B.; Badet-Denisot, M. A. *Arch. Biochem. Biophys.* **2008***, 474*, 302-317.

(60) Jaeger, T.; Mayer, C. *Cellular and Molecular Life Sciences* **2008**, *65*, 928-939.

(61) Bateman, A. *Trends Biochem. Sci.* **1999**, *24*, 94-95.

(62) Hofstein, H. A.; Feng, Y.; Anderson, V. E.; Tonge, P. J. *Biochemistry* **1999**, *38*, 9508-9516.

(63) Yip, V. L. Y.; Withers, S. G. *Curr. Opin. Chem. Biol.* **2006**, *10*, 147-155.

(64) Yip, V. L. Y.; Varrot, A.; Davies, G. J.; Rajan, S. S.; Yang, X.; Thompson, J.; Anderson, W. F.; Withers, S. G. *J. Am. Chem. Soc.* **2004**, *126*, 8354-8355.

(65) Kim, Y.; Quartey, P.; Ng, R.; Zarembinski, T.; Joachimiak, A. *J. Struct. Funct. Genomics* **2009**, *10*, 151-156.

(66) Bradford, M. M. *Anal. Biochem.* **1976**, *72*, 248-254.

(67) Arnold, K.; Bordoli, L.; Kopp, J.; Schwede, T. *Bioinformatics* **2006**, *22*, 195-201.

(68) Lovell, S. C.; Davis, I. W.; Arendall III, W. B.; De Bakker, P. I. W.; Word, J. M.; Prisant, M. G.; Richardson, J. S.; Richardson, D. C. *Proteins: Struct. , Funct. , Genet.* **2003**, *50*, 437-450.

(69) Emsley, P.; Cowtan, K. *Acta Crystallogr.* **2004**, *60*, 2126-2132.

Appendix: NMR Spectra of Selected Compounds

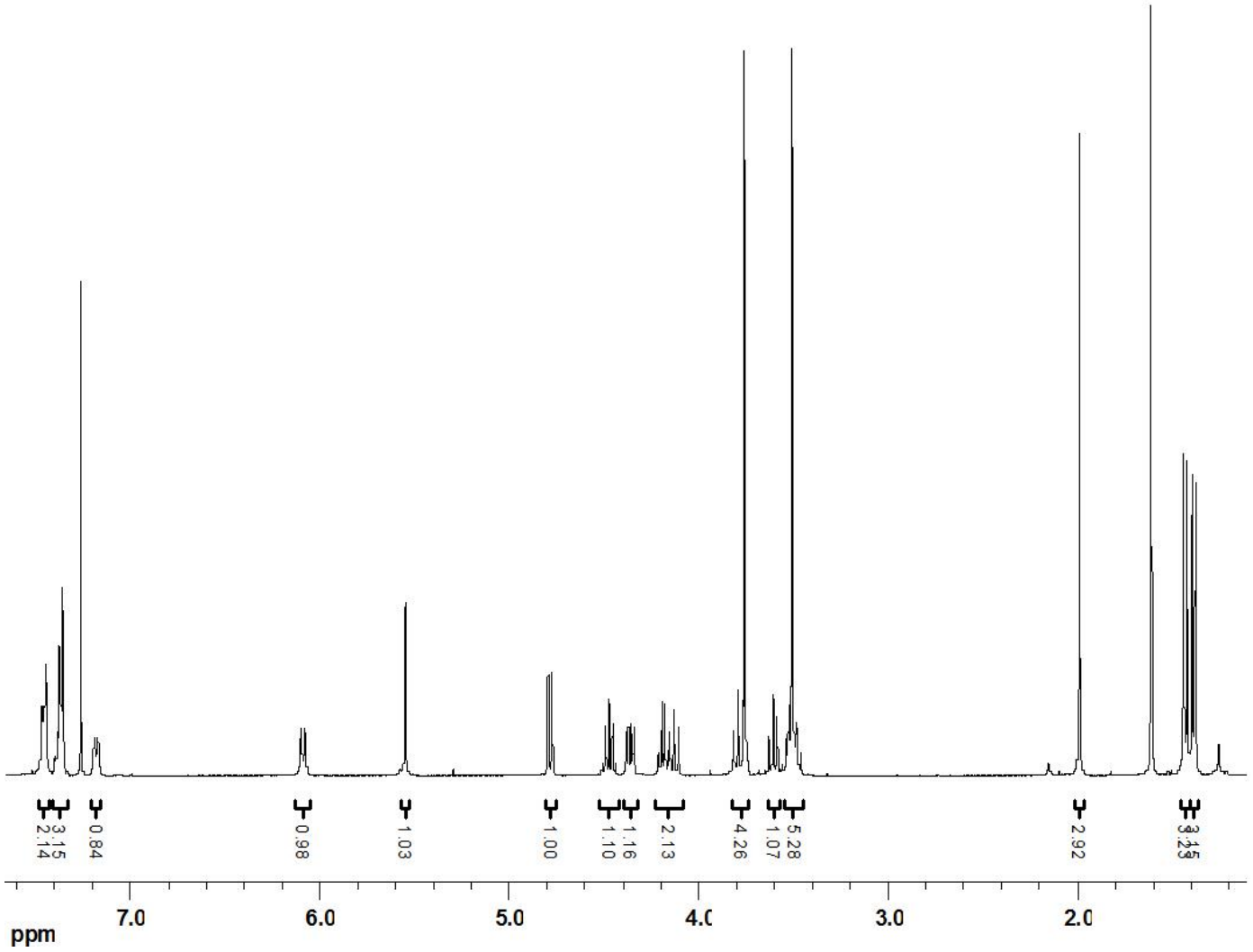

Figure A. 1 ^{1}H NMR (400 MHz, $CDCl_3$) spectrum of compound **6**.

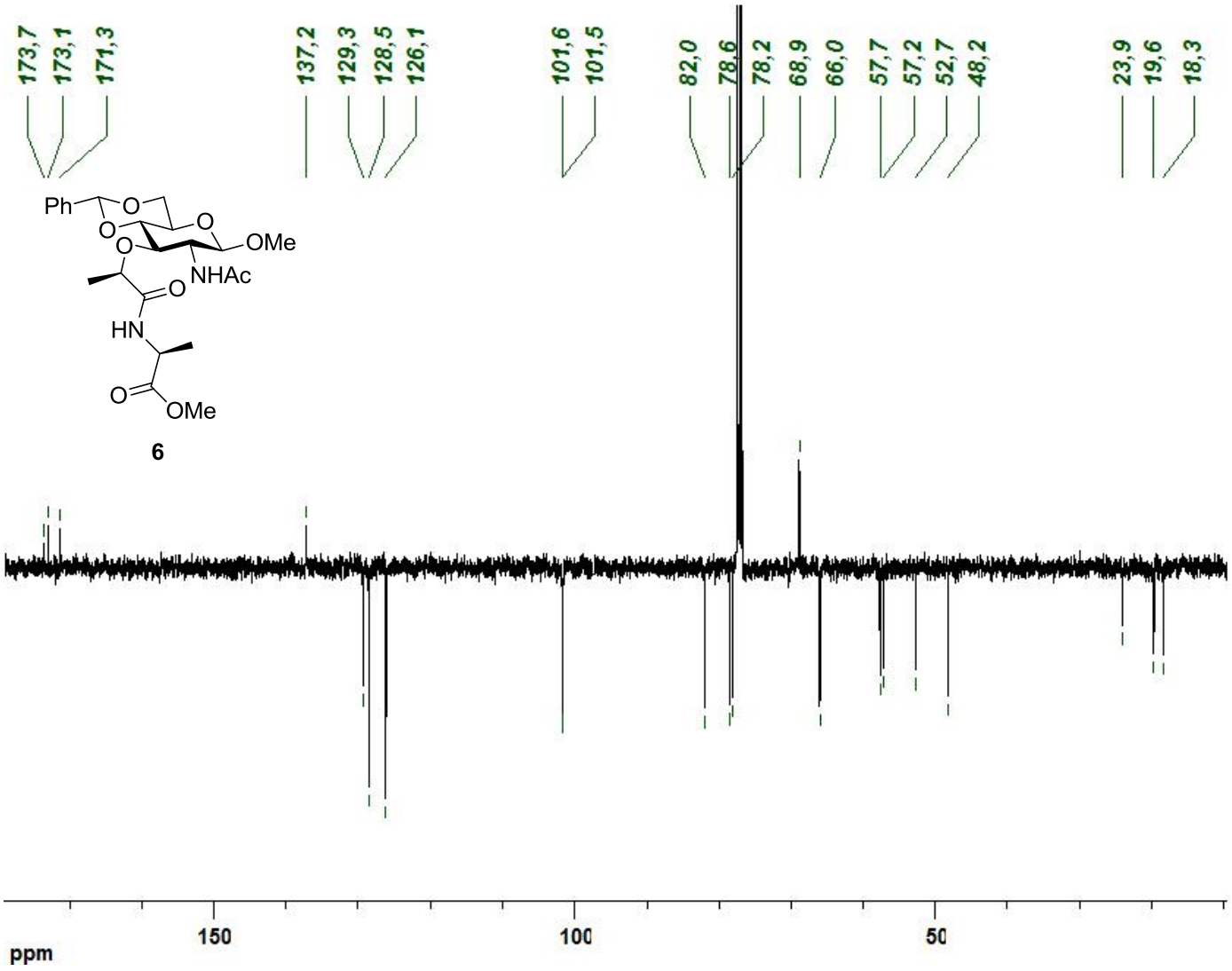

Figure A. 2 ^{13}C NMR (100 MHz, $CDCl_3$) spectrum (APT) of compound **6**.

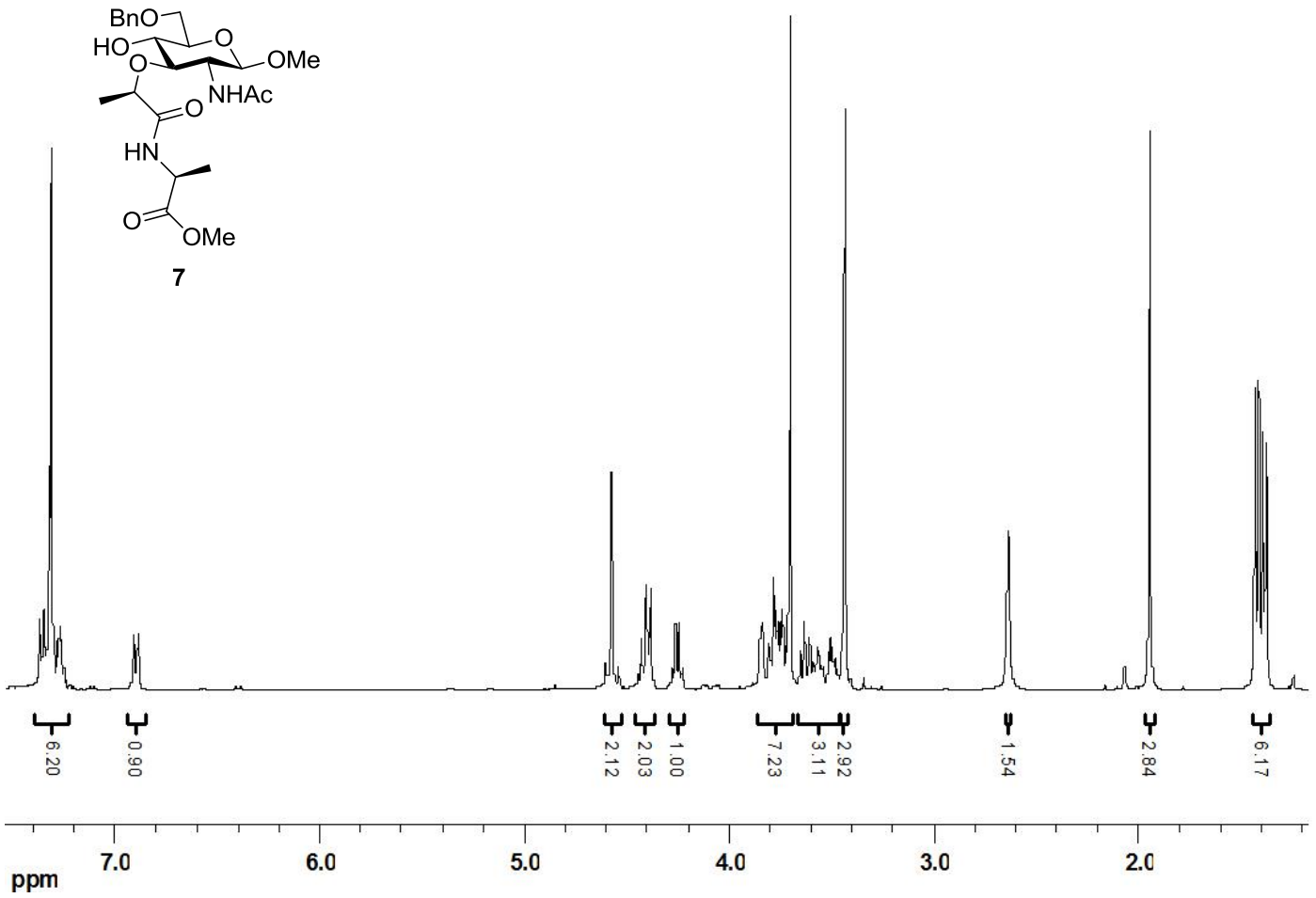

Figure A. 3 ^{1}H NMR (400 MHz, $CDCl_3$) spectrum of compound **7**.

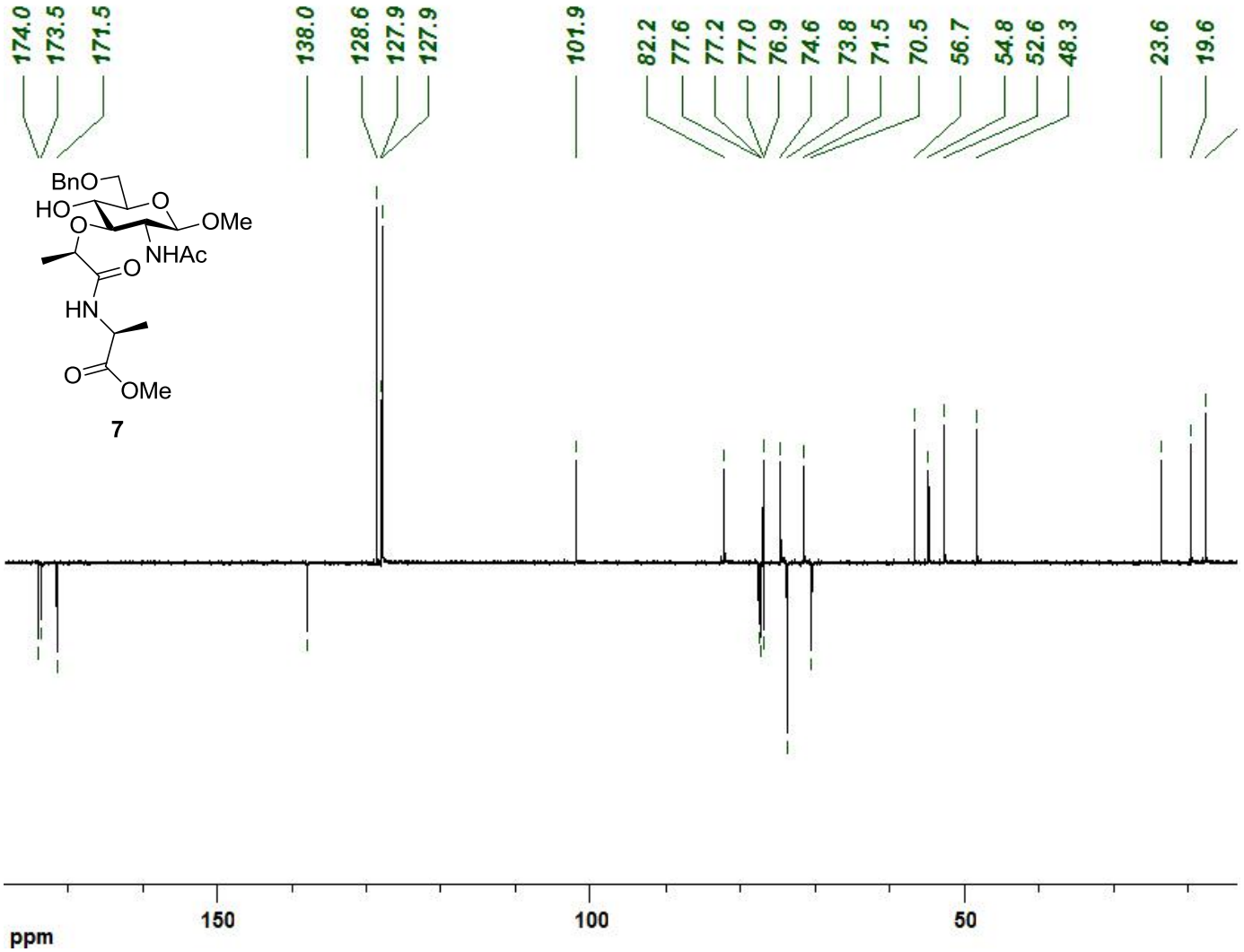

Figure A. 4 ^{13}C NMR (100 MHz, $CDCl_3$) spectrum (APT) of compound **7**.

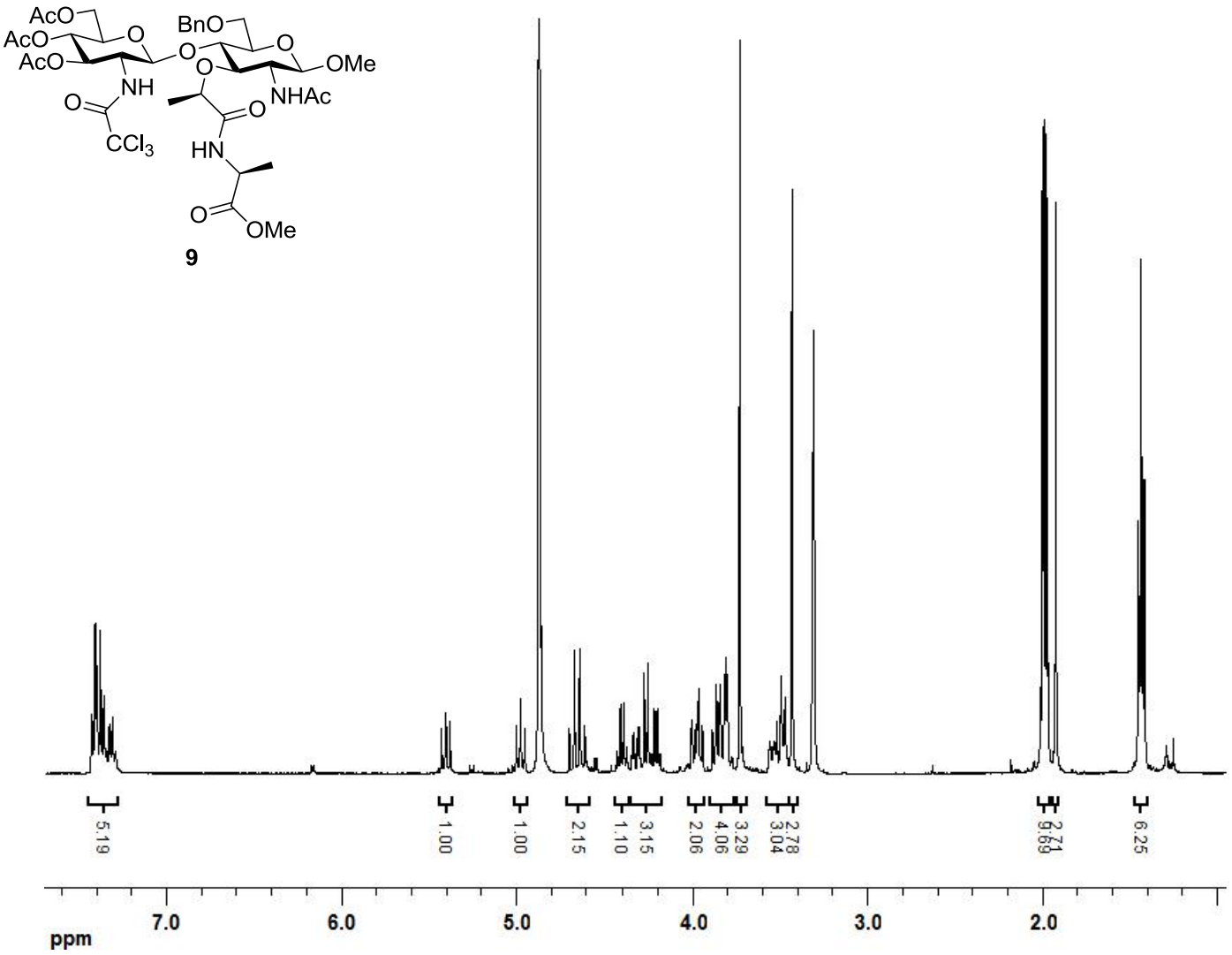

Figure A. 5 ^{1}H NMR (400 MHz, MeOD) spectrum of compound **9**.

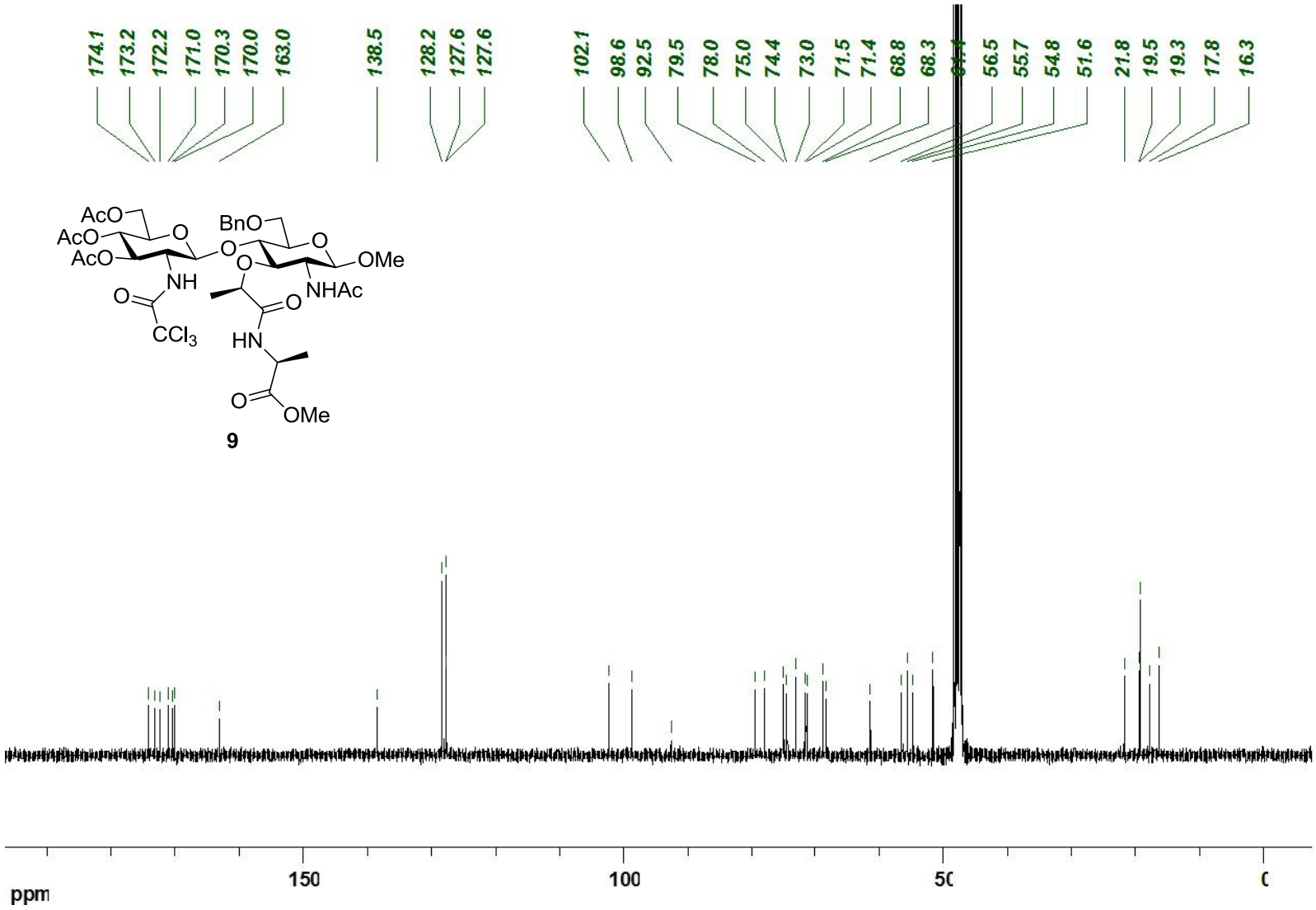

Figure A. 6 ^{13}C NMR (100 MHz, MeOD) spectrum of compound **9**.

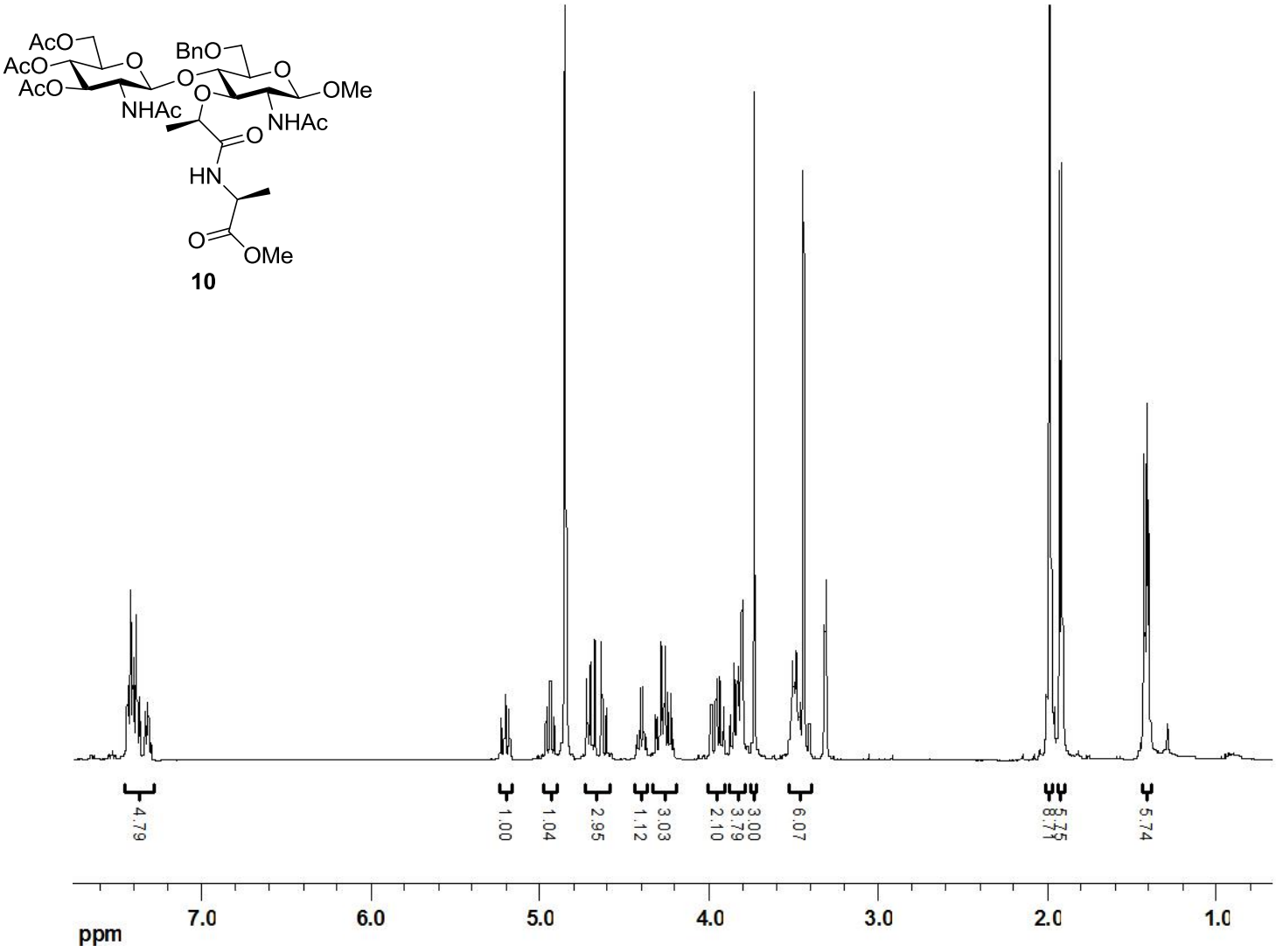

Figure A. 7 ^{1}H NMR (400 MHz, MeOD) spectrum of compound **10**.

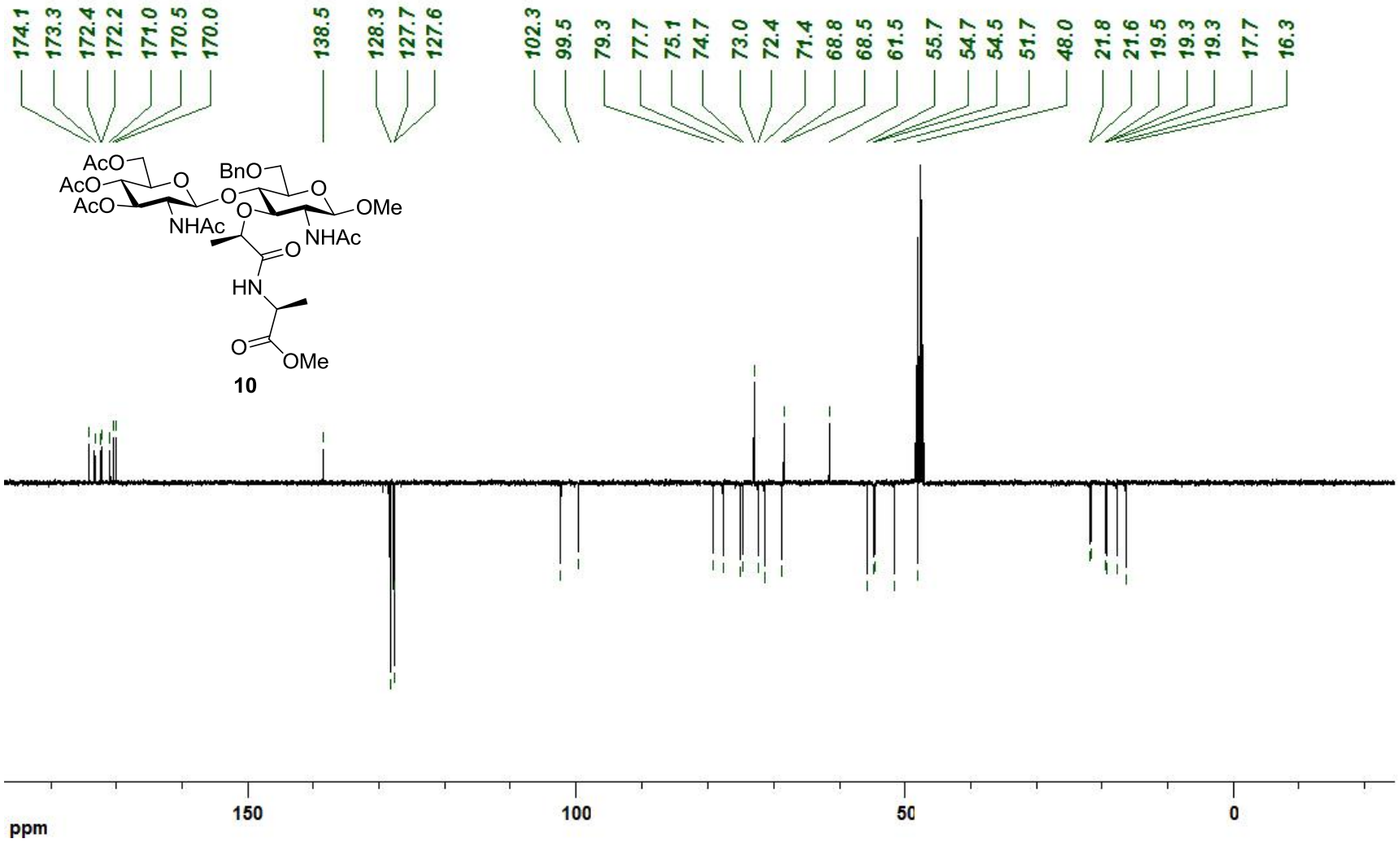

Figure A. 8 ^{13}C NMR (100 MHz, MeOD) spectrum (APT) of compound **10**.

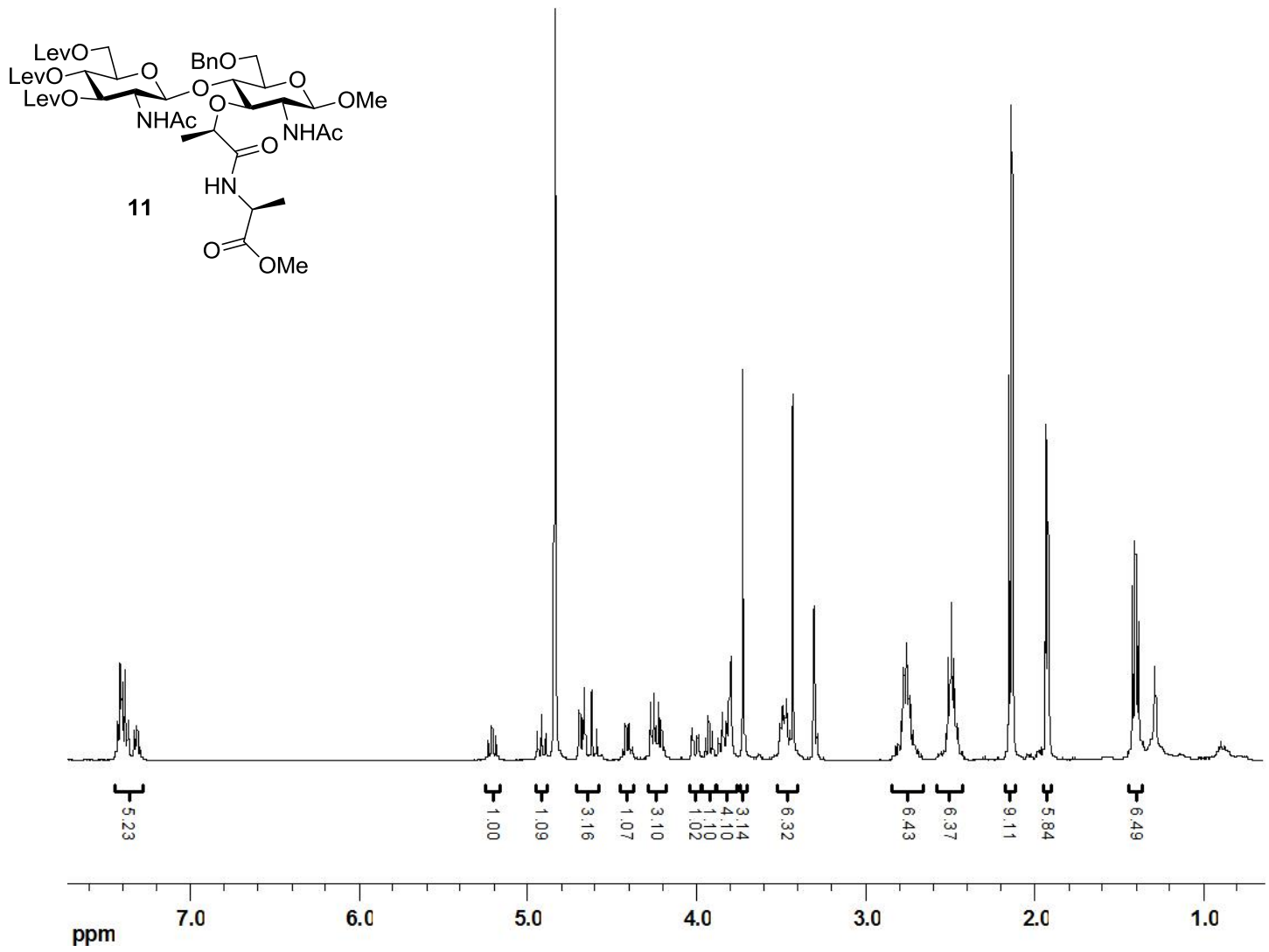

Figure A. 9 ^{1}H NMR (400 MHz, MeOD) spectrum of compound **11**.

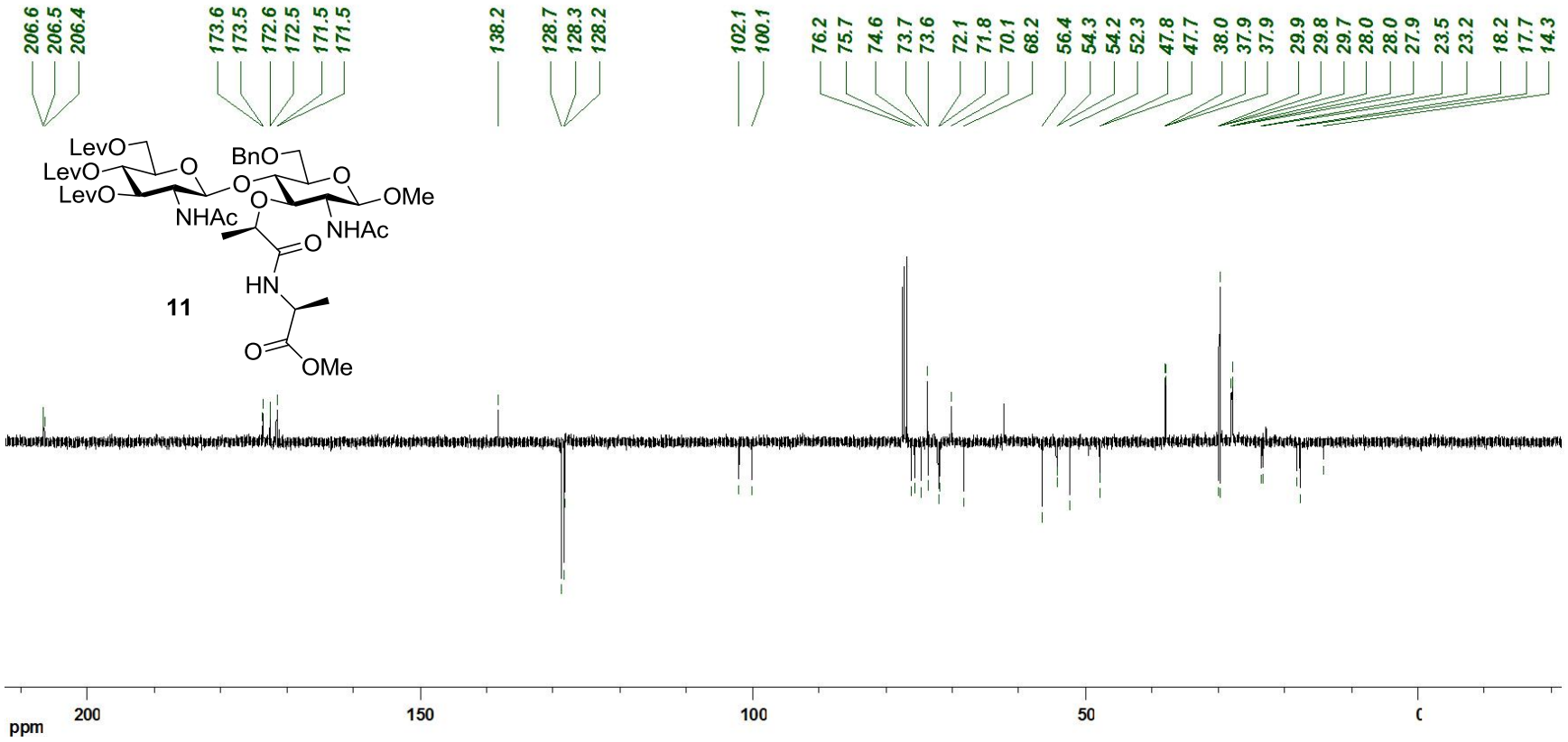

Figure A. 10 ^{13}C NMR (100 MHz, MeOD) spectrum (APT) of compound **11**.

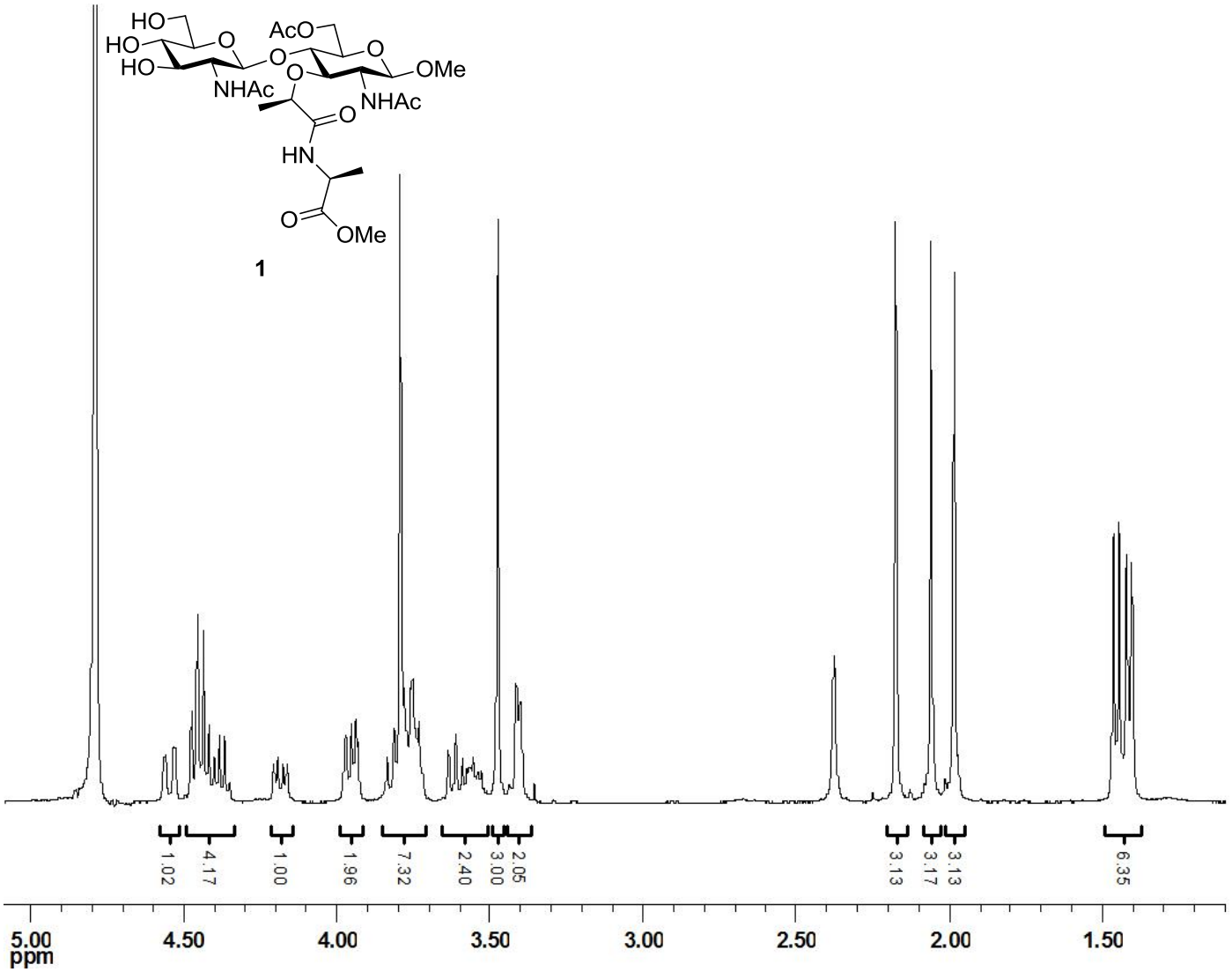

Figure A. 11 ^{1}H NMR (400 MHz, D_2O) spectrum of compound **1**.

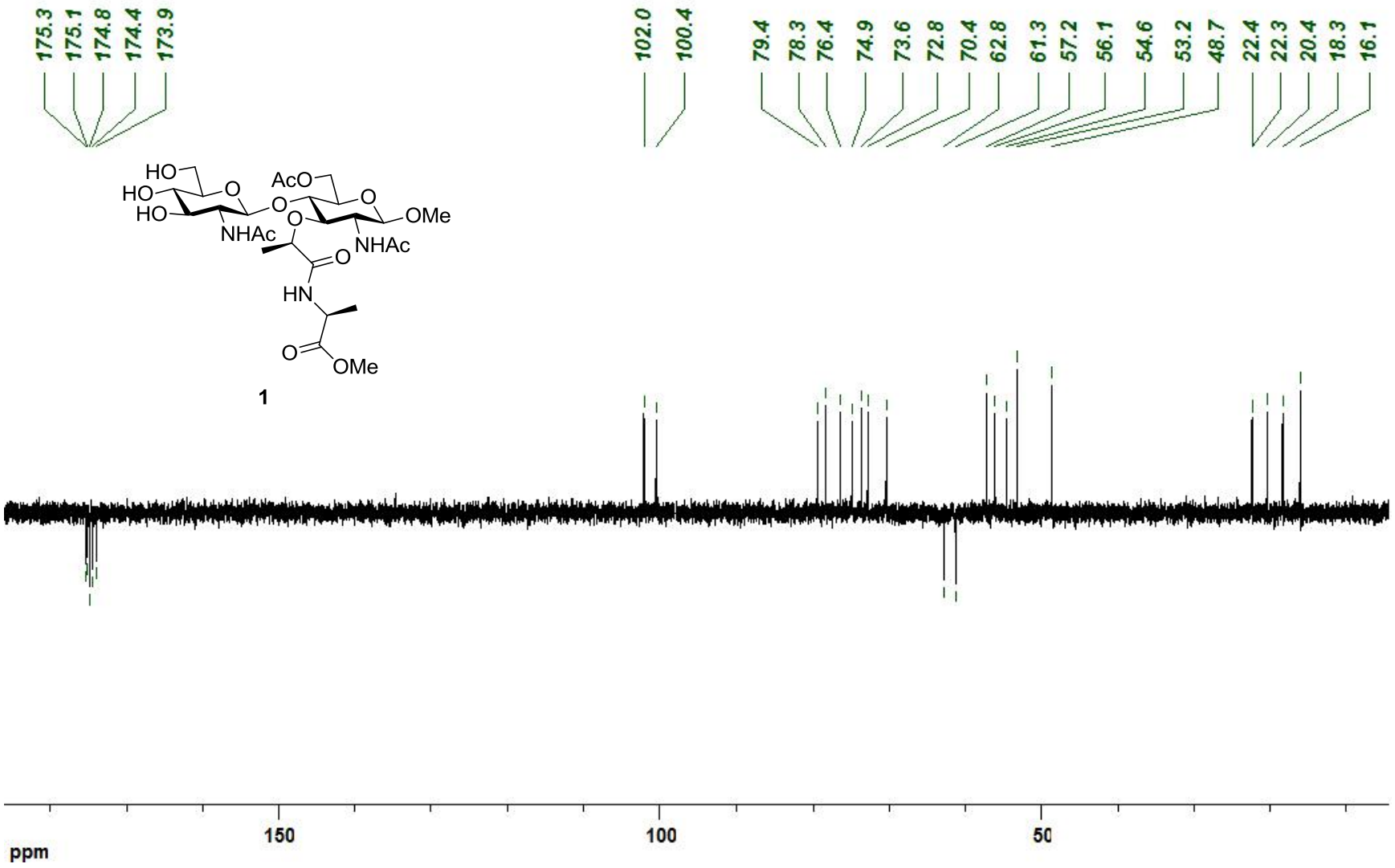

Figure A. 12 ^{13}C NMR (100 MHz, D_2O) spectrum (APT) of compound **1.**

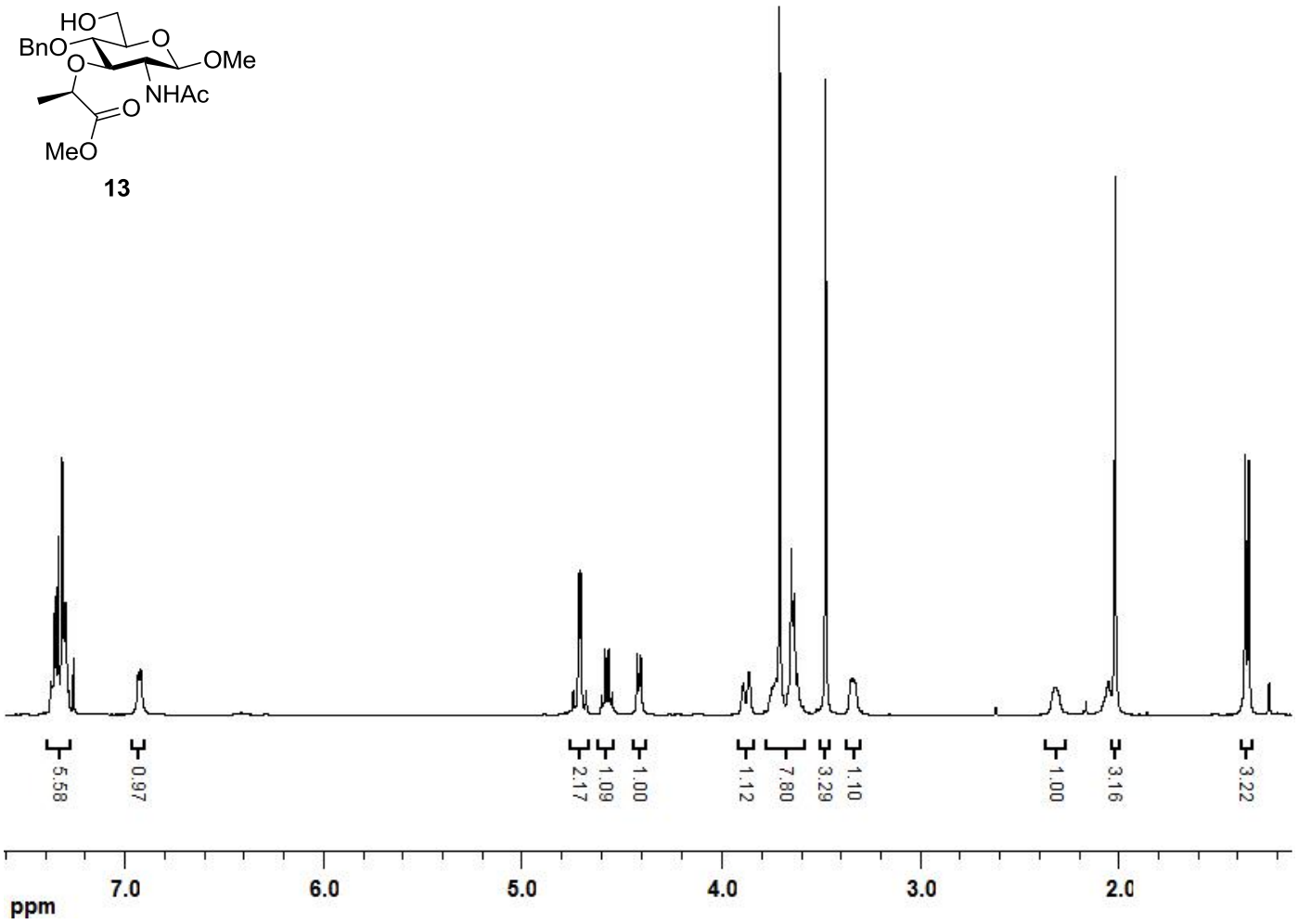

Figure A. 13 ^{1}H NMR (400 MHz, $CDCl_3$) spectrum of compound **13**.

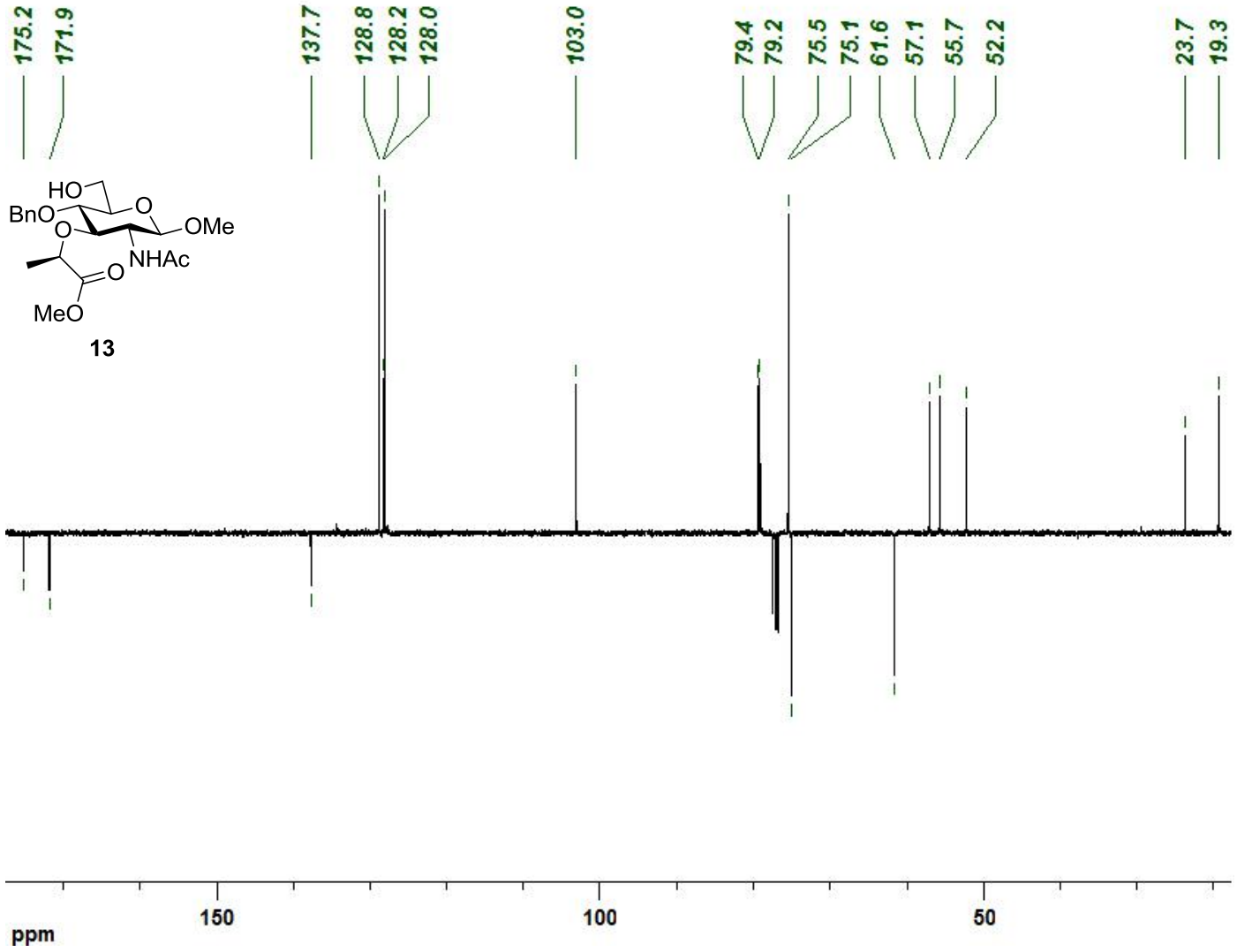

Figure A. 14 ^{13}C NMR (100 MHz, $CDCl_3$) spectrum (APT) of compound **13**.

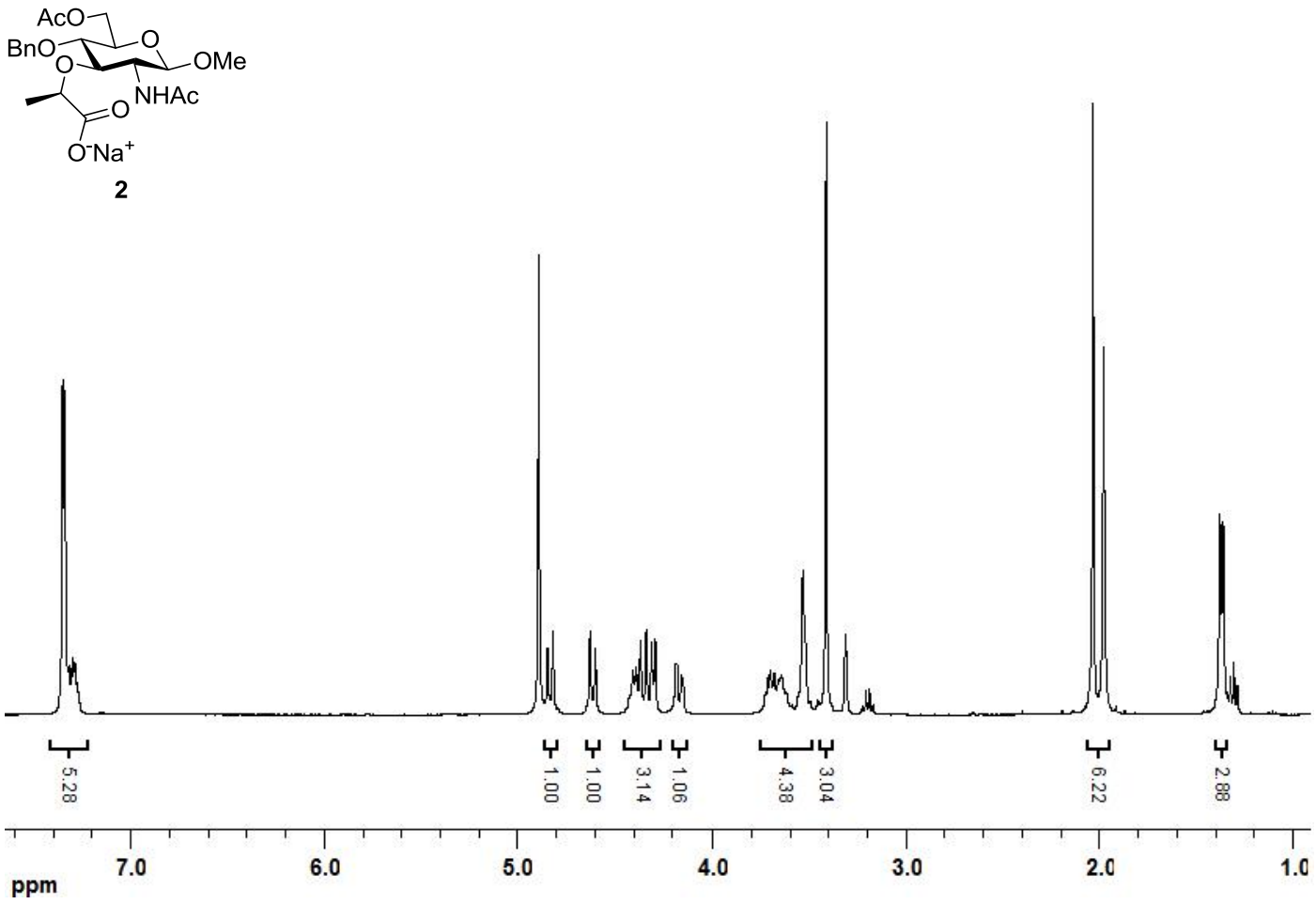

Figure A. 15 ^{1}H NMR (400 MHz, MeOD) spectrum of compound **2**.

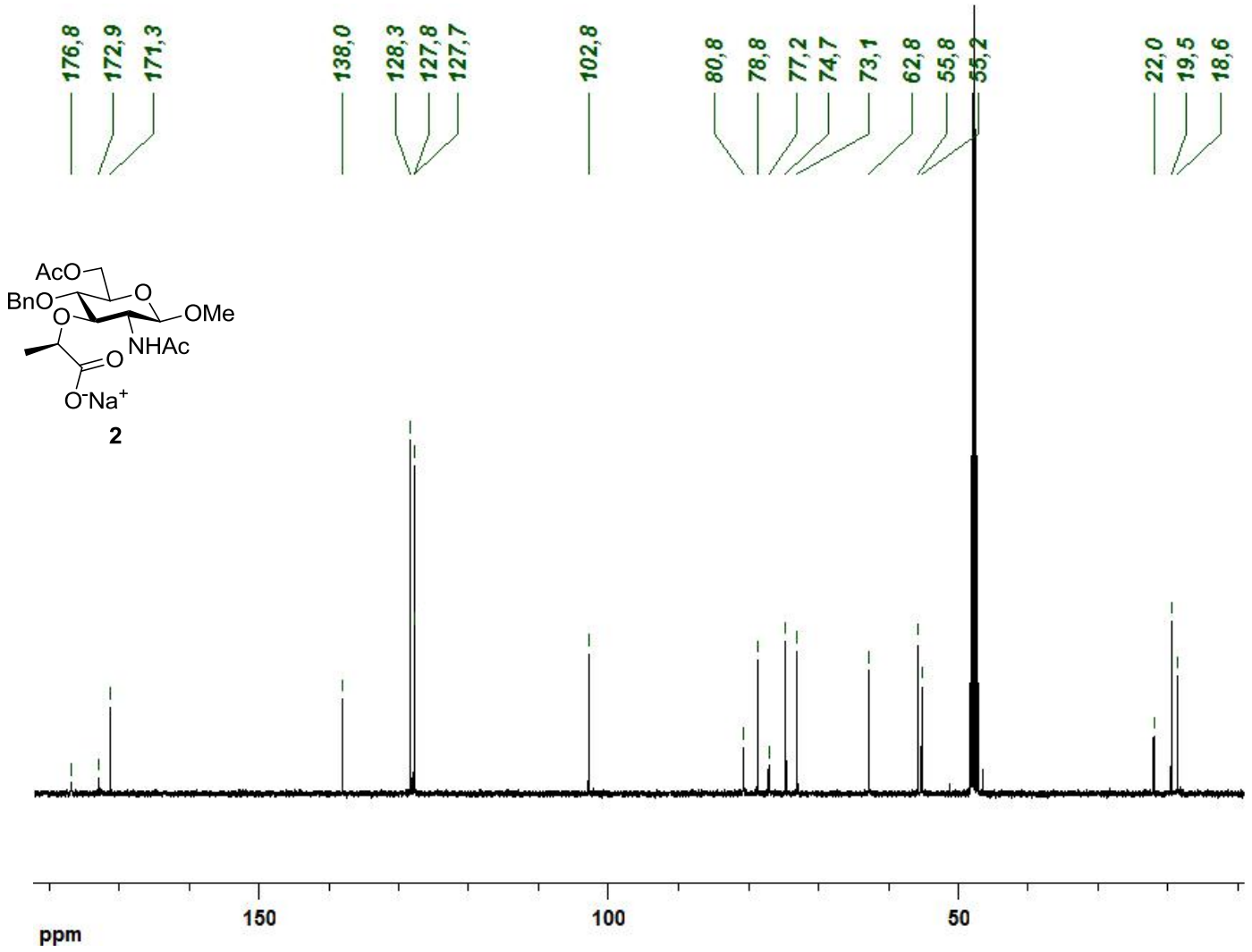

Figure A. 16 ^{13}C NMR (100 MHz, MeOD) spectrum of compound **2**.

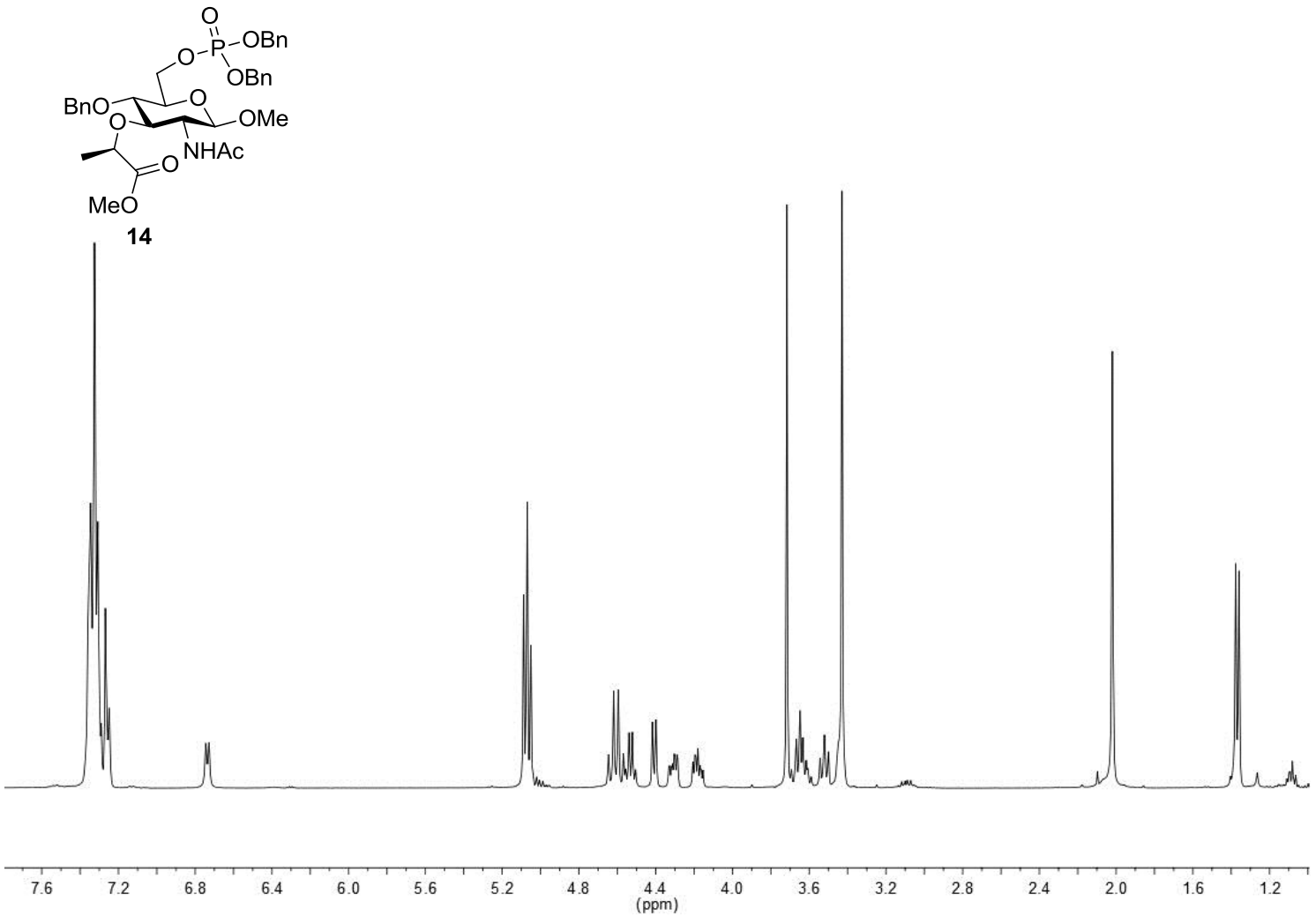

Figure A. 17 ^{1}H NMR (300 MHz, $CDCl_3$) spectrum of compound **14**.

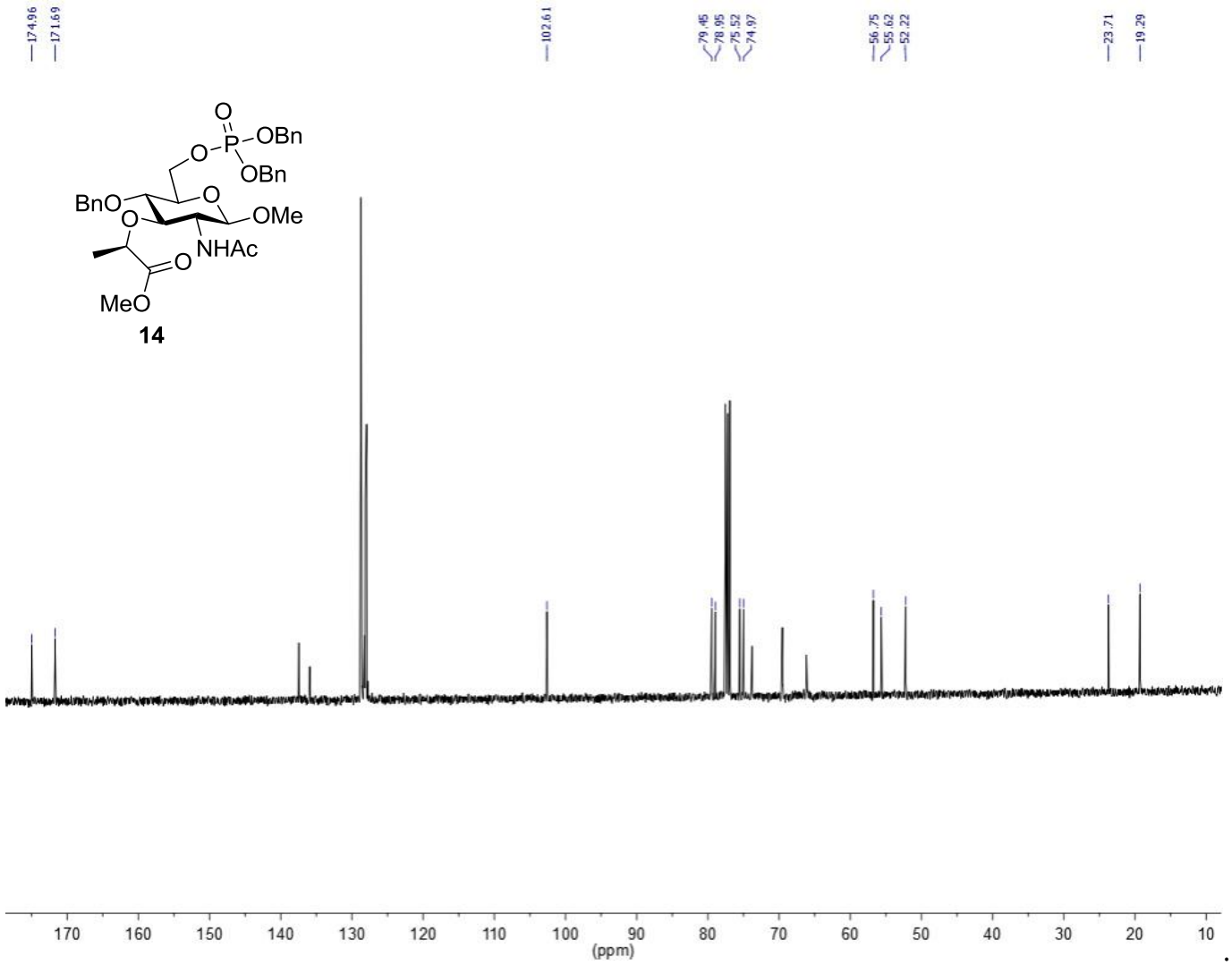

Figure A. 18 ^{13}C NMR (75 MHz, $CDCl_3$) spectrum of compound **14**.

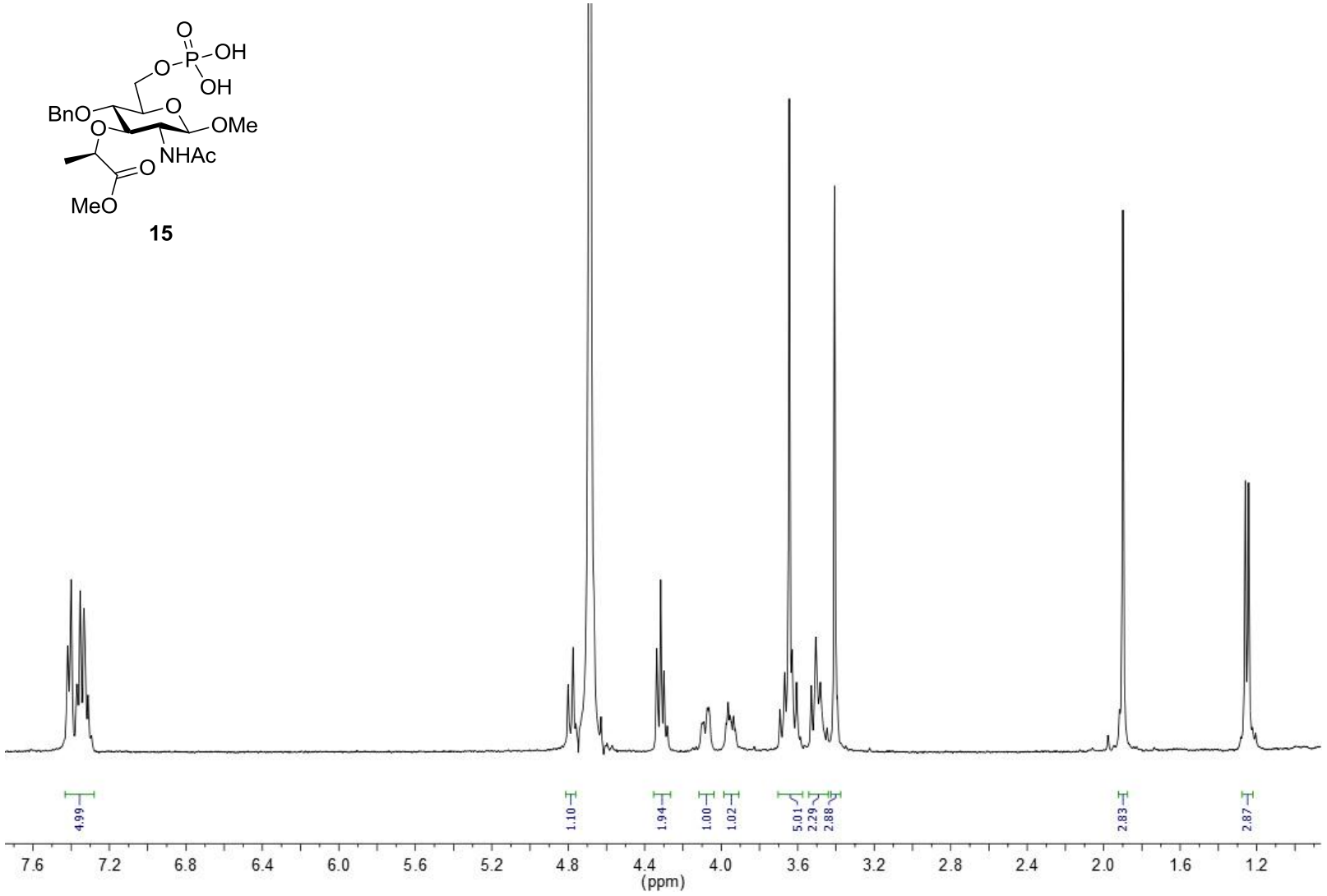

Figure A. 19 ^{1}H NMR (400 MHz, D_2O) spectrum of compound **15**.

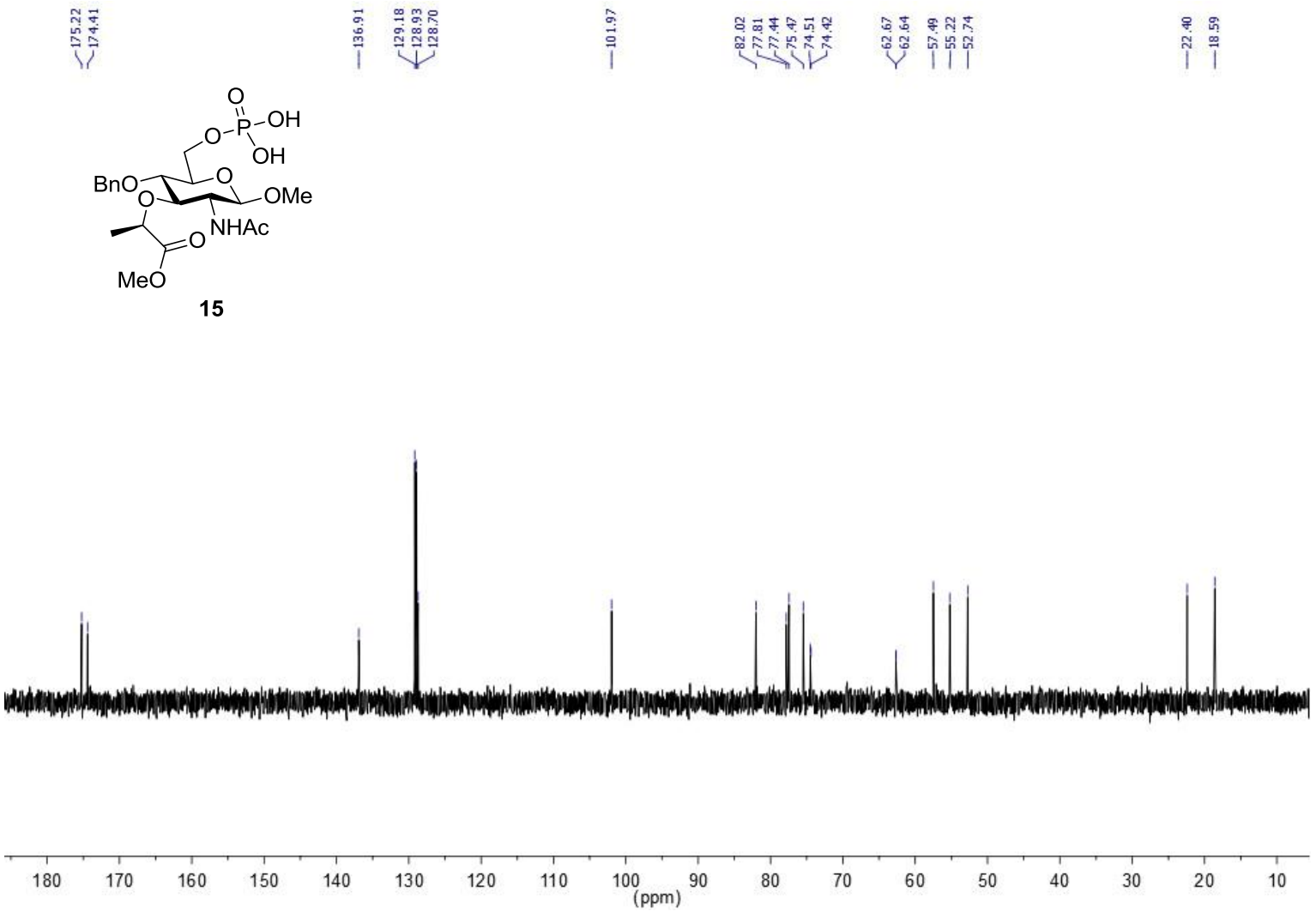

Figure A. 20 ^{13}C NMR (100 MHz, D_2O) spectrum of compound **15**.

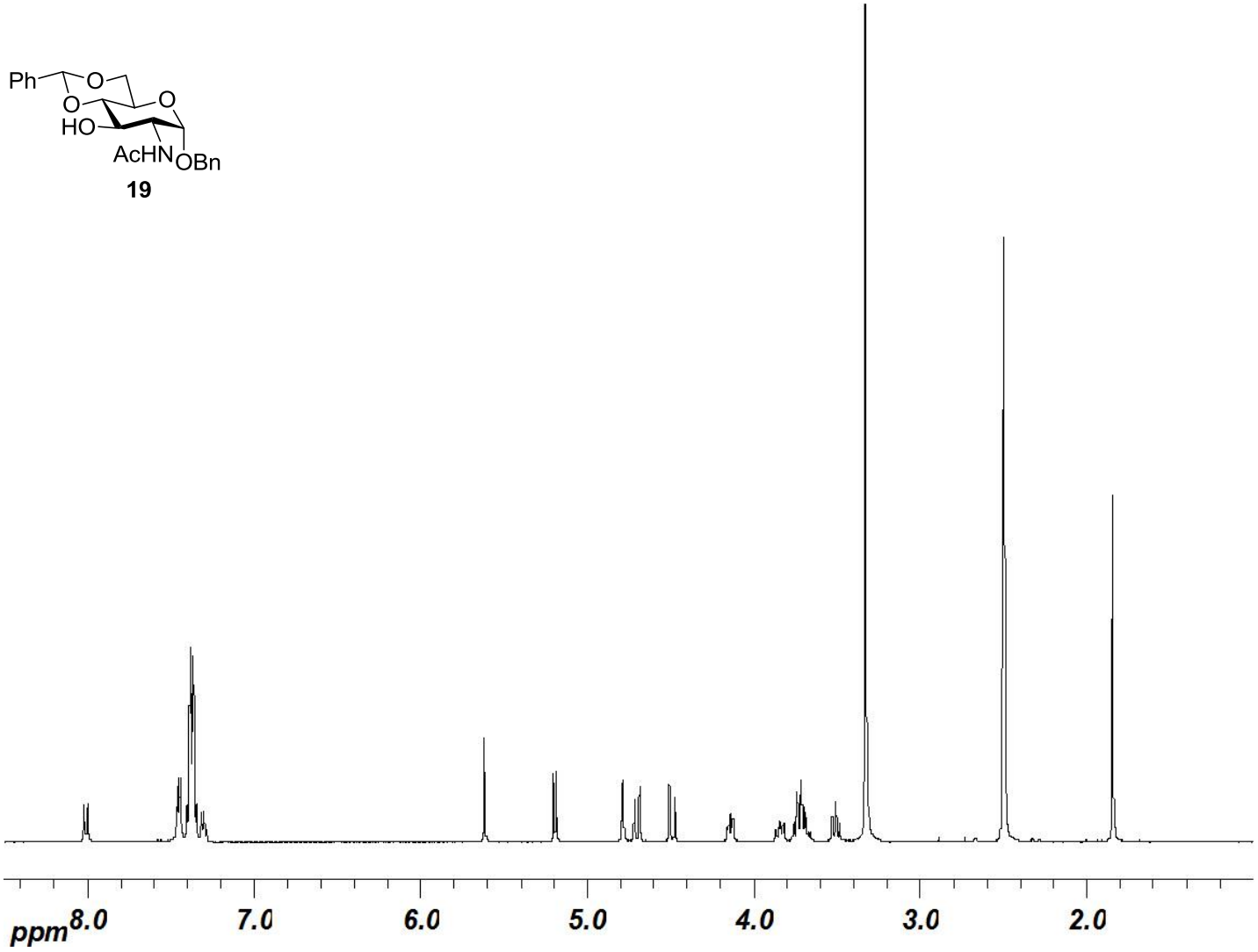

Figure A. 21 ^{1}H NMR (400 MHz, DMSO-d_6) spectrum of compound **19**.

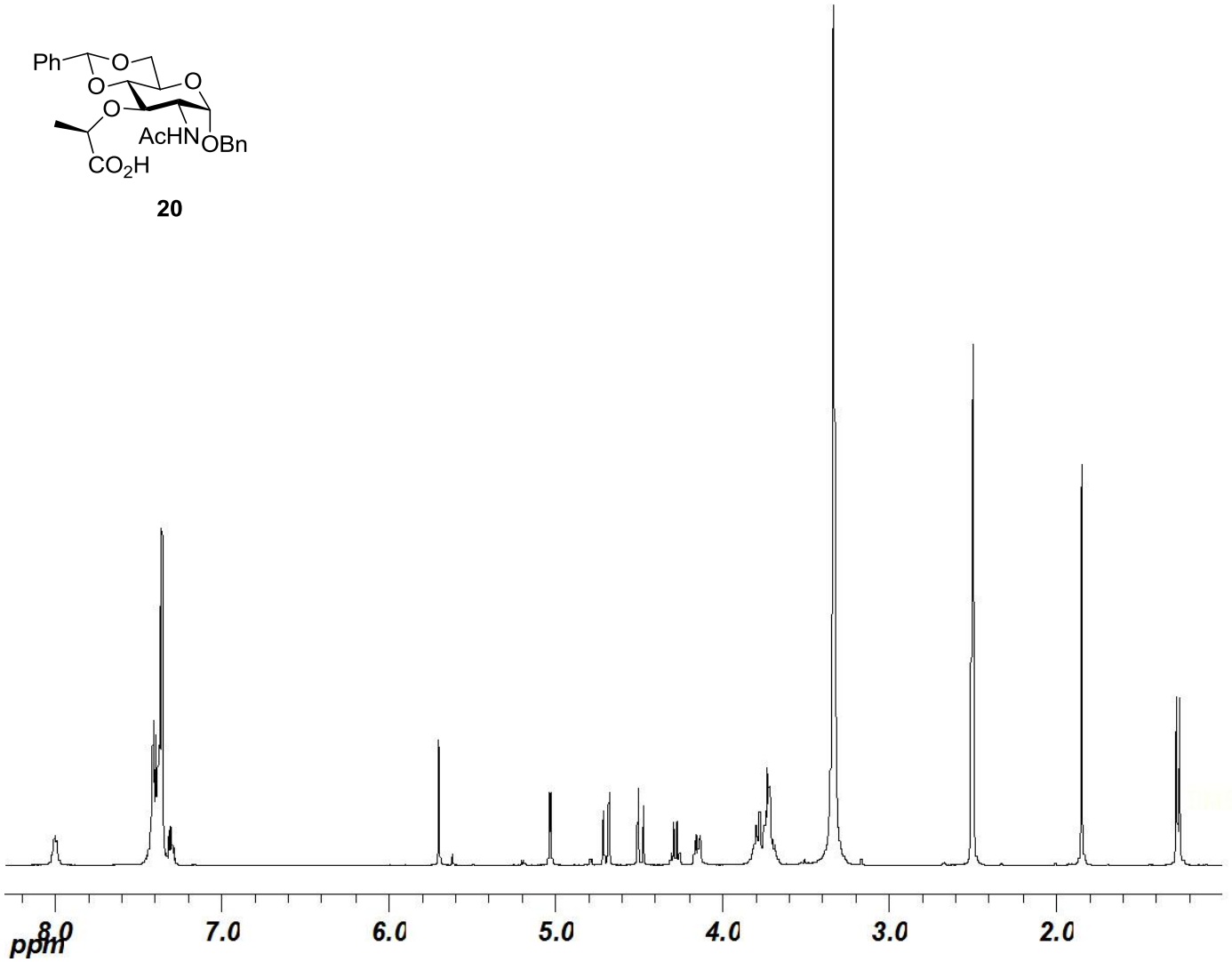

Figure A. 22 ^{1}H NMR (400 MHz, DMSO-d_6) spectrum of compound **20**.

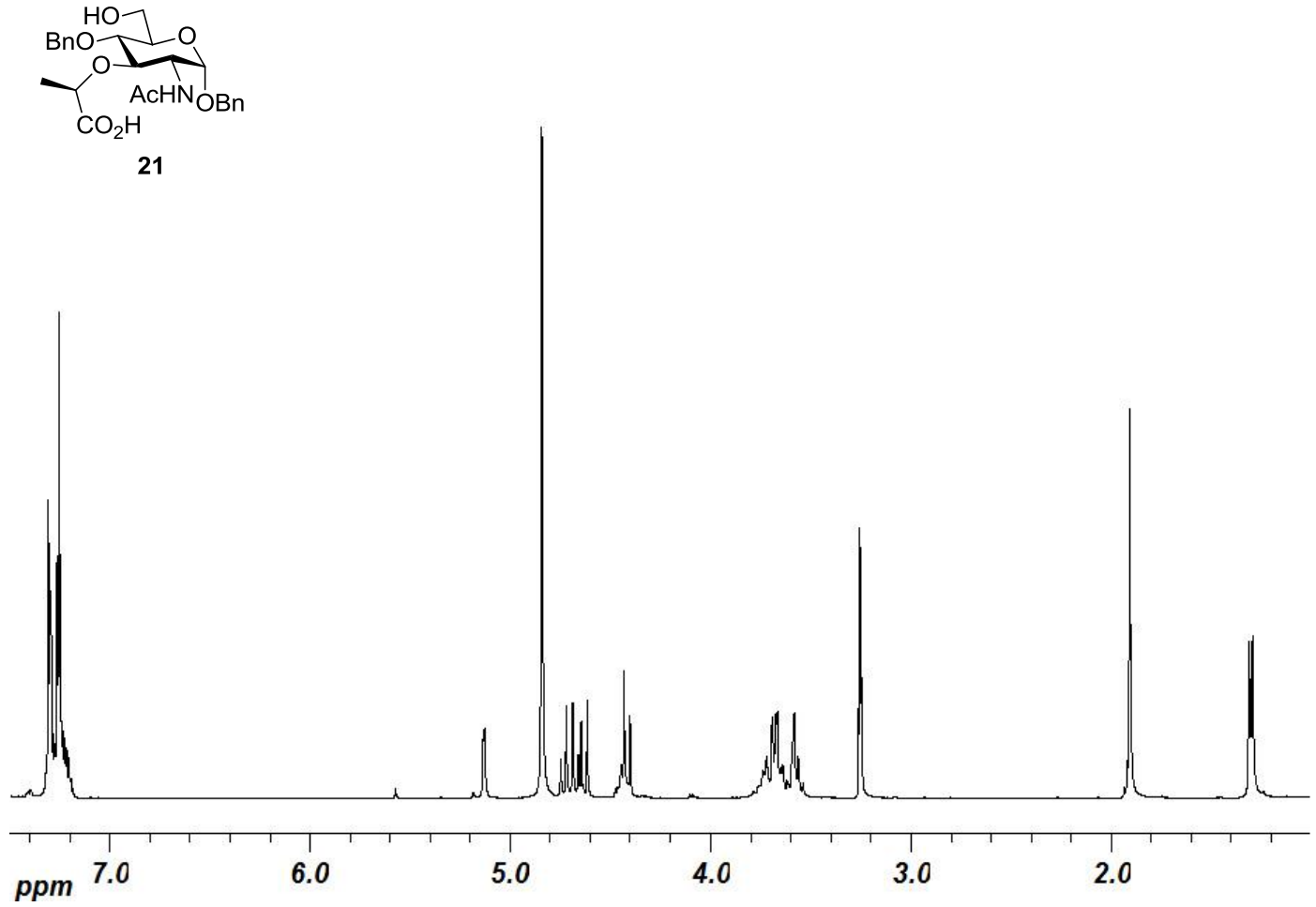

Figure A. 23 ^{1}H NMR (400 MHz, MeOD) spectrum of compound **21**.

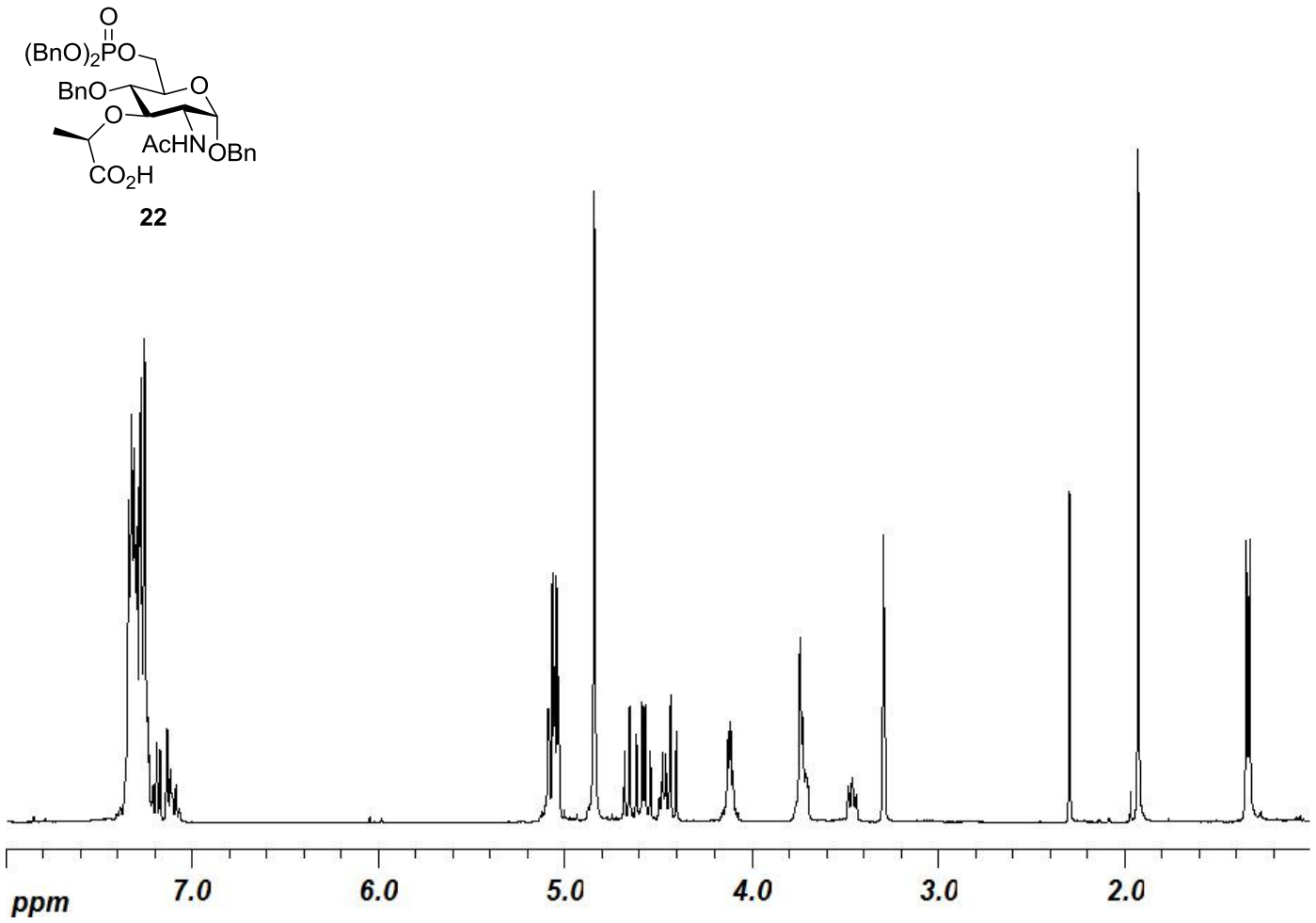

Figure A. 24 ^{1}H NMR (400 MHz, MeOD) spectrum of compound **22**.

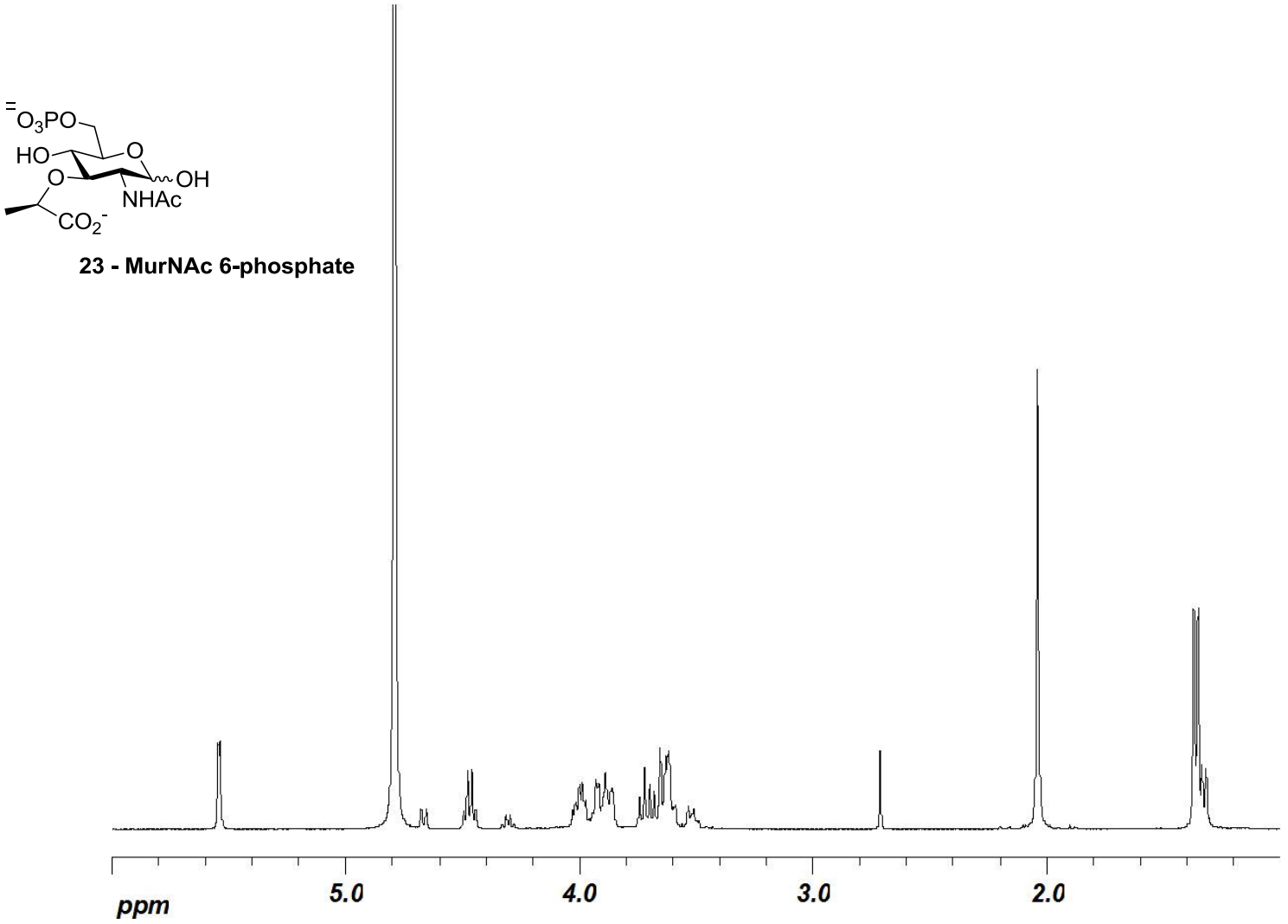

Figure A. 25 ^{1}H NMR (400 MHz, D_2O) spectrum of compound **23**.

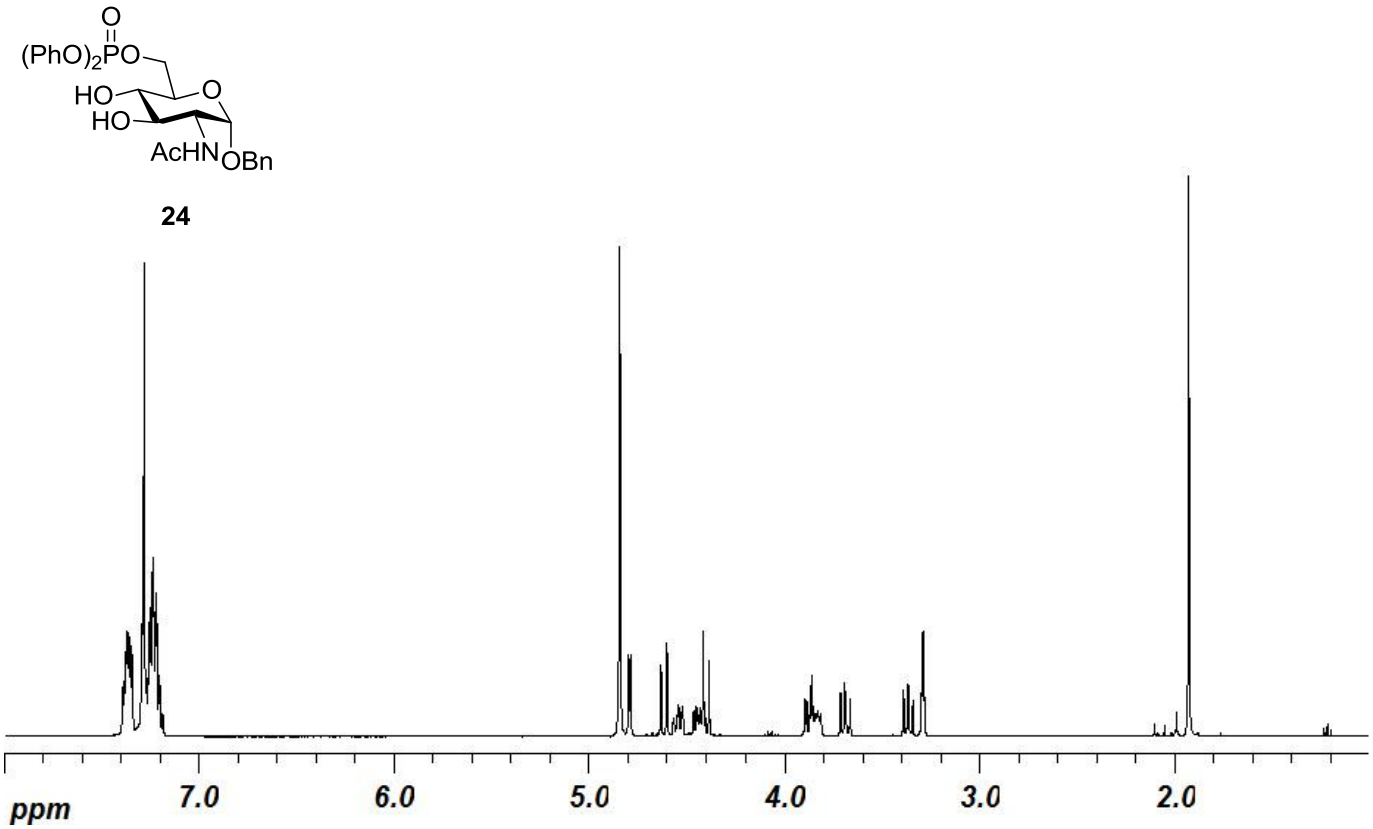

Figure A. 26 ^{1}H NMR (400 MHz, MeOD) spectrum of compound **24**.

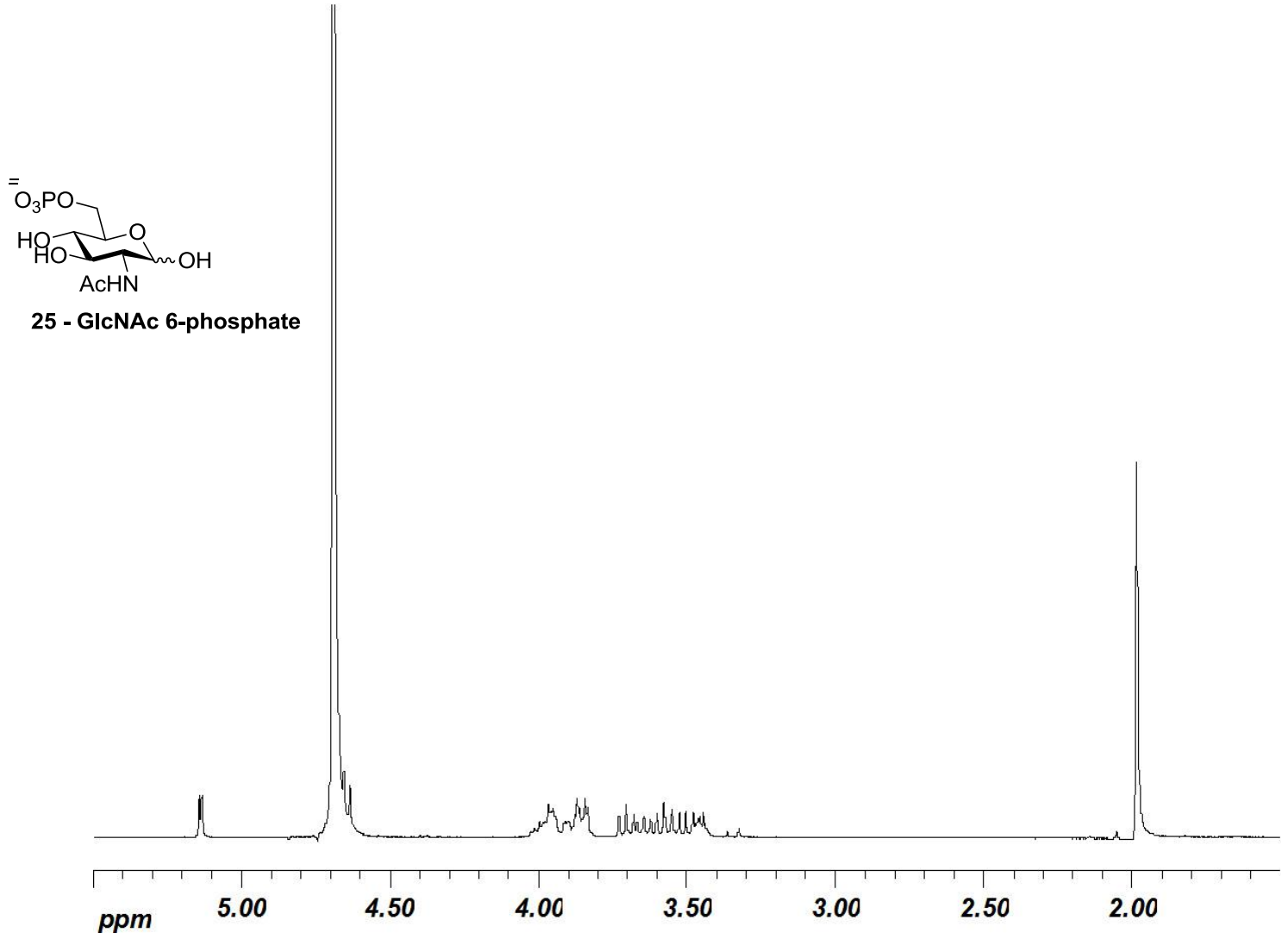

Figure A. 27 ^{1}H NMR (400 MHz, D_2O) spectrum of compound **25**.

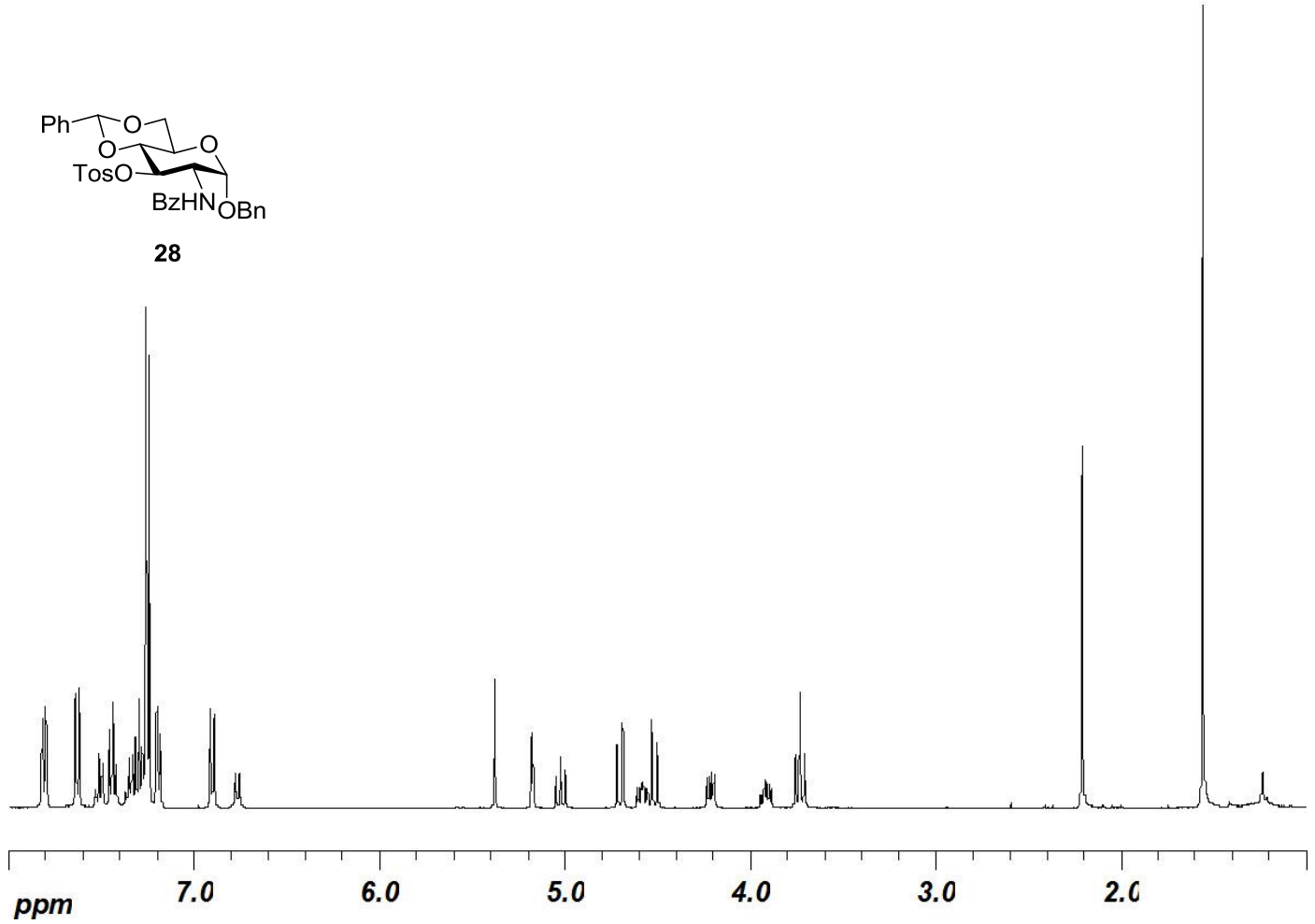

Figure A. 28 ^{1}H NMR (400 MHz, $CDCl_3$) spectrum of compound **28**.

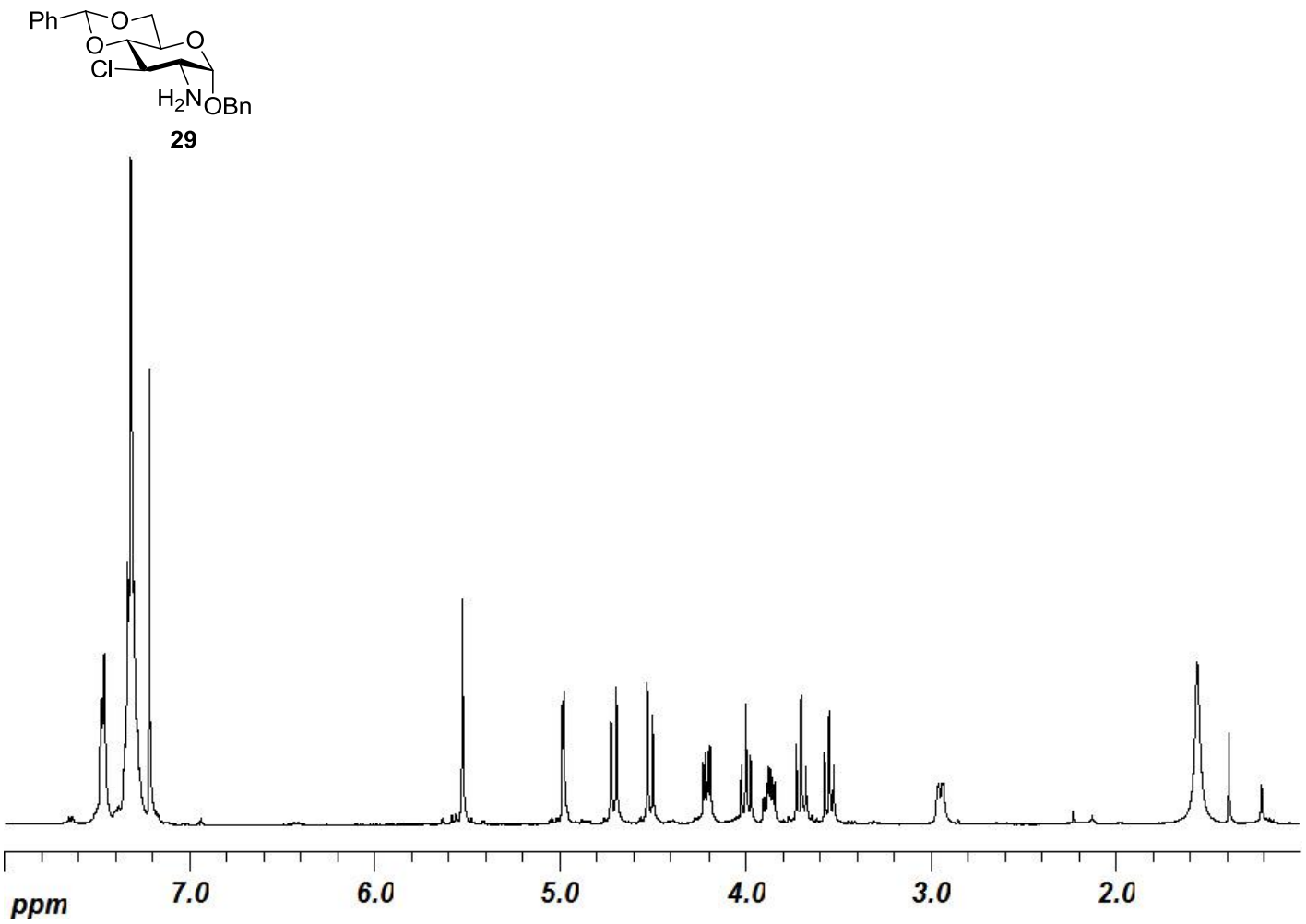

Figure A. 29 ^{1}H NMR (400 MHz, $CDCl_3$) spectrum of compound **29**.

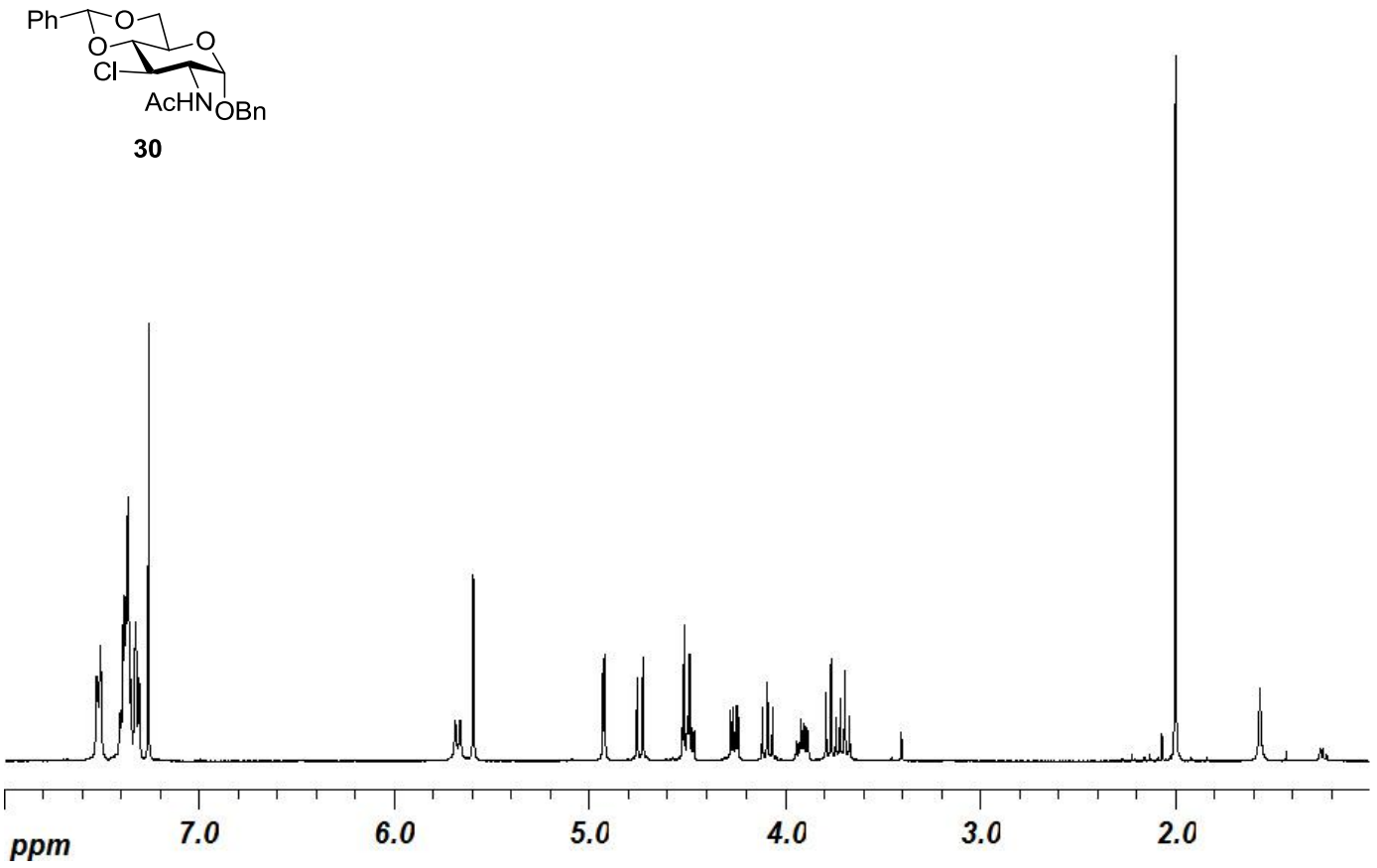

Figure A. 30 ^{1}H NMR (400 MHz, $CDCl_3$) spectrum of compound **30**.

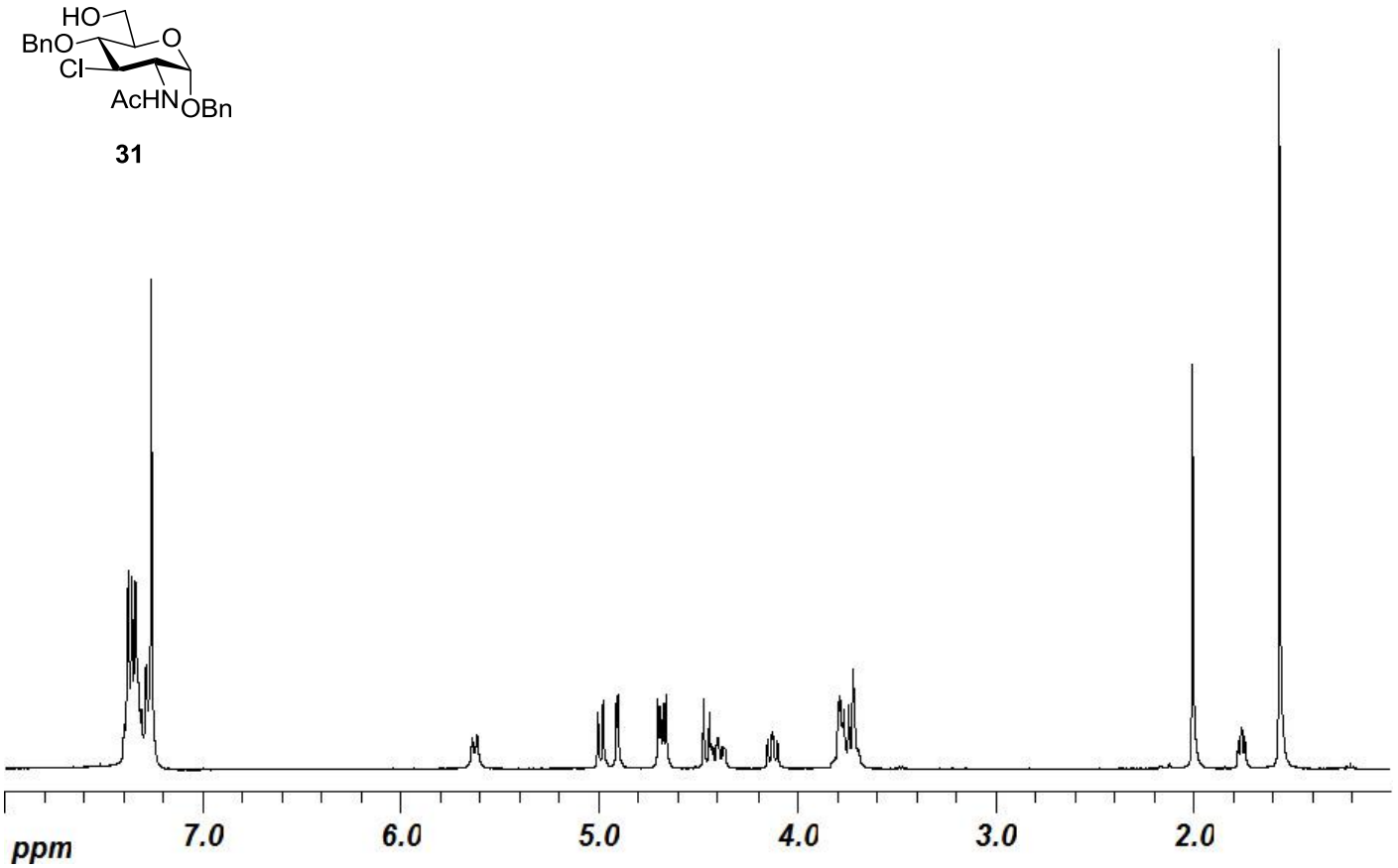

Figure A. 31 ^{1}H NMR (400 MHz, $CDCl_3$) spectrum of compound **31**.

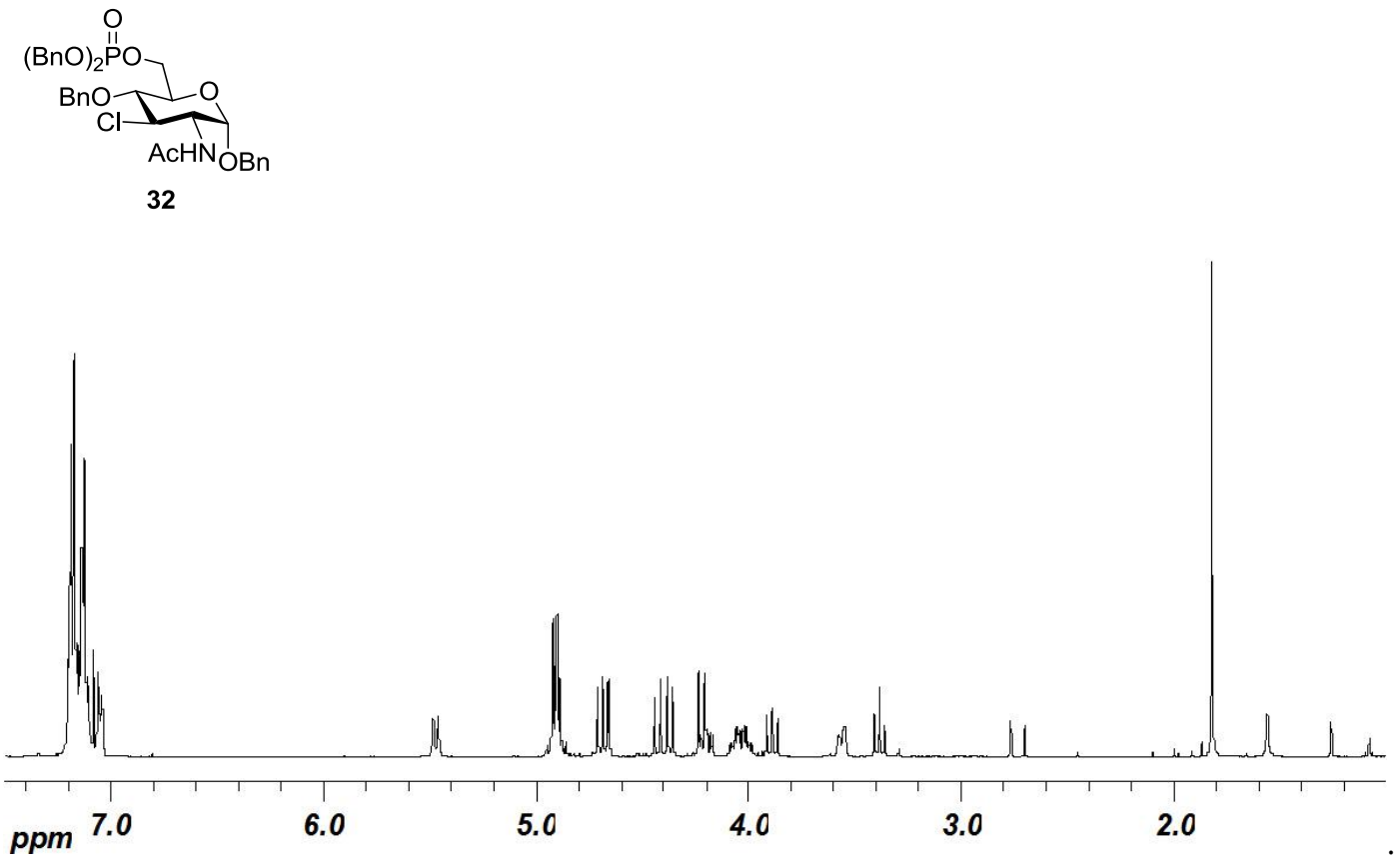

Figure A. 32 ^{1}H NMR (400 MHz, $CDCl_3$) spectrum of compound **32**.

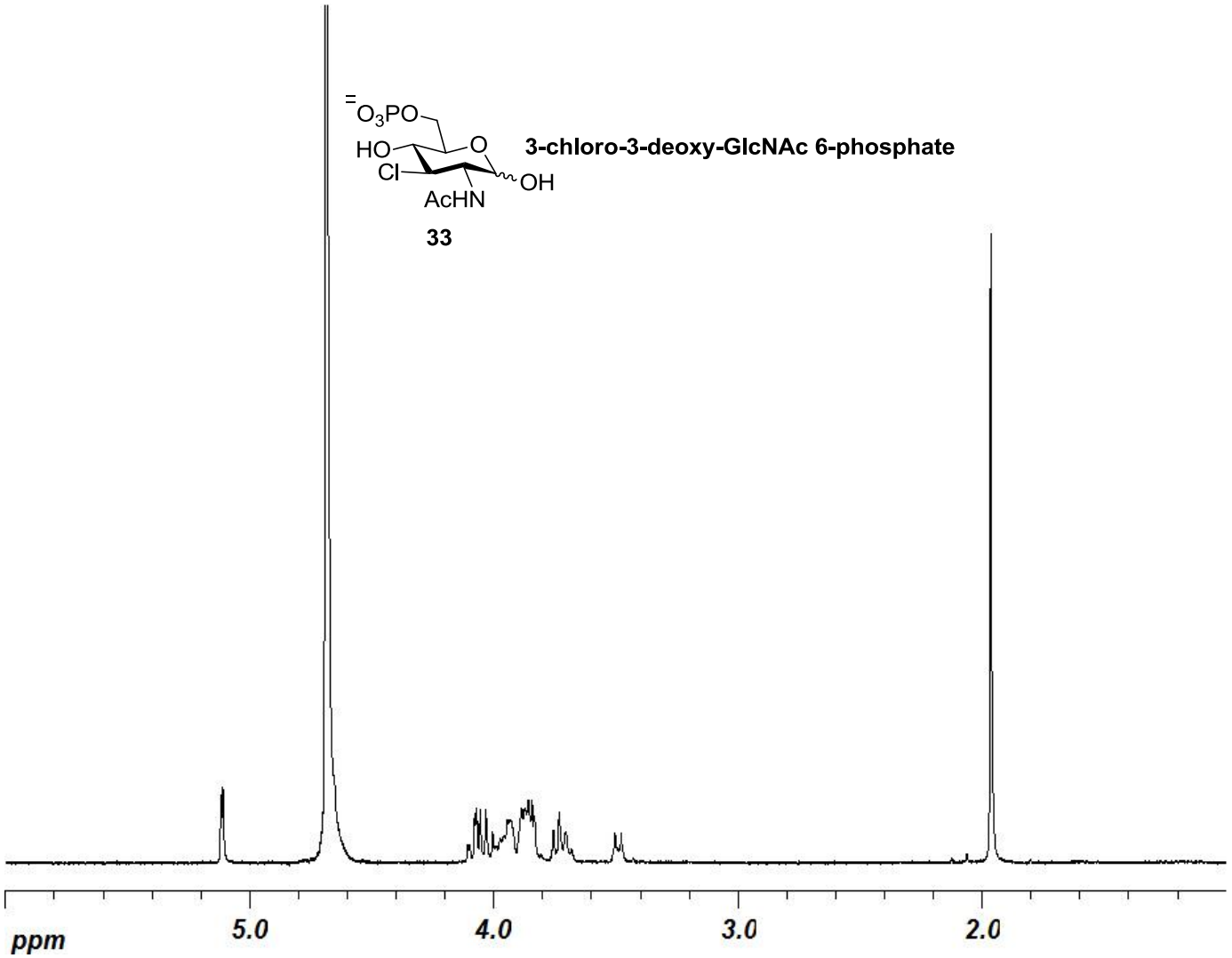

Figure A. 33 ^{1}H NMR (400 MHz, D_2O) spectrum of compound **33**